DISSERTATION

MODELING HUMAN TROPHOBLAST DEVELOPMENT DURING THE PERI-IMPLANTATION PERIOD USING EXTENDED EMBRYO CULTURE

Submitted by

Deirdre Maria Logsdon

Department of Biomedical Sciences

In partial fulfillment of the requirements

For the Degree of Doctor of Philosophy

Colorado State University

Fort Collins, Colorado

Summer 2023

Doctoral Committee:

Advisor: Quinton Winger
Co-Advisor: Rebecca Krisher

Ye Yuan
Dawit Tesfaye
Jennifer DeLuca

ABSTRACT

MODELING HUMAN TROPHOBLAST DEVELOPMENT DURING THE PERI-IMPLANTATION PERIOD USING EXTENDED EMBRYO CULTURE

During the peri-implantation period, a human embryo must transition from a pre-implantation stage blastocyst to a gastrulating embryonic disc surrounding by the primitive placenta. The primitive placenta establishes contact, proliferates, invades, modulates the maternal immune system, and provides a primitive form of nutrients to the implanting embryo proper. Insights into this period have been largely stunted due to the ethical and technical challenges that accompany human embryo research. Studies using donated human embryos following fertility treatment are complicated by confounding infertility diagnoses and limited sample sizes. The development of the extended culture system has provided an avenue to functionally study the peri-implantation period. By using a variety of models including mouse embryos, human embryos, and stem cell-derived blastoids in the extended culture system, researchers are finally able to begin to piece together the puzzle of the peri-implantation period. Here, our objectives were to demonstrate the utility of mouse models in modeling human trophoblast during peri-implantation extended culture, examine and summarize human development during peri-implantation in the context of confounding fertility diagnoses, compare human trophoblast in extended culture to other widely available regenerative trophoblast models, and determine to what extent blastoids are able to reflect human peri-implantation development and maternal-fetal crosstalk in extended culture. Further, we show that estrogen signaling in trophectoderm may be conserved between mouse and human embryos, aged embryos exhibit hindered growth in extended culture, peri-implantation trophoblast cells have unique transcriptional

priorities, and the presence of endometrial stromal cells encourage fusion of trophoblasts. Our studies both reinforce the significance of the extended culture system and lay the groundwork for future studies on early trophoblast and embryo development during peri-implantation.

ACKNOWLEDGEMENTS

Rebecca, I appreciate so many things about you as a mentor and as a human. You have modeled for me the strength and stability of a good leader, and I can always count on you to give me thoughtful advice and feedback while somehow simultaneously juggling all of your other roles. I am grateful that you stuck with me through the move, and I can't emphasize enough how much of an impact you have made on me. I often ask myself, "What would Rebecca do?" Even though we don't talk often, your presence has persisted, and your strength will carry through me as I navigate this world. Thank you for everything.

Ye, I know that adopting a PhD student while being thrust into a new position must have not been easy. But, you have taken it in stride. I am grateful that you stayed down in the trenches with me to help guide me through this journey. You are one of the most ambitious people I know, and I appreciate your unwillingness to settle. You have advocated for me endlessly and encouraged me to push the boundaries of my experiments. Thank you for all that you have done for me, it doesn't go unnoticed, and I will try to carry your ambition forward with me throughout my life.

Dr. Winger, Dr. DeLuca, and Dr. Tesfaye, thank you for your support through this journey. Each of you have been easy to work with, gracious, and thoughtful in your feedback. I appreciate the time that it takes to serve on a committee, and I am grateful that you each were on mine.

Mom and Dad, you are my best friends. There were times during this process that I was so frustrated in the nitty gritty details, and you were both always willing to take my call and listen to my experiences. You have been my biggest cheerleaders, and I attribute everything that I have accomplished to your unwavering support. I love you both.

DEDICATION

This work is dedicated to my husband, William, and two children, William and Emelia.

Juggling this degree with our day-to-day has not been easy, and I appreciate your endless support and love when I walk in the door.

TABLE OF CONTENTS

LIST OF TABLES

CHAPTER I

CHAPTER II

CHAPTER III

CHAPTER IV

LIST OF FIGURES

CHAPTER I

CHAPTER II

CHAPTER III

CHAPTER IV

CHAPTER V

APPENDIX I

APPENDIX II

APPENDIX III

APPENDIX IV

APPENDIX V

CHAPTER I: REVIEW OF THE LITERATURE

Introduction

Human reproduction is incredibly inefficient, with an estimated 40-50% of fertilized ova during natural conception failing to implant successfully, and remains a significant barrier to successful pregnancies both naturally and from assisted reproductive technologies (1-4). As the pluripotent inner cell mass (ICM) proliferates and begins to self-organize into what will eventually be a post-implantation epithelial disk-like shape, trophectoderm (TE) cells must prepare to make contact and communicate with the endometrium, appose to the endometrial epithelial tissue, and breach the epithelial layer in their pursuit of the endometrial stroma and ultimately the maternal blood supply (5-9). Immediately following, TE cells will differentiate into nascent trophoblast (TB) populations and TB sublineages that will perform highly specialized functions for the establishment of a healthy placenta. Though critically important for pregnancy, implantation is one of the most puzzling milestones in human development, as most of the underlying mechanisms are largely unknown (10). Ethically, human embryos are impossible to secure for research unless they are donated following infertility treatment. In the United States, even this donation can become ethically complicated given recent shifts in embryo termination laws (11-13). Technically, in vivo monitoring of implantation poses different hurdles. At this early point in pregnancy, the mother is still unaware of the implanting embryo and monitoring techniques including ultrasonography are useless due to the poor resolution (10).

To overcome these hurdles, researchers have used a combination of animal models, regenerative cell lines, and donated human embryos to study early implantation events and early TB differentiation during the peri-implantation period (14-16). Rapid advances in human embryo implantation models over the last decade have given unprecedented insight into the mechanisms of human implantation and TB differentiation (17-21). Continuing to optimize

working models of the peri-implantation period will help to reveal mechanisms for the establishment of a healthy placenta for long term health of both the mother and child. Additionally, these insights will prove essential for the development of contraception for family planning and for the mitigation of placental pathologies including recurrent pregnancy loss and preeclampsia.

Here, we review the rapid development of models for the peri-implantation development of human TB from a historical perspective. We will emphasize the development and utility of the peri-implantation extended embryo culture (EEC) model in the absence of maternal tissues, including the preceding development of the mouse EEC system, focus on human EEC in the broader context of modeling TB differentiation, and compare human EEC with commonly used regenerative stem cell models. Finally, we explore the ability of stem-cell-derived blastoids to model TB differentiation during the peri-implantation period, discuss opportunities for developments in each model system, and highlight unanswered questions still in need of exploration.

The Primitive Placenta

The earliest published report of human embryonic development in 1883 contains detailed descriptions and vivid drawings depicting human development at 8 weeks gestation (22). Over the next century, more detailed descriptions emerged, though the implantation stage remained particularly unexplored due to technical and ethical limitations (23-25). Thus, our insights into implantation and early TB differentiation in humans through the 20th century has been gleaned almost entirely from histological sections from hysterectomies from 1941-1956 by Hertig and Rock (26-29). These and others contributed to a collection established by Francis Mall in 1914 that comprise the Carnegie Collection of Human Embryos (23, 30, 31). From this collection of histological sections, the 23 Carnegie stages were eventually described by O'Rahilly and Muller which capture embryo development through approximately 8 weeks post fertilization (23, 24).

For the scope of this review, we will focus on modeling the developmental events of Carnegie Stages 4-5b in vitro.

At Carnegie Stage 4, the blastocyst is comprised of three main cell types. Pluripotent cells that will comprise the epiblast and hypoblast cells that will become the extra embryonic endoderm (XEN) both comprise the ICM and are encapsulated by a balloon-like structure comprised of TE, destined to differentiate into the tissues of the placenta (18). The balloon-like blastocoele cavity is expanded with fluid and the blastocyst has attached to the surface of the endometrial epithelial cells via the polar TE lying just underneath the ICM (32).

Once attached, the mural TE opposite of the ICM eventually collapses as the polar TE breaches the endometrial epithelium to gain access to the underlying endometrial stromal cells (Carnegie Stage 5a). The TE in direct contact with maternal cells undergoes an epithelial to mesenchyme transition (EMT, 33), proliferates, and differentiates into two subpopulations of TB; the progenitor stem cell TB population of cytotrophoblasts (CTB) and the multinucleate syncytiotrophoblasts (STB) that together will form the trophoblastic shell (34). At this point in development, there is no emergence of an apparent chorionic villous structure, and the embryo has not yet accessed the maternal spiral arteries. Therefore, the short-lived trophoblastic shell comprised of the proliferative CTB and multinucleate STB become the primitive placenta and are entirely reliant on histotrophic secretions from the endometrium (34). In Carnegie stage 5b, histologic sections of the trophoblastic shell including the primitive syncytium measure approximately 500 μm, have entirely breached the endometrial epithelial layer, and are completely embedded in the underlying endometrial stromal cells. Within the trophoblastic shell, the primitive syncytium matures to create large empty lacunae that fill with maternal blood to nourish the embryo until villous columns of CTB are able to breach the STB and extra villous TB (EVT) are able to differentiate reach and recolonize the inner wall of the maternal vasculature (26, 29).

TB of the primitive placenta differ from definitive TB as mature villous columns have not emerged to interdigitate with maternal tissues. Because TB cells are responsible for interfacing with maternal tissues and mediating the exchange of nutrients and waste between the mother and the fetus, improper TB differentiation and invasion is the one of the putative causes of various pregnancy complications including spontaneous pregnancy loss and early onset pre-eclampsia (34, 35).

The Rapid Advancement of Human Trophoblast Models

Remarkably, histological sectioning of in vivo implanting embryos remains the gold standard representation of the peri-implantation period in humans. Advances in culturing human oocytes and embryos (37-39) and modeling implantation in vitro over the past century have been limited largely by inadequate culture conditions (Figure 1.1). Additionally, the ability to obtain human oocytes for in vitro fertilization and blastocyst culture didn't emerge until the late 1970's, nearly 30 years after our first glimpse of implantation from Hertig and Rock. In vitro culture of human blastocysts up to embryonic day (D) 9 was achieved with co-culture of endometrial epithelial and stromal cells, though trophoblast invasion and outgrowth was severely stunted and could not progress pass a strong adhesive phase (40). In the subsequent decade, various human embryo-endometrial co-culture experiments emerged (extensively reviewed elsewhere, 41), and the first co-culture experiment to closely examine trophoblast invasion came in 2003 (42). However, researchers were still unable to culture human embryos past the apposition and adhesion events up to D 9, and all in vitro models of human embryo implantation at the time utilized the co-culture of embryos with endometrial cells for support and communication (6, 43-49). Therefore, research regarding TB differentiation and development during implantation still relied heavily on regenerative TB cell models.

Regenerative cell models of TB include those fused with choriocarcinomas, immortalized first trimester TB, and primary TB cell lines (50-56) and are widely used to investigate TB cell

differentiation and function. However, many immortalized TB as well as those fused with choriocarcinoma are problematic in that they are derived from a TB population later in gestation, and because of their immortalization or fusion with choriocarcinoma, do not truly recapitulate some behaviors of physiologically normal primitive TB (14). For the scope of this review, we do not delineate the shortcoming of each TB cell model as they have already been extensively reviewed (57, 14).

For investigators studying the primitive placenta during peri-implantation and the de novo differentiation of a TB cell fate, the aforementioned cell lines are not an option. Instead, inducing a TB identity from hESC became possible in 2002 with the exposure to bone morphogenic protein 4 (BMP4, 69). Transcriptomic analyses between human TE and BMP-treated hESC reveal similarities during the implantation period (58), and further optimization of the protocol in 2013 (addition of A83-01 and PD0325901, BAP) allowed for unidirectional conversion of hESC to TB without contaminating amnion-like cells (59). Still, the identity of BAP-treated hESCs is controversial. Several groups have challenged the identity of BAP cells as amnion (60, 61). However, these reports are based on a modification to the differentiation protocol and with proper exclusion of FGF2 and a full 8 day differentiation, BAP cells are much more similar to TB than amnion (62, 63) Additionally, direct transcriptional comparisons indicate the true TB identity of BAP does not resemble first-trimester or term TB (64), and novel early BAP markers may be indicative of the primitive placenta (65).

In 2018, Okae et al. derived true human TB stem cell (hTSC) lines (both male and female) from extended culture blastocysts as well as first trimester villous columns. It became possible to maintain a TB stem cell population in vitro that would self-renew with continued Wnt activiation via GSK3 inhibitor CHIR99021, epidermal growth factor (EGF), TGFβ inhibitors A83-01 and SB431542, the histone deacetylase inhibitor valproic acid (VPA), and the Rho-associated protein kinase (ROCK) inhibitor Y27632 (66). Self-renewing CTB are also capable of

differentiating to STB following treatment with forskolin to upregulate cAMP or EVT following treatment with A83-01, neuroregulin 1 (NRG1), and Matrigel (66). The hTSC and BAP-treated hESC are the closest regenerative TB lines that could theoretically model the primitive placenta, however their similarity to peri-implantation stage TB cells will need to be intentionally and functionally compared before researchers can confidently rely on their ability to model the TB in the primitive placenta.

Peri-implantation Extended Culture of Mouse Embryos

Key developments in mouse embryo culture medium and technologies typically precede and pave the way for advances in human embryo culture (8, 87). During normal peri-implantation development in vivo, mouse embryos attach to the endometrium via interactions with the mural TE rather than the polar TE. Once apposed, the embryo interdigitates with the epithelial cells of the endometrium and the TE cells undergo endoreduplication to form TB giant cells. Extraembryonic endoderm cells opposite the epiblast eventually develop a protruding ectoplacental cone as the epiblast cavitates to form the pro amniotic sac around D 6.5 in vivo (80). Mouse extended culture was attempted in 1966 and was later more successful with inclusion of a bovine lens substrate (67, 81, 82). Several other in vitro culture systems with modified substrates emerged, none of which are conducive to modern day imaging advances. The development of the mouse peri-implantation EEC system on optical grade culture dishes in a defined in vitro culture medium (IVC1: Advanced DMEM/F12 base with 20% (v/v) fetal bovine serum (FBS), 2mM glutamine, penicillin (25U/mL), streptomycin (25 µg/mL), 1X ITS-X, 8nM estradiol, 200 ng/mL progesterone, 25 uM N-acetyl-L-cysteine; IVC2: IVC1 with 30% (v/v) knockout serum replacer (KOSR) instead of FBS) allowed for a more accessible model to examine peri-implantation dynamics (71).

Mouse implantation on fibronectin has been used historically as a measure of implantation potential for embryos (83, 84). We showed that the improved mouse EEC protocol could act as

a proxy to further measure developmental potential of the embryo as evidenced by epiblast proliferation and organization of advanced morphological structures including the ectoplacental cone, a proamniotic cavity, and morphological stratification of the epiblast cells into a columnar epithelium (85). Assuming that embryo quality would increase with the amount of time the embryo spent in vivo, we used in vitro matured oocytes, in vivo matured oocytes fertilized in vitro, and in vivo flushed blastocysts to show that high quality embryos would develop further in EEC, and the observations made in EEC are able to mimic the development following surgical embryo transfer. Indeed, poor quality embryos have fewer epiblast cells, smaller TB outgrowths, and fewer incidence of advanced morphological structures.

There are several limitations to the mouse EEC model in regards to human trophoblast development during implantation. Pluripotency factor POU5F1 persists in the TE of human blastocysts and is associated with the downstream expression of TE marker CDX2 in humans, whereas POU5F1 is restricted to the ICM of mouse blastocysts and disruption does not hinder cell lineage specification during blastocyst development (86). Mouse embryos attach via the mural TE, whereas human embryos appose and attach to the polar TE just below the ICM (87, 88). In regards to TB development, mice do not develop the TB subpopulations unique to humans. TB giant cells, analogous to STB in human, are present but they do not fuse to form a multinuceate syncytium (88). Mouse embryos also do not develop a highly invasive MTB, and invade relatively superficially compared to human TB that invade as deep as the myometrial layer of the uterus (90). Despite glaring differences in regards to peri-implantation, the development of mouse EEC was a critical stepping stone to the development of human EEC (18).

Peri-implantation Extended Culture of Human Embryos in the Absence of Maternal Tissues

It was not until 2016 when Shahbazi et al. and Deglincerti et al. were able to culture human embryos during the peri-implantation period in the absence of maternal tissues and replicate the

morphological hallmarks of the primitive placenta that were first observed in the mid-1950's (17, 18). By culturing human embryos in IVC1 for 48 h undisturbed and exchanged ½ volume with IVC2 for 5 additional days, Shahbazi et al. observed populations of round, mono-nucleated cytokeratin 7 (CK7)-positive TB cells proximal to the hypoblast and epiblast while large multinucleate TB cells lay at the distal periphery of the embryo (17). Not only were authors able to finally mimic the morphogenesis of the primitive placenta that was first seen nearly a century earlier, but they were able to show that human embryos were able to self-organize and exhibit advanced morphological development without maternal contributions. Shahbazi et al. showed that by D 7, the human embryo fully collapses after a series of blastocoel contractions. Once collapsed, the embryo is comprised of POU5F1-positive epiblast cells that begin to organize radially to generate the pro-amniotic cavity. A GATA3-positive population proximal to the epiblast also cavitates to form the prospective yolk sac. These two populations work to generate the bilaminar disk of the developing embryo and are surrounded by mono nucleated CTB and an outer perimeter of multinucleated STB.

Deglencerti also demonstrated the culture of human embryos in the absence of maternal tissues. Deglencerti describes TB development more in depth confirming that CDX2 expression diminishes and that GATA binding protein 3 (GATA3) acts as an appropriate TB marker during peri-implantation. Multinucleate cytokeratin 7(CK7)/ GATA3-positive cells on the periphery of the embryo also stained positive for human chorionic gonadotropin beta (CGB, 18); a hallmark of STB and a key player in the maternal recognition of pregnancy in humans (89). They also identify lacunar pockets within the syncytium, and though MTB are not described in detail, TB cells detached from the main embryo are shown in one figure at 12 d. p. f. Since the development of EEC, several modifications have been made to the culture conditions and medium formulation (Table 1.1), and the observations made in these two studies has provided the research community with a usable model to replicate the observations that were made nearly 80 years earlier.

Table 1.1 Modifications to the Extended Embryo Culture Conditions and Medium Formulations

Publication	Medium	Culture System Modifications	IVC1/2 Recipe Modifications
91	mIVC1/2	Non-adherent 96 well plate 10% Matrigel on D 9	10 µM ROCK inhibitor Y27632, 1mM sodium pyruvate, 0.22% (v/v) sodium lactate
92-94	IVC1/2	Fibronectin substrate	NA
95, 96	IVC1/2	NA	IVC1/2 + 50 ng/mL IGF
97	IVC1/2	Primate model	8 µM ROCK inhibitor Y27632 in IVC2
98	IVC1/2	Primate model, Matrigel substrate	1XN2/B27 supplement replacement for the exclusion of 2mM glutamine, penicillin (25U/mL), streptomycin(25uG/mL), 1X ITS-X, 8nM estradiol, 200 ng/mL progesterone, 25 uM N-acetyl-L-cysteine in IVC2
73	mIVC1/2	Blastoid model	10 µM ROCK inhibitor Y27632, 1mM sodium pyruvate, 0.22% (v/v) sodium lactate
78	CMRL1/2/3	Blastoid model	CMRL 1066 base medium, 10% FBS (CMRL1), 20% FBS (CMRL2), 30% KOSR (CMRL3), 1mM sodium pyruvate, 10 nM estradiol, 1 µM progesterone, 5% Matrigel, 1XN2/B27, 10 µM ROCK inhibitor Y27632, exclusion of N-acetyl-L-cysteine and ITS-X
74	IVC1/2	Blastoid model, Eppendorf optical grade tissue culture plates	NA

75	mIVC1/2	Blastoid model	10 µM ROCK inhibitor Y27632, 1mM sodium pyruvate, 0.22% (v/v) sodium lactate
76	IVC1/2	Blastoid model	NA
77	N2B27	Blastoid model, Geltrex substrate	Exclusion of 20% FBS, 2mM glutamine, penicillin (25U/mL), streptomycin(25µg/mL), 1X ITS-X, 8nM E2, 200 ng/mL Progesterone, 25 uM N-acetyl-L-cysteine
99	EBC	Blastoid model, fibronectin substrate	DMEM/F12 1:1 with Neurobasal, 15% FBS, 0.5X NEAA, 1mM sodium pyruvate, 0.5X N2, 1X B27, 50 nM Chroman 1, 5µM Emricasan, 1X Polyamine supplement, 0.7 µM Trans-ISRIB

Blastoid Models During Peri-implantation

The development of EEC has provided an avenue to overcome the technical limitation of observation and manipulation during the peri-implantation period. However, the nebulous ethical boundaries are insurmountable for research groups that are funded federally, and privately funded organizations that are able to utilize human embryos are limited in that most are donated from fertility patients with confounding infertility diagnoses. The development of an appropriate regenerative model integrated with both embryonic and extra-embryonic cell lineages that mimic the human blastocyst, termed blastoid, will open the doors for research institutions to investigate the peri-implantation period. Furthermore, high throughput blastoid production would increase sample sizes while reducing variability providing for more meaningful experimental outcomes.

The first appearance of a blastoid solely derived from stem cells came in the mouse model in 2018 in which mouse ESCs and TSCs were co-aggregated and were capable of reorganizing, developing a blastocoele cavity, and implanting into the uterine horn of a recipient mouse (72).

Later iterations of blastoids from co-aggregated cell lineages, termed assembloids, continue to show progress in terms of their implantation potential (100). In 2021, several methods of human blastoid emerged which have allowed researchers the opportunity to not only model human embryos, but to do so with large scale production while simultaneously reducing genetic heterogeneity between samples (73-76, 78). Development of stem-cell derived blastoids from naïve hESCs (PAY, PALLY, and HDM/TDM blastoids), from reprogrammed fibroblasts (iblastoids) or assembled epiblast and trophoblast-like cells (assembloids) have been further evaluated using single cells RNA-sequencing to evaluate the identity of each cell lineage. Further, each model has used peri-implantation extended culture in lieu or in parallel with human embryos to evaluate the ability of blastoid models to represent implantation events (73, 74, 76, 78, 99).

Although several methods of blastoid production are able to differentiate the appropriate cell lineages of the human blastocyst including the extra embryonic endoderm, trophectoderm, and epiblast, there are still considerable differences between human embryos and blastoids in extended culture (99). Initial apposition and attachment of blastoids compared to blastocysts remains misaligned. In our latest work, we showed that HDM/TDM blastoids are approximately 48 h ahead of attaching human embryos in comparable culture conditions. Similarly, 90% of iBlastoids attach to the surface of an optical grade tissue culture dish (74). This 48h advantage leaves little room for continued proliferation and expansion of the blastocoele cavity and a significant reduction in GATA3 cell number and trophectoderm outgrowth (99). The initial “attachment gap” between human blastocysts and blastoids may be attributed to the over-differentiated state of the TE. TE differentiation mediums were largely developed following the report of hTSC differentiation medium. Blastoid TE may represent a more “primed” state of TE development (20). This is further bolstered by differential POU5F1 expression in the TE of a blastoid compared to a D5 or later D6 human embryo (99). Though PALLY blastoids retain a blastocoele cavity for approximately 48 h post attachment, PALLY TE does not co-express

POU5F1 similarly to a D5 human blastocyst (18). Efforts in blastoid protocol optimization need to address the inappropriate willingness of blastoids to attach within 24h and develop culture conditions which encourage a more “naïve” TE that co-expresses POU5F1. Despite the discrepancy in timing, both HDM/TDM and PALLY blastoids do attach via the polar TE that lay just beneath the ICM and co-express markers of polar TE (73, 78).

Although blastoids do survive in the IVC system (73, 74), we showed that by marrying the IVC medium with the blastoid induction medium, our blastoid survival in extended culture was significantly improved. We found that not only did our medium improvement improve blastoid extended culture, they also improved human EEC health likely due to the added supplements and apoptotic inhibitors (99, Table 1.3). Several other groups including Kagawa et al. also implemented minor to significant changes to the culture conditions and base IVC1/2 recipe, though they do not always describe their reasoning (Table 1.3). Regardless of medium, each blastoid model exhibits attachment, eventual collapse of the blastocoele cavity, and presence of CK7 and GATA3 positive TB like cells throughout the duration of extended culture (73-78, 99).

Remarkably, most blastoid models exhibit advanced differentiation of TB lineages similar to those in human embryos in peri-implantation extended culture. Each blastoid model reports either secretion of CGB and/or differentiated STB lineages appropriately identified using STB markers SDC1, CGB, with enlarged, multinucleated, irregularly shaped nuclei (18, 73, 74, 77, 78, 99). Fan assembloids identify their STB using transcriptional data, though the morphology in representative imaging does not resemble peri-implantation human STB (75, 92). STB morphology in iblastoids also do not resemble human STB as flattened multinucleated plaques, and the STB represented are only binuclear (92, 106). Zhao et al. point out that iblastoid generation develops cells much closer to amnion or extraembryonic endoderm rather than true TE (101). This was similarly noted in Sozen et al. assembloids (76), and may be due in part to the inclusion of FGF2 during assembloid production, as FGF2 inclusion in the BAP model also

encourages amnion differentiation (63, 102, 103). In HDM/TDM blastoids, there are obvious CGB positive, flattened, multinucleated cells on the periphery of the implanting blastoid, though the numbers that are actually fused into multinucleated plaques were very low (99).

Apparent MTB lineages are more elusive in the blastoid models during peri-implantation. There has been no mention of a migratory TB cell in the assembloids or PAY blastoids, and though iblastoids and PALLY blastoids show representative staining of MMP2 and HLA-G- positive regions respectively, positive immunofluorescence signals reside proximal to the epiblast just inside the peripheral STB-like populations. Additionally, the “spindle- like” morphology of EVT-like cells from the iblastoids do not quite resemble the exaggerated stretched morphology of hTSC EVT or even human EEC MTB (66, 106, 92). It is possible that blastoid models have a “pre-MTB” population similar to human embryos (92), but MTB are not able to migrate away from the implanting blastoids due to the short duration of blastoid survival in extended culture. No papers have reported blastoid survival longer than 5 days in extended culture, and in our experience, blastoid health drops significantly after 3 days (99). Future studies for peri-implantation blastoid culture will likely be needed to improve blastoid health and continued proliferation past 5 days in culture to see evidence of migratory TB.

Trophoblast sublineage specification timing and transcriptional program shifts

Several groups, including ours, have probed the transcriptional program dynamics during the peri-implantation period. Blastocyst TE express transcripts that call GO terms associated with epithelial morphogenesis, metabolism, energy production, and assembly of cell junctions (104, 105). Over the course of 7 days in extended culture, the TB cells of the implanting human embryo develop unique transcriptional programs geared toward the propagation of the self-renewing stem cell population of CTB. Lineage specification timing is remarkably similar amongst observers. CTB is capable of bifurcation into the specialized TB subtypes STB as early as D 7/8 (104, 92, 91) and MTB around and D 12 (92, 91). General priorities of the TB

populations shift from cell proliferation and rise in energy metabolism on D8, to post translational processing, syncytialization, and steroidogenesis on D10, and finally upregulate the immunomodulation and response to hypoxia by D12. CTB cells as early as D8 show transcriptional preference biased toward STB or MTB, and we considered these as “pre-MTB” or “pre-STB” (92). Several other groups noted similar cell types which align transcriptionally with those in early 8-week placental CTB (91, 104-106). Additionally, several putative markers of TB lineages in the primitive placenta have emerged and have been confirmed via confocal microscopy (Figure 1.3).

Table 1.2 Human EEC Manuscripts and their Significance to Early Trophoblast Development

Year	Citation	Intervention	Significance to TB differentiation
2016	17	Immunoflourescence	• Culture of human embryos up to day 14 without maternal tissues • Multinucleated STB on periphery • Mononucleated CTB proximal to epiblast
2016	18	Immunoflourescence	• Culture of human embryos up to day 14 without maternal tissues • GATA3, CK7 confirmed as TB markers • CGB expressed in STB at 10 d.p.f.
2019	108	RNA-seq (Smartseq2) STRT-seq scBS-seq Immunoflourescence	• Initiation of X inactivation • Stepwise route for TE lineage specification • Hypermethylation of epiblast and hypoblast markers in TE lineage
2019	92	RNA-seq (SmartSeq2) Immunoflourescence Western blotting	• Describes TB subpopulations and transcriptional programs • Interferon signaling is upregulated during peri-implantation

2020	109	Immunoflourescence	• Compared developmental potential of common chromosomal aneuploidies • Validated aberrant expression of CDH1 in trisomy 16 embryos
2020	91	RNA-seq (SmartSeq2) Immunoflourescence	• 3-dimensional peri-implantation extended culture
2021	110	Immunoflourescence	• Epiblast measurements presented from previously unpublished retrospective data in human embryos bolster that polar TE may direct epiblast disc shape
2021	95	RNA-seq (10X Genomics Chromium) Immunoflourescence Pharmacological inhibition	• First functional manipulation of human embryos using pharmacological inhibitors during EEC • Disruption of FGF signaling impairs TB proliferation
2021	93	Immunoflourescence	• First use of peri-implantation extended culture as a quality control and safety assay for ART
2022	94	Immunoflourescence CGB secretion	• Trophoblast outgrowth area and CGB secretion mimics clinical live birth data
2022	105	RNA-seq (SmartSeq2) Immunoflourescence	• Transcriptional program for two subtypes of CTB (CTB and pFCC), 2 subtypes of STB (pSTb1 and pSTB2), and MTB • Upregulation of cellular aging program during implantation • Nuclear deformation in STB

Discussion

Culture conditions for the establishment of the EEC during peri-implantation have allowed researchers to push the boundaries of human embryo culture to uncharted territory and have prompted the reconsideration of the previously established 14-day rule (111,112). Continued advancements in culture conditions will undoubtedly take human embryo culture through gastrulation soon and incorporation of advanced models including co-culture with endometrial stromal, epithelial, vascular, and immune cells are likely on the horizon which will provide profound insight (113, 107, 99). Future observational studies including rapidly advancing molecular technologies using single-cell multi-omics and spatially resolved ‘omics technologies will pave the way for novel functional investigations. However, as we approach new horizons using EEC, there are still many trophoblast questions remain to be answered that can still provide valuable insight for TB development during peri-implantation.

Our group incorporated the addition of a fibronectin coating to the bottom of the optical grade coverslip to facilitate TB attachment and differentiation. Interestingly, we are one of the few groups that note a significant population of migratory TB cells that rapidly migrate away from the embryo at approximately D10-12. Integrin subunits ITGA5/ITGB1 are highly expressed in the migratory TB cells and comprise a heterodimer that acts as the receptor for the extracellular matrix protein fibronectin (114). By adding fibronectin to the culture dish, it is possible that we are encouraging the differentiation or motility of the migratory TB cells in the extended culture system. Several groups note the presence of an EVT-like cell, but almost all groups show representative staining within the boundaries of the STB and no apparent migratory TB break free from the embryo. Are the emergence of migratory TB before the formation of the villous column an artifact of the system? Or do migratory TB represent a population of uncharacterized cells that precede the development or more advanced EVT? Additionally, expression of EVT-like markers including HLA-G are consistently noted within the boundaries of STB. We have also

noted channels of migratory TB squeezing through STB plaques. What is the mechanism that drives the migratory TB to push through STB during implantation?

The addition of pyruvate, lactate, the ROCK inhibitor Y27632 as well as 10% Matrigel has allowed scientists to culture embryos in 3D suspension and allows marked progression of the embryonic epiblast (91). In histological sections, the TB comprise approximately 359 μm or 75% of the diameter at the midpoint of a Carnegie 5a implanting embryo, whereas the embryo proper measures only 126 μm of the 485 μm cross section. Using this sectioning as the gold standard, TB in the aforementioned 3D system are severely stunted and begs the question; what is the optimal extra-embryonic: embryonic cell ratio during peri-implantation? TB actively secrete hormones that may play critical roles in embryo development (106). Additionally, the use of ROCK inhibitors critically effects implantation events (115). Inclusion of ROCK inhibitors should be minimized or examined more closely for their effects in EEC.

Following initial apposition and adhesion, implanting blastocysts up to Carnegie stage 5a have an identifiable blastocoele cavity. In traditional EEC, we note complete collapse of the blastocoele cavity after about 3 d. With our newly formulated EBC recipe, the blastocoele cavity persists through for about 5 days. We also notice that blastoids fully collapse their blastocoels on the first day of EEC suggesting that the TE may be overly differentiated, or the tight junctions between TE cells are not strong enough to continue to retain fluid. PALLY blastoids retain their blastocele cavities for two days in EEC. Future blastoid generation protocols should be aimed at generating blastoids with TE capable of continued proliferation and blastocoele retention during EEC.

The future of EEC is promising. Blastoids can now be produced with high efficiency, vitrified, and warmed according to human embryo vitrification protocols (116, 99), and cues from long-term culture of monkey embryos in EEC help to drive novel insights for human development (97,

98). Rotating 3D culture incubators allow advanced development of embryonic lineages from blastoid models that do not currently support advanced TE development at this time, but may in years to come (117, 118). The development of the extended culture system was a landmark development in modeling human implantation. This system has allowed researchers to see the unseen and tease apart early events that lead to proper cell fate specification of the epiblast, diversification of the extra embryonic primitive endoderm, and differentiation of early TB. Though our earliest glimpses of human embryo implantation and development were nearly 80 years ago, our best models of TB development and differentiation have only been developed in the last ten years. Undoubtedly, we will continue to see rapid growth in our understanding of human peri-implantation development.

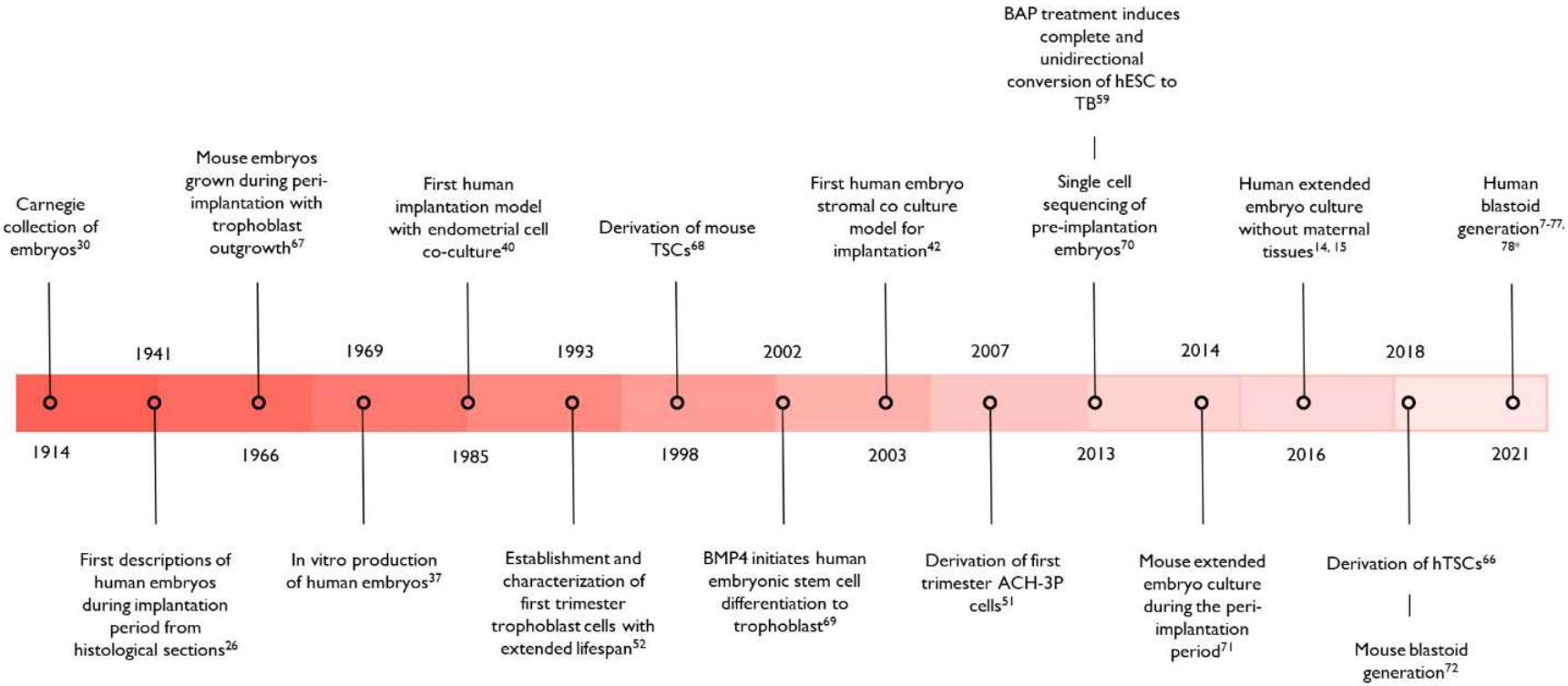
Carnegie collection of embryos[30]
1914
First descriptions of human embryos during implantation period from histological sections[26]
1941
Mouse embryos grown during peri-implantation with trophoblast outgrowth[67]
1966
In vitro production of human embryos[37]
1969
First human implantation model with endometrial cell co-culture[40]
1985
Establishment and characterization of first trimester trophoblast cells with extended lifespan[52]
1993
Derivation of mouse TSCs[68]
1998
BMP4 initiates human embryonic stem cell differentiation to trophoblast[69]
2002
First human embryo stromal co culture model for implantation[42]
2003
Derivation of first trimester ACH-3P cells[51]
2007
BAP treatment induces complete and unidirectional conversion of hESC to TB[59]
Single cell sequencing of pre-implantation embryos[70]
2013
Mouse extended embryo culture during the peri-implantation period[71]
2014
Human extended embryo culture without maternal tissues[14, 15]
2016
Derivation of hTSCs[66]
Mouse blastoid generation[72]
2018
Human blastoid generation[7-77, 78*]
2021

Figure 1.1 Timeline of key events leading to our current understanding of peri-implantation trophoblast development. TSC=trophoblast stem cells, BMP4=Bone morphogenic protein 4, hESC= human embryonic stem cell, ACH-3P=primary human first-trimester human trophoblast cells fused with choriocarcinoma cells

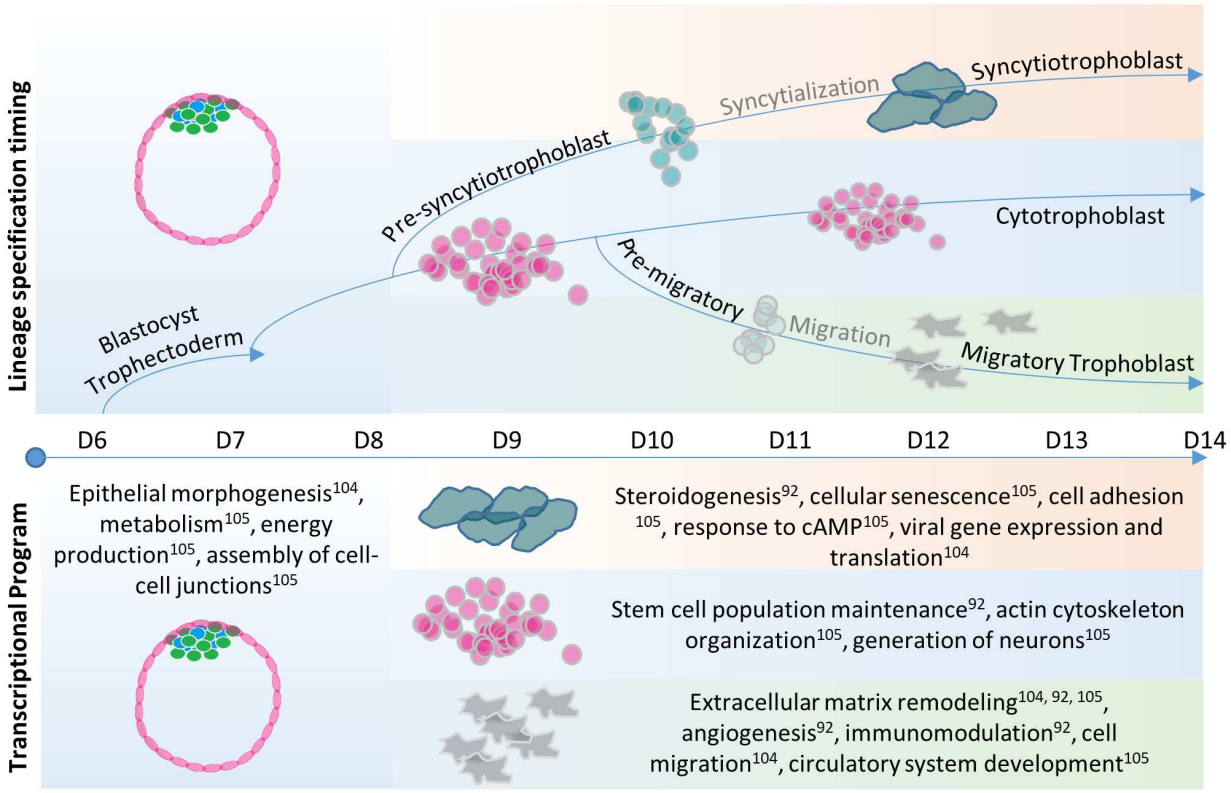

Figure 1.2 Trophoblast sublineage specification timing and transcriptional program shifts during the peri-implantation period. D= embryonic day.

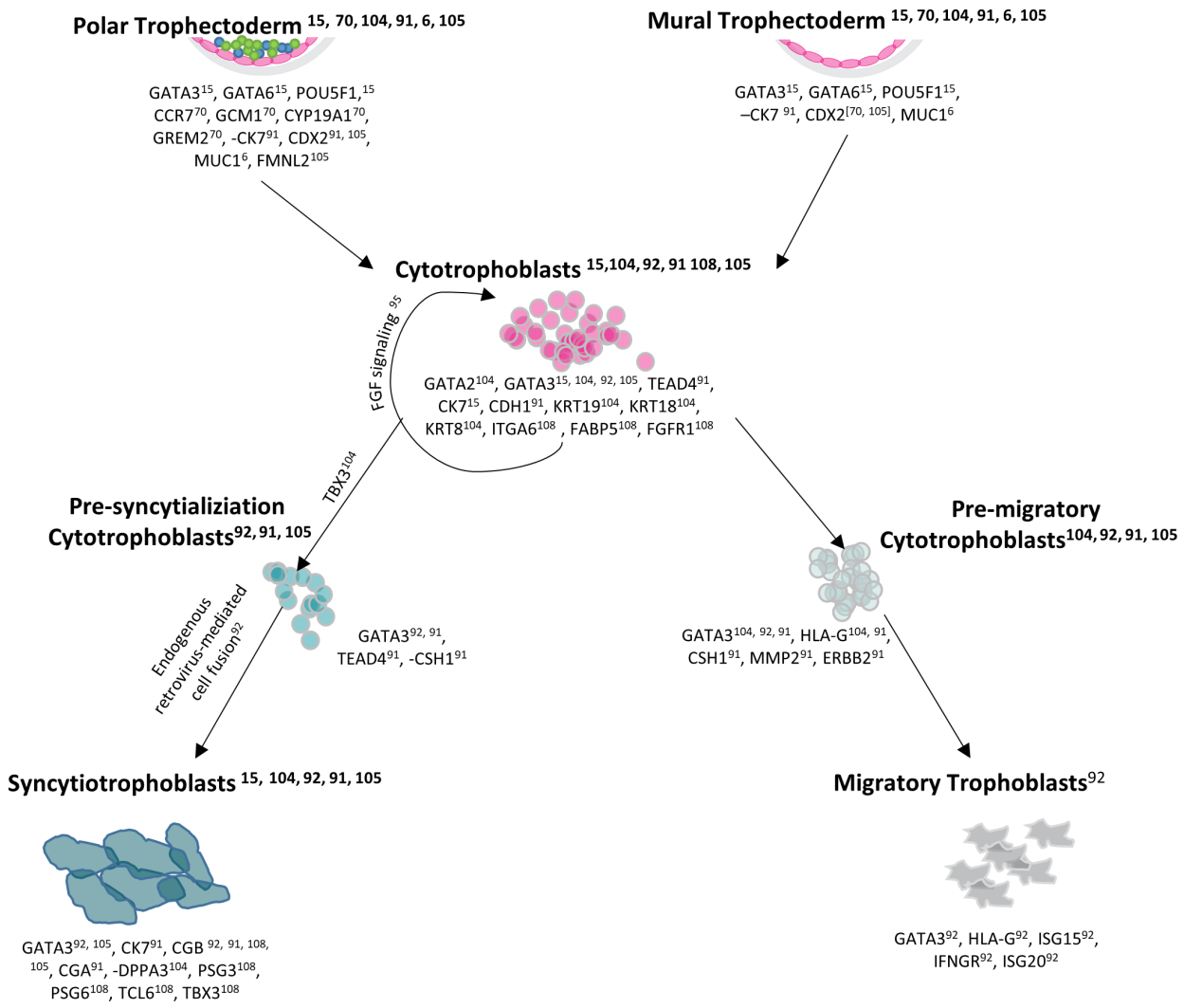

Figure 1.3. Validated markers in peri-implantation trophoblast subpopulations.

REFERENCES

1. Larsen EC, Christiansen OB, Kolte AM, Macklon N. New insights into mechanisms behind miscarriage. BMC Med. 2013 Jun 26;11:154. doi: 10.1186/1741-7015-11-154. PMID: 23803387; PMCID: PMC3699442.
2. Wilcox AJ, Harmon Q, Doody K, Wolf DP, Adashi EY. Preimplantation loss of fertilized human ova: estimating the unobservable, *Human Reproduction*, Volume 35, Issue 4, April 2020, Pages 743–750, https://doi.org/10.1093/humrep/deaa048
3. Laufer N, Simon A. Recurrent implantation failure: current update and clinical approach to an ongoing challenge. Fertil Steril. 2012 May;97(5):1019-20. doi: 10.1016/j.fertnstert.2012.03.033. PMID: 22542141.
4. Chard T. Frequency of implantation and early pregnancy loss in natural cycles. Baillieres Clin Obstet Gynaecol. 1991 Mar;5(1):179-89. doi: 10.1016/s0950-3552(05)80077-x. PMID: 1855339.
5. James JL, Carter AM, Chamley LW. Human placentation from nidation to 5 weeks of gestation. Part I: What do we know about formative placental development following implantation? Placenta. 2012 May;33(5):327-34. doi: 10.1016/j.placenta.2012.01.020. Epub 2012 Feb 26. PMID: 22374510.
6. Meseguer M, Aplin JD, Caballero-Campo P, O'Connor JE, Martín JC, Remohí J, Pellicer A, Simón C. Human endometrial mucin MUC1 is up-regulated by progesterone and down-regulated in vitro by the human blastocyst. Biol Reprod. 2001 Feb;64(2):590-601. doi: 10.1095/biolreprod64.2.590. PMID: 11159362.
7. Hyland RA, Shaw TJ, Png FY, Murphy CR. Pan-cadherin concentrates apically in uterine epithelial cells during uterine closure in the rat. Acta Histochem. 1998 Feb;100(1):75-81. doi: 10.1016/S0065-1281(98)80007-X. PMID: 9542582.
8. Cohen M, Meisser A, Bischof P. Metalloproteinases and human placental invasiveness. Placenta. 2006 Aug;27(8):783-93. doi: 10.1016/j.placenta.2005.08.006. Epub 2005 Oct 24. PMID: 16249026.

9. Ashary N, Tiwari A, Modi D. Embryo Implantation: War in Times of Love. Endocrinology. 2018 Feb 1;159(2):1188-1198. doi: 10.1210/en.2017-03082. PMID: 29319820.
10. Macklon NS, Geraedts JP, Fauser BC. Conception to ongoing pregnancy: the 'black box' of early pregnancy loss. Hum Reprod Update. 2002 Jul-Aug;8(4):333-43. doi: 10.1093/humupd/8.4.333. PMID: 12206468.
11. Matthews KRW, Morali D. Can we do that here? An analysis of US federal and state policies guiding human embryo and embryoid research. J Law Biosci. 2022 Jun 9;9(1):lsac014. doi: 10.1093/jlb/lsac014. PMID: 35692936; PMCID: PMC9183789.
12. Reynolds M. Embryonic research could be the next target after Roe. *Wired* 2022 July https://www.wired.com/story/roe-wade-embryo-research/
13. Greely HT. The death of *Roe* and the future of *ex vivo* embryos. J Law Biosci. 2022 Jul 3;9(2):lsac019. doi: 10.1093/jlb/lsac019. PMID: 35795073; PMCID: PMC9252173.
14. Hannan NJ, Paiva P, Dimitriadis E, Salamonsen LA, Models for Study of Human Embryo Implantation: Choice of Cell Lines?, *Biology of Reproduction*, Volume 82, Issue 2, 1 February 2010, Pages 235–245, https://doi.org/10.1095/biolreprod.109.077800
15. Horii M, Bui T, Touma O, Cho HY, Parast MM. An improved two-step protocol for trophoblast differentiation of human pluripotent stem cells. *Curr Protoc Stem Cell Biol* 2019; 50:e96.
16. Lee KY, DeMayo FJ. Animal models of implantation. Reproduction. 2004 Dec;128(6):679-95. doi: 10.1530/rep.1.00340. PMID: 15579585.
17. Shahbazi MN, Jedrusik A, Vuoristo S, Recher G, Hupalowska A, Bolton V, Fogarty NNM, Campbell A, Devito L, Ilic D, Khalaf Y, Niakan KK, Fishel S, Zernicka-Goetz M. Self-organization of the human embryo in the absence of maternal tissues. Nat Cell Biol. 2016 Jun;18(6):700-708. doi: 10.1038/ncb3347. Epub 2016 May 4. PMID: 27144686; PMCID: PMC5049689.
18. Deglincerti A, Croft GF, Pietila LN, Zernicka-Goetz M, Siggia ED, Brivanlou AH. Self-organization of the in vitro attached human embryo. Nature. 2016 May 12;533(7602):251-4. doi: 10.1038/nature17948. Epub 2016 May 4. PMID: 27144363.

19. Ban Z, Knöspel F, Schneider MR. Shedding light into the black box: Advances in in vitro systems for studying implantation. Dev Biol. 2020 Jul 1;463(1):1-10. doi: 10.1016/j.ydbio.2020.04.003. Epub 2020 Apr 30. PMID: 32360630.
20. Ai Z, Yin Y, Niu B, Li T. Deconstructing human peri-implantation embryogenesis based on embryos and embryoids†. Biol Reprod. 2022 Jul 25;107(1):212-225. doi: 10.1093/biolre/ioac096. PMID: 35552636.
21. Zhou J, West RC, Ehlers EL, Ezashi T, Schulz LC, Roberts RM, Yuan Y, Schust DJ. Modeling human peri-implantation placental development and function†. Biol Reprod. 2021 Jul 2;105(1):40-51. doi: 10.1093/biolre/ioab080. PMID: 33899095; PMCID: PMC8256105.
22. Foster, M. (1874). *The elements of embryology*. Macmillan and Company.
23. Gasser RF, Cork RJ, Stillwell BJ, McWilliams DT. Rebirth of human embryology. Dev Dyn. 2014 May;243(5):621-8. doi: 10.1002/dvdy.24110. Epub 2014 Feb 27. PMID: 24395627; PMCID: PMC4310677.
24. Mall FP. Report upon the collection of human embryos at the johns Hopkins university. *Anat Rec* 2005; 5:343–357.
25. Philipp T, Philipp K, Reiner A, Beer F, Kalousek D. Embryoscopic and cytogenetic analysis of 233 missed abortions: Factors involved in the pathogenesis of developmental defects of early failed pregnancies. *Hum Reprod* 2003; 18:1724–1732.
26. Hertig AT, Rock J. Two human ova of the pre-villous stage, having an ovulation age of about eleven and twelve days, respectively. *Contrib Embryol Carnegie Inst.* 1941;29:127–156.
27. Hertig AT, Rock J. Two human ova of the pre-villous stage, having a development age of about eight and nine days, respectively. *Contrib Embryol Carnegie Inst.* 1945;33:169–186.
28. Hertig AT, Rock J. Two human ova of the pre-villous stage, having a development age of about seven and nine days respectively. *Contrib Embryol Carnegie Inst.* 1949;31:65–84.
29. Hertig AT, Rock J, Adams EC. A description of 34 human ova within the first 17 days of development. *Am J Anat* 1956; 98:435–493.

30. Washington CIo . Contributions to embryology. In: *Carnegie institution of Washington*. Washington, D.C.: The Carnegie Institute of Washington; 1921.
31. Buettner KA. Franklin Paine Mall (1862-1917). In: *Embryo Project Encyclopedia*. Arizona State University. School of Life Sciences. Center for Biology and Society; 2007.
32. Heuser CH, and Streeter GL. 1941. Development of the macaque embryo. *Contrib Embryol.* Carnegie Institution of Washington. 29:15-55.
33. Cuman C, Menkhorst E, Winship A, Van Sinderen M, Osianlis T, Rombauts LJ, Dimitriadis E. Fetal-maternal communication: the role of Notch signalling in embryo implantation. Reproduction. 2014 Feb 4;147(3):R75-86. doi: 10.1530/REP-13-0474. PMID: 24357662.
34. Burton GJ, Jauniaux E. The cytotrophoblastic shell and complications of pregnancy. Placenta. 2017 Dec;60:134-139. doi: 10.1016/j.placenta.2017.06.007. Epub 2017 Jun 13. PMID: 28651899.
35. Enders AC, Schlafke S. Cytological aspects of trophoblast-uterine interaction in early implantation. Am J Anat. 1969 May;125(1):1-29. doi: 10.1002/aja.1001250102. PMID: 5770161.
36. Rock J, Menkin MF. In vitro fertilization and cleavage of human ovarian eggs. Science. 1944 Aug 4;100(2588):105-7. doi: 10.1126/science.100.2588.105. PMID: 17788930.
37. Edwards RG, Bavister BD, Steptoe PC. Early stages of fertilization in vitro of human oocytes matured in vitro. Nature. 1969 Feb 15;221(5181):632-5. doi: 10.1038/221632a0. PMID: 4886881.
38. Shettles LB. A morula stage of human ovum developed in vitro. Fertil Steril. 1955 Jul-Aug;6(4):287-9. doi: 10.1016/s0015-0282(16)32040-4. PMID: 14391412.
39. Edwards RG. Human implantation: the last barrier in assisted reproduction technologies? Reprod Biomed Online. 2006 Dec;13(6):887-904. doi: 10.1016/s1472-6483(10)61039-5. PMID: 17169215.
40. Lindenberg S, Nielsen MH, Lenz S. In vitro studies of human blastocyst implantation. Ann N Y Acad Sci. 1985;442:368-74. doi: 10.1111/j.1749-6632.1985.tb37541.x. PMID: 3925843.

41. Weimar CH, Post Uiterweer ED, Teklenburg G, Heijnen CJ, Macklon NS. In-vitro model systems for the study of human embryo-endometrium interactions Reprod Biomed Online. 2013 Nov;27(5):461-76. doi: 10.1016/j.rbmo.2013.08.002. Epub 2013 Aug 28. PMID: 24055530.
42. Carver, J. et al. *Hum. Reprod.* **18**, 283–290, (2003).
43. Simón C, Mercader A, Garcia-Velasco J, Nikas G, Moreno C, Remohí J, Pellicer A. Coculture of human embryos with autologous human endometrial epithelial cells in patients with implantation failure. J Clin Endocrinol Metab. 1999 Aug;84(8):2638-46. doi: 10.1210/jcem.84.8.5873. PMID: 10443653.
44. Simón C, Gimeno MJ, Mercader A, O'Connor JE, Remohí J, Polan ML, Pellicer A. Embryonic regulation of integrins beta 3, alpha 4, and alpha 1 in human endometrial epithelial cells in vitro. J Clin Endocrinol Metab. 1997 Aug;82(8):2607-16. doi: 10.1210/jcem.82.8.4153. PMID: 9253342.
45. Caballero-Campo P, Domínguez F, Coloma J, Meseguer M, Remohí J, Pellicer A, Simón C. Hormonal and embryonic regulation of chemokines IL-8, MCP-1 and RANTES in the human endometrium during the window of implantation. Mol Hum Reprod. 2002 Apr;8(4):375-84. doi: 10.1093/molehr/8.4.375. PMID: 11912286.
46. Dominguez F, Galan A, Martin JJ, Remohi J, Pellicer A, Simón C. Hormonal and embryonic regulation of chemokine receptors CXCR1, CXCR4, CCR5 and CCR2B in the human endometrium and the human blastocyst. Mol Hum Reprod. 2003 Apr;9(4):189-98. doi: 10.1093/molehr/gag024. PMID: 12651900.
47. González RR, Caballero-Campo P, Jasper M, Mercader A, Devoto L, Pellicer A, Simon C. Leptin and leptin receptor are expressed in the human endometrium and endometrial leptin secretion is regulated by the human blastocyst. J Clin Endocrinol Metab. 2000 Dec;85(12):4883-8. doi: 10.1210/jcem.85.12.7060. PMID: 11134157.
48. Teklenburg G, Salker M, Molokhia M, Lavery S, Trew G, Aojanepong T, Mardon HJ, Lokugamage AU, Rai R, Landles C, Roelen BA, Quenby S, Kuijk EW, Kavelaars A, Heijnen

CJ, Regan L, Brosens JJ, Macklon NS. Natural selection of human embryos: decidualizing endometrial stromal cells serve as sensors of embryo quality upon implantation. PLoS One. 2010 Apr 21;5(4):e10258. doi: 10.1371/journal.pone.0010258. PMID: 20422011; PMCID: PMC2858159.

49. Bentin-Ley U, Sjögren A, Nilsson L, Hamberger L, Larsen JF, Horn T. Presence of uterine pinopodes at the embryo-endometrial interface during human implantation in vitro. Hum Reprod. 1999 Feb;14(2):515-20. doi: 10.1093/humrep/14.2.515. PMID: 10100003.
50. Feng HC, Choy MY, Deng W, Wong HL, Lau WM, Cheung AN, Ngan HY, Tsao SW. Establishment and characterization of a human first-trimester extravillous trophoblast cell line (TEV-1). J Soc Gynecol Investig. 2005 May;12(4):e21-32. doi: 10.1016/j.jsgi.2005.02.008. PMID: 15866109.
51. Hiden U, Wadsack C, Prutsch N, Gauster M, Weiss U, Frank HG, Schmitz U, Fast-Hirsch C, Hengstschläger M, Pötgens A, Rüben A, Knöfler M, Haslinger P, Huppertz B, Bilban M, Kaufmann P, Desoye G. The first trimester human trophoblast cell line ACH-3P: a novel tool to study autocrine/paracrine regulatory loops of human trophoblast subpopulations--TNF-alpha stimulates MMP15 expression. BMC Dev Biol. 2007 Dec 19;7:137. doi: 10.1186/1471-213X-7-137. PMID: 18093301; PMCID: PMC2263055.
52. Graham CH, Hawley TS, Hawley RG, MacDougall JR, Kerbel RS, Khoo N, Lala PK. Establishment and characterization of first trimester human trophoblast cells with extended lifespan. Exp Cell Res. 1993 Jun;206(2):204-11. doi: 10.1006/excr.1993.1139. PMID: 7684692.
53. Fournier T, Handschuh K, Tsatsaris V, Evain-Brion D. Involvement of PPARgamma in human trophoblast invasion. Placenta. 2007 Apr;28 Suppl A:S76-81. doi: 10.1016/j.placenta.2006.12.006. Epub 2007 Feb 23. Erratum in: Placenta. 2007 Aug-Sep;28(8-9):974-6. PMID: 17321592.
54. Husslein H, Haider S, Meinhardt G, Prast J, Sonderegger S, Knöfler M. Expression, regulation and functional characterization of matrix metalloproteinase-3 of human

trophoblast. Placenta. 2009 Mar;30(3):284-91. doi: 10.1016/j.placenta.2008.12.002. Epub 2009 Jan 19. PMID: 19155066; PMCID: PMC2974218.

55. Li L, Schust DJ. Isolation, purification and in vitro differentiation of cytotrophoblast cells from human term placenta. Reprod Biol Endocrinol. 2015 Jul 9;13:71. doi: 10.1186/s12958-015-0070-8. PMID: 26156160; PMCID: PMC4497497.
56. Stromberg K, Azizkhan JC, Speeg KV Jr. Isolation of function human trophoblast cells and their partial characterization in primary cell culture. In Vitro. 1978 Jul;14(7):631-8. doi: 10.1007/BF02617924. PMID: 208965.
57. Sullivan MH. Endocrine cell lines from the placenta. Mol Cell Endocrinol. 2004 Dec 30;228(1-2):103-19. doi: 10.1016/j.mce.2003.03.001. PMID: 15541575.
58. Aghajanova L, Shen S, Rojas AM, Fisher SJ, Irwin JC, Giudice LC. Comparative transcriptome analysis of human trophectoderm and embryonic stem cell-derived TB reveal key participants in early implantation. Biol Reprod. 2012 Jan 16;86(1):1-21. doi: 10.1095/biolreprod.111.092775. PMID: 21865555.
59. Amita M, Adachi K, Alexenko AP, Sinha S, Schust DJ, Schulz LC, Roberts RM, Ezashi T. Complete and unidirectional conversion of human embryonic stem cells to trophoblast by BMP4. *Proc Natl Acad Sci* 2013; 110:E1212–E1221. [PMC free article] [PubMed] [Google Scholar]
60. Io S, Kabata M, Iemura Y, Semi K, Morone N, Minagawa A, Wang B, Okamoto I, Nakamura T, Kojima Y, Iwatani C, Tsuchiya H, Kaswandy B, Kondoh E, Kaneko S, Woltjen K, Saitou M, Yamamoto T, Mandai M, Takashima Y. Capturing human trophoblast development with naive pluripotent stem cells in vitro. Cell Stem Cell. 2021 Jun 3;28(6):1023-1039.e13. doi: 10.1016/j.stem.2021.03.013. Epub 2021 Apr 7. PMID: 33831365.
61. Guo G, Stirparo GG, Strawbridge SE, Spindlow D, Yang J, Clarke J, Dattani A, Yanagida A, Li MA, Myers S, Özel BN, Nichols J, Smith A. Human naive epiblast cells possess unrestricted lineage potential. Cell Stem Cell. 2021 Jun 3;28(6):1040-1056.e6. doi: 10.1016/j.stem.2021.02.025. Epub 2021 Apr 7. PMID: 33831366; PMCID: PMC8189439.

62. Seetharam AS, Vu HTH, Choi S, Khan T, Sheridan MA, Ezashi T, Roberts RM, Tuteja G. The product of BMP-directed differentiation protocols for human primed pluripotent stem cells is placental trophoblast and not amnion. Stem Cell Reports. 2022 Jun 14;17(6):1289-1302. doi: 10.1016/j.stemcr.2022.04.014. Epub 2022 May 19. PMID: 35594861; PMCID: PMC9214062.
63. Roberts RM, Ezashi T, Sheridan MA, Yang Y. Specification of trophoblast from embryonic stem cells exposed to BMP4. Biol Reprod. 2018 Jul 1;99(1):212-224. doi: 10.1093/biolre/ioy070. PMID: 29579154; PMCID: PMC6044404.
64. Yabe S, Alexenko AP, Amita M, Yang Y, Schust DJ, Sadovsky Y, Ezashi T, Roberts RM. Comparison of syncytiotrophoblast generated from human embryonic stem cells and from term placentas. *Proc Natl Acad Sci* 2016; 113:E2598–E2607.
65. Karvas RM, McInturf S, Zhou J, Ezashi T, Schust DJ, Roberts RM, Schulz LC. Use of a human embryonic stem cell model to discover GABRP, WFDC2, VTCN1 and ACTC1 as markers of early first trimester human trophoblast. *Mol Hum Reprod* 2020; 26:425–440.
66. Okae H, Toh H, Sato T, Hiura H, Takahashi S, Shirane K, Kabayama Y, Suyama M, Sasaki H, Arima T. Derivation of human trophoblast stem cells. *Cell Stem Cell* 2018; 22:50–63.e56.
67. Gwatkin RB, Meckley PE. Chromosomes of the mouse blastocyst following its attachment and outgrowth in vitro. Ann Med Exp Biol Fenn. 1966;44(2):125-7. PMID: 6007522.
68. Tanaka S, Kunath T, Hadjantonakis AK, Nagy A, Rossant J. Promotion of trophoblast stem cell proliferation by FGF4. Science. 1998 Dec 11;282(5396):2072-5. doi: 10.1126/science.282.5396.2072. PMID: 9851926.
69. Xu R-H, Chen X, Li DS, Li R, Addicks GC, Glennon C, Zwaka TP, Thomson JA. BMP4 initiates human embryonic stem cell differentiation to trophoblast. *Nat Biotechnol* 2002; 20:1261–1264.
70. Petropoulos S., Edsgard D., Reinius B., Deng Q., Panula S. P., Codeluppi S., Plaza Reyes A., Linnarsson S., Sandberg R. and Lanner F. (2016). Single-Cell RNA-Seq Reveals

Lineage and X Chromosome Dynamics in Human Preimplantation Embryos. *Cell*, 165, 1012-1026.

71. Bedzhov, I., Leung, C., Bialecka, M. *et al. In vitro* culture of mouse blastocysts beyond the implantation stages. *Nat Protoc* **9**, 2732–2739 (2014). https://doi.org/10.1038/nprot.2014.186
72. Rivron NC, Frias-Aldeguer J, Vrij EJ, Boisset JC, Korving J, Vivié J, Truckenmüller RK, van Oudenaarden A, van Blitterswijk CA, Geijsen N. Blastocyst-like structures generated solely from stem cells. Nature. 2018 May;557(7703):106-111. doi: 10.1038/s41586-018-0051-0. Epub 2018 May 2. PMID: 29720634.
73. Yu, L., Wei, Y., Duan, J. *et al.* Blastocyst-like structures generated from human pluripotent stem cells. *Nature* **591**, 620–626 (2021). https://doi.org/10.1038/s41586-021-03356-y
74. Liu X, Tan JP, Schröder J, Aberkane A, Ouyang JF, Mohenska M, Lim SM, Sun YBY, Chen J, Sun G, Zhou Y, Poppe D, Lister R, Clark AT, Rackham OJL, Zenker J, Polo JM. Modelling human blastocysts by reprogramming fibroblasts into iBlastoids. Nature. 2021 Mar;591(7851):627-632. doi: 10.1038/s41586-021-03372-y. Epub 2021 Mar 17. PMID: 33731926.
75. Fan Y, Min Z, Alsolami S, Ma Z, Zhang E, Chen W, Zhong K, Pei W, Kang X, Zhang P, Wang Y, Zhang Y, Zhan L, Zhu H, An C, Li R, Qiao J, Tan T, Li M, Yu Y. Generation of human blastocyst-like structures from pluripotent stem cells. Cell Discov. 2021 Sep 7;7(1):81. doi: 10.1038/s41421-021-00316-8. PMID: 34489415; PMCID: PMC8421367.
76. Sozen B, Jorgensen V, Weatherbee BAT, Chen S, Zhu M, Zernicka-Goetz M. Reconstructing aspects of human embryogenesis with pluripotent stem cells. Nat Commun. 2021 Sep 21;12(1):5550. doi: 10.1038/s41467-021-25853-4. PMID: 34548496; PMCID: PMC8455697.
77. Yanagida A, Spindlow D, Nichols J, Dattani A, Smith A, Guo G. Naive stem cell blastocyst model captures human embryo lineage segregation. Cell Stem Cell. 2021 Jun 3;28(6):1016-1022.e4. doi: 10.1016/j.stem.2021.04.031. Epub 2021 May 5. PMID: 33957081; PMCID: PMC8189436.

78. Kagawa, H., Javali, A., Khoei, H.H. *et al.* Human blastoids model blastocyst development and implantation. *Nature* **601**, 600–605 (2022). https://doi.org/10.1038/s41586-021-04267-8

79. Cohen J, Rieger D. Historical background of gamete and embryo culture. Methods Mol Biol. 2012;912:1-18. doi: 10.1007/978-1-61779-971-6_1. PMID: 22829365.

80. Woods L, Perez-Garcia V, Hemberger M. Regulation of Placental Development and Its Impact on Fetal Growth-New Insights From Mouse Models. Front Endocrinol (Lausanne). 2018 Sep 27;9:570. doi: 10.3389/fendo.2018.00570. PMID: 30319550; PMCID: PMC6170611.

81. Jenkinson EJ, Wilson IB. In vitro support system for the study of blastocyst differentiation in the mouse. Nature. 1970 Nov 21;228(5273):776-8. doi: 10.1038/228776a0. PMID: 5472970.

82. Hsu Y-C. Differentiation in vitro of mouse embryos beyond the implantation stage. *Nature* 1972; 239:200–202.

83. Kim J, Lee J, Jun JH. Advantages of the outgrowth model for evaluating the implantation competence of blastocysts. Clin Exp Reprod Med. 2020 Jun;47(2):85-93. doi: 10.5653/cerm.2019.03216. Epub 2020 May 7. PMID: 32521581; PMCID: PMC7315857.

84. Wang J, Rout UK, Bagchi IC, Armant DR. Expression of calcitonin receptors in mouse preimplantation embryos and their function in the regulation of blastocyst differentiation by calcitonin. Development. 1998 Nov;125(21):4293-302. doi: 10.1242/dev.125.21.4293. PMID: 9753683.

85. Logsdon DM, Ermisch AF, Kile R, Schoolcraft WB, Krisher RL, Yuan Y. Egg cylinder development during in vitro extended embryo culture predicts the post transfer developmental potential of mouse blastocysts. J Assist Reprod Genet. 2020 Apr;37(4):747-752. doi: 10.1007/s10815-020-01714-9. Epub 2020 Feb 18. PMID: 32072379; PMCID: PMC7183034.

86. Fogarty NME, McCarthy A, Snijders KE, Powell BE, Kubikova N, Blakeley P, Lea R, Elder K, Wamaitha SE, Kim D, Maciulyte V, Kleinjung J, Kim JS, Wells D, Vallier L, Bertero A, Turner JMA, Niakan KK. Genome editing reveals a role for OCT4 in human embryogenesis. Nature.

2017 Oct 5;550(7674):67-73. doi: 10.1038/nature24033. Epub 2017 Sep 20. Erratum in: Nature. 2017 Oct 04;: PMID: 28953884; PMCID: PMC5815497.

87. Shahbazi MN, Zernicka-Goetz M. Deconstructing and reconstructing the mouse and human early embryo. Nat Cell Biol. 2018 Aug;20(8):878-887. doi: 10.1038/s41556-018-0144-x. Epub 2018 Jul 23. PMID: 30038253.
88. Molè MA, Weberling A, Zernicka-Goetz M. Comparative analysis of human and mouse development: From zygote to pre-gastrulation. Curr Top Dev Biol. 2020;136:113-138. doi: 10.1016/bs.ctdb.2019.10.002. Epub 2019 Dec 26. PMID: 31959285.
89. Cole LA. Biological functions of hCG and hCG-related molecules. Reprod Biol Endocrinol. 2010 Aug 24;8:102. doi: 10.1186/1477-7827-8-102. PMID: 20735820; PMCID: PMC2936313.
90. Soares MJ, Iqbal K, Kozai K. Hypoxia and Placental Development. Birth Defects Res. 2017 Oct 16;109(17):1309-1329. doi: 10.1002/bdr2.1135. PMID: 29105383; PMCID: PMC5743230.
91. Xiang L, Yin Y, Zheng Y, Ma Y, Li Y, Zhao Z, Guo J, Ai Z, Niu Y, Duan K, He J, Ren S, Wu D, Bai Y, Shang Z, Dai X, Ji W, Li T. A developmental landscape of 3D-cultured human pre-gastrulation embryos. Nature. 2020 Jan;577(7791):537-542. doi: 10.1038/s41586-019-1875-y. Epub 2019 Dec 12. PMID: 31830756.
92. West RC, Ming H, Logsdon DM, Sun J, Rajput SK, Kile RA, Schoolcraft WB, Roberts RM, Krisher RL, Jiang Z, Yuan Y. Dynamics of trophoblast differentiation in peri-implantation-stage human embryos. Proc Natl Acad Sci U S A. 2019 Nov 5;116(45):22635-22644. doi: 10.1073/pnas.1911362116. Epub 2019 Oct 21. PMID: 31636193; PMCID: PMC6842583.
93. Logsdon DM, Grimm CK, Schoolcraft WB, McCormick S, Schlenker T, Swain JE, Krisher RL, Yuan Y, Collins MG. Evaluation of the TMRW vapor phase cryostorage platform using reproductive specimens and in vitro extended human embryo culture. F S Sci. 2021 Aug;2(3):268-277. doi: 10.1016/j.xfss.2021.06.005. Epub 2021 Jul 6. PMID: 35560277.

94. Logsdon DM, Grimm CK, West RC, Engelhorn HJ, Kile R, Reed LC, Swain JE, Katz-Jaffe M, Schoolcraft WB, Krisher RL, Yuan Y. Maternal physiology and blastocyst morphology are correlated with an inherent difference in peri-implantation human embryo development. Fertil Steril. 2022 Jun;117(6):1311-1321. doi: 10.1016/j.fertnstert.2022.02.018. Epub 2022 Mar 30. PMID: 35367060.

95. Molè MA, Coorens THH, Shahbazi MN, Weberling A, Weatherbee BAT, Gantner CW, Sancho-Serra C, Richardson L, Drinkwater A, Syed N, Engley S, Snell P, Christie L, Elder K, Campbell A, Fishel S, Behjati S, Vento-Tormo R, Zernicka-Goetz M. A single cell characterisation of human embryogenesis identifies pluripotency transitions and putative anterior hypoblast centre. Nat Commun. 2021 Jun 17;12(1):3679. doi: 10.1038/s41467-021-23758-w. PMID: 34140473; PMCID: PMC8211662.

96. Molè MA, Weberling A, Fässler R, Campbell A, Fishel S, Zernicka-Goetz M. Integrin β1 coordinates survival and morphogenesis of the embryonic lineage upon implantation and pluripotency transition. Cell Rep. 2021 Mar 9;34(10):108834. doi: 10.1016/j.celrep.2021.108834. PMID: 33691117; PMCID: PMC7966855.

97. Niu Y, Sun N, Li C, Lei Y, Huang Z, Wu J, Si C, Dai X, Liu C, Wei J, Liu L, Feng S, Kang Y, Si W, Wang H, Zhang E, Zhao L, Li Z, Luo X, Cui G, Peng G, Izpisúa Belmonte JC, Ji W, Tan T. Dissecting primate early post-implantation development using long-term in vitro embryo culture. Science. 2019 Nov 15;366(6467):eaaw5754. doi: 10.1126/science.aaw5754. Epub 2019 Oct 31. PMID: 31672917.

98. Ma H, Zhai J, Wan H, Jiang X, Wang X, Wang L, Xiang Y, He X, Zhao ZA, Zhao B, Zheng P, Li L, Wang H. In vitro culture of cynomolgus monkey embryos beyond early gastrulation. Science. 2019 Nov 15;366(6467):eaax7890. doi: 10.1126/science.aax7890. Epub 2019 Oct 31. PMID: 31672918.

99. Yu L, Ezashi T, Wei Y, Duan J, Logsdon D, Zhan L, Nahar A, Pinzon-Arteaga CA, Liu L, Stobbe C, Katz-Jaffe M, Schoolcraft WB, Wang L, Tan T, Hon GC, Yuan Y, Wu J. Large scale production of human blastoids amenable to modeling blastocyst development and

maternal-fetal crosstalk BioRxiv. 2022 Sept. 14 doi: httsp://doi.org/ 10.1101/2022.09.14.507946

100. Sozen B, Cox AL, De Jonghe J, Bao M, Hollfelder F, Glover DM, Zernicka-Goetz M. Self-Organization of Mouse Stem Cells into an Extended Potential Blastoid. Dev Cell. 2019 Dec 16;51(6):698-712.e8. doi: 10.1016/j.devcel.2019.11.014. PMID: 31846649.

101. Zhao C, Reyes AP, Schell JP, Weltner J, Ortega NM, Zheng Y, Björklund AK, Rossant J, Fu J, Petropoulos S, Lanner F. Reprogrammed blastoids contain amnion-like cells but not trophectoderm. BioRxiv 2021 doi: https://doi.org/10.1101/2021.05.07.442980

102. Yu P, Pan G, Yu J, Thomson JA. FGF2 sustains NANOG and switches the outcome of BMP4-induced human embryonic stem cell differentiation. *Cell Stem Cell* 2011; 8:326–334.

103. Das P, Ezashi T, Schulz LC, Westfall SD, Livingston KA, Roberts RM. Effects of fgf2 and oxygen in the bmp4-driven differentiation of trophoblast from human embryonic stem cells. *Stem Cell Res* 2007; 1:61–74.

104. Lv B, An Q, Zeng Q, Zhang X, Lu P, Wang Y, Zhu X, Ji Y, Fan G, Xue Z. Single-cell RNA sequencing reveals regulatory mechanism for trophoblast cell-fate divergence in human peri-implantation conceptuses. PLoS Biol. 2019 Oct 9; 17(10):e3000187. doi: 10.1371/ journal.pbio.3000187. PMID: 31596842; PMCID: PMC6802852.

105. Wang Y, Jiang X, Jia L, Wu X, Wu H, Wang Y, Li Q, Yu R, Wang H, Xiao Z, Liang X. A Single-Cell Characterization of Human Post-implantation Embryos Cultured *In Vitro* Delineates Morphogenesis in Primary Syncytialization. Front Cell Dev Biol. 2022 Jun 15; 10:835445. doi: 10.3389/fcell.2022.835445. PMID: 35784461; PMCID: PMC9240912.

106. Liu Y, Fan X, Wang R, Lu X, Dang YL, Wang H, Lin HY, Zhu C, Ge H, Cross JC, Wang H. Single-cell RNA-seq reveals the diversity of trophoblast subtypes and patterns of differentiation in the human placenta. Cell Res. 2018 Aug;28(8):819-832. doi: 10.1038/ s41422-018-0066-y. Epub 2018 Jul 24. PMID: 30042384; PMCID: PMC6082907.

107. Liu D, Chen Y, Ren Y, Yuan P, Wang N, Liu Q, Yang C, Yan Z, Yang M, Wang J, Lian Y, Yan J, Zhai F, Nie Y, Zhu X, Chen Y, Li R, Chang HM, Leung PCK, Qiao J, Yan L. Primary

specification of blastocyst trophectoderm by scRNA-seq: New insights into embryo implantation. Sci Adv. 2022 Aug 12; 8(32):eabj3725. doi: 10.1126/sciadv.abj3725. Epub 2022 Aug 10. PMID: 35947672; PMCID: PMC9365277.

108.Zhou F, Wang R, Yuan P, Ren Y, Mao Y, Li R, Lian Y, Li J, Wen L, Yan L, Qiao J, Tang F. Reconstituting the transcriptome and DNA methylome landscapes of human implantation. Nature. 2019 Aug;572(7771):660-664. doi: 10.1038/s41586-019-1500-0. Epub 2019 Aug 21. PMID: 31435013.

109.Shahbazi MN, Wang T, Tao X, Weatherbee BAT, Sun L, Zhan Y, Keller L, Smith GD, Pellicer A, Scott RT Jr, Seli E, Zernicka-Goetz M. Developmental potential of aneuploid human embryos cultured beyond implantation. Nat Commun. 2020 Aug 10; 11(1):3987. doi: 10.1038/s41467-020-17764-7. PMID: 32778678; PMCID: PMC7418029.

110.Weberling A, Zernicka-Goetz M. Trophectoderm mechanics direct epiblast shape upon embryo implantation. Cell Rep. 2021 Jan 19; 34(3):108655. doi: 10.1016/j.celrep.2020.108655. PMID: 33472064; PMCID: PMC7816124.

111.Lovell-Badge R, Anthony E, Barker RA, Bubela T, Brivanlou AH, Carpenter M, Charo RA, Clark A, Clayton E, Cong Y, Daley GQ, Fu J, Fujita M, Greenfield A, Goldman SA, Hill L, Hyun I, Isasi R, Kahn J, Kato K, Kim JS, Kimmelman J, Knoblich JA, Mathews D, Montserrat N, Mosher J, Munsie M, Nakauchi H, Naldini L, Naughton G, Niakan K, Ogbogu U, Pedersen R, Rivron N, Rooke H, Rossant J, Round J, Saitou M, Sipp D, Steffann J, Sugarman J, Surani A, Takahashi J, Tang F, Turner L, Zettler PJ, Zhai X. ISSCR Guidelines for Stem Cell Research and Clinical Translation: The 2021 update. Stem Cell Reports. 2021 Jun 8;16(6):1398-1408. doi: 10.1016/j.stemcr.2021.05.012. Epub 2021 May 27. PMID: 34048692; PMCID: PMC8190668.

112.Clark AT, Brivanlou A, Fu J, Kato K, Mathews D, Niakan KK, Rivron N, Saitou M, Surani A, Tang F, Rossant J. Human embryo research, stem cell-derived embryo models and in vitro gametogenesis: Considerations leading to the revised ISSCR guidelines. Stem Cell Reports.

2021 Jun 8;16(6):1416-1424. doi: 10.1016/j.stemcr.2021.05.008. Epub 2021 May 27. PMID: 34048690; PMCID: PMC8190666.

113.Rawlings TM, Makwana K, Taylor DM, Molè MA, Fishwick KJ, Tryfonos M, Odendaal J, Hawkes A, Zernicka-Goetz M, Hartshorne GM, Brosens JJ, Lucas ES. Modelling the impact of decidual senescence on embryo implantation in human endometrial assembloids. Elife. 2021 Sep 6;10:e69603. doi: 10.7554/eLife.69603. PMID: 34487490; PMCID: PMC8523170.

114.Sechler JL, Corbett SA, Schwarzbauer JE. Modulatory roles for integrin activation and the synergy site of fibronectin during matrix assembly. Mol Biol Cell. 1997 Dec;8(12):2563-73. doi: 10.1091/mbc.8.12.2563. PMID: 9398676; PMCID: PMC25728.

115.Grewal S, Carver JG, Ridley AJ, Mardon HJ. Implantation of the human embryo requires Rac1-dependent endometrial stromal cell migration. Proc Natl Acad Sci U S A. 2008 Oct 21;105(42):16189-94. doi: 10.1073/pnas.0806219105. Epub 2008 Oct 6. PMID: 18838676; PMCID: PMC2562412.

116.Heidari Khoei H, Javali A, Kagawa H, Sommer TM, Sestini G, David L, Slovakova J, Novatchkova M, Scholte Op Reimer Y, Rivron N. Generating human blastoids modeling blastocyst-stage embryos and implantation. Nat Protoc. 2023 Feb 15. doi: 10.1038/s41596-023-00802-1. Epub ahead of print. PMID: 36792779.

117.Lau KYC, Rubinstein H, Gantner CW, Hadas R, Amadei G, Stelzer Y, Zernicka-Goetz M. Mouse embryo model derived exclusively from embryonic stem cells undergoes neurulation and heart development. Cell Stem Cell. 2022 Oct 6;29(10):1445-1458.e8. doi: 10.1016/j.stem.2022.08.013. Epub 2022 Sep 8. PMID: 36084657; PMCID: PMC9648694.

118.Amadei G, Handford CE, Qiu C, De Jonghe J, Greenfeld H, Tran M, Martin BK, Chen DY, Aguilera-Castrejon A, Hanna JH, Elowitz MB, Hollfelder F, Shendure J, Glover DM, Zernicka-Goetz M. Embryo model completes gastrulation to neurulation and organogenesis. Nature. 2022 Oct;610(7930):143-153. doi: 10.1038/s41586-022-05246-3. Epub 2022 Aug 25. PMID: 36007540; PMCID: PMC9534772.

CHAPTER II: ESTROGEN SIGNALING ENCOURAGES BLASTOCYST DEVELOPMENT AND IMPLANTATION POTENTIAL

This work was published in the Journal of Assisted Reproduction and Genetics in March, 2023

Summary

Purpose: Estrogen is well-known for preparing uterine receptivity. However, its roles in regulating embryo development and implantation are unclear. Our objective was to characterize estrogen receptor 1 (ESR1) in human and mouse embryos and determine the effect of estradiol (E_2) supplementation on pre- and peri-implantation blastocyst development.

Methods: Mouse embryos, 8-cell through hatched blastocyst stages, and human embryonic day 5-7 blastocysts were stained for ESR1 and imaged using confocal microscopy. We then treated 8-cell mouse embryos with 8 nM E_2 during in vitro culture (IVC) and examined embryo morphokinetics, blastocyst development, and cell allocation into the inner cell mass (ICM) and trophectoderm (TE). Finally, we disrupted ESR1, using ICI 182, 780, and evaluated peri-implantation development.

Results: ESR1 exhibits nuclear localization in early blastocysts followed by aggregation, predominantly in the TE of hatching and hatched blastocysts, in human and mouse embryos. During IVC, most E_2 was absorbed by the mineral oil, and no effect on embryo development was found. When IVC was performed without an oil overlay, embryos treated with E_2 exhibited increased blastocyst development and ICM:TE ratio. Additionally, embryos treated with ICI 182,780 had significantly decreased trophoblast outgrowth during extended embryo culture.

Conclusion: Similar ESR1 localization in mouse and human blastocysts suggest a conserved role in blastocyst development. These mechanisms may be underappreciated due to the use of mineral oil during conventional IVC. This work provides important context for how estrogenic

toxicants may impact reproductive health and offers an avenue to further optimize human assisted reproductive technology (ART) to treat infertility.

Key Words: Estradiol, Pre-implantation Embryo, Implantation, Embryo Development, Estrogen Receptor, In Vitro Culture

Introduction

Uterine preparation for implantation is carefully dictated by a precise ratio of estrogen and progesterone [1, 2, 3]. Although circulating 17-β-estradiol (E_2) is considerably reduced during the luteal phase compared to the follicular phase, a nidatory wave of E_2 peaks during the time of implantation in both mice and humans. This nidatory estrogen acts directly on the endometrial stromal and epithelial cells to prepare for receptivity [4, 5] and induces uterine secretion of factors such as leukemia inhibitory factor (LIF) that facilitate embryo implantation [6, 7]. However, it is still unclear if E_2 acts directly on the embryo itself and if so, provides any benefit to embryo implantation.

Estrogens signal through two known nuclear transcription factor receptors, estrogen receptor 1 (ESR1) [8] and estrogen receptor 2 (ESR2) [9] and one G-coupled protein receptor, GPER1 [10, 11]. Transcription of *Esr1* is active after mouse zygotic genome activation, becomes silent during the morula stage, and reappears with the emergence of the blastocoele [12], suggesting a stage-specific role for ESR1 just prior to implantation. ESR1 protein is present in the zygote to the blastocyst stage [13-15], followed by targeted degradation that is necessary to initiate implantation [16]. However, *Esr1/Esr2* double knockout embryos are still able to successfully implant and produce pups [17, 18], calling into question the role of estrogen signaling in pre-implantation embryo development [18-23].

High levels of E_2 (≥ 100 nM) during in vitro culture are deleterious at the two-cell stage [13, 24], but E_2 supplementation at 8 nM during the peri-implantation period successfully facilitates in vitro attachment and outgrowth of both human and mouse embryos [25-28]. We hypothesized that 8 nM E_2 acts directly on the implanting embryo through ESR1 to support blastocyst development and implantation. Thus, our objectives were to determine the subcellular localization of ESR1 in mouse and human embryos and to determine if 8nM E_2 supplementation past the 8-cell stage improves mouse blastocyst development and implantation potential.

Materials and Methods

All chemicals were purchased through Sigma Aldrich unless otherwise stated.

Animals

All animal protocols were performed in line with animal care and use guidelines [29]. Female and male mice were housed separately and kept in a 14:10 (light: dark, h) cycle with food and water offered ad libitum. CF1 outbred female mice (Envigo, Indianaplois, IN) between 4-8 weeks old were housed in groups and 3-4 month old BDF1 outbred male mice (Envigo) were housed individually.

In vitro fertilization and in vitro culture of mouse embryos

Female mice were stimulated with a 5 IU intraperitoneal (i.p.) injection of pregnant mare serum gonadotropin (PMSG, Calbiochem, Millerica, MA) followed by 5 IU i.p. human chorionic gonadotropin (hCG, Calbiochem) 48 h later. Approximately 17 h following hCG injection, cumulus-oocyte-complexes (COC's) were collected from the ampullae and placed into a 3-(N-morpholino)-propanesulfonic acid (MOPS) buffered handling medium supplemented with 5% (v/v) fetal calf serum (Hyclone, Waltham, MA, USA) [30].

Fresh sperm was retrieved from the vas deferentia and caudae epididymides and left to capacitate in fertilization medium [30, 31] supplemented with 10% bovine serum albumin (BSA, Probumin, Millipore Sigma, Burlington, MA), under mineral oil (Spectrum, New Brunswick, NJ) for 1 h. Ten COC's were inseminated with 1 x 10^6 capacitated sperm/mL in 50 µL drops under mineral oil. COC's were incubated with sperm for 6 h before visual confirmation of two distinct pronuclei, at which time zygotes were moved to 20 µL drops of phenol-free culture media under oil [30, 31]. Cleavage was evaluated 24 h post fertilization (h.p.f.) and cleaved embryos were cultured until 54 h.p.f. before distribution into treatment groups. For embryo culture under oil, embryos were distributed into 20 µL of phenol-free media (10 embryos per drop) containing no E_2, E_2, or E_2 with the nuclear estrogen receptor antagonist, ICI 182,780 (Tocris, Minneapolis, MN) under oil for an additional 66 h (120 h.p.f). E_2 and ICI 182,780 products were diluted initially in 100% ethanol and were further diluted in culture medium to a final concentration of 8 nM (E_2) or 165 nM (ICI 182, 780. For embryo culture in the absence of oil, at 54 h.p.f. embryos were distributed into groups of 60-90 in wells of 250 µL in a 6-well plate without an oil overlay for an additional 66 h (120 h.p.f.). Water was added to the center of the 6-well plate to minimize well evaporation, and dishes were cultured in a humidified incubator. Blastocyst formation and hatching was evaluated at 102 h.p.f. For morphokinetic evaluations, embryos were cultured as single embryos in 22 µL drops under 1.5 mL oil in in the Embryoscope time-lapse imaging system (Vitrolife, Englewood, CO) from 54 h.p.f. through blastocyst hatching. Due to the high elevation of our laboratory, all embryo culture was carried out under 6.5% O_2 and 7.5% CO_2 at 37°C to mimic 5% O_2 and 6% CO_2 at sea level.

Vitrified human blastocyst warming and recovery

Human embryos were donated with informed consent following IVF treatment at the Colorado Center for Reproductive Medicine in Lone Tree, CO (WIRB study no. 1179872). Vitrified aneuploid embryonic day (D) 5 embryos were warmed using the Kitazato method (Kitazato, Japan) and left to recover in 20 µL drops of in-house prepared culture media with 20% (v/v)

Quinn's Advantage Serum Protein Substitute (SPS, Origio, Cooper Surgical, Trumbull, CT) under oil for 2 h, 24 h, or 48 h before fixation in 4% paraformaldehyde (PFA, Electron Microscopy Sciences, Hatfield, PA) in phosphate-buffered saline (PBS) for 20 min for immunofluorescence staining.

Immunofluorescence staining and imaging

Mouse 8-cell embryos at 48 h.p.f., morulae at 72 h.p.f, early blastocysts at 78 h.p.f., blastocysts at 96 h.p.f., hatching blastocysts at 102 h.p.f., and hatched blastocysts at 120 h.p.f. were collected for immunofluorescence staining. All embryos (human and mouse) at varying stages were fixed in 4% PFA in PBS for 20 min, then washed three times for 5 minutes each wash in PBS containing 0.1% Tween 20 (Fisher Scientific, Fair Lawn, NJ) and 0.1% polyvinylpyrrolidone (PVP; wash buffer,), and permeabilized in 0.3% Triton X-100 in PBS for 30 min. Following permeabilization, embryos were washed once in wash buffer for 5 min and moved to blocking buffer with 0.1% Tween 20, 1.0% BSA, 0.1 M glycine, and 10% horse serum for 2 h. Embryos were washed in wash buffer once for 5 min and moved to primary antibodies diluted in antibody buffer (0.1% Tween 20 and 1.0% BSA in PBS) overnight in 4 °C. Antibody information is listed in Table 2. After overnight incubation with primary antibodies, embryos were washed three times in wash buffer for 5 min and transferred to secondary antibodies, Alexaflour 488 (1:200; donkey anti-rabbit IgG, Invitrogen, Carlsbad, CA) and Alexafluor 568 (1:200; goat anti-mouse IgG, Invitrogen) for 1 h. Embryos were then washed in wash buffer for 5 min, once in 1:1 wash buffer and antibody buffer for 5 min, and washed a final time in wash buffer for 5 min before mounting onto a poly-L-lysine coated slide with Prolong Diamond antifade mountant with DAPI (ThermoFisher, Waltham, MA), and covered with a coverslide.

Hatching embryos fixed for cell number determination were visualized using an OlympusBX52 microscope with UV illumination filters specific to secondary antibodies. Images were captured using the Photometrics CoolSnap HQ camera and were counted using the Metamorph

Advanced software version 7.7.0.0 using the hand count tool. Embryos fixed for receptor localization were imaged using the Olympus Fluoview FV10i confocal microscope with FV10-ASW software version 04.01 and fluorescence intensities were measured using FIJI (a version of ImageJ2) [32].

Estradiol Quantification in Culture Medium

To determine if E_2 was being absorbed by the oil overlay, we supplemented 8 nM E_2 into culture medium and left it in the incubator with (20 µL drops) or without an oil overlay (5 mL in a snap cap tube) for 48 h. After 48 h, 200 µL of each medium were snap frozen in triplicate in liquid nitrogen and stored in -80 °C. E_2 concentration was measured using a Roche Cobas e601 and reported as nM.

Capillary Electrophoresis Protein Quantification

Mouse hatching blastocysts from each treatment were snap frozen in LN_2 in groups of 10 in minimal volume of PBS + 0.1% PVP and stored in -80°C up to four weeks before use. Samples were lysed using 6µL RIPA lysis buffer with 1X Halt Phosphatase inhibitor Cocktail (ThermoFisher) and 1X cOmplete EDTA-free Protease Inhibitor. Samples were run on the ProteinSimple Jess® System (ProteinSimple, San Jose, CA) according to manufacturer protocols. Briefly, a fluorescent master mix was mixed with each sample at a 1:5 dilution and boiled for 10 min at 95°C. Wash Buffer, luminol/peroxide mix, secondary antibody anti-rabbit HRP, antibody diluent, primary antibodies (p44/42 MAPK rabbit, 1:20, cat#4695S, Cell Signaling; phosphor-p44/42 MAPK (Thr202/Tyr204), 1:20, cat#4370S, Cell Signaling, Danvers, MA), total protein normalization reagent, ladder, and samples were loaded onto the cartridge for a 25 capillary, 12-230 kd separation module (ProteinSimple). Each sample was split equally into two lanes measuring either total or phosphor-MAPK. Final analysis of band separation was quantified automatically using the corrected area under the curve in the expected kd range for

MAPK normalizing against the amount of total protein in the capillary. We then used a ratio of phospho/total MAPK for each paired sample.

Mouse Blastocyst Extended Culture

Extended culture of mouse blastocysts to D 9 post fertilization was used as a proxy to evaluate blastocyst implantation potential [26, 33]. Hatching blastocysts at 102 h.p.f. were treated with acidic Tyrode's solution to remove the zona pellucida and placed into equilibrated wells of Advanced DMEM/F12 with 20% fetal calf serum (FCS, Hyclone, SH30070.02), 25 μM N-acetyl-cysteine, 8nM E_2, 200 ng/mL progesterone, 1X ITS-X (ThermoFisher), 5 mg/mL Gentamicin (Cellgro), and 2 mM GlutaGro (FisherSci) (IVC1) in fibronectin-coated (30 μg/ml fibronectin in PBS incubated overnight) 8-well chambered coverslips (ibidi, Martinsried, Germany). Embryos were left to incubate in atmospheric O_2 and 7.5% CO_2 to mimic 6.5% CO_2 at sea level for 72 h before checking attachment. At 72 h (D 7) in extended culture, embryo attachment was examined and ½ medium was exchanged with equilibrated IVC2 medium (IVC1 with 30% Knockout Serum Replacement (ThermoFisher) instead of 20% FCS). Embryos were imaged daily using an Olympus DP22 camera attached to a stereoscope and FIJI was used to quantify the area of trophectoderm outgrowth [33].

Statistical Analysis

All continuous data were evaluated for normality using a Shapiro-Wilks test. Those datasets with equal variance and normal distribution were compared using a one-way ANOVA with Tukey's post hoc comparison test. Non-normal data was compared using a Kruskal Wallis test. Embryo development data was analyzed as binomial proportions and compared using a chi-squared test. All data analyses were completed using GraphPad Prism 8.4.2. Significance was noted at $p<0.05$. Data are presented as mean ± SEM.

Results

Stage-specific ESR1 localization in mouse pre-implantation stage embryos

ESR1 showed strong immunofluorescent staining throughout mouse embryo development from the 8-cell to the hatched blastocyst stage with dynamic changes of its subcellular localization (Fig. 2.1, 2.6). ESR1 localized to the nucleus during the 8-cell stage, waned during the morula stage, maintained stable with the emergence of the blastocoele cavity, followed by a sharp decline at the hatched blastocyst stage. (Fig. 1.1A). At the early blastocyst stage, embryos began to develop bright punctate aggregates of ESR1 that then decreased in intensity as the embryos fully hatched from the zona pellucida (Fig. 1.1B). The nuclear/cytoplasmic ESR1 ratio, which correlates with estrogen signaling activity [34], was stable from 8-cell to hatching blastocyst and rapidly increased in the TE of fully hatched blastocysts (Fig. 1.1C). By examining the three different staining patterns of ESR1 in mouse embryos (nuclear, cytoplasmic, and punctate, Fig. 1.1D), we demonstrated the dynamic changes of estrogen signaling activity during blastocyst formation and hatching, suggesting a direct role of E_2 on embryo development and TE differentiation.

Subcellular Localization of ESR1 in Human Blastocysts Mimics the Pattern Found in Mouse Blastocysts

We used SOX2 expression to identify the ICM of human D5 blastocysts and POU5F1 to identify the ICM in D6 and D7 embryos (Fig. 2.7). After 2 h of recovery post-warming, D5 human blastocysts showed bright staining of ESR1 localized to the nucleus and cytoplasm of all cells (n=8, Fig. 2.2A). On D6 (24 h post warming, n=8) and D7 (48 h post warming, n=6), nuclear localization of ESR1 decreased in both the ICM and TE (Fig. 2.2B), while the punctate ESR1 aggregates increased in all TE cells (Fig. 2.2C), demonstrating a similar pattern to that found in mouse embryos. The ICM of human embryos also developed aggregate ESR1 patterns, though this was significantly reduced compared to TE (Fig. 2.2C). The nuclear/cytoplasmic ESR1 ratio dipped slightly at D6 for both ICM and TE and increased again at D7 in human blastocysts and

remained consistently above a 1:1 ratio (Fig. 2.2D), suggesting continued estrogen signaling activity in human blastocysts at this stage. A decrease in nuclear intensity, increase in punctate aggregates, and increase in nuclei/cytoplasmic ratio in late blastocysts is remarkably similar to similar measurements in mouse embryos (Fig. 2.1).

Estradiol supplementation improves blastocyst development and hatching

Embryos treated with 8 nM E_2 under an oil overlay showed no differences in blastocyst development (control, n=112/140, 80.0%; E_2, n=131/153, 85.6%; p=0.22) or blastocyst hatching (control, n=76/140, 54.3%; E_2, n=86/153, 56.2%; p=0.81) 102 h.p.f. (D4) compared to control (Fig. 2.3A, left panel). However, we suspected that the oil overlay may be absorbing E_2 out of the culture medium. Without an oil overlay, embryos supplemented with 8 nM E_2 developed to blastocyst more frequently than control embryos (control, n=141/205, 68.8%; E_2, n=178/222, 80.2%; p<0.01) and tended to have increased blastocyst hatching on D4 (control, n=97/205 47.3%; E_2, n=124/222 55.9%; p=0.08; Fig. 2.3A, right panel). To verify whether E_2 was being actively absorbed by the oil overlay of our culture system, we sampled culture medium supplemented with E_2 with or without an oil overlay after 48 h in the incubator without embryos. We found that the concentration of E_2 was significantly reduced in culture drops under oil compared to medium without an oil overlay (with oil: 0.66 ± 0.01 nM, without oil: 2.62 ±0.04 nM; p<0.0001, Fig. 2.3B). On D4, we saved hatching blastocysts from each group and performed immunofluorescence staining with antibodies against SOX2 and CDX2 to count the number of ICM and TE cells respectively. Embryos grown in E_2-supplemented culture medium with no oil overlay had significantly increased ICM: TE ratio (control without oil: 0.17 ± 0.02, n= 10; E_2 without oil: 0.25 ± 0.02, n=29, p<0.01, Fig. 2.3C) compared to those in the control group or with an oil overlay (control with oil: 0.10 ± 0.01, n=40; E_2 with oil: 0.11 ± 0.01, n=38, Fig. 3C). No differences were noted for ICM number, TE number, or total cell number between control or estradiol groups with (Fig. 2.8) or without an oil overlay (Fig. 2.3D). Morphokinetic timing to developmental stages evaluated using a time-lapse imaging system was not different between

groups (data not shown) which may be due to the necessity of an oil overlay during culture in a non-humidified time-lapse incubator.

Inhibition of estrogen signaling *impairs peri-implantation development of mouse embryos*

Embryos were treated with 0 nM E_2 (Control), 8 nM E_2, or 8 nM E_2 + 165 nM ICI 182, 780 for 48 h from the 8-cell stage to the hatching blastocyst stage (Fig. 2.4A). Treatment of embryos with E_2 and the nuclear estrogen receptor antagonist, ICI 182,780 (Robertson) did not change the proportion of embryos that were able to initiate blastocyst formation on D4 compared to those cultured with E_2 alone or in control conditions (Fig. 2.4B). The number of hours to initiate blastocoele formation or hatching from the zona pellucida was also not different in embryos treated with ICI 182,780 compared to control embryos or those treated with E_2 (data not shown). However, when morphologically similar D4 hatching blastocysts from each group were cultured to D9 during peri-implantation extended culture, embryos that were exposed to ICI 182,780 during the 8-cell to blastocyst stage had significantly reduced trophectoderm outgrowth at D7 (control: 0.12 ± 0.01 mm^2, n=36; E_2: 0.12 ± 0.01 mm^2, n=36; E_2+ ICI 182, 780: 0.08 ± 0.01 mm^2, n=36) and D9 (control: 0.37 ± 0.02 mm^2, n=36; E_2: 0.37 ± 0.02 mm^2, n=36; E_2+ ICI 182, 780: 0.27 ± 0.02 mm^2, n=36; $p<0.05$, Fig. 2.4C, D). Advanced morphological structure formation, including the ectoplacental cone and proamniotic cavity, was not different between treatments (Supplementary Fig. 2.3B, C). Interestingly, both control embryos and embryos that were treated with E_2+ICI 182, 780 showed a decrease in phosphorylated MAPK1/3: total MAPK1/3 compared to embryos treated with E_2 (control: 0.14 ± 0.02, n=5; E_2: 0.27 ± 0.05, n=3; E_2+ ICI 182, 780: 0.09 ± 0.03, n=7, Fig. 2.4E).

Discussion

Though we show here that estrogen signaling certainly encourages blastocyst development, and disruption of ESR1 signaling impairs implantation, the question of necessity still remains. *Esr1/Esr2* double knockout embryos are still able to implant and make pups [17,18]. However,

the efficiency (i.e. litter sizes, health, implantation efficiency, etc.) of those double knockouts embryos is not reported. It is possible that estrogen receptors that are carried over from the maternal oocyte are sufficient to carry a mutant blastocyst through development as some maternal proteins do persist through to the blastocyst stage [35, 36]. We propose that although ESR1/2 are not *necessary* for blastocyst development and implantation, they do play an important role, particularly in TE differentiation and embryo implantation, and has been overlooked. Supplementation with 8 nM E_2 improved blastocysts' ability to form a blastocoele cavity, hatch from the zona pellucida, and increased the ICM:TE ratio in hatching blastocysts. Furthermore, addition of ICI 182, 780 during the 8-cell stage caused a profound reduction in downstream trophoblast development in extended culture. Further investigations will be useful in determining an E_2 concentration, potentially even below 8nM, for optimal pre-implantation embryo culture.

Mouse embryos, unlike pigs, rats, and rabbits, do not have the functional enzymes to produce their own E_2 at the blastocyst stage [37-40]. In accordance with other species, human blastocysts express both aromatase (CYP19A1) as well as 17-β-hydroxysteroid dehydrogenase (HSD17B1) which make them capable of producing their own E_2 [41], though this has never been quantitatively measured. Single-cell RNA-sequencing in human blastocysts also revealed that human embryo TE upregulate transcripts relating to the GO term "response to estrogen stimulus" when compared to the ICM and primitive endoderm [42]. Interestingly, the benefit of E_2 was lost when mouse embryos were cultured with E_2 under oil. This is particularly important when considering the possibility that human embryos may produce endogenous E_2 into their microenvironment. The absorption of estradiol, progesterone, and androstenedione out of culture medium into an oil overlay has been previously reported [43]. Since the oil overlay in the culture system is absorbing steroid hormones, it is likely that endogenously produced E_2 by human embryos may be unintentionally lost into the oil and may affect blastocyst development and implantation potential.

Despite differences in endogenous production of E_2 between mouse and human blastocysts, we found strong similarities in ESR1 localization at the blastocyst and late blastocyst stage, suggesting that signaling downstream of estrogen may be conserved between the two species. Mouse embryos, as opposed to humans, undergo lactational diapause in which the embryo enters a quiescent state. Diapausing mouse embryos in vivo can be activated with administration of an E_2 injection [4, 45]. Though E_2 itself through ESR1 is not solely responsible for activating dormant embryos out of diapause [20], it may be involved in encouraging proliferation and transcriptional events that follow activation out of diapause in mouse embryos. In this case, mouse embryos would be reliant on an exogenous source of E_2 to prime trophoblast for implantation. However, because human, pig, and rabbit embryos do not exhibit an extended diapause [46], endogenous production of E_2 may allow them to proceed through development and prepare for implantation with a minor or negligible paused pluripotent state.

We did not find that ESR2 and GPER1 localization was similar between mouse and human embryos. However, both mouse and human embryos display similar localization patterns of ESR1 in the nucleus prior to bright aggregations at the late blastocyst stage. Similar aggregations were noted when late mouse blastocysts in vivo were activated from diapause and flushed from ovarectomized mothers [16]. ESR1 generally colocalized with ubiquitin and researchers previously hypothesized that targeted degradation must proceed *before* ESR1 can translocate to the nucleus [16]. We show that embryos produced in vitro display varying levels of ESR1 expression throughout development and that ESR1 is localized to the nucleus *prior* to aggregation, not after. We therefore propose that ESR1 translocation to the nucleus may be involved in normal embryonic development in preparation for implantation, and only afterwards forms ESR1 aggregates. This hypothesis is further bolstered by previous reports that predict ESR1's potential involvement in blastocyst production through trophoblast-specific lineage markers (CDX2, GATA3, and TEAD4) [15] or through other estrogen responsive genes (CLDN4,

etc.) [47]. ESR1 is held in the cytoplasm bound in complexes with heat shock protein chaperones [48, 49]. Upon binding with E_2, ESR1 is free to dimerize and translocate into the nucleus to alter transcription via binding with estrogen response elements or indirectly through interactions with tethering factors [50]. ESR1 enters the nucleus via two known mechanisms, passive diffusion or shuttling via importin-α/β1. TNPO2 is a molecule that binds the nuclear localization signal on ESR1 competitively with importin-α/β1 and restricts ESR1 from entering the nucleus [51]. In some cases, we noticed specific retention of ESR1 in the cytoplasm (Fig. 2.8C) similar to reported ESR1 mutants without a functional nuclear localization signal [50]. Further studies are warranted to determine whether TNPO2, or another mechanism, is responsible for ESR1 translocation during embryonic development.

Aggregations of ESR1 in both mouse and human embryos are remarkably similar to those present in estrogen responsive MCF-7 breast cancer cells [52]. In this cancer cell model, ESR1 were identified as membrane-bound aggregations that were increased in estrogen-starved cells and displayed significantly increased MAPK1/3 activity when cells were treated with E_2 [52]. Previous reports also link MAPK phosphorylation as a stimulated downstream response of ESR1 interaction with IGF1R [53, 54]. Additionally, aggregate staining of ESR1 in MCF-7 cells also results in proteasomal degradation unless ESR1 can be rescued by the presence of fibronectin [55]. As fibronectin binds integrins that are associated with ESR1 aggregations, the receptors avoid lysosomal degradation preserving and strengthening their transcriptional activity [55]. We also found increased MAPK1/3 activity when embryos were treated with 8 nM E_2, which is particularly intriguing due to the necessary role MAPK1/3 play in cell proliferation, cell survival, and normal trophoblast development in mouse embryos [56-58]. We did not find obvious colocalization of ESR1 with ubiquitin (Fig. 2.8D) and hypothesize that embryos may aggregate ESR1 for an unknown physiological role in TE development, potentially through MAPK signaling mechanisms. Interestingly, mouse homozygous MAPK mutant embryos do not survive past D 8.5 during the peri-implantation period and are severely stunted from D6.5-7.5,

particularly in the extraembryonic tissues [57]. If TE cells use a similar mechanism to MCF-7 cells, contact with fibronectin from the endometrium may rescue degradation of ESR1 or could act as a checkpoint before proceeding through implantation and increase MAPK1/3 to ramp up proliferation and prime embryos for implantation. Further studies are warranted to demonstrate the connection between membrane-bound ESR1 and MAPK signaling during the peri-implantation period in mouse embryos.

Conclusion

We propose that estrogen receptors assist in blastocyst development, act to prime the trophoblast for implantation, and that low levels of E_2 are beneficial for both mouse and human embryos. Though ESR1/2 may not be necessary for mouse embryo development and implantation, they may participate in mechanisms that encourage embryo development and implantation that are currently overlooked. Uncovering these signaling mechanisms in the early embryo has implications for human IVF culture conditions, treatment for fertility complications such as recurrent pregnancy loss, and considerations around environmental exposure to estrogenic toxicants. Additionally, our work highlights important opportunities to develop optimal culture conditions without the use of an oil overlay, to supplement steroid hormones that may be lost in the oil over time, and improve the implantation potential of human embryos cultured in vitro.

Table 2. Primary Antibodies

Protein of interest	**Host**	**Supplier**	**Catalog Number**
SOX2	Rabbit	Biogenex	AN833GP
ESR1	Mouse	Invitrogen	MA3-310
ESR2	Rabbit	Invitrogen	PA1-313
GPER1	Rabbit	Invitrogen	PA5-28647
Ubiquitin	Rabbit	Sigma	ABS1513-I
MAPK p44/42	Rabbit	Cell Signaling	4695S
phosphor-p44/42 MAPK (Thr202/Tyr204)	Rabbit	Cell Signaling	4370S
POU5F1	Rabbit	Cell Signaling	2750
POU5F1	Mouse	Santa Cruz	sc-5279

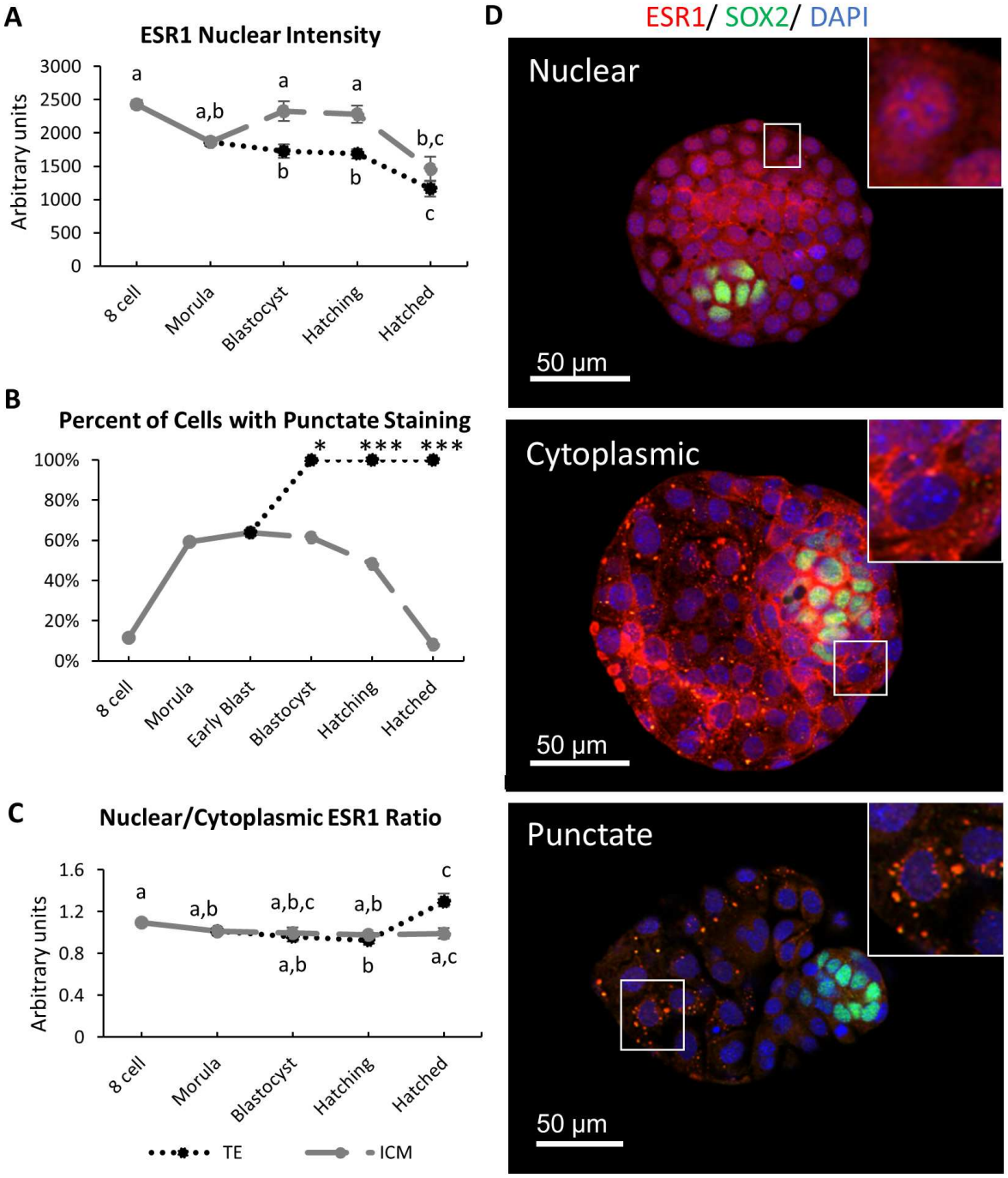

Figure 2.1 A) Fluorescence intensity of estrogen receptor alpha (ESR1) in the nuclei of 8-cell embryos (n=26), morulae (n=27), blastocysts (n=16), hatching blastocysts (n=30), and hatched blastocysts (n=12). B) Proportion of embryos displaying an aggregate punctate staining pattern of ESR1 throughout development. C) Nuclei:cytoplasm fluorescence intensity ratio throughout embryo development. ICM=GREEN, SOX-2 positive, inner cell mass; TE=RED, CDX2- positive, trophectoderm. D) Representative patterns of ESR1 in embryonic day (D) 5 mouse blastocysts. Top panel= nuclear, middle panel= cytoplasmic, bottom panel= punctate aggregate staining.

ESR1= Red, DAPI= Blue, SOX2= Green. Scale bars= 50 µm. Alphabet designations denote significance p<0.05 after one-way ANOVA. Chi-squared contingency test significance noted with *p<0.05, ***p<0.001.

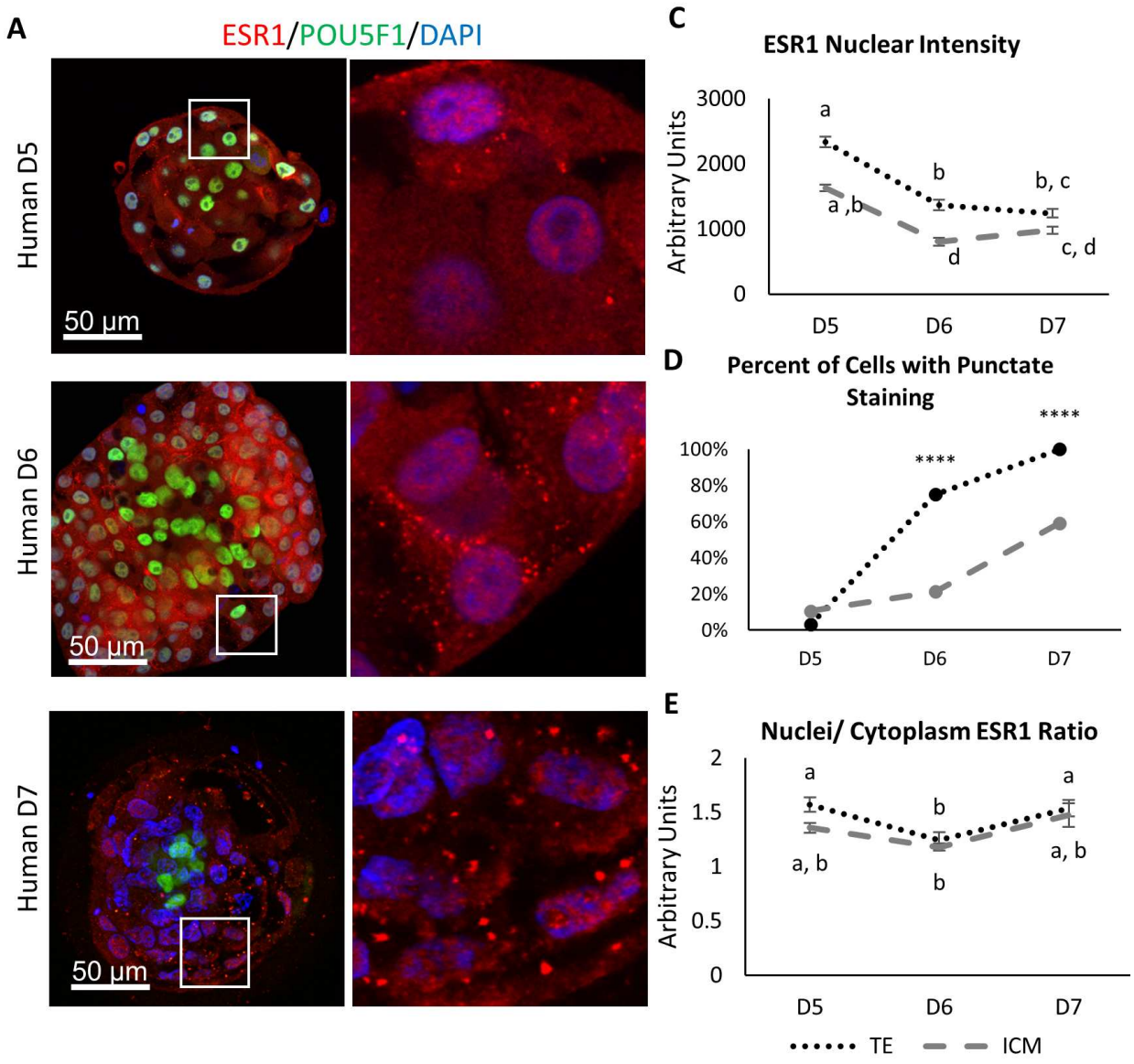

Figure 2.2 A) Estrogen receptor alpha (ESR1) in embryonic day (D) 5 human blastocysts following a 2 h, 24 h (D6), and 48 h (D7) recovery period after warming. ESR1=Red, DAPI= Blue. Scale bars= 50 µm. White boxes outline zoomed in images in right panels. B) Fluorescence intensity of estrogen receptor alpha (ESR1) in the nuclei of D5 human blastocyst trophectoderm and inner cell mass following a 2 h, 24 h (D6), and 48 h (D7) recovery period after warming. C) Proportion of cells within embryos displaying an aggregate punctate staining pattern of ESR1 throughout development in trophectoderm and inner cell mass. C) Nuclei:cytoplasm fluorescence intensity ratio throughout recovery up to D7 (48 h). n=30 cells from 3 blastocysts (D5), 30 cells from 3 blastocysts (D6), 10 cells from 3 blastocysts (D7). Alphabet designations denote significance p<0.05 after Kruskal-Wallis test (panel B) or one-way ANOVA (panel D). Chi-squared contingency test significance noted with ****p<0.0001.

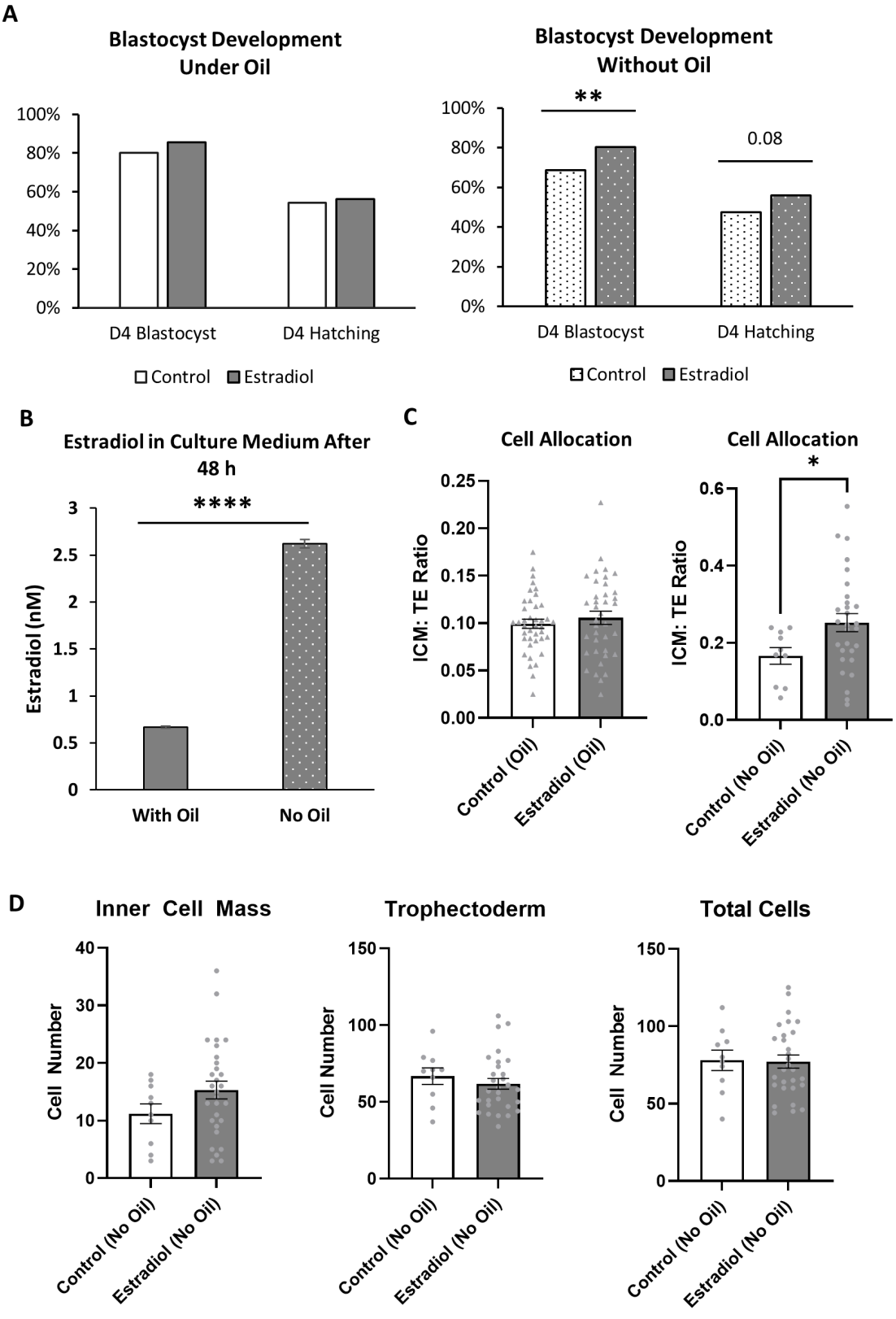
A
Blastocyst Development Under Oil
100%
80%
60%
40%
20%
0%
D4 Blastocyst
D4 Hatching
Control
Estradiol
Blastocyst Development Without Oil
**
0.08
100%
80%
60%
40%
20%
0%
D4 Blastocyst
D4 Hatching
Control
Estradiol
B
Estradiol in Culture Medium After 48 h
****
Estradiol (nM)
3
2.5
2
1.5
1
0.5
0
With Oil
No Oil
C
Cell Allocation
ICM: TE Ratio
0.25
0.20
0.15
0.10
0.05
0.00
Control (Oil)
Estradiol (Oil)
Cell Allocation
*
ICM: TE Ratio
0.6
0.4
0.2
0.0
Control (No Oil)
Estradiol (No Oil)
D
Inner Cell Mass
Cell Number
40
30
20
10
0
Control (No Oil)
Estradiol (No Oil)
Trophectoderm
Cell Number
150
100
50
0
Control (No Oil)
Estradiol (No Oil)
Total Cells
Cell Number
150
100
50
0
Control (No Oil)
Estradiol (No Oil)

Figure 2.3 A) Mouse embryo development on embryonic day (D)4 for embryos treated with 0 nM estradiol (Control) or 8 nM estradiol (Estradiol) at the 8-cell stage under oil (left, Control n=140, Estradiol n=153) or in wells without oil (right, Control n=205, Estradiol n=222). Fishers Exact test **p<0.01 B) Estradiol concentration (nM) in medium left for 48 h with or without an oil overlay. Student t-test ****p<0.0001C) Cell allocation into the inner cell mass (ICM, SOX-2 positive) or trophectoderm (TE, CDX2-positive) in embryos cultured in 0 nM (Control) or 8 nM estradiol (Estradiol) with (Control n=40, Estradiol n=38; left panel) or without (Control n=10, Estradiol n=29; right panel) an oil overlay. D) Cell number for ICM (left panel), TE (center panel) or F) total (CDX2 + SOX2 positive cells, right panel) amongst treatments without oil. Student t-test *p<0.05.

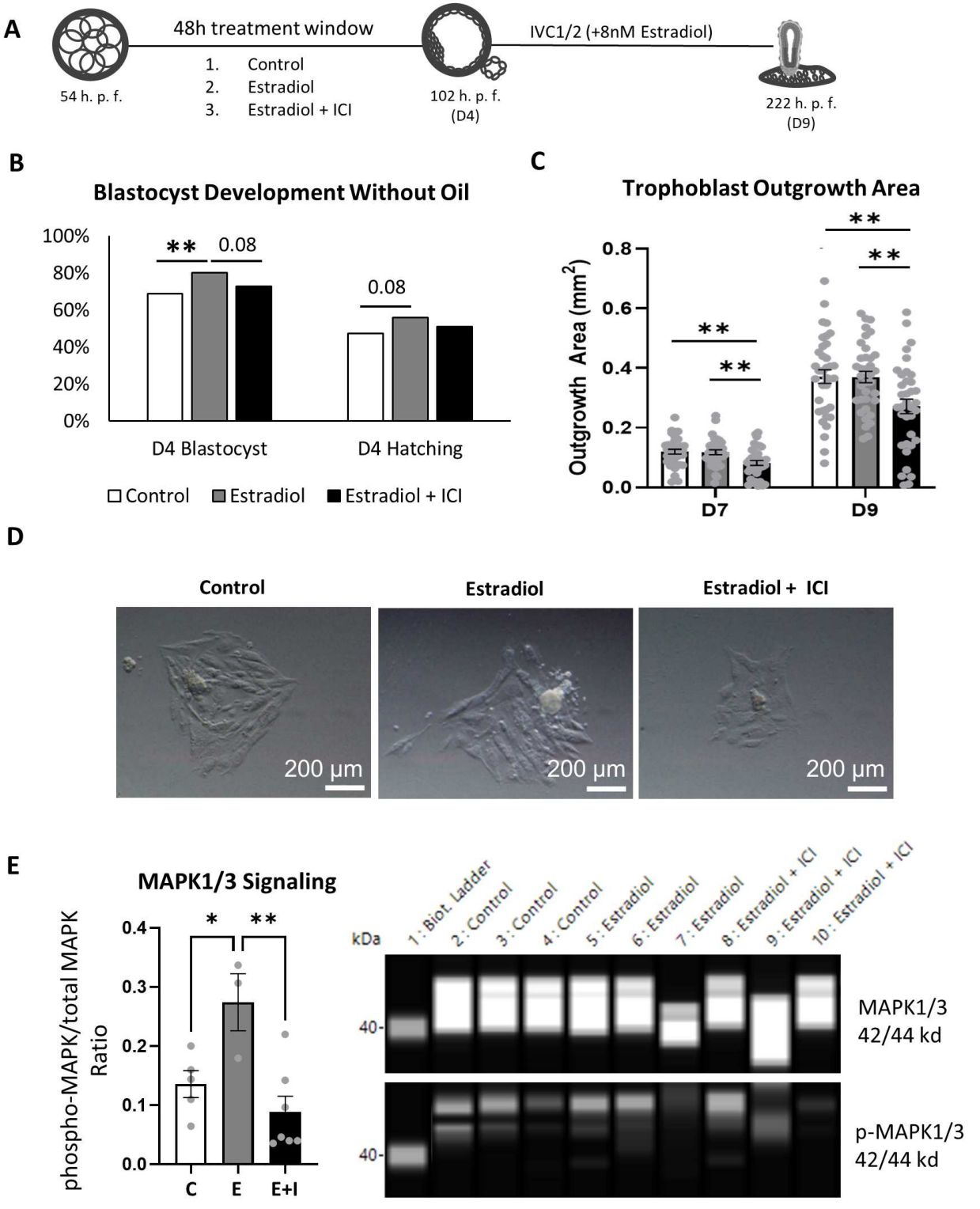

Figure 2.4 A) Schematic diagram of extended culture treatment conditions. B) Mouse embryo development on embryonic day (D)4 for embryos treated with 0 nM estradiol (Control, n=205), 8 nM estradiol (Estradiol, n=222), or 8 nM estradiol + 165 nM ICI 182, 780 (Estradiol + ICI, n=229)

at the 8-cell stage. C) Trophectoderm outgrowth area (mm^2) from control (n=36), estradiol (n=36), and estradiol + ICI (n=36) treated mouse embryos at embryonic day (D) 7 and 9. D) Representative stereomicroscope images of mouse embryos at embryonic day 9 in extended embryos culture. Scale bar= 200 µm. E) Protein quantification using capillary electrophoresis against MAPK1/3 (kd=42/44) and p-MAPK1/3 (kd=42/44) in control (n=5 tubes of 10 hatching blastocysts), estradiol (n=3 tubes of 10 hatching blastocysts), or estradiol +ICI treated (n=7 tubes of 10 hatching blastocysts embryos (right panel). Ratio of p-MAPK1/3:total MAPK1/3 in each treatment (left panel). One way ANOVA *$p<0.05$ **$p<0.01$.

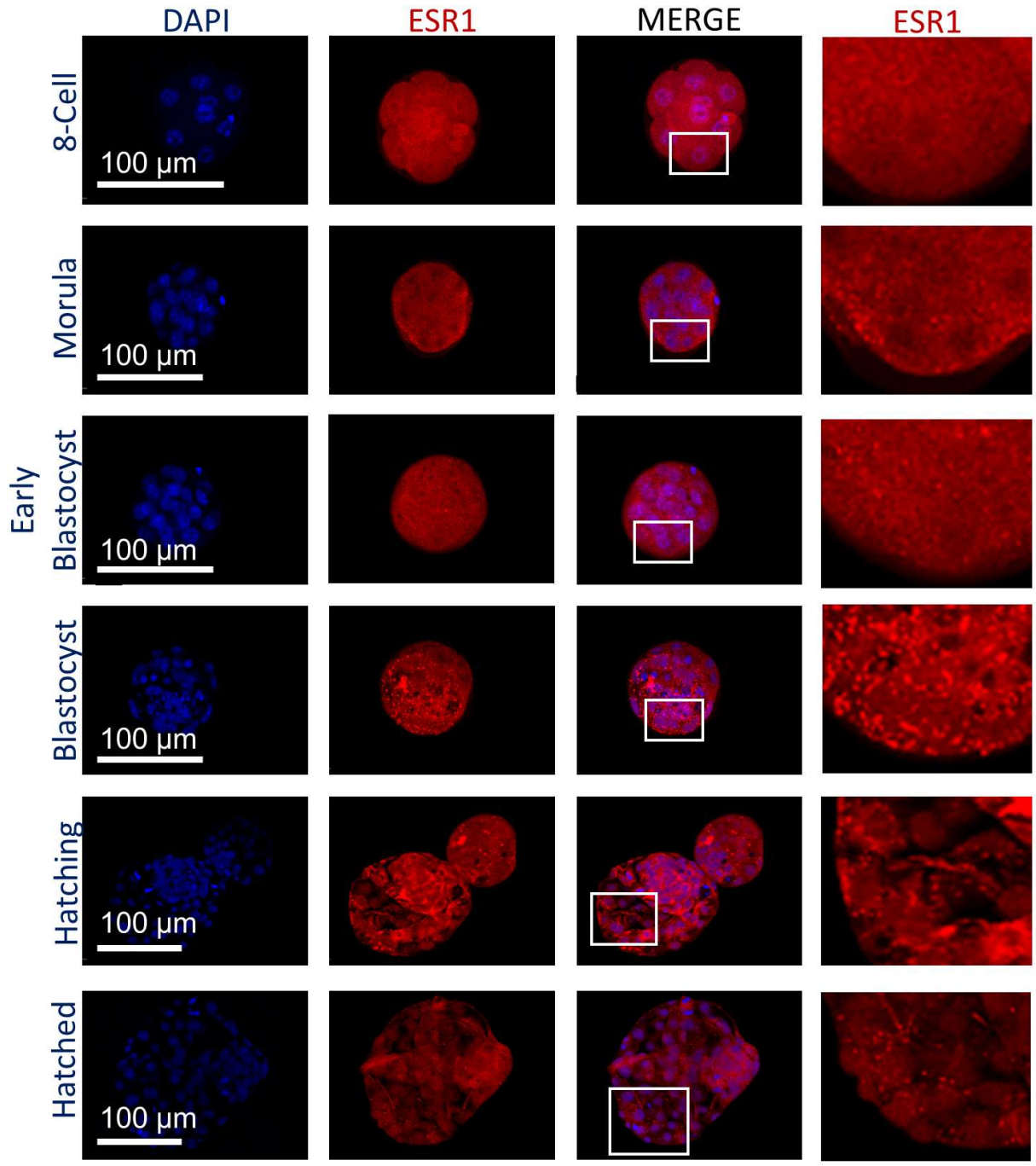

Figure 2.5 Representative confocal images of estrogen receptor (ESR1) throughout embryo development. Scale bar= 100 µm.

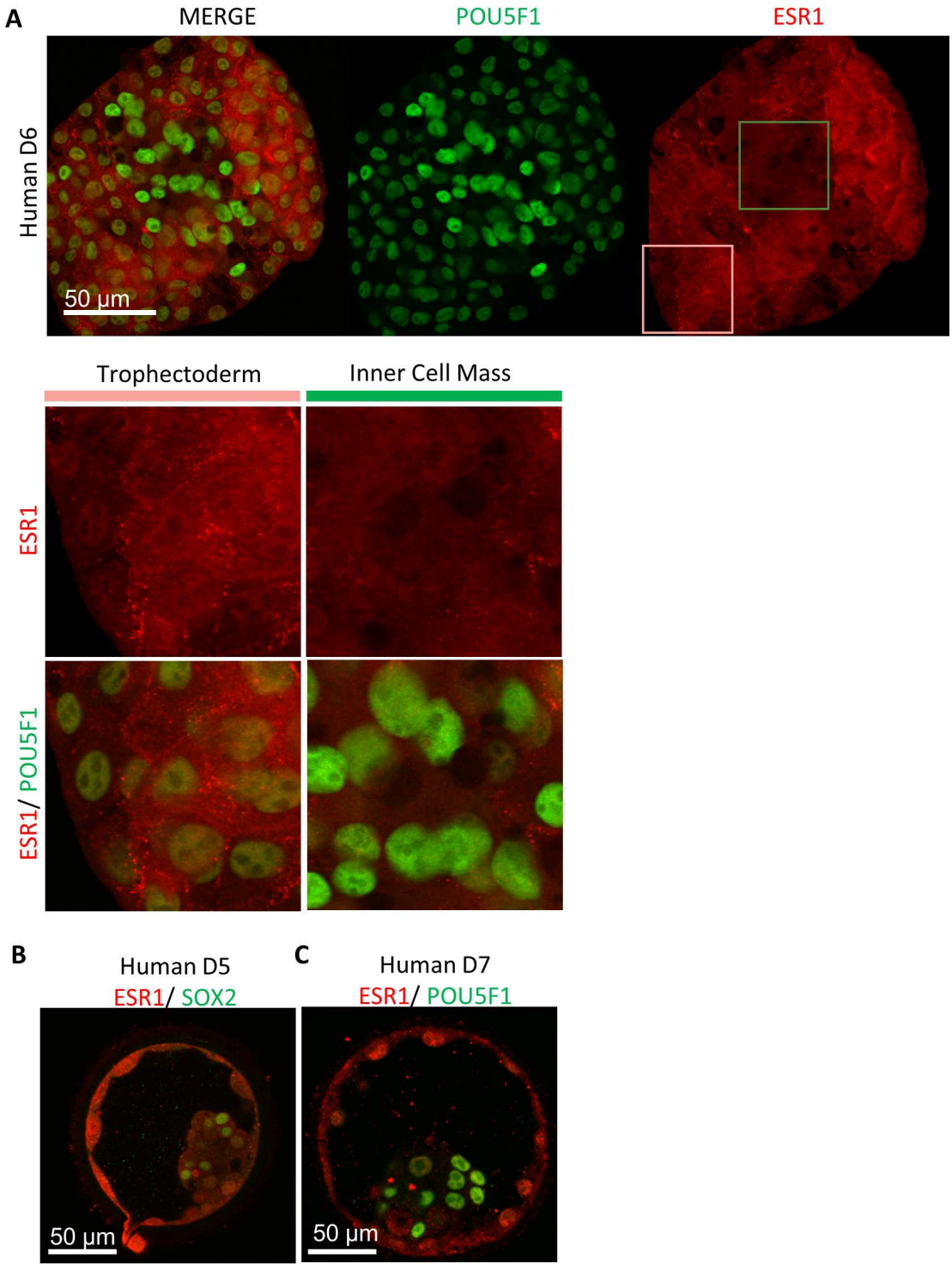

Figure 2.6 A) Representative confocal image of a human blastocyst after 24 h (D6) in recovery droplets following warming. Embryo stained with antibodies against POU5F1 for the inner cell mass and ESR1. Small boxes are magnified in color-matched bottom panels for trophectoderm and inner cell mass and highlight the differences in POU5F1 and ESR1 between the two cell types. Scale bar= 50 µm. B) Representative confocal image of a human blastocyst after 2 h (D5) in recovery droplets following warming. Embryo stained with antibodies against SOX2 for

the inner cell mass and ESR1. Scale bar= 50 μm. C) Representative confocal image of a human blastocyst after 48 h (D7) in recovery droplets following warming. Embryo stained with antibodies against POU5F1 for the inner cell mass and ESR1. Scale bar= 50 μm.

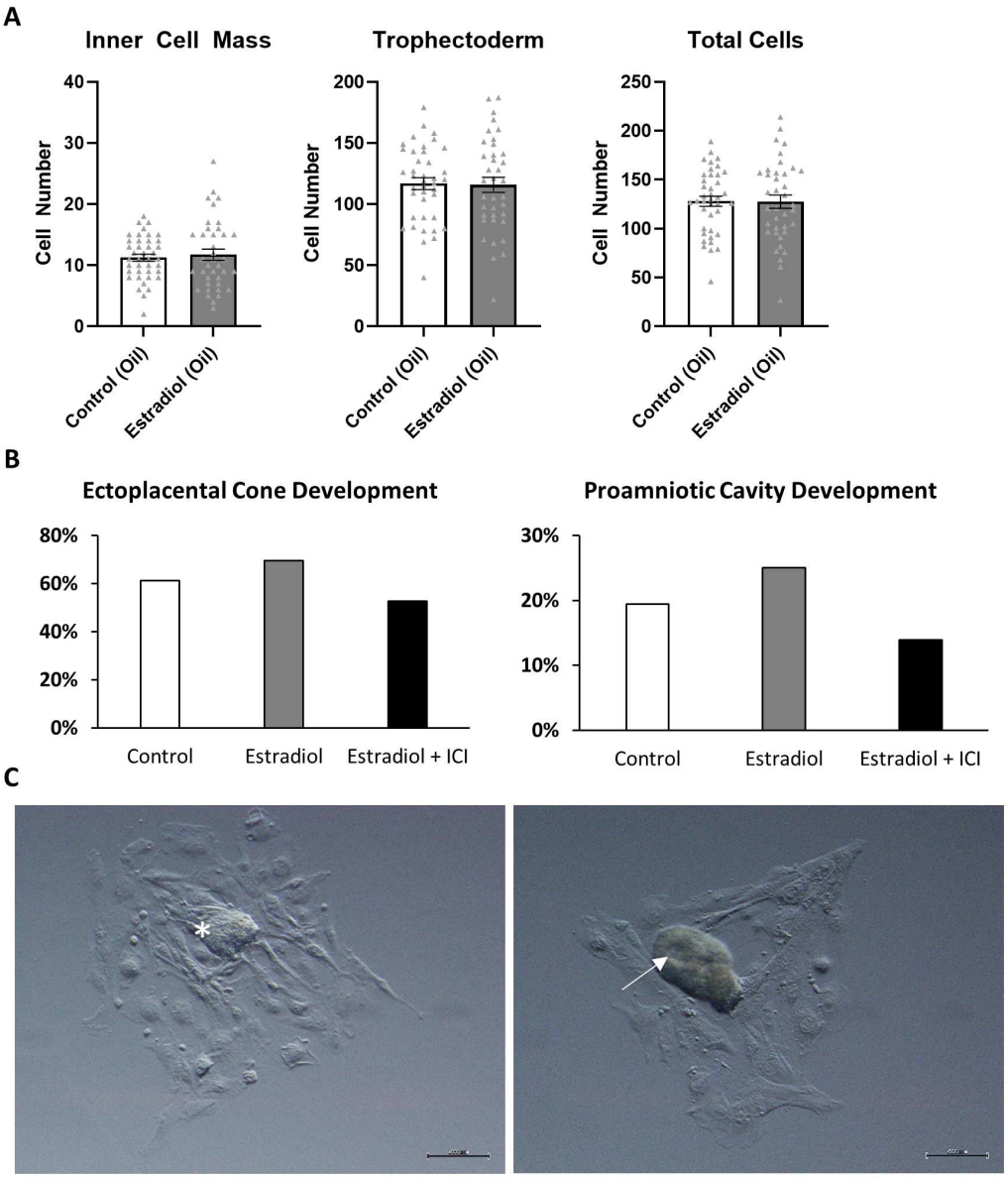

Figure 2.7 A) Cell number for ICM (left panel), TE (center panel) or F) total (CDX2 + SOX2 positive cells, right panel) amongst treatments under oil. B) Ectoplacental cone development (left) and proamniotic cavity development (right) in embryos grown in extended culture to D9. C) Representative stereomicroscope images of mouse embryos in extended culture with the development of an emerging ectoplacental cone (star, left) and a proamniotic cavity (white arrow, right). Scale bar = 200 μm.

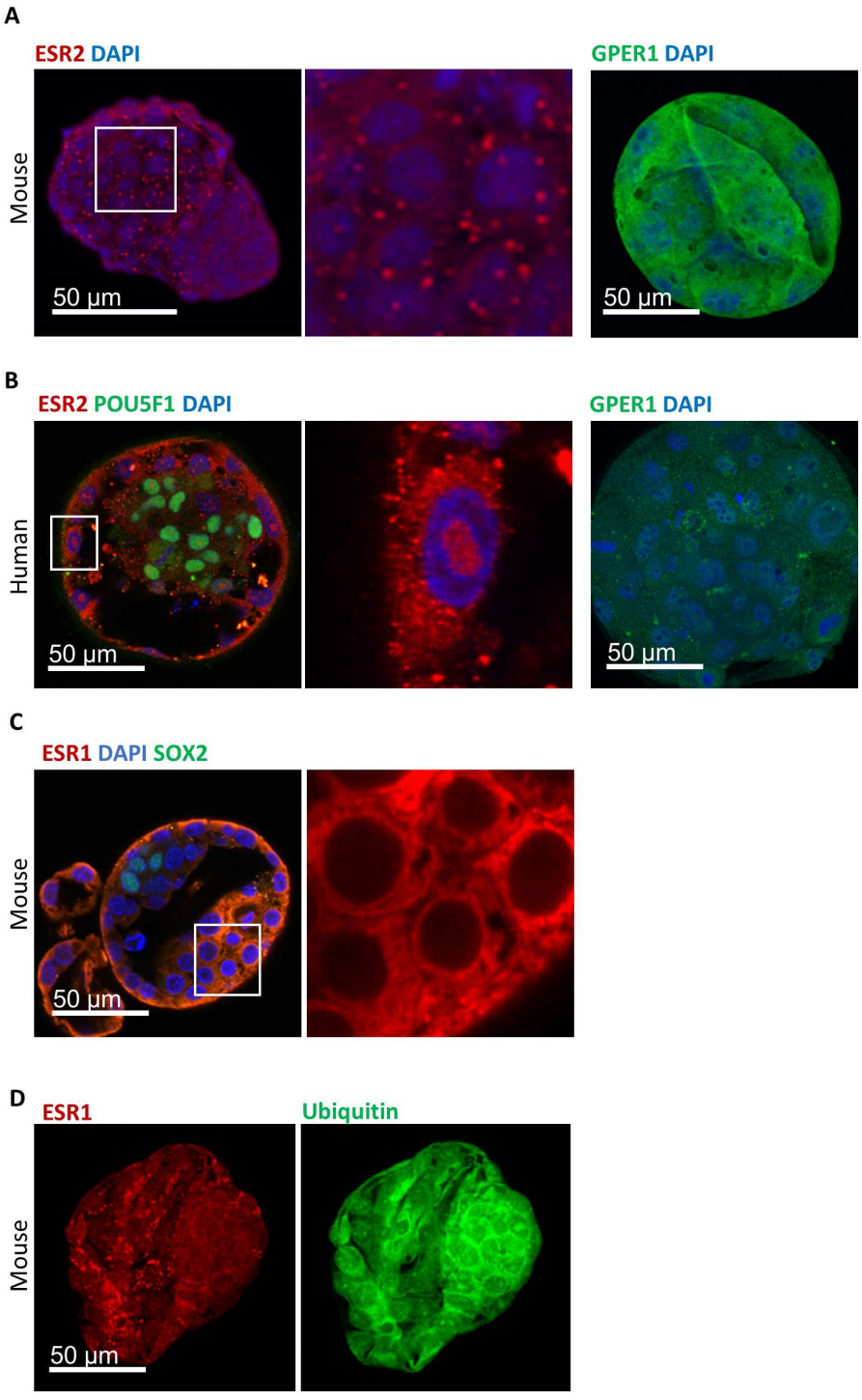

Figure 2.8 A) Representative confocal image of ESR2 (red, left) and GPER1 (green, right) in embryonic D5 mouse blastocysts. B) Representative confocal image of ESR2 (red, left) and GPER1 (green, right) in embryonic D7 human blastocysts. C) ESR1 localization restricted to the cytoplasm of mouse blastocyst on D5. Green= SOX2, red= ESR1, blue=DAPI. D) Representative confocal image of ESR1 (red, left) and Ubiquitin (green, right) in embryonic D5 mouse blastocysts. Scale bars= 50 µm.

REFERENCES

1. Vasquez YM, DeMayo FJ. Role of nuclear receptors in blastocyst implantation. *Seminars in cell & developmental biology*, 2013; **24** (10-12), 724–735. https://doi.org/10.1016/j.semcdb.2013.08.004
2. Martin L, Finn CA, Carter J. Effects of Progesterone and oestradiol-17β on the luminal epithelium of the mouse uterus. *Reproduction* 1970 **21** (3):461-469. https://rep.bioscientifica.com/view/journals/rep/21/3/jrf_21_3_010.xml
3. Finn CA, Martin L. Hormone secretion during early pregnancy in the mouse. *J Endocrinol.* 1969 Sep;45 (1):57-65. doi: 10.1677/joe.0.0450057. PMID: 5347379.
4. Ma WG, Song H, Das SK, Paria BC, Dey SK. Estrogen is a critical determinant that specifies the duration of the window of uterine receptivity for implantation. *Proc Natl Acad Sci* U S A. 2003 Mar 4;100 (5):2963-8. doi: 10.1073/pnas.0530162100
5. Huet-Hudson YM, Andrews GK, Dey SK. Cell Type-Specific Localization of c-Myc Protein in the Mouse Uterus: Modulation by Steroid Hormones and Analysis of the Periimplantation Period. *Endocrinology*, **125** (3) 1683- 1690. https://doi.org/10.1210/endo-125-3-1683
6. McCormack JT, Greenwald GS. Evidence for a preimplantation rise in oestradiol-17β levels on day 4 of pregnancy in the mouse. *Reproduction* 1974 **41**(2), 297-301.
7. Bhatt H, Brunet LJ, Stewart CL. Uterine expression of leukemia inhibitory factor coincides with the onset of blastocyst implantation. *Proceedings of the National Academy of Sciences* 1991 **88**(24), 11408-11412.
8. Kumar V, Green S, Sftack G, Berry M, Jinn J, Chambon P. Functional domains of the human estrogen receptor. Cell.1987; **51**:941–945.
9. Kuiper GG, Enmark E, Pelto-Huikko M, Nilsson S, Gustafsson JA. Cloning of a novel estrogen receptor expressed in rat prostate and ovary. *Proc Nat Acad Sci U S A.*1996; *93*:5925–5930.
10. Filardo EJ, Quinn JA, Bland KI, Frackelton Jr AR. Estrogen-induced activation of Era–1 and Erk–2 requires the G protein-coupled receptor homolog, GPR30, and occurs via trans-

activation of the epidermal growth factor receptor through release of HB-EGF. *Mol Endocrinol.* 2000;14:1649–1660.

11. Prossnitz ER, Arterburn, JB, Sklar LA. GPR30: A G protein-coupled receptor for estrogen. *Molecular and cellular endocrinology* 2007, 265-266, 138–142. https://doi.org/10.1016/j.mce.2006.12.010
12. Hou Q, Gorski J. Estrogen receptor and progesterone receptor genes are expressed differentially in mouse embryos during preimplantation development. *Proc Nat Acad Sci U S A* 1993 90(20):9460-4.
13. Chang KT, Su YT, Thai YR, Lan KC, Hsuuw YD, Kang HY, Chan WH, Huang FJ. High levels estradiol affect blastocyst implantation and post-implantation development directly in mice. *Biomed J.* 2021 Jan 16:S2319-4170(21)00003-2. doi: 10.1016/j.bj.2021.01.004
14. Hou Q, Paria BC, Mui C, Dey SK, Gorski J. Immunolocalization of estrogen receptor protein in the mouse blastocyst during normal and delayed implantation. *Proc Natl Acad Sci U S A.* 1996 Mar 19;**93**(6):2376-81. doi: 10.1073/pnas.93.6.2376. PMID: 8637881; PMCID: PMC39804.
15. Cheng X, Xu S, Song C, He L, Lian X, Liu Y, Wei J, Pang L, Wang S. Roles of ERα during mouse trophectoderm lineage differentiation: revealed by antagonist and agonist of ERα. *Dev Growth Differ.* 2016 Apr;58(3):327-38. doi: 10.1111/dgd.12276. Epub 2016 Apr 1. PMID: 27037955.
16. Saito K, Furukawa E, Kobayashi M, Fukui E, Yoshizawa M, Matsumoto H. Degradation of estrogen receptor α in activated blastocysts is associated with implantation in the delayed implantation mouse model. *Mol Hum Reprod.* 2014 May;20(5):384-91. doi: 10.1093/molehr/gau004. Epub 2014 Jan 16. PMID: 24442344.
17. Dupont S, Krust A, Gansmuller A, Dierich A, Chambon P, Mark M. Effect of single and compound knockouts of estrogen receptors alpha (ER alpha) and beta (ER beta) on mouse reproductive phenotypes. *Development*. 2000 Oct;127 (19):4277-91. doi: 10.1242/dev.127.19.4277. PMID: 10976058.

18. Walker VR, Korach KS. Estrogen receptor knockout mice as a model for endocrine research. ILAR J. 2004;45(4):455-61. doi: 10.1093/ilar.45.4.455. PMID: 15454684.
19. Gorski J, Hou Q. Embryonic estrogen receptors: do they have a physiological function? Environ Health Perspect. 1995 Oct;103 Suppl 7(Suppl 7):69-72. doi: 10.1289/ehp.95103s769. PMID: 8593878; PMCID: PMC1518884.
20. Paria BC, Lim H, Wang XN, Liehr J, Das SK, Dey SK. Coordination of Differential Effects of Primary Estrogen and Catecholestrogen on Two Distinct Targets Mediates Embryo Implantation in the Mouse, *Endocrinology*, Volume 139, Issue 12, 1 December 1998, Pages 5235–5246, https://doi.org/10.1210/endo.139.12.6386
21. Paria BC, Chakraborty C, Dey SK. Catechol estrogen formation in the mouse uterus and its role in implantation, *Molecular and Cellular Endocrinology,* Volume 69, Issue 1, 1990, Pages 25-32, ISSN 0303-7207, https://doi.org/10.1016/0303-7207(90)90085-M.
22. Hernández N, López-Morató M, Perianes MJ, Sánchez-Mateos S, Casas-Rua V, Domínguez-Arroyo JA, Sánchez-Margallo FM, Álvarez IS. 4-Hydroxyestradiol improves mouse embryo quality, epidermal growth factor-binding capability in vitro and implantation rates. *Mol Hum Reprod.* 2021 Feb 5;27(2):gaaa075. doi: 10.1093/molehr/gaaa075. PMID: 33237288.
23. Dickmann Z, Gupta JS, Dey SK. Does "blastocyst estrogen" initiate implantation? *Science.* 1977 Feb 18;195 (4279):687-8. doi: 10.1126/science.841306. PMID: 841306.
24. Valbuena D, Martin J, de Pablo JL, Remohí J, Pellicer A, Simón C. Increasing levels of estradiol are deleterious to embryonic implantation because they directly affect the embryo. *Fertil Steril.* 2001 Nov;76(5):962-8. doi: 10.1016/s0015-0282(01)02018-0. PMID: 11704118.
25. Deglincerti A, Croft GF, Pietila LN, Zernicka-Goetz M, Siggia ED, Brivanlou AH. Self-organization of the in vitro attached human embryo. *Nature.* 2016 May 12;533(7602):251-4. doi: 10.1038/nature17948. Epub 2016 May 4. PMID: 27144363.

26. Bedzhov I, Leung CY, Bialecka M, Zernicka-Goetz M. In vitro culture of mouse blastocysts beyond the implantation stages. *Nat Protoc.* 2014 Dec;9(12):2732-9. doi: 10.1038/nprot.2014.186. Epub 2014 Oct 30. PMID: 25356584.
27. Shahbazi MN, Jedrusik A, Vuoristo S, Recher G, Hupalowska A, Bolton V, Fogarty NNM, Campbell A, Devito L, Ilic D, Khalaf Y, Niakan KK, et al. Self-organization of the human embryo in the absence of maternal tissues. *Nat Cell Biol.* 2016 Jun;18(6):700-708. doi: 10.1038/ncb3347. Epub 2016 May 4. PMID: 27144686; PMCID: PMC5049689.
28. Logsdon DM, Grimm CK, West RC, Engelhorn HJ, Kile R, Reed LC, Swain JE, Katz-Jaffe M, Schoolcraft WB, Krisher RL, Yuan Y. Maternal physiology and blastocyst morphology are correlated with an inherent difference in peri-implantation human embryo development. *Fertil Steril.* 2022 Mar 30:S0015-0282(22)00137-6. doi: 10.1016/j.fertnstert.2022.02.018. Epub ahead of print. PMID: 35367060.
29. Institute of Laboratory Animal Resources (ILAR). Guide for the care and use of laboratory animals. [8th] ed. Washington, D.C.: National Academy Press, 2011.
30. Ermisch AF, Herrick JR, Pasquariello R, Dyer MC, Lyons SM, Broeckling CD, Rajput SK, Schoolcraft WB, Krisher RL. A novel culture medium with reduced nutrient concentrations supports the development and viability of mouse embryos. Sci Rep. 2020 Jun 9;10(1):9263. doi: 10.1038/s41598-020-66019-4. PMID: 32518371; PMCID: PMC7283311.
31. Herrick JR, Strauss KJ, Schneiderman A, Rawlins M, Stevens J, Schoolcraft WB *et al.* The beneficial effects of reduced magnesium during the oocyte-to-embryo transition are conserved in mice, domestic cats and humans. Reproduction, Fertility and Development 2015;27:323-31.
32. Schindelin J, Arganda-Carreras I, Frise E, Kaynig V, Longair M, Pietzsch T et al. Fiji: an open-source platform for biological-image analysis. Nature Methods 2012; 9:676-82.
33. Logsdon DM, Ermisch AF, Kile R, Schoolcraft WB, Krisher RL, Yuan Y. Egg cylinder development during in vitro extended embryo culture predicts the post transfer developmental potential of mouse blastocysts. J Assist Reprod Genet. 2020

Apr;37(4):747-752. doi: 10.1007/s10815-020-01714-9. Epub 2020 Feb 18. PMID: 32072379; PMCID: PMC7183034.

34. Hayward MA, Mitchell TA, Shapiro DJ. Induction of estrogen receptor and reversal of the nuclear/cytoplasmic receptor ratio during vitellogenin synthesis and withdrawal in Xenopus laevis. J Biol Chem. 1980 Dec 10;255 (23):11308-12. PMID: 7440543.
35. Gao Y, Liu X, Tang B, Li C, Kou Z, Li L, Liu W, Wu Y, Kou X, Li J, Zhao Y, Yin J, Wang H, Chen S, Liao L, Gao S. Protein Expression Landscape of Mouse Embryos during Pre-implantation Development. Cell Rep. 2017 Dec 26;21(13):3957-3969. doi: 10.1016/j.celrep.2017.11.111. PMID: 29281840.
36. Chen F, Ma B, Lin Y, Luo X, Xu T, Zhang Y, Chen F, Li Y, Zhang Y, Luo B, Zhang Q, Xie X. Comparative maternal protein profiling of mouse biparental and uniparental embryos. Gigascience. 2022 Sep 3;11:giac084. doi: 10.1093/gigascience/giac084. PMID: 36056732; PMCID: PMC9440387.
37. Strömstedt M, Keeney DS, Waterman MR, Paria BC, Conley AJ, Dey SK. Preimplantation mouse blastocysts fail to express CYP genes required for estrogen biosynthesis. Mol Reprod Dev. 1996 Apr;43 (4):428-36. doi: 10.1002/(SICI)1098-2795(199604)43:4<428::AID-MRD4>3.0.CO;2-R. PMID: 9052933. Yu LL, Qu T, Zhang SM, Yuan DZ, Xu Q, Zhang JH, He
38. Dey SK, Dickmann Z. Δ^5-3^2-Hydroxysteroid Dehydrogenase Activity in Rat Embryos on Days 1 Through 7 of Pregnancy, *Endocrinology*, Volume 95, Issue 1, 1 July 1974, Pages 321–322, https://doi.org/10.1210/endo-95-1-321
39. Hoversland RC, Dey SK, Johnson DC. Aromatase activity in the rabbit blastocyst. J Reprod Fertil. 1982 Sep;66(1):259-63. doi: 10.1530/jrf.0.0660259. PMID: 7120190.
40. Dey SK, Dickmann Z. Estradiol-17β-hydroxysteroid dehydrogenase activity in preimplantation rat embryos, Steroids,Volume 24, Issue 1,1974,Pages 57-62,ISSN 0039-128X,https://doi.org/10.1016/0039-128X(74)90045-2.

41. Gene Expression Omnibus (GEO) National Center for Biotechnology Information. Bethesda, MD; 2010, 17βHSD in human blastocysts: https://www.ncbi.nlm.nih.gov/geo/query/acc.cgi?acc=GSM456658 CYP19A1 in human blastocysts: https://www.ncbi.nlm.nih.gov/geo/tools/profileGraph.cgi?ID=GDS3959:203475_at Accessed on 12/29/2022
42. Petropoulos S, Edsgärd D, Reinius B, Deng Q, Panula SP, Codeluppi S, Plaza Reyes A, Linnarsson S, Sandberg R, Lanner F. Single-Cell RNA-Seq Reveals Lineage and X Chromosome Dynamics in Human Preimplantation Embryos. Cell. 2016 May 5;165(4):1012-26. doi: 10.1016/j.cell.2016.03.023. Epub 2016 Apr 7. Erratum in: Cell. 2016 Sep 22;167(1):285. PMID: 27062923; PMCID: PMC4868821.
43. Miller KF, Pursel VG. Absorption of compounds in medium by the oil covering microdrop cultures. Gamete Res. 1987 May;17(1):57-61. doi: 10.1002/mrd.1120170107. PMID: 3148538.
44. Yoshinaga K, Adams CE. Delayed implantation in the spayed, progesterone treated adult mouse. J Reprod Fertil. 1966 Dec;12(3):593-5. doi: 10.1530/jrf.0.0120593. PMID: 5928277.
45. Ptak GE, Tacconi E, Czernik M, Toschi P, Modlinski JA, Loi P. Embryonic diapause is conserved across mammals. PLoS One. 2012;7(3):e33027. doi: 10.1371/journal.pone.0033027. Epub 2012 Mar 12. PMID: 22427933; PMCID: PMC3299720.
46. Liu Y, Jones C, Coward K. An investigation of mechanisms underlying mouse blastocyst hatching: a ribonucleic acid sequencing study. F S Sci. 2022 Feb;3(1):35-48. doi: 10.1016/j.xfss.2021.12.003. Epub 2021 Dec 22. PMID: 35559994.
47. Segnitz B, Gehring U. Subunit structure of the nonactivated human estrogen receptor. Proc Natl Acad Sci U S A. 1995 Mar 14;92(6):2179-83. doi: 10.1073/pnas.92.6.2179. PMID: 7892243; PMCID: PMC42447.
48. Echeverria PC, Picard D. Molecular chaperones, essential partners of steroid hormone receptors for activity and mobility. Biochim Biophys Acta. 2010 Jun;1803(6):641-9. doi: 10.1016/j.bbamcr.2009.11.012. Epub 2009 Dec 16. PMID: 20006655.

49. Kushner PJ, Agard DA, Greene GL, Scanlan TS, Shiau AK, Uht RM, Webb P. Estrogen receptor pathways to AP-1. J Steroid Biochem Mol Biol. 2000 Nov 30;74(5):311-7. doi: 10.1016/s0960-0760(00)00108-4. PMID: 11162939.

50. Moriyama T, Yoneda Y, Oka M, Yamada M. Transportin-2 plays a critical role in nucleocytoplasmic shuttling of oestrogen receptor-α. Sci Rep. 2020 Oct 29;10(1):18640. doi: 10.1038/s41598-020-75631-3. PMID: 33122699; PMCID: PMC7596556.

51. Zivadinovic D, Watson CS. (2005). Membrane estrogen receptor-alpha levels predict estrogen-induced ERK1/2 activation in MCF-7 cells. *Breast cancer research: BCR*, *7*(1), R130–R144. https://doi.org/10.1186/bcr959

52. Kahlert S, Nuedling S, van Eickels M, Vetter H, Meyer R, Grohe C. Estrogen receptor alpha rapidly activates the IGF-1 receptor pathway. J Biol Chem. 2000 Jun 16;275(24):18447-53. doi: 10.1074/jbc.M910345199. PMID: 10749889.

53. Lee JS, Tocheny CE, Shaw LM. The Insulin-like Growth Factor Signaling Pathway in Breast Cancer: An Elusive Therapeutic Target. Life (Basel). 2022 Nov 29;12(12):1992. doi: 10.3390/life12121992. PMID: 36556357; PMCID: PMC9782138

54. Sampayo RG, Toscani AM, Rubashkin MG, Thi K, Masullo LA, Violi IL, Lakins JN, Cáceres A, Hines WC, Coluccio Leskow F, Stefani FD, Chialvo DR, et al. Fibronectin rescues estrogen receptor α from lysosomal degradation in breast cancer cells. *J Cell Biol.* 2018 Aug 6;217(8):2777-2798. doi: 10.1083/jcb.201703037. Epub 2018 Jul 6. PMID: 29980625; PMCID: PMC6080927.

55. Corson LB, Yamanaka Y, Lai KM, Rossant J. Spatial and temporal patterns of ERK signaling during mouse embryogenesis. *Development.* 2003 Oct;130(19):4527-37. doi: 10.1242/dev.00669. PMID: 12925581.

56. Saba-El-Leil MK, Vella FD, Vernay B, Voisin L, Chen L, Labrecque N, Ang SL, Meloche S. An essential function of the mitogen-activated protein kinase Erk2 in mouse trophoblast development. *EMBO* Rep. 2003 Oct;4(10):964-8. doi: 10.1038/sj.embor.embor939. Epub 2003 Sep 19. PMID: 14502223; PMCID: PMC1326397.

57. Chang L, Karin M. Mammalian MAP kinase signalling cascades. *Nature* 410, 37–40 (2001). https://doi.org/10.1038/35065000\

CHAPTER III: MATERNAL PHYSIOLOGY AND BLASTOCYST MORPHOLOGY CORRELATE WITH AN INHERENT DIFFERENCE IN PERI-IMPLANTATION HUMAN EMBRYO DEVELOPMENT

This work was published in the journal Fertility and Sterility in June, 2022

Summary

Objective: To determine what patient and embryo characteristics are correlated with the developmental potential of the peri-implantation embryo.

Design: Retrospective study.

Setting: Research laboratory.

Patients: Six hundred fifty-one cryopreserved human blastocysts donated for research with informed patient consent.

Interventions: Not applicable.

Main Outcome Measures: Blastocyst attachment to fibronectin-coated plates, trophectoderm outgrowth area, epiblast cell number, total cell number, human chorionic gonadotropin secretion.

Results: Patients' body mass index, age, follicle-stimulating hormone: luteinizing hormone ratio on menstrual cycle day 3, antral follicle count on menstrual cycle day 3, antimüllerian hormone level on menstrual cycle day 3, and blastocyst morphological grade were correlated with peri-implantation development outcomes. After controlling for good-quality morphological grades, blastocysts from patients of advanced maternal age developed fewer epiblast cells than blastocysts from younger patients.

Conclusions: Extended embryo culture during the peri-implantation period mirrors several disparities in fertility treatment outcome that we see clinically, including those from patients with advanced maternal age, high body mass index, and low ovarian reserve and from embryos with

lower-quality morphological grades. This model system may be useful by providing an alternative or more sensitive endpoint assessment in studying patient, clinical, or laboratory factors that may influence preimplantation embryo developmental potential.

Introduction

Approximately 40%–50% of human embryos are lost before a clinically diagnosable pregnancy, 75% of which are believed to be a result of implantation failure (1, 2). Because of the cryptic nature of human embryo implantation, it is difficult to understand why a large proportion of pregnancies are lost during implantation. Advances in human extended embryo culture (EEC) to embryonic day 14 (ED 14) (3, 4) have allowed researchers to study peri-implantation-stage embryos in the absence of maternal tissues (5, 6, 7). In the mouse, development in the EEC system is indicative of fetal developmental potential and can act as a proxy for surgical embryo transfers (8, 9). If peri-implantation embryo development in the absence of maternal tissues correlates with live birth outcomes similarly in human embryos, the EEC system would be valuable for providing additional information about how fertility treatments and maternal physiology may affect implantation.

Clinicians use several indicators to assess a woman's fertility (10), not only to estimate ovarian reserve but also to predict live birth outcomes (11, 12, 13). However, the complex relationship between the uterine environment and embryo quality, which is affected by both maternal and paternal physiology, makes it difficult to determine which factors influence the potential of having a live birth. Identifying relationships between maternal physiological markers and the peri-implantation developmental potential of the embryo would provide valuable predictive power to guide clinicians to make more informed decisions for patients undergoing in vitro fertilization (IVF). In addition, experimental manipulations can be performed in EEC without compromising patient care in the clinical setting. For example, this system has already been used to provide

meaningful data to improve human embryo culture conditions and to evaluate the safety of cryostorage with regard to the developmental potential of human blastocysts (14, 15, 16).

A retrospective analysis of all human blastocysts in EEC in our laboratory over the course of 2 years was performed to identify relationships between maternal physiology and the peri-implantation development of blastocysts. It was hypothesized that maternal physiology at oocyte retrieval, including age, body mass index (BMI), and ovarian reserve, influences the developmental capacity of the resulting embryos during the peri-implantation period. In this study, previously established EEC quality markers were examined—total nuclei, epiblast cell number, outgrowth area, and human chorionic gonadotropin (hCG) production in spent media (5, 14)—in a historical data set compiled from the EEC of 651 human blastocysts donated to research. Statistical assessments were then performed to look for correlations between these quantitative developmental potential parameters and patient characteristics commonly used to assess fertility.

Methods

All reagents were purchased from Sigma Aldrich (St. Louis, MO) unless otherwise stated.

Ethics Statement

Surplus cryopreserved human blastocysts were donated with informed consent from patients after completion of their infertility treatment in our clinic. No embryos were cultured beyond ED 14, in agreement with the “14-day rule” that was in place during the course of the experiments. The study was approved by the Western Institutional Review Board-Copernicus Group, formally the Western Institutional Review Board (no. 1179872).

Extended Embryo Culture

The embryos were kept in culture for varying amounts of time from EEC day (EECD) 3 up to EECD7 depending on the experiment. In many experiments, culture was concluded on EECD5 as a standardized endpoint for epiblast cell number and total cell number staining. In experiments aimed to explore transcriptomic and epigenetic changes during the peri-implantation period, culture was concluded on EECD 3, 5, or 7. Early experiments were concluded on EECD 2, 4, or 6, and thus, very few data points were collected for those time points. Extended embryo culture experiments were performed as previously described (3, 4, 5, 17). Vitrified embryos were warmed according to a standard warming protocol and recovered in equilibrated 20-µL drops of Sage BM (Origio, Cooper Surgical, Trumbull, CT) supplemented with 10% v/v Quinn's Advantage SPS (Origio, Cooper Surgical) under mineral oil (Spectrum, New Brunswick, NJ) for 2 hours at 37 °C in 6.5% O2 and 7.5% CO2, which mimics 5% O2 and 6% CO2 at sea level.

After recovery, the embryos were briefly treated with acidic Tyrode solution to remove the zona pellucida, washed in in vitro culture 1 (IVC1, Cell Guidance Systems, St. Louis, MO), and placed into EEC. The embryos were cultured in 8-well ibi-Treat microslides (Ibidi, Martinsried, Germany) coated with fibronectin from human plasma (30 µg/mL) in 300 µL of IVC1 or in vitro culture 2 (IVC2, Cell Guidance Systems) for the duration of EEC. The embryos were cultured for 48 hours in equilibrated IVC1 medium without disturbance. On the second day of EEC, the embryos were examined for attachment to the fibronectin-coated dish by gently moving the dish and watching for movement of the embryo. If the embryo was attached, 150 µL of medium was replaced with fresh IVC2 on each day of EEC. While the medium was being exchanged, the embryos were observed for any movement in case they were detached in the process of medium exchange. Any unattached embryos were kept in culture in IVC1 until the conclusion of the experiment in case of later attachment, although late attachment was not quantified in this data set past 72 hours in extended culture. All embryos in EEC were cultured in atmospheric O2

(21%) and 7.5% CO2 at 37 °C. Any embryos that failed to attach for the duration of EEC or that detached and/or disintegrated were discarded from the final data set.

Measurement of Outgrowth Area

Images of embryos were obtained each day of EEC with an Olympus DP22 camera (Olympus, Melville, NY) attached to a stereo microscope. The images were then imported into open source software FIJI (a version of ImageJ) (18), and the edges of trophoblast outgrowth were outlined with the use of the freehand selection tool. Outgrowth areas were measured in arbitrary units and converted to square millimeters with the use of the scale bar as a reference.

Quantification of Human Chorionic Gonadotropin

If the embryos were attached, 150 µL of spent medium was collected and snap frozen in liquid nitrogen during each medium exchange with IVC2 after 24, 48, 72, 96, and 120 hours postattachment (h. p. a.). Spent medium was analyzed for hCG by electrochemiluminescence with a Roche Cobas e601 analyzer (Roche, Indianapolis, IN), and the hCG content was reported in mIU/mL.

Immunofluorescence Staining and Confocal Microscopy

At the conclusion of culture, the embryos were fixed with 4% paraformaldehyde (Electron Microscopy Science, Hatfield, PA) in phosphate-buffered saline (PBS) for 20 minutes. After fixation, the embryos were washed 3 times in PBS with 0.1% Tween 20 (PBST, Fisher Scientific, Fair Lawn, NJ) for 10 minutes and stored in PBST at 4 °C. The embryos were stained with antibodies against POU5F1 (sc-5279, Santa Cruz Biotechnology, Dallas, TX), NucBlue (Hoechst 33342, R37605, Life Technologies), and rhodamine phalloidin (Cytoskeleton, Denver, CO) to visualize the F-actin cytoskeleton. The embryos were washed in PBST and permeabilized with PBS + 0.5% (v/v) Triton X-100. The embryos were washed and held in blocking buffer containing 10% (v/v) fetal calf serum (Cytiva Hyclone, SH3007002E, Marlborough, MA), 3%

bovine serum albumin (MP Biomedicals MFCD00130384, Irvine, CA), and 0.1% Tween 20 in PBS overnight and subsequently moved to primary antibodies (1:200) diluted in blocking buffer overnight. The embryos were washed 3 times for 10 minutes and moved to secondary antibody Alexa Fluor 488 (1:200, A-11001, Invitrogen, Carlsbad, CA), NucBlue, and rhodamine phalloidin (1:200) diluted in blocking buffer overnight. The embryos were washed 3 times and mounted using 5–10 μL of ProLong Diamond Antifade (ThermoFisher, Waltham, MA) mountant with 4, 6-diamino-2-phenylindole.

Imaging experiments were performed with a 3i Marianas inverted spinning disk confocal microscope, as previously described (8, 14). The images were then analyzed for epiblast cell number with the surface tool and object identification within the surface of approximately 5–10 μM in diameter with Imaris ×64 9.20 software (Oxford Instruments, Abingdon, UK).

Patient Data

Patient data were obtained retrospectively from scanned patient records from an electronic medical record system. Embryos were used from a mix of egg donors (n = 123), nondonor infertility patients (n = 427), and embryos that were deidentified or whose donor status was not available (n = 101) (Figure 3.5, available online). Data from these groups were analyzed both together and separately. Diagnoses of fertility patients were categorized into unexplained infertility (n = 211), ovulation dysfunction (Ovulation Dys., n = 25), polycystic ovary syndrome (n = 56), advanced maternal age (AMA, n = 159), male factor (n = 127), recurrent implantation failure (n = 21), recurrent pregnancy loss (n = 65), diminished ovarian reserve (n = 87), history of endometriosis (n = 16), and uterine or tubal factors, including abnormalities and blockages (n = 84), and were used for nondonor, autologous, oocyte-derived embryo comparisons only. On menstrual cycle day 3, patient serum was analyzed for estradiol (E2, pg/mL), follicle-stimulating hormone (FSH, mIU/mL), luteinizing hormone (LH, mIU/mL), and antimüllerian hormone (AMH, ng/mL) concentrations, and antral follicle count (AFC) was determined by transvaginal

ultrasound. Patients with multiple diagnoses were included separately in the analysis of each diagnosis. Regardless of their *International Classification of Diseases*, 10th revision designation, patients >37 years old were considered of AMA for all AMA vs. young comparisons. Patient age and BMI were noted on the day of oocyte retrieval.

Embryo Data

Embryo age was reported beginning on ED 0 on the day of retrieval, and experienced embryologists assessed the embryos according to embryo stage, degree of expansion, inner cell mass grade, and trophectoderm (TE) grade using the Gardner embryo grading scale (19). The embryos ranged from ED 5–ED 7 (ED 5, n = 322; ED 6, n = 232; ED 7, n = 8). In total, 651 embryos comprised the data set; 313 embryos did not undergo preimplantation genetic testing for aneuploidy (PGT-A); 194 did undergo PGT-A; and whether or not the remaining 144 had undergone PGT-A was unknown, either because they were deidentified upon their donation to research or their PGT-A records were not available. Of the embryos that did undergo PGT-A, 34 were euploid and 160 were aneuploid. Of our aged (>37 years) nondonor population, 88 embryos were aneuploid, 9 were euploid, 10 were nonbiopsied, and 24 were of unknown PGT-A status. Of our young (<35 years) nondonor population, 23 embryos were aneuploid, 5 were euploid, 100 were nonbiopsied, and 33 were of unknown PGT-A status.

Statistical Analysis

Summary statistics, including means, standard deviations, minimum values, and maximum values for both the patient and embryo predictor data as well as the EEC outcomes were calculated by Microsoft Excel. Additionally, the mean ± SEM was calculated for all pooled EEC outcomes with the use of GraphPad Prism 8.4.2.

Correlative analyses between continuous variables were performed with the use of a Spearman's nonparametric correlation matrix, and significance was noted at $P<.05$. Because

the numbers of days in EEC within each EEC outcome were correlated, one representative day in EEC was used for each comparison to maximize the number for each comparison while keeping the matrix as simple as possible. Thus, staining outcomes, including total cell nuclei and epiblast cell number, are represented by embryos fixed on EECD5. Human chorionic gonadotropin in spent media is represented by spent media collected 24 h. p. a., and outgrowth areas are represented by embryos measured on EECD3. The resulting comparisons for each Spearman's correlation matrix were as follows: maternal age, BMI, AFC, E2, FSH, LH, FSH:LH, [hCG] 24 h. p. a., outgrowth area on EECD3, total cell nuclei on EECD5, and epiblast cell number on EECD5. Correlation matrices were computed on the entire data set and for donors and nondonors separately with the use of GraphPad Prism 8.4.2. The direction and strength of the relationship between 2 variables is represented as rho, whereas a negative value reflects a negative relationship and a positive value reflects a positive relationship. All P values and sample sizes have been included for each correlation matrix in the Supplemental Information. Significance was noted at $P<.05$. Many of the independent and dependent variables exhibited multicollinearity and would interfere with a multivariate analysis. Significant P values between 2 patient predictors or 2 extended culture outcomes highlight multicollinearity.

For binomial variables with categorical predictors, we used the $\chi 2$ test or Fisher's exact test with the use of GraphPad Prism 8.4.2. All continuous variable data were checked for normality with the Shapiro-Wilk test. For parametric continuous variables with categorical predictors, we used Student's t-test or ANOVA where appropriate. For nonparametric comparisons between continuous variables from categorical predictors, we used the Mann-Whitney U test or Kruskal-Wallis test where appropriate with the use of GraphPad Prism 8.4.2. Significance was noted at $P<.05$.

Results

Summary Statistics for the Dataset

First, we quantified all summary statistics for each embryo cultured in our EEC system (Table 3.1) and for patient predictors (Table 3.2). On average, 78.5% of embryos were able to attach to fibronectin-coated dishes within 48 hours after being plated. After 72 hours, 88.8% of embryos were attached (Figure 3.6).

Upon attachment, the embryos began to collapse, differentiate, and outgrow (Figure 3.6A, left panel). Over the course of 7 days in EEC (ED 12–14), the embryos showed continued growth, as measured by total area of the trophoblast outgrowth (Figure 3.6B). The total number of cell nuclei was stable from EECD3–EECD6 but increased on EECD7 (Figure 3.6C). After attachment, the embryos secreted hCG from differentiated syncytiotrophoblast (5) (Figure 3.6D). Approximately 54% of embryos that were stained contained an epiblast, as determined by POU5F1-positive staining (Figure 3.6E). Epiblast cell number did not vary significantly during the course of EEC, likely due to the variability in embryo quality and reduced sample size for some days in EEC (Figure 3.6E).

Extended Culture Outcomes According to Embryo Stage and Grade

In assessing EEC outcomes according to embryo grade, no significance was noted for any parameter according to inner cell mass grade, embryonic day, or level of expansion alone. Outgrowth areas for embryos with TE score C were significantly reduced compared with those with TE scores A or B (Figure 3.7, available online). Historical data from our clinic show that ED 5 euploid blastocysts of at least grade 3BB (good quality) yielded a live birth rate of at least 65%, whereas ED 6 euploid blastocysts either fully hatched or of grade 3AA or below (fair quality) yielded a live birth rate of 50% at best (Fig. 3.1A). In comparison of the EEC outcomes between these 2 groups, the good-quality blastocysts had increased outgrowth areas compared with the fair-quality blastocysts (Fig. 3.1B). No differences were found between embryo quality

and epiblast cell number (Fig. 3.1C), [hCG] in spent media (Fig. 3.1D), or total cell nuclei (Fig. 3.1E).

Correlations Within the Entire Dataset

All patient physiological predictors (age, BMI, E2, FSH, LH, FSH: LH, AMH, and AFC) were compared with EEC outcomes (outgrowth area, total cell nuclei, [hCG], and epiblast cell number) by Spearman's correlation. Many patient predictors and EEC outcomes were highly correlated within each other (e.g., outgrowth area vs. total cell nuclei; Table 3.3). These correlations are beyond the scope of this study and will not be discussed further. Here we focus on the correlations between patient predictors and EEC outcomes. Age and outgrowth area (rho = −0.14, P =.0110), age and [hCG] (rho = −0.26, P=.0005), BMI and epiblast cell number (rho = −0.33, P=.0298), and FSH:LH and total nuclei (rho = −0.34, P=.0039) were negatively correlated. Positive correlations were found between AFC and [hCG] (rho = 0.18, P=.0106) and between BMI and total nuclei (rho = 0.23, P=.0468) (Fig. 3.2).

Extended Culture Outcomes in Nondonor Fertility Patients

We examined the data for donors and nondonors separately. Outgrowth areas were larger for embryos from donors than for embryos from nondonor fertility patients (Fig. 3.3A). However, when nondonor fertility patients were separated by diagnosis, only the outgrowth areas for embryos from patients with AMA were significantly reduced compared with donor-derived embryo outgrowth areas (P=.0089) (Fig. 3.3B). When correlations between continuous variables for nondonor fertility patients were examined, significance was noted between 3 ovarian reserve test predictors (FSH:LH, AMH, and AFC) and total cell nuclei (rho = −0.3563, P=.0031; rho = 0.2507, P=.0363; rho = 0.2554, P=.0329, respectively) (Fig. 3.3C). Additional correlations between 2 EEC outcomes or 2 patient predictors can be found in Table 3.4. Rho values were similar between correlation matrices from the entire data set (Fig. 3.2 and Supplemental

Table 3), donors (Figure 3.8 and Table 3.4), and nondonor fertility patients (Fig. 3.3C and Table 3.5).

Maternal age vs. outgrowth area was the most consistently significant patient predictor/EEC outcome pair across all data sets. Patients with AMA had significantly reduced outgrowth areas compared with young patients across the entire data set (Fig. 3.4A). Embryos from AMA nondonor fertility patients also showed reduced outgrowth areas compared with embryos from younger nondonor fertility patients (Fig. 3.4B). Interestingly, even in healthy donors, outgrowth areas were negatively correlated with donor age (rho = −0.3874, P<.0001) (Fig. 3.4C). Because AMA can affect preimplantation embryo development, we also performed an AMA vs. young comparison of EEC outcomes for good-quality embryos only (≥65% or higher live birth rate). Considering only good-quality embryos (Fig. 3.1A), epiblast cell number was greater in EEC embryos from young patients than in those from patients with AMA (P<.0001) (Fig. 3.4D and E).

Discussion

Embryo culture during the peri-implantation period enabled us to correlate patient characteristics and preimplantation embryo morphology with EEC outcomes to evaluate the developmental potential of human blastocysts in a new way. It is important to note that strong correlations are not indicative of causal relationships, and they do not offer explanations for why embryo developmental potential may differ. Still, the relationships we describe here can provide meaningful insight into embryo quality based on patient physiology and embryo morphology.

In this retrospective analysis, many of the embryos from this data set were cultured primarily for other studies, and not every embryo was measured for every EEC outcome. Thus, the sample size is reduced for some outcomes, and this limits our ability to effectively explore them as they relate to patient diagnoses or PGT-A status. For example, most of the embryos used for this study either were chromosomally aneuploid (n = 160) or were not tested for aneuploidy (n = 313), making it impossible to compare the EEC outcomes between different PGT-A diagnoses.

Additionally, the average maternal age in the aneuploid group (37.97 years, compared with 30.75 years for the untested group and 35.94 years for the euploid group) is biased toward an older patient demographic, which, as we have shown here, affects peri-implantation development. Comparisons of outgrowth areas between young and aged nondonor fertility patients according to PGT-A status can be found in Figure 3.9 (available online). Therefore, we are limited in our analytic capabilities despite the large number of embryos in the data set, and interpretations regarding the direct comparison of AMA and young patients should be made with caution.

It is widely established that AMA affects fertility, primarily because of the lack of high-quality oocytes. In addition to low abundance due to diminished ovarian reserve following natural follicular atresia, oocytes from patients with AMA have altered mitochondrial membrane potential, mitochondrial copy number, and spindle formation (20, 21, 22). Live birth rates after IVF treatment decline with age (21, 23, 24). We showed that maternal age negatively affected the development of embryos in EEC, as evidenced by decreased outgrowth area and epiblast cell number. Several ovarian test results were significantly correlated with the total number of nuclei, including menstrual cycle day 3 AMH, AFC, and FSH:LH ratio (Fig. 3.3C). Advanced maternal age may affect these parameters (25) (Table 3.3); however, a high FSH:LH ratio is also correlated with poor IVF outcome, regardless of maternal age (26, 27, 28, 29). Because AMA is the most significant risk factor for aneuploidy and is significantly associated with pregnancy failure, aneuploidy status may be a confounding variable here that we are unable to control for. However, peri-implantation development in EEC declines with age for our nondonor fertility patients as well as healthy donors, mimicking the pattern that we would expect to see clinically.

Patients with high BMI are more likely to have early miscarriage and placental hypertrophy (30, 31, 32, 33, 34). In this study, BMI was negatively correlated with epiblast cell number but

positively correlated with total nuclei, suggesting increased growth in the trophoblast population that becomes the placenta. This is similar to what is seen clinically in women with high BMI, with decreased viability in early fetal development and inappropriate overgrowth in trophoblast cells (35). It is intriguing that this phenotype may be exhibited at this early time in development. In the mouse, both diet-induced as well as genetically induced obesity affects oocyte quality, as evidenced by impaired meiotic maturation, impaired spindle formation, oxidative stress, and induced epigenetic changes in deoxyribonucleic acid methylation, as well as histone modifications (36). Furthermore, the negative effects of increased maternal BMI on the quality of oocytes cannot be reversed by resumption of a control diet (37). Because all embryos in EEC experienced the same in vitro conditions, differences among patients with high BMI may be due to inherent differences in their oocytes and not to the uterine environment alone. We may be seeing altered peri-implantation development as a result of epigenetic programming at the oocyte stage. The consistency we see between clinical and EEC patterns further bolsters the argument that EEC provides an accurate model to predict embryonic developmental potential.

Conclusion

In conclusion, we have provided a detailed summary of the in vitro peri-implantation development of 651 human blastocysts in EEC. With the large number of embryos in our data set, we provide valuable information for clinicians regarding which maternal factors may affect the inherent developmental potential of a resulting blastocyst. The use of EEC to predict developmental potential also expands our ability to use donated human embryos for various research studies in a controlled in vitro environment. Finally, this system may help us better understand how maternal physiology and IVF interventions affect the developmental potential of embryos after embryo transfer and thus provide valuable information for further improvement of the current practice.

Notes

The authors thank the patients who donated embryos for research at the Colorado Center for Reproductive Medicine. We also thank the IVF Laboratory for their dedication to patient care and help with the disposition of embryos to research and the Clinical Laboratory for measurements of human chorionic gonadotropin. Finally, Radu Moldovan and Dominik Stich from the University of Colorado–Denver Advanced Light Microscopy Core were instrumental in helping with confocal microscopy.

A

	Embryo Grades
Good Quality n=268	D5 5AA D5 5BA D5 5AB D5 5BB D5 4AA D5 4BA D5 4AB D5 4BB D5 3AA D5 3BA D5 3AB D5 3BB
Fair Quality n=106	D6 3AA D6 3AB D6 2/3 D6 6AA D6 6BA D6 6AB D6 5BB D6 4BB D6 3BB D6 6BB D7 6BB D6 3BC D6 4BC D6 5BC

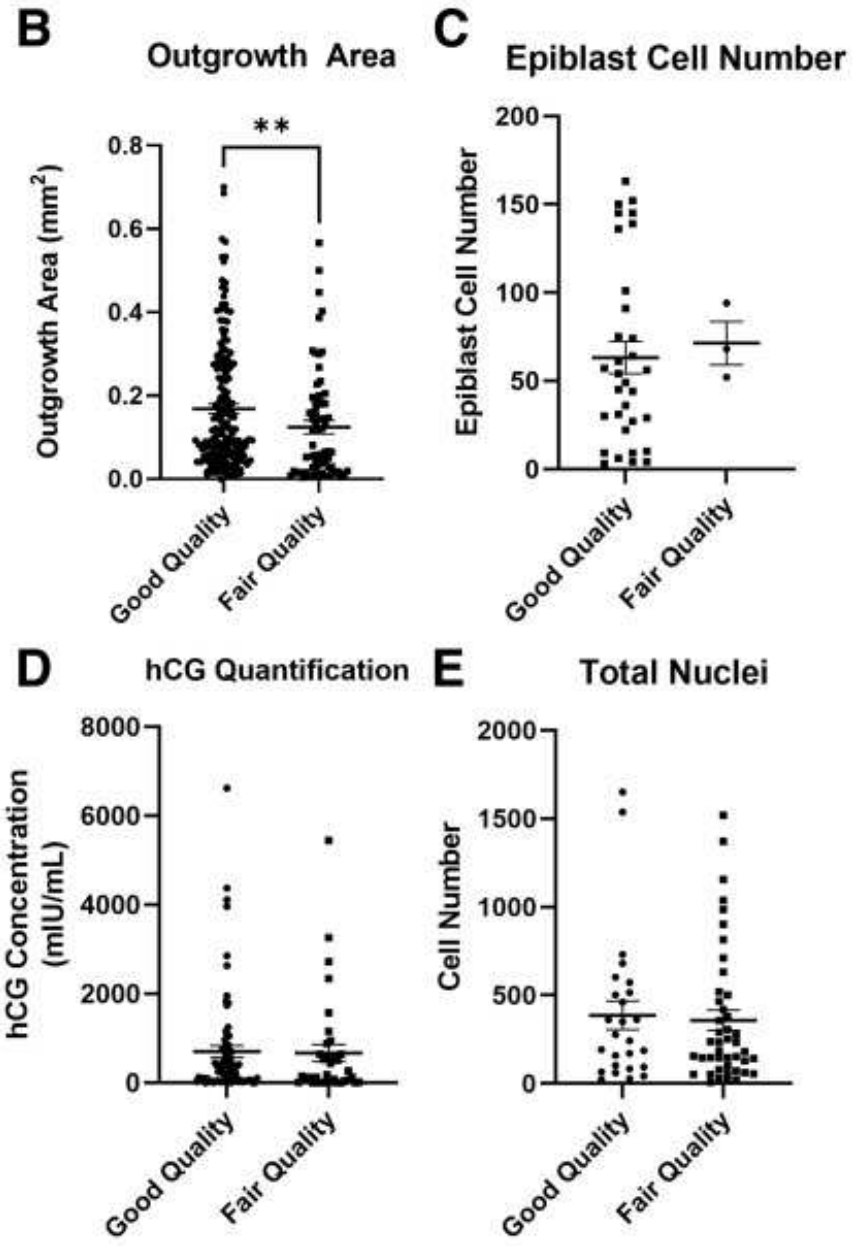

Figure 3.1. Peri-implantation development of embryos in extended embryo culture (EEC) based on morphological grade. (A) Embryo quality assignment as good (n = 268) or fair (n = 106) according to morphological grades with historical live birth rates of >65% (good) or <50% (fair). (B) Outgrowth areas (good n = 179, fair n = 68), (C) epiblast cell number according to cell nuclei stained positive for POU5F1 (good n = 32, fair n = 3), (D) human chorionic gonadotropin concentration (mIU/mL) in spent media (good n = 76, fair n = 36), and (E) total cell nuclei as determined by 4,6-diamino-2-phenylindole (good n = 26, fair n = 44), in good- and fair-quality embryos in EEC. Outgrowth areas were measured on day 3 during peri-implantation stage EEC. Total cell nuclei and epiblast cell number were measured on day 5 of peri-implantation stage EEC. Human chorionic gonadotropin concentration was measured 24 hours post attachment to fibronectin-coated dishes. Significance was noted at $**P<.01$ after a Mann-Whitney *U* test. D = embryonic day; hCG = human chorionic gonadotropin.

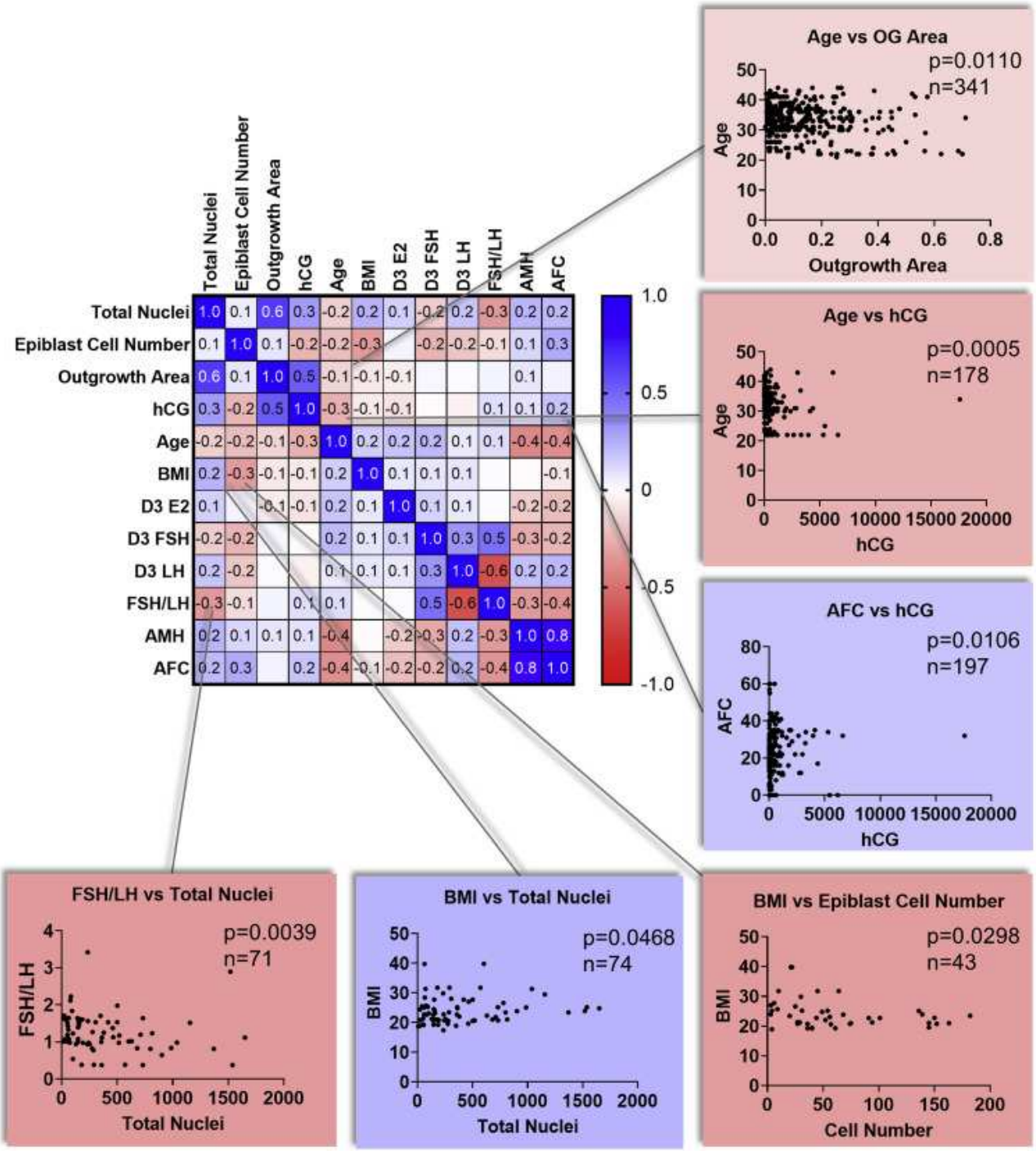

Figure 3.2. Correlations within the entire data set. Spearman's correlation matrix comparing patient predictors and extended embryo culture outcomes. Scale represents Spearman's *rho* values describing the positivity of each correlation. Significant correlations (*P*<.05) are pulled out and depicted as scatter plots along the correlation matrix. AFC = antral follicle count; AMH = antimüllerian hormone (ng/mL); BMI = body mass index; D3 = menstrual cycle day 3; E2 = estradiol (pg/mL); FSH = follicle-stimulating hormone (mIU/mL); hCG = human chorionic gonadotropin in spent media (mIU/mL); LH = luteinizing hormone (mIU/mL); OG area = outgrowth area (mm^2).

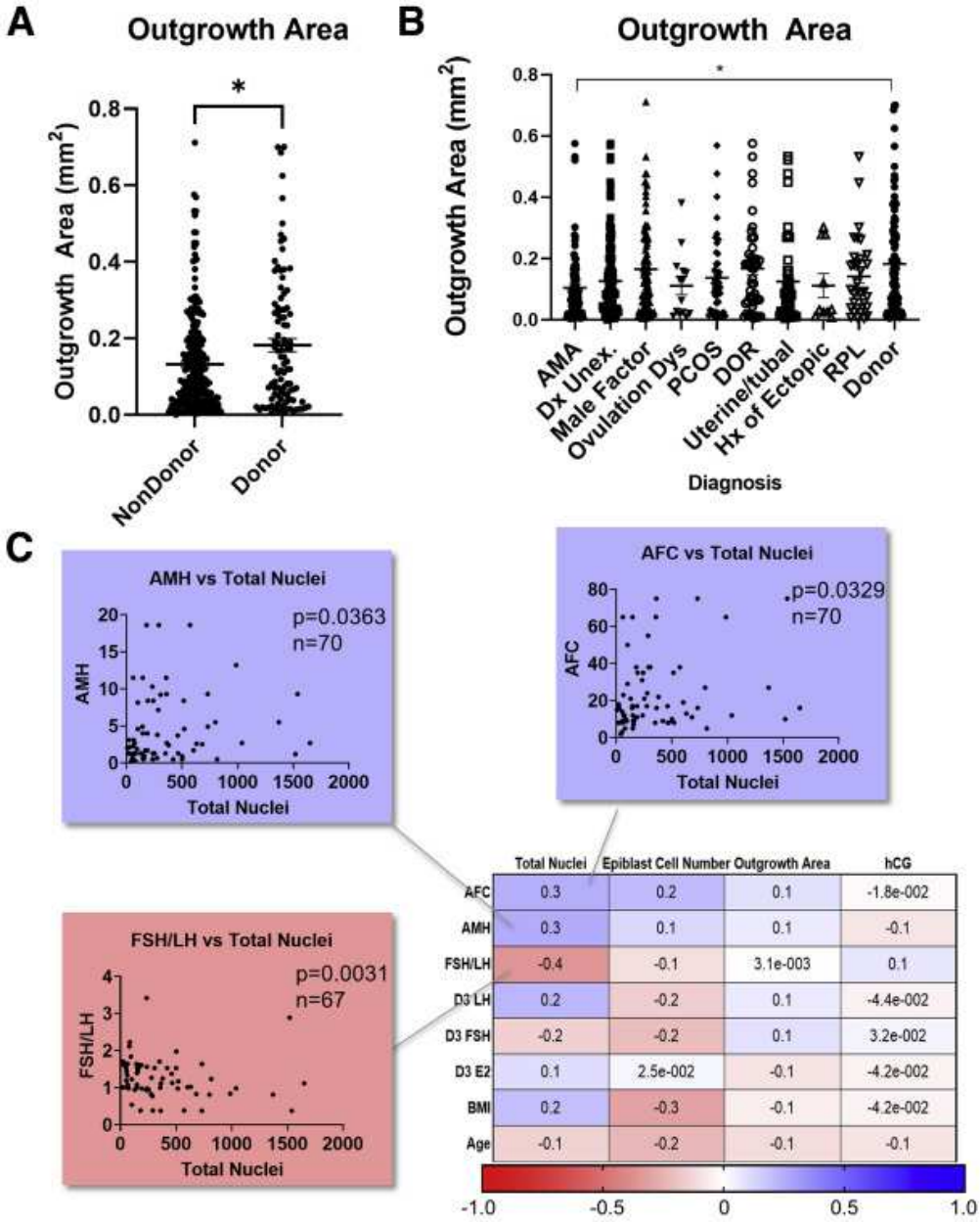

Figure 3.3. Peri-implantation embryonic development from nondonor fertility patients. (A) Outgrowth areas (mm^2) from nondonor (n = 254) and donor-derived (n = 99) embryos. (B) Outgrowth areas (mm^2) from nondonors by diagnosis (Dx; AMA n = 77, Dx Unex. n = 138, male factor n = 89, ovulation Dys. n = 14, PCOS n = 46, DOR = 46, uterine/tubal n = 43, history (Hx) of ectopic pregnancy n = 10, RPL n = 32) and donor-derived embryos (n = 99) on extended embryo culture (EEC) day 3. (C) Spearman's correlation matrix comparing patient predictors with EEC outcomes. Scale represents Spearman's *rho* values describing the positivity of each correlation. Significant

correlations between patient predictors and EEC outcomes are pulled out as scatter plots. AFC = antral follicle count; AMA = advanced maternal age; AMH = antimüllerian hormone (ng/mL); BMI = body mass index; D3 = day 3; DOR = diminished ovarian reserve; Dx Unex = unexplained infertility; E2 = estradiol (pg/mL); FSH = follicle-stimulating hormone (mIU/mL); hCG = human chorionic gonadotropin; LH = luteinizing hormone (mIU/mL); PCOS = polycystic ovary syndrome; RPL = recurrent pregnancy loss. Significance is noted at $*P<.05$.

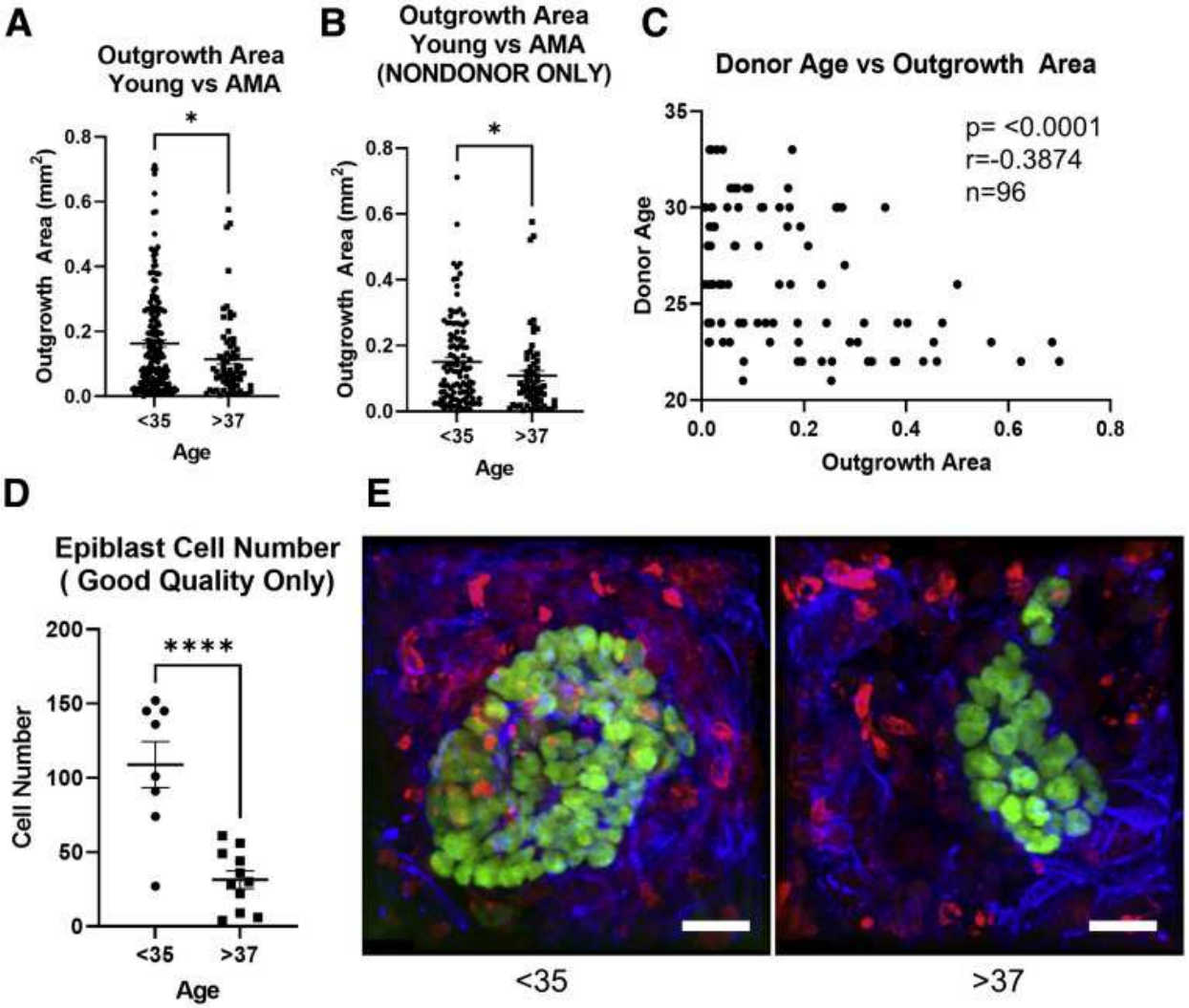

Figure 3.4. Effect of age on peri-implantation development. (A) Outgrowth areas (mm^2) from advanced maternal age (AMA, >37 years, n = 68) and young (<35 years, n = 193) embryos. (B) Outgrowth areas (mm^2) from AMA (n = 63) and young (n = 111) embryos from nondonors only. (C) Scatter plot of age vs. outgrowth area for embryos from healthy donors. r = rho depicts a negative Spearman's correlation (rho = −0.3874). (D) Epiblast cell number from good-quality embryos only from AMA (n = 11) and young (n =

8) patients. (E) Representative confocal images of AMA and young epiblast cells. *Red* = 4,6-diamino-2-phenylindole, *blue* = rhodamine phalloidin, *green* = POU5F1. Scale bar = 15 μM. Values reported as mean ± SEM. Significance is noted at $*P<.05$, $****P<.0001$. AMA = advanced maternal age.

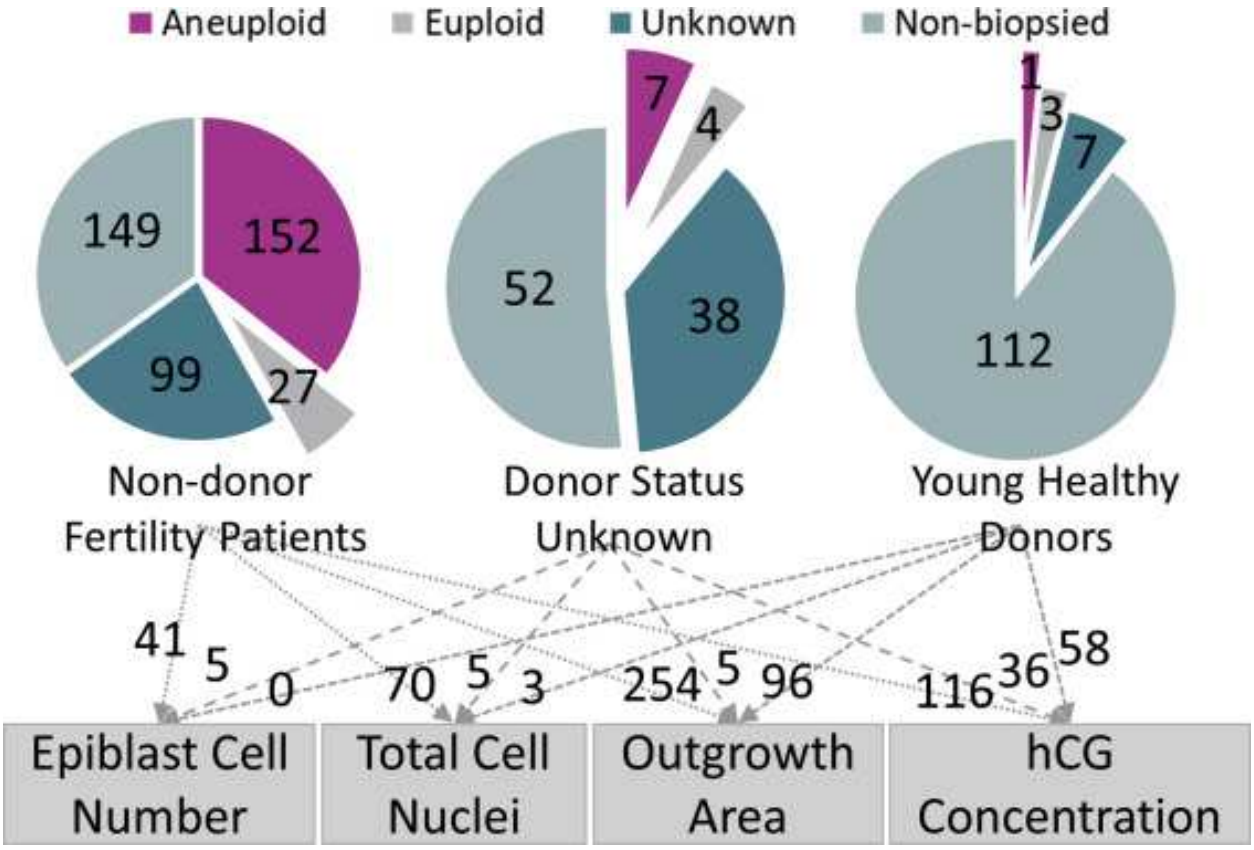

Figure 3.5. Flow diagram illustrating the sample distribution of the extended culture data set. A total of 651 donated human blastocysts were warmed and cultured during the peri-implantation stage and measured for four extended culture outcomes; epiblast cell number, total cell nuclei, outgrowth area, and hCG concentration. Preimplantation genetic testing for aneuploidy status is shown in pie graphs for the embryos from non-donor fertility patients, young healthy donors, or those with unknown donor status. The numbers on the pie graphs indicate the number of embryos for each PGT-A status, and the numbers next to the dashed line indicate the number of embryos measured for each outcome.

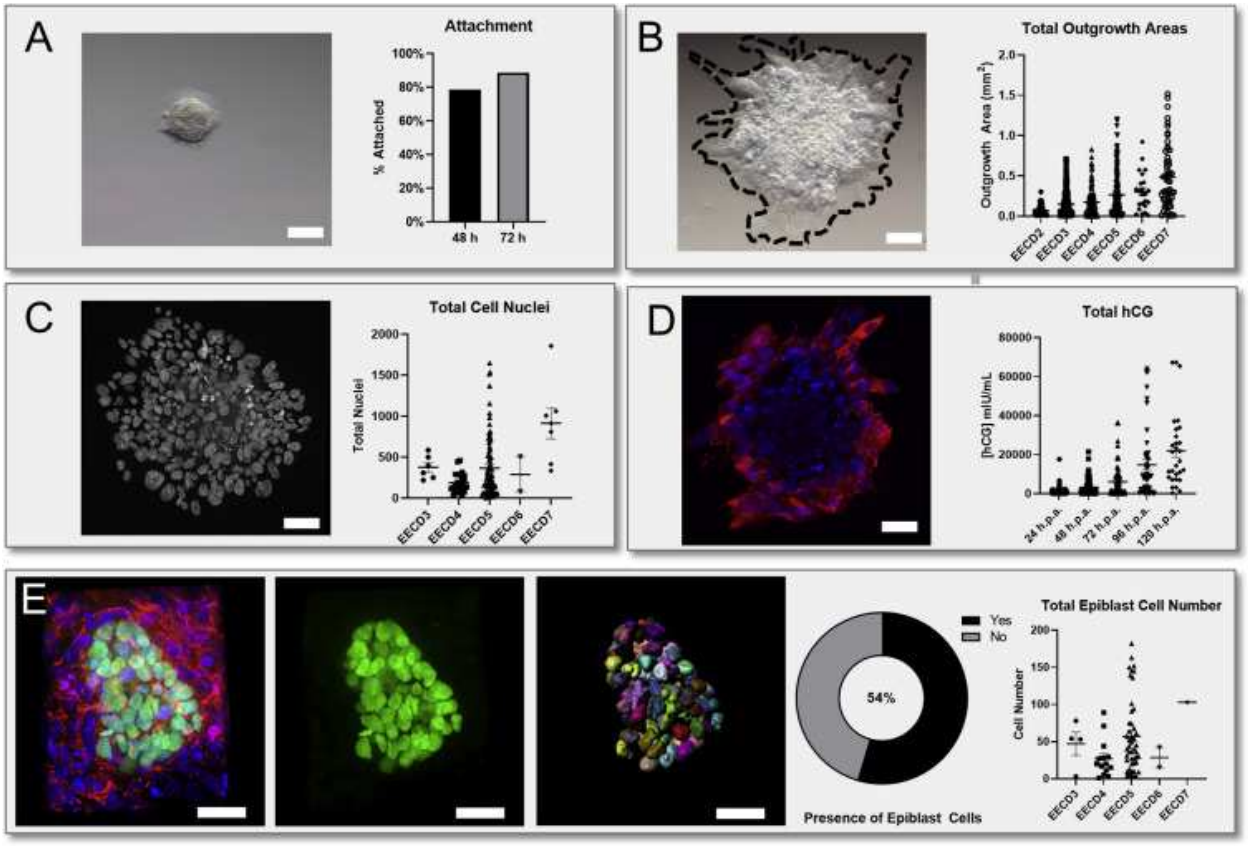

Figure 3.6. EEC Outcomes for Entire Data set. A) Representative stereomicroscope image of an attached embryo on EEC day (EECD) 3. Scale bar= 200 μM (left). Percent of attached embryos after 48 h (0.79 ± 0.016, n=624) and 72 h (0.89 ± 0.013, n=590) in culture (right). B) Representative stereomicroscope image of embryo on EECD 5 with example trophectoderm outgrowth area outlined in black. Scale bar= 200 μM (left). Total outgrowth areas over during the course of 7 d (EECD2 n=53, EECD3 n=390, EECD4 n=117, EECD5 n=185, EECD6 n=23, EECD7 n=56) in EEC (right). C) Representative confocal image of total cell nuclei on EECD 5. Gray= DAPI Scale bar= 200 μM (left). Total cell nuclei during the course of 7 d (EECD3 n=6, EECD4 n=25, EECD5 n=79, EECD6 n=2, EECD7 n=7) in EEC (right). D) Representative confocal image of embryo on EECD 5. Red= human chorionic gonadotropin (hCG), BLUE= DAPI. Scale bar= 200 μM (Left). Total hCG concentration (mIU/mL) from spent media following 24 (n=206), 48 (n=124), 72 (n=83), 96 (n=46), and 120 (n=29) hours post attachment (h. p. a.) to fibronectin- coated plates. E) Representative confocal images (Left, Center) and software analysis (right) of epiblast cells on EECD 5. RED=rhodamine phalloidin, BLUE= DAPI, GREEN= POU5F1. Scale bar= 15 μM. F) Percentage of embryos with POU5F1 cells present upon staining (54%, n=161, left). Total epiblast cell number during the course (EECD3 n=4, EECD4 n=14, EECD5 n=47, EECD6 n=2, EECD7 n=1) of EEC (right). All values reported as mean ± SEM. Statistical comparisons were not made for each group and are meant to be descriptive only.

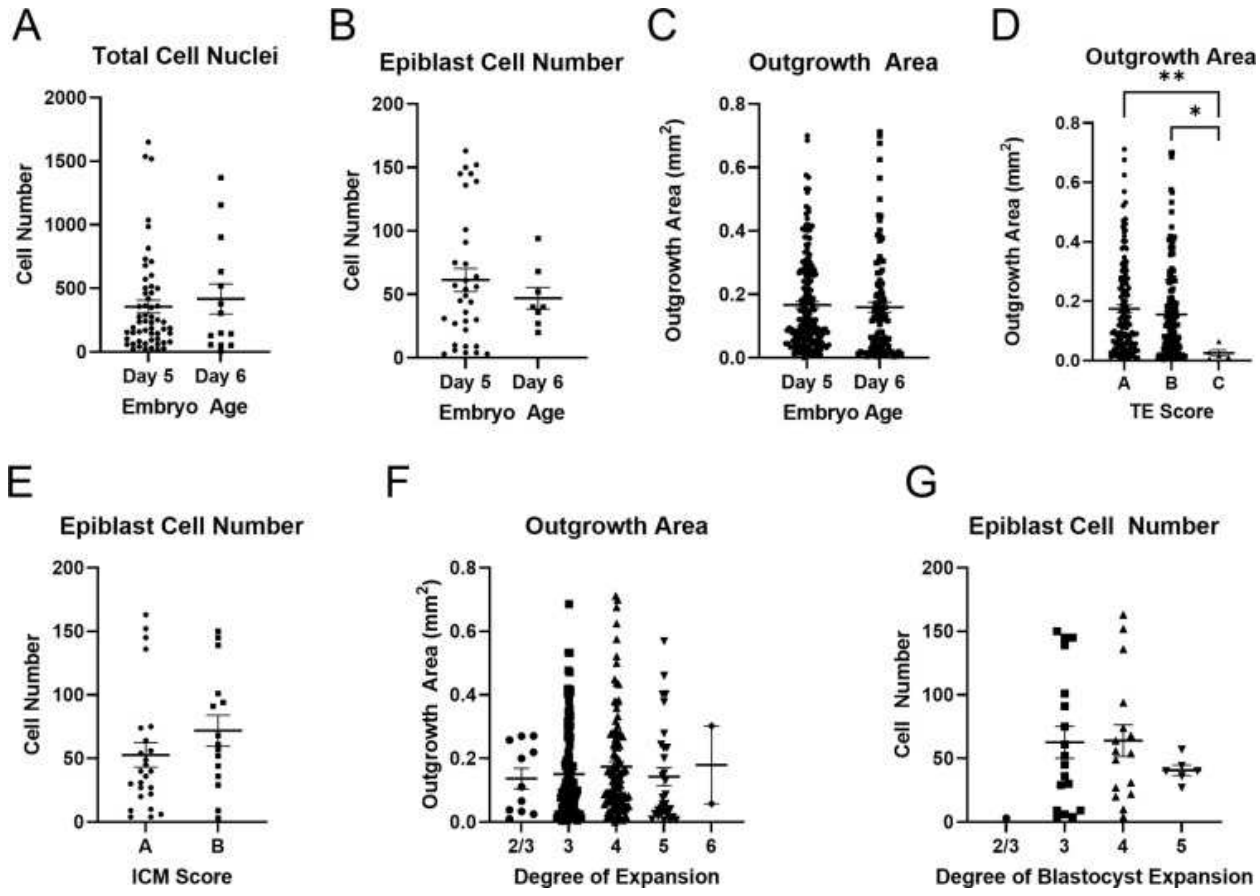

Figure 3.7. Effect of Embryo Morphology Scores on EEC Outcomes. A) Total cell nuclei in embryos vitrified at embryonic day (Day) 5 (n=56) and 6 (n=14). B) Epiblast cell number in embryos vitrified at embryonic day 5 (n=33) and 6 (n=8). C) Outgrowth areas (mm2) for embryos vitrified at embryonic day 5 (n=188) and 6 (n=107). D) Outgrowth areas (mm2) for embryos with a trophectoderm (TE) grade of A (138), B (n=159), or C (n=5) as determined by the Gardner grading scale. E) Epiblast cell numbers in embryos with an inner cell mass (ICM) grade of A (n=25) or B (n=15) as determined by the Gardner grading scale. F) Outgrowth areas (mm2) for embryos with expansion grades 2/3-6 (2/3 n=11, 3 n=105, 4 n=106, 5 n=31, 6 n=2) as determined by the Gardner grading scale. G) Epiblast cell number in embryos with expansion grades 2/3-6 (2/3 n=1, 3 n=18, 4 n=16, 5 n=6) as determined by the Gardner grading scale. Values reported as mean ± SEM. P-values are reported as $*$ $p<0.05$ or $**p<0.01$.

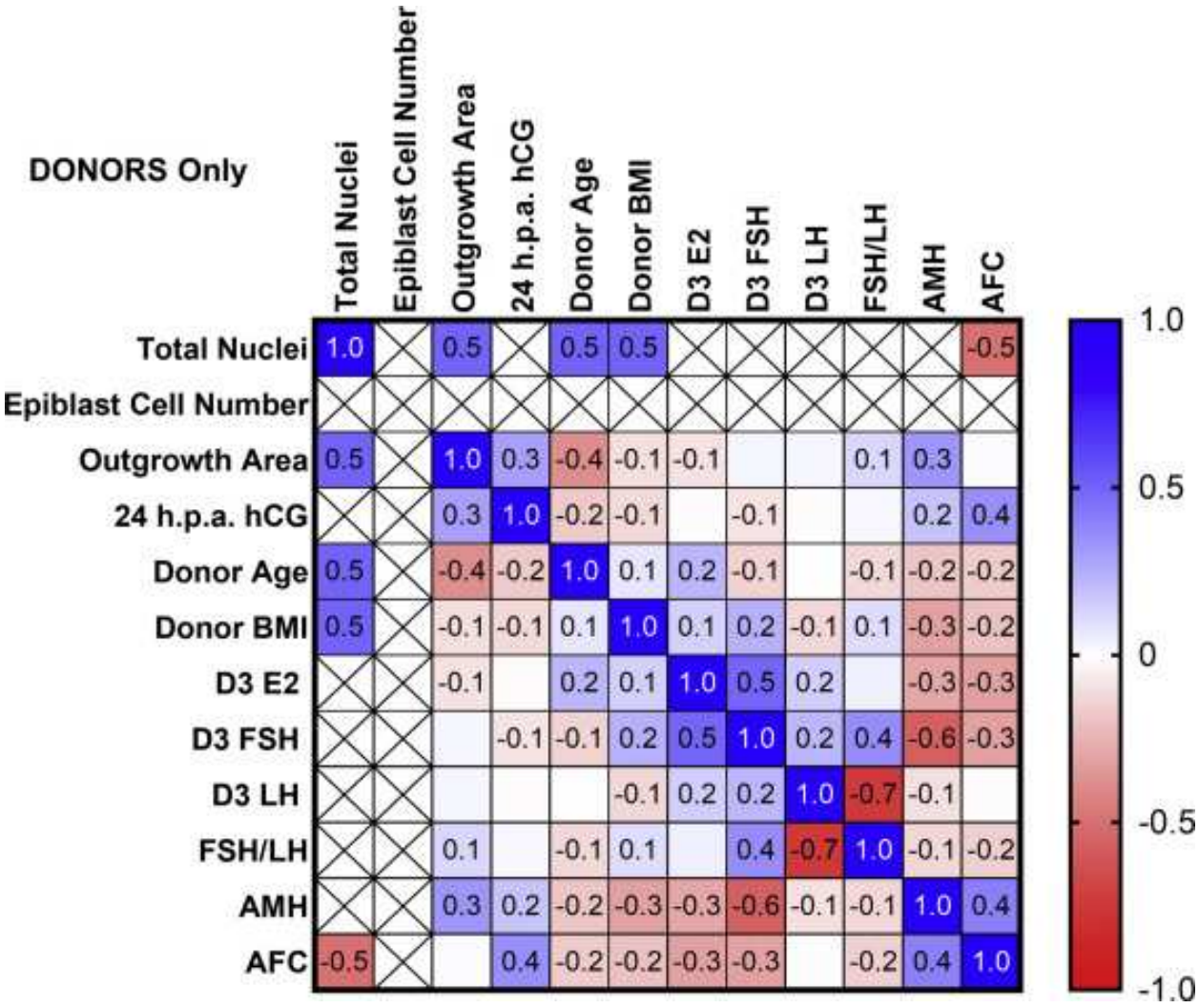

Figure 3.8 Correlations within Donor Patients. Spearman correlation matrix comparing patient predictors and EEC outcomes only in healthy donors. Scale represents spearman *rho* values describing the positivity of each correlation. hCG= human chorionic gonadotropin (mIU/mL), BMI= body mass index, D3= menstrual cycle day 3, E2= estradiol (pg/mL), FSH= follicle-stimulating hormone (mIU/mL), LH= luteinizing hormone (mIU/mL), AMH= anti-müllerian hormone (ng/mL), AFC= antral follicle count.

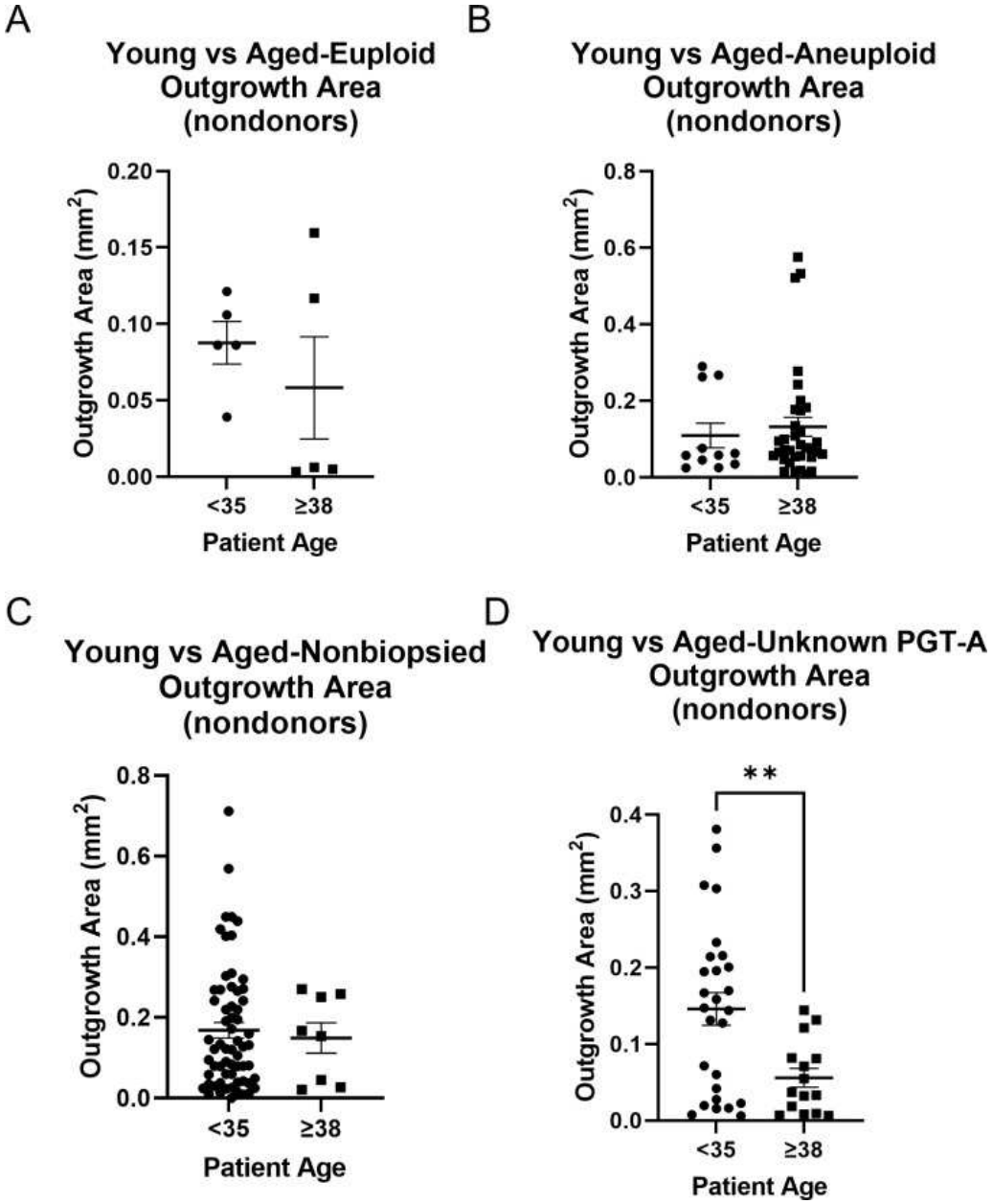

Figure 3.9 Outgrowth areas (mm^2) between young (<35 years) and aged (>37) non-donor fertility patients with A) euploid (young n=5, aged n=5), B) aneuploid (young n=11, aged n=34), C) nonbiopsied (young n=63, aged n=8), or embryos of D) unknown PGT-A status (young n=27, aged n=15). All values reported as mean ± SEM. Significance is noted $**p<0.01$.

Table 3.1. Summary statistics for extended culture outcomes.

	Sample Size	Mean	Standard Deviation	Minimum	Maximum
Outgrowth Area	389	0.15 mm²	0.15 mm²	0.003 mm²	0.71 mm²
Total Cell Nuclei	79	368 nuclei	382 nuclei	7 nuclei	1651 nuclei
hCG Concentration	206	682 mIU/mL	1606 mIU/mL	0.59 mIU/mL	17,610 mIU/mL
Epiblast Cell Number	47	57 cells	50 cells	3 cells	182 cells

Table 3.2. Descriptive Statistics for Patient Predictors

	Sample Size	Mean	Standard Deviation	Minimum	Maximum
Age	563	33.89	5.56	20	44
BMI	558	23.42	3.89	17.45	40.5
Cycle D3 Estradiol (pg/mL)	534	40.01	17.22	5.02	98
Cycle D3 FSH (mIU/mL)	545	6.94	2.21	2.50	15.1
Cycle D3 LH (mIU/mL)	545	6.05	2.29	0.20	16.3
Cycle D3 FSH:LH	544	1.18	0.24	0.87	6.5
Cycle D3 AMH (ng/mL)	549	4.16	3.54	0.10	23.6
Cycle D3 AFC	553	22.78	13.49	2	75

Table 3.3. Spearman Correlation P-Values for Entire Dataset

	Total Nuclei	***Epiblast Cell***	***Outgrowth Area***	***hCG (mIU/***	***Age***	***BMI***	***D3 E2 (pg/mL)***	***D3 FSH (mIU/***	***D3 LH (mIU/***	***FSH/ LH***	***AMH (ng/***	***AFC***
Total Nuclei		0.73	**2.88E-10**	0.20	0.18	**0.0**	0.23	0.18	0.14	**3.92E-**	0.05*	0.07
Epiblast Cell Number	0.73		0.62	0.43	0.17	**0.03**	0.84	0.12	0.24	0.46	0.44	0.07
Outgrowth	**2.88E-10**	0.62		**1.42E-1**	**0.01**	0.1	0.25	0.67	0.85	0.60	0.15	0.44
hCG (mIU/	0.20	0.43	**1.42E-11**		**4.80E-04**	0.40	0.24	0.86	0.55	0.20	0.26	**0.01**
Age	0.18	0.17	**0.01**	**4.80E-04**		**3.66E-**	**3.15E-05**	**1.22E-06**	0.18	0.02	**7.95E-22**	**1.66E-20**
BMI	**0.05**	**0.03**	0.15	0.40	**3.66E-04**		0.123	0.10	0.08	0.89	0.74	0.12
D3 E2 (pg/mL)	0.23	0.84	0.25	0.24	**3.15E-05**	0.12		**1.38E-03**	0.14	0.81	**9.17E-05**	**2.87E-07**
D3 FSH (mIU/mL)	0.18	0.12	0.67	0.86	**1.22E-06**	0.10	**1.38E-03**		**1.43E-15**	**1.29693E-29**	**1.25E-11**	**1.43E-08**
D3 LH (mIU/	0.14	0.24	0.85	0.55	0.18	0.08	0.14	**1.43E-15**		**2.72744E-60**	**6.33E-06**	**3.63E-07**
FSH/LH	**3.92E-03**	0.46	0.60	0.20	**0.02**	0.8	0.81	**1.30E-2**	**2.73E-6**		**6.91E-**	**6.00E-**
AMH (ng/mL)	0.05*	0.44	0.15	0.26	**7.95E-22**	0.74	**9.17E-05**	**1.25E-11**	**6.33E-06**	**6.91E-16**		**1.22E-117**
AFC	0.07	0.07	0.44	**0.01**	**1.66E-20**	0.12	**2.87E-07**	**1.43E-08**	**3.63E-07**	**6.00E-18**	**1.22E-117**	

Table 3.4 Spearman Correlation P-Values for Non-donor Fertility Patients

	Total Nuclei	*Epiblast Cell Number*	*Outgrowth Area*	*hCG (mIU/mL)*	*Age*	*BMI*	*D3 E2 (pg/mL)*	*D3 FSH (mIU/mL)*	*D3 LH (mIU/mL)*	*FSH/LH*	*AMH (ng/mL)*	*AFC*
Total Nuclei		0.81	**3.21E-10**	0.13	0.23	0.10	0.39	0.22	0.07	**3.09E-0**	**0.03**	**0.04**
Epiblast Cell Number	0.81		0.54	0.06	0.13	0.05*	0.88	0.18	0.33	0.52	0.46	0.20
Outgrowth Area	**3.21E-10**	0.54		**1.69E-07**	0.07	0.38	0.14	0.17	0.35	0.96	0.35	0.15
hCG (mIU/	0.13	0.06	**1.69E-07**		0.33	0.65	0.66	0.74	0.65	0.42	0.38	0.85
Age	0.23	0.13	0.07	0.33		**2.68E-**	**2.02E-**	**1.92E-0**	0.698	4.92E-0	9.97E-1	1.69E-
BMI	0.10	0.05*	0.38	0.65	**2.68E-**		0.64	0.50	**0.02**	0.47	0.49	0.55
D3 E2 (pg/	0.39	0.88	0.14	0.66	**2.02E-**	0.64		**1.04E-0**	**0.01**	0.79	0.16	**0.01**
D3 FSH (mIU/mL)	0.22	0.18	0.17	0.74	**1.92E-08**	0.50	**1.04E-03**		**3.6E-10**	**7.76E-23**	**6.42E-12**	**2.08E-10**
D3 LH (mIU/mL)	0.07	0.33	0.35	0.65	0.70	**0.02**	**0.01**	**3.6E-10**		**2.21E-51**	**1.28E-05**	**4.37E-07**
FSH/LH	**3.09E-**	0.52	0.96	0.42	**4.92E-**	0.47	0.79	**7.76E-2**	**2.21E-5**		**1.08E-2**	**5.58E-**
AMH (ng/	**0.03**	0.46	0.35	0.38	**9.97E-14**	0.49	0.16	**6.42E-12**	**1.28E-05**	**1.08E-20**		**6.02E-93**
AFC	**0.04**	0.20	0.15	0.85	**1.69E-**	0.55	**0.01**	**2.08E-1**	**4.37E-0**	**5.58E-2**	**6.02E-9**	

Table 3.5 Spearman Correlation P-Values for Donors

	Total Nuclei	***Epiblast Cell Numb***	***Outgrowth Area***	***hCG (mIU/mL)***	***Age***	***BMI***	***D3 E2 (pg/mL)***	***D3 FSH (mIU/mL)***	***D3 LH (mIU/mL)***	***FSH/LH***	***AMH (ng/mL)***	***AFC***
Total Nuclei			1.00		1.00	1.00						1.00
Epiblast Cell Number												
Outgrowth Area	1.00			0.04	**9.66E-05**	0.30	0.37	0.80	0.81	0.26	**1.42E-03**	0.92
hCG (mIU/			**0.04**		0.20	0.36	0.95	0.51	0.95	0.88	0.17	**0.01**
Age	1.00		**9.66E-05**	0.20		0.41	**0.02**	0.13	0.98	0.18	**0.04**	0.06
BMI	1.00		0.30	0.36	0.41		0.12	**0.01**	0.17	0.27	**5.82E-0**	**0.02**
D3 E2 (pg/			0.37	0.95	**0.02**	0.12		**2.05E-08**	0.11	0.63	**1.24E-0**	**5.06E-04**
D3 FSH (mIU/mL)			0.80	0.51	0.13	**0.01**	**2.05E-08**		0.02	**7.99E-05**	**6.54E-11**	**6.03E-04**
D3 LH (mIU/			0.81	0.95	0.98	0.17	0.11	**0.02**		1**.58E-2**	0.28	0.92
FSH/LH			0.26	0.88	0.18	0.27	0.63	**7.99E-05**	**1.58E-21**		0.17	0.09
AMH (ng/mL)			**1.42E-03**	0.17	**0.04**	**5.82E-04**	**1.24E-03**	**6.54E-11**	0.28	0.17		**6.60E-06**
AFC	1.00		0.92	**0.01**	0.06	**0.02**	**5.06E-0**	**6.03E-04**	0.92	0.09	**6.60E-0**	

Table 3.6 Spearman Correlation Sample Sizes for Entire Dataset

	Total Nuclei	***Epiblast Cell Numbe***	***Outgrowth Area***	***hCG (mIU/mL)***	***Age***	***BMI***	***D3 E2 (pg/mL)***	***D3 FSH (mIU/mL)***	***D3 LH (mIU/mL)***	***FSH/LH***	***AMH (ng/mL)***	***AFC***
Total	79	46	77	19	73	74	71	71	71	71	74	79
Epiblast Cell	46	47	45	13	43	43	41	41	41	41	43	47
Outgrowth Area	77	45	390	143	341	343	353	353	353	353	357	388
hCG (mIU/mL)	19	13	143	206	178	178	171	172	171	171	174	197
Age	73	43	341	178	563	544	518	518	517	516	522	556
BMI	74	43	343	178	544	558	514	514	513	512	521	551
D3 E2 (pg/mL)	71	41	353	171	518	514	546	545	544	543	542	546
D3 FSH (mIU/mL)	71	41	353	172	518	514	545	546	545	544	542	546
D3 LH (mIU/mL)	71	41	353	171	517	513	544	545	545	544	541	545
FSH/LH	71	41	353	171	516	512	543	544	544	544	540	544
AMH (ng/	74	43	357	174	522	521	542	542	541	540	550	550
AFC	79	47	388	197	556	551	546	546	545	544	550	639

Table 3.7 Spearman Correlation Sample Sizes for Non-donor Fertility Patients

	Total Nuclei	*Epiblast Cell Number*	*Outgrowth Area*	*hCG (mIU/mL)*	*Age*	*BMI*	*D3 E2 (pg/mL)*	*D3 FSH (mIU/mL)*	*D3 LH (mIU/mL)*	*FSH/LH*	*AMH (ng/mL)*	*AFC*
Total Nuclei	70	40	68	16	70	70	67	67	67	67	70	70
Epiblast Cell Number	40	41	39	11	41	41	39	39	39	39	41	41
Outgrowth Area	68	39	254	85	254	246	247	247	247	247	250	254
hCG (mIU/	16	11	85	116	114	115	111	112	111	111	113	116
Age	70	41	254	114	421	411	412	413	412	411	415	421
BMI	70	41	246	115	411	412	403	404	403	402	409	412
D3 E2 (pg/mL)	67	39	247	111	412	403	414	414	413	412	411	414
D3 FSH (mIU/mL)	67	39	247	112	413	404	414	415	414	413	411	415
D3 LH (mIU/mL)	67	39	247	111	412	403	413	414	414	413	410	414
FSH/LH	67	39	247	111	411	402	412	413	413	413	409	413
AMH (ng/	70	41	250	113	415	409	411	411	410	409	417	417
AFC	70	41	254	116	421	412	414	415	414	413	417	425

Table 3.8 Spearman Correlation Sample Sizes for Donors

	Total Nuclei	*Epiblast Cell Number*	*Outgrowth Area*	*hCG (mIU/mL)*	*Age*	*BMI*	*D3 E2 (pg/mL)*	*D3 FSH (mIU/mL)*	*D3 LH (mIU/mL)*	*FSH/LH*	*AMH (ng/mL)*	*AFC*
Total Nuclei	3		3		3	3						3
Epiblast Cell Number												
Outgrowth	3		96	49	96	94	91	91	91	91	92	96
hCG (mIU/			49	58	57	55	54	54	54	54	55	57
Age	3		96	57	122	120	116	115	115	115	117	122
BMI	3		94	55	120	120	114	113	113	113	115	120
D3 E2 (pg/			91	54	116	114	116	115	115	115	115	116
D3 FSH (mIU/mL)			91	54	115	113	115	115	115	115	115	115
D3 LH (mIU/			91	54	115	113	115	115	115	115	115	115
FSH/LH			91	54	115	113	115	115	115	115	115	115
AMH (ng/mL)			92	55	117	115	115	115	115	115	117	117
AFC	3		96	57	122	120	116	115	115	115	117	122

REFERENCES

1. Macklon NS, Geraedts JPM, Fauser BCJM. Conception to ongoing preg- nancy: the 'black box' of early pregnancy loss. Hum Reprod Update 2002; 8:333–43.

2. Wilcox AJ, Harmon Q, Doody K, Wolf DP, Adashi EY. Preimplantation loss of fertilized human ova: estimating the unobservable. Hum Reprod 2020;35: 743–50.

3. Shahbazi MN, Jedrusik A, Vuoristo S, Recher G, Hupalowska A, Bolton V, et al. Self-organization of the human embryo in the absence of maternal tis- sues. Nat Cell Biol 2016;18:700–8.

4. Deglincerti A, Croft GF, Pietila LN, Zernicka-Goetz M, Siggia ED, Brivanlou AH. Self-organization of the in vitro attached human embryo. Na- ture 2016;533:251–4.

5. West RC, Ming H, Logsdon DM, Sun J, Rajput SK, Kile RA, et al. Dynamics of trophoblast differentiation in peri-implantation-stage human embryos. Proc Natl Acad Sci U S A 2019;116:22635–44.

6. Lv B, An Q, Zeng Q, Zhang X, Lu P, Wang Y, et al. Single-cell RNA sequencing reveals regulatory mechanism for trophoblast cell-fate divergence in human peri-implantation conceptuses. PLoS Biol 2019;17:e3000187.

7. Zhou F, Wang R, Yuan P, Ren Y, Mao Y, Li R, et al. Reconstituting the tran- scriptome and DNA methylome landscapes of human implantation. Nature 2019;572:660–4.

8. Logsdon DM, Ermisch AF, Kile R, Schoolcraft WB, Krisher RL, Yuan Y. Egg cylinder development during in vitro embryo culture predicts the post trans- fer developmental potential of mouse blastocysts. J Assist Reprod Genet 2020;37:747–52.

9. Logsdon DM, Ermisch AF, Herrick JR, Becker J, Yao L, Broeckling C, et al. Fatty acids present in commercial albumin preparations differentially affect development of murine embryos before and during implantation. F&S Sci 2021;2:50–8.

10. Lee TH, Liu CH, Huang CC, Hsieh KC, Lin PM, Lee MS. Impact of female age and male infertility on ovarian reserve markers to predict outcome of assis- ted reproduction technology cycles. Reprod Biol Endocrinol 2009;7:100.

11. Broer SL, van Disseldorp J, Broeze KA, Dolleman M, Opmeer BC, Bossuyt P, et al. Added value of ovarian reserve testing on patient characteristics in the prediction of ovarian response and ongoing pregnancy: an individual patient data approach. Hum Reprod Update 2013;19:26–36.
12. van Rooij IA, Broekmans FJM, Hunault CC, Scheffer GJ, Eijkemans MJC, de Jong FH, et al. Use of ovarian reserve tests for the prediction of ongoing pregnancy in couples with unexplained or mild male infertility. Reprod Bio- med Online 2006;12:182–90.
13. Tal R, Seifer DB. Ovarian reserve testing: a user's guide. Am J Obstet Gynecol 2017;217:129–40.
14. Logsdon DM, Grimm CK, Schoolcraft WB, McCormick S, Schlenker T, Swain JE, et al. Evaluation of the TMRW vapor phase cryostorage platform using reproductive specimens and in vitro extended human embryo culture. F&S Sci 2021;2:268–77.
15. Logsdon DM, Rajput SK, Grimm CK, Schoolcraft WB, Yuan Y, Krisher RL. Exposure of human blastocysts to specific growth factors based on receptor presence improves epiblast formation in extended embryo culture. Fertil Steril 2020;114:e350.
16. Ermisch AF, Logsdon DM, Schlenker TW, Hamm JM, McCormick S, Schoolcraft WB, et al. A novel embryo culture system with reduced nutrients supports development of human 3PN embryos and extended embryo outgrowth. Fertil Steril 2018;110:e360–1.
17. Logsdon DM, Kile RA, Schoolcraft WB, Krisher RL, Yuan Y. Single cell collec- tion of trophoblast cells in peri-implantation stage human embryos. J Vis Exp 2020. https://doi.org/10.3791/61476.
18. Schindelin J, Arganda-Carreras I, Frise E, Kaynig V, Longair M, Pietzsch T, et al. Fiji: an open-source platform for biological-image analysis. Nat Methods 2012;9:676–82.
19. Gardner DK, Lane M, Stevens J, Schlenker T, Schoolcraft WB. Blastocyst score affects implantation and pregnancy outcome: towards a single blasto- cyst transfer. Fertil Steril 2000;73:1155–8.

20. Faddy MJ, Gosden RG, Gougeon A, Richardson SJ, Nelson JF. Accelerated disappearance of ovarian follicles in mid-life: implications for forecasting menopause. Hum Reprod 1992;7:1342–6.

21. Cimadomo D, Fabozzi G, Vaiarelli A, Ubaldi N, Ubaldi FM, Rienzi L. Impact of maternal age on oocyte and embryo competence. Front Endocrinol (Lau- sanne) 2018;9:327.

22. Pasquariello R, Ermisch AF, Silva E, McCormick S, Logsdon DM, Barfield JP, et al. Alterations in oocyte mitochondrial number and function are related to spindle defects and occur with maternal aging in mice and humans. Biol Re- prod 2019;100:971–81.

23. van Kooij RJ, Looman CW, Habbema JD, Dorland M, te Velde ER. Age- dependent decrease in embryo implantation rate after in vitro fertilization. Fertil Steril 1996;66:769–75.

24. Hsu MI, Mayer J, Aronshon M, Lanzendorf S, Muasher S, Kolm P, et al. Em- bryo implantation in in vitro fertilization and intracytoplasmic sperm injec- tion: impact of cleavage status, morphology grade, and number of embryos transferred. Fertil Steril 1999;72:679–85.

25. Lenton EA, Sexton L, Lee S, Cooke ID. Progressive changes in LH and FSH and LH: FSH ratio in women throughout reproductive life. Maturitas 1988;10: 35–43.

26. Seckin B, Turkcapar F, Ozaksit G. Elevated day 3 FSH/LH ratio: a marker to predict IVF outcome in young and older women. J Assist Reprod Genet 2012;29:231–6.

27. Prasad S, Gupta T, Divya A. Correlation of the day 3 FSH/LH ratio and LH con- centration in predicting IVF outcome. J Reprod Infertil 2013;14:23–8.

28. Liu KE, Greenblatt EM. Elevated day 3 follicle-stimulating hormone/lutei- nizing hormone ratio >or 1⁄4 2 is associated with higher rates of cancella- tion in in vitro fertilization-embryo transfer cycles. Fertil Steril 2008;90: 297–301.

29. Mukherjee T, Copperman AB, Lapinski R, Sandler B, Bustillo M, Grunfeld L. An elevated day three follicle-stimulating hormone:luteinizing hormone ra- tio (FSH:LH) in the presence of a normal day 3 FSH predicts a poor response to controlled ovarian hyperstimulation. Fertil Steril 1996;65:588–93.

30. Brouwers L, Franx A, Vogelvang TE, Houben ML, van Rijn BB, Nikkels PGJ. Association of maternal prepregnancy body mass index with placental histo- pathological characteristics in uncomplicated term pregnancies. Pediatr Dev Pathol 2019;22:45–52.
31. Howell KR, Powell TL. Effects of maternal obesity on placental function and fetal development. Reproduction 2017;153:R97–108.
32. van der Steeg JW, Steures P, Eijkemans MJC, Habbema JDF, Hompes PGA, Burggraaff JM, et al. Obesity affects spontaneous pregnancy chances in sub- fertile, ovulatory women. Hum Reprod 2008;23:324–8.
33. Hindmarsh PC, Geary MPP, Rodeck CH, Kingdom JCP, Cole TJ. Factors pre- dicting ante- and postnatal growth. Pediatr Res 2008;63:99–102.
34. L'Abee C, Vrieze I, Kluck T, Erwich JJHM, Stolk RP, Sauer PJJ. Parental factors affecting the weights of the placenta and the offspring. J Perinat Med 2011; 39:27–34.
35. Leon-Garcia SM, Roeder HA, Nelson KK, Liao X, Pizzo DP, Laurent LC, et al. Maternal obesity and sex-specific differences in placental pathology. Placenta 2016;38:33–40.
36. Hou YJ, Zhu CC, Duan X, Liu HL, Wang Q, Sun SC. Both diet and gene mutation induced obesity affect oocyte quality in mice. Sci Rep 2016;6: 18858.
37. Reynolds KA, Boudoures AL, Chi MMY, Wang Q, Moley KH. Adverse effects of obesity and/or high-fat diet on oocyte quality and metabolism are not reversible with resumption of regular diet in mice. Reprod Fertil Dev 2015;27:716–24.

CHAPTER IV: TRANSCRIPTOME COMPARISON OF REGENERATIVE TROPHOBLAST MODELS AND THE PRIMITIVE PLACENTA DURING PERI-IMPLANTATION

Significance

Successful implantation acts as the rate-limiting step to a healthy pregnancy. Two distinct, easily accessible in vitro models have recently emerged to study differentiation and function of human placental trophoblast but it remains unclear how well either mimic the cells of the emerging placenta during the first two weeks of embryo development. Here, we compare the phenotypes of the two most widely used models with trophoblasts derived from peri-implantation stage conceptuses to validate their usefulness in modeling the primitive placenta.

Summary

The mechanisms controlling trophoblast proliferation and differentiation during embryo implantation are fundamentally important in defining a successful pregnancy, yet poorly understood. Human trophoblast stem cells (TSC) and BMP4/A83-01/PD17034-treated pluripotent stem cell derived trophoblast cells (BAP) are two widely employed, contemporary models to study trophoblast development and function, but how faithfully they mimic the identity of early stage trophoblast cells has not been fully examined. Here, we evaluate the transcriptomic profiles of trophoblast cells from these two widely used cell models and directly compare them with trophoblast cells from peri-implantation stage human embryos during extended embryo culture (EEC) between embryonic d 8 to d 10 12. Cells from BAP and TSC models all grouped closely with trophoblast cells from EEC, with the trophoblast sublineages, including cytotrophoblast (CTB), syncytiotrophoblast (STB), and extravillous-like migratory trophoblast (MTB), clustered together following dimensional analysis and unsupervised hierarchical clustering. However, subtle differences amongst models exist for each trophoblast sublineages. TSC-CTB is more similar to EEC-CTB from d 8 embryos with transcripts

associated with increased Wnt signaling activities important for trophoblast stemness. BAP-CTB are more similar to EEC-CTB from d 10 and 12 embryos and upregulate transcripts important for trophoblast differentiation and invasion. For STB, EEC-STB showed enriched GO terms related to oxygen-dependent metabolism, while BAP and TSC-derived STB both prioritize lipid and membrane synthesis as well as actin reorganization and cell spreading. EEC-MTB transcripts indicate an increased level of invasiveness and motility compared to TSC-MTB with increased proliferative capacity. We also provide a pool of novel lineage markers in early trophoblast that were upregulated (>4-fold) across all three models and validate the presence of 11 genes prominent in peri-implantation human embryos. Together, our comprehensive analysis revealed that both commonly used BAP and TSC models resemble features of peri-implantation trophoblasts, while still maintaining subtle transcriptomic differences within the trophoblast sublineages.

Key Words: trophoblast, human embryo, implantation, pluripotent stem cells, trophoblast stem cells, RNA-sequencing

Introduction

Placental insufficiency, along with other pathologies that include pre-eclampsia and recurrent implantation failure, is believed to originate from improper trophoblast (TB) invasion into the maternal endometrium during early stages of pregnancy (1). While surveillance of the implanting embryo during this time is impossible, most of our understanding about the peri-implantation stage human development has been gleaned entirely from histological sectioning of implanting embryos (2). Recently, an extended embryo culture (EEC) system has allowed researchers to observe human peri-implantation stage development in vitro (3, 4). However, opportunities to access human embryos to study implantation and early placentation remain limited to most researchers due to government regulation, and animal models do not fully recapitulate physiological events that accompany human implantation (5). Additionally, choriocarcinoma and

other commonly used immortalized TB cell lines, as well primary cultures from later-stage placentas appear not to simulate peri-implantation stage TB development (6).

Human embryonic stem cells (hESC), though resembling a primed state during peri- or post-implantation, can be prompted to differentiate into TB-like cells with treatment of BMP4 (7). Original BMP4 treatment protocols give rise to a mixed population of TB-like cells contaminated with populations of mesodermal amnion-like cells (8, 9). Additional refinement to culture conditions with the intentional exclusion of FGF2, inhibition of FGF2R with PD17034, and inhibition of TGFβ signal transduction with A83-01 (BAP, 10) yields a mixed population of stem-cell progenitor cytoTB (CTB) as well as large, multinucleate syncytioTB (STB) –like cells that produce human chorionic gonadotropin, a hallmark of the implanting human embryo. The importance of excluding all traces of FGF2 over the full course of an eight-d differentiation procedure has been particularly emphasized in order to exclude mesoderm formation and to generate bona fide TB cells from hESC (6, 11-15). However, some continue to refute the validity of the BAP protocol and claim that the treatment of hESC with either BMP4 alone or through use of BAP leads primarily to the appearance of mesoderm in the form of amnion-like cells, but only as defined by upregulation of several mRNA markers, including those for *GABRP* and *VTCN1* discussed below, considered to be amnion-specific (16, 17).

Human TB stem cells (TSCs) can be generated from either 1st trimester placenta or outgrowths of peri-implantation conceptuses (18). They have become a widely used model that can give rise to three TB subtypes; CTB, STB, and MTB. TSC are selected and maintained on a culture medium supplemented with the TGFB inhibitor A83-10, a Rho-associated kinase inhibitor Y27632, a WNT activator CHIR99021, the HDAC inhibitor valproic acid (VPA), and epidermal growth factor (EGF). STB can be differentiated from CTB with the exclusion of VPA, CHIR99021, and A83-01, and the addition of forskolin to increase the intracellular cAMP

production. MTB can be induced from CTB with the exclusion of VPA, CHIR99021, and EGF, and the additional supplementation of neuregulin 1 (NRG1, 18).

Both the BAP and TSC models have become widely used in the past decade to study early TB development. Because BAP-treated hESC capture active differentiation into TB-like cells from a pluriptotent state, and their transcriptional profile does not provide a good match for third trimester placental TB, it is hypothesized that BAP hESC capture TB differentiation that resembles the primitive placenta during human implantation (19, 6, 15). TSC are themselves TB and cannot by definition mimic the transition from pluripotency to the TB lineage, but since some TSC lines (BTS5 and BTS11) were derived from blastocysts and are morphologically indistinct from villous column TSC lines (CT27 and CT29), it has been assumed that they too imitate differentiating TB from the peri-implantation period (18). Here, we compare transcriptional profiles of BAP, TSC, and human EEC TB and evaluate to what extent these two regenerative models are truly able to model the primitive placenta.

Materials and Methods

All reagents were purchased from Sigma Aldrich unless otherwise specified.

Ethics statement

All embryos used in this study were donated with informed consent following completion of IVF treatment at our facility. Experiments were approved by the Western Institutional Review Board (WIRB study no. 1179872).

Trophoblast stem cell culture and differentiation

TSC lines CT-27 (female) and CT-29 (male) were obtained from the RIKEN Cell Engineering Division (https://cell.brc.riken.jp/en/) and cultured as previously described (18). In brief, stem-state CTB cells were plated on plates pre-coated with 5 µg/mL collagen IV (Corning, cat #

354277) and maintained in stem state medium containing DMEM/F12 with 0.3 % w/v bovine serum albumin (BSA, FisherSci, BP9704100), 1X insulin, transferrin, selenium- ethanol amine (ITS-X, ThermoFisher, cat # 51500056), 0.2 % v/v fetal bovine serum (ThermoFisher, cat # 16141061), 0.1 mM 2-mercaptoethanol, 50 ng/mL epidermal growth factor, 1.5 µg/mL L-ascorbic acid, 0.8 mM valproic acid, 5 µM Y27632 (ReproCell, cat #04-0012), 2 µM CHIR99021 (ReproCell, cat #04-0004), 0.5 µM A83-01 (ReproCell, cat #04-0004), and 1 µM SB431542 (ReproCell, cat #04-0010). Monolayers were rinsed with phosphate-buffered saline, dispersed to single cells with TrypLE Express for approximately 15 min, and passaged at 75% confluence.

To induce STB differentiation in TSC, cells were passaged to a plate coated with 2.5 µg/mL collagen IV and seeded at 1 x 10^5 cells per 35 mm well of a 6 well plate. Cells were differentiated over the course of 6 d in medium containing DMEM/F12 with 0.3% w/v BSA, 1X ITS-X, 0.1 mM 2-mercaptoethanol, 2.5 µM Y27632, 2 µM Forskolin, and 4% v/v Knockout Serum Replacement (KSR) with medium changes every other day.

To induce MTB differentiation in TSC, cells were passaged to a plate coated with 1 µg/mL collagen IV and seeded at 1 x 10^5 cells per 35 mm well of a 6 well plate. Cells were differentiated over the course of 6 d in medium containing DMEM/F12 with 0.3 % w/v BSA, 1X ITS-X, 0.1 mM 2-mercaptoethanol, 2.5 µM Y27632, 7.5 µM A83-01, 100 ng/mL neuroregulin 1 (NRG1), 2% Matrigel, and 4 % v/v KSR with medium changes every other day. On d 3 of differentiation, medium was exchanged with the above recipe without NRG1. On d 6, medium was exchanged with the above recipe without NRG1 and KSR and cells were passaged a final time to enhance MTB differentiation.

BAP-treated hESC culture

Human embryonic stem cell (hESC) lines H1 (WA01, male, XY) and H9 (WA09, female, XX) were obtained from the WiCell Research in Madison, WI (Thomson et al.) Cells were seeded at

a density of 50,000 cells/well onto Matrigel (Corning)-coated 6-well plates in mTESR1 medium (Stem Cell Technologies). Cells were then cultured in basal DMEM/F12 with 20 % v/v KOSR, non-essential amino acids, 2mM L-glutamine, and FGF2 (4 ng/mL) for 24 h. The TB phenotype was initiated using an established protocol (10). Medium was exchanged with the same recipe without FGF2, and additional supplementation of BMP4 (10 ng/mL), A83-01 (1 μm), and PD173074 (0.1 μm) (BAP) each day over the course of 8 days. Upon completion of BAP treatment, cells were dispersed and passed through a cell strainer to separate small, CTB-like cells (<40 μm) and large, STB-like cells (>70 μm) (19). After separation, cells were centrifuged and snap frozen for downstream assays. All cell culture was completed at 37 °C in a humidified incubator at 5% CO_2 and atmospheric oxygen.

Human embryo extended culture

Vitrified human embryos 5 or 6 days post fertilization (d. p. f.) were thawed according to standard protocols (23) and were left to recover for 2 h in 20 μL drops of single step human culture medium (Sage 1-step, Cooper Surgical) supplemented with 20% Quinn's Advantage Serum Protein Substitute (Cook) in 37 °C at 7.5% CO_2 and 6.5% O_2 to mimic 6 % CO_2 and 5 % O_2 at sea level. Following recovery, the zona pellucidae were removed with brief exposure to acidic Tyrode's solution (24) and embryos were placed into an extended embryo culture (EEC) system for 3 or 5 days. EEC and downstream single-cell dissociation was performed as described previously (24). In brief, embryos were cultured on a chambered coverslip (ibidi, Martinsreid, Germany) coated with 30 μg/mL fibronectin from human plasma. Embryos were cultured in in vitro culture medium 1 (IVC1) containing Advanced DMEM/F12, 20% fetal calf serum (FCS, Hyclone), 200ng/mL water soluble progesterone, 8 nM water soluble estradiol, 25 μM N-acetyl cysteine, 1X ITS-X (ThermoFisher), 2 mM GlutaGro (Fisher Scientific), and 10 μg/mL Gentamicin (Cellgro) for the first 48 h in EEC. At this time, embryos were checked for attachment and a one-half volume of medium was replaced with in vitro culture medium 2 (IVC2) containing Advanced DMEM/F12, 30 % v/v KSR (ThermoFisher), 200ng/mL water

soluble progesterone, 8 nM water soluble estradiol, 25 μM N-acetyl cysteine, 1X ITS-X (ThermoFisher), 2 mM GlutaGro (Fisher Scientific), and 5 mg/mL Gentamicin (Cellgro). Half medium exchanges were made daily for an additional 3 to 5 days.

Trypsin digestion and sample collection

TSC were washed once with PBS before trypsin digestion with TrypLE for 15 min. BAP cells were washed once with PBS before trypsin digestion using 10x TrypLE for 7 minutes. Cell line digestions were quenched using DMEM/F12 before collection and centrifugation. Approximately 1,000 cells for each cell line sample were resuspended in Collection Buffer (PicoPure, Applied BioSystems, ThermoFisher, KIT0204) and stored in -80 °C before RNA extraction. Following TrypLE dispersion, we collected TB subtypes from peri-implantation embryos as previously described (25, 24) in groups of approximately 10-40 cells per tube in minimal volume of PBS + 0.1% PVP, snap frozen in LN_2 and saved at -80 °C (24).

RNA-seq library preparation and sequencing

RNA was extracted from cells by using PicoPure column-based RNA isolation kit according to manufacturer protocol (Applied BioSystems, ThermoFisher). RNA was eluted twice with 11 μL Elution Buffer and RNA concentration measured by using QuBit RNA High Sensitivity reagents according to manufacturer protocol (Invitrogen). The RNA-seq libraries were generated from extracted RNA by using the Smart-seq2 v4 kit with minor modification from manufacturer's instructions. Briefly, mRNA was captured and amplified with the Smart-seq2 v4 kit (Clontech). After AMPure XP beads purification, the high-quality amplified RNAs were subject to library preparation (Nextera XT DNA Library Preparation Kit; Illumina) and multiplexed by Nextera XT Indexes (Illumina). The concentration of sequencing libraries was determined by using Qubit dsDNA HS Assay Kit (Life Technologies) and KAPA Library Quantification Kits (KAPA Biosystems). The size of sequencing libraries was determined by means of Agilent D5000 ScreenTape system at Tapestation 4200 system (Agilent). Pooled indexed libraries were then

sequenced on the Illumina HiSeq X platform with 150-bp pair-end reads. For each group, at least 3 replicates were processed to profile transcriptomes by RNA-seq with the Smart-seq2 protocol as described above. We generated approximately 60 million 150bp paired-end reads per sample.

RNA-seq data processing

Multiplexed sequencing reads that passed filters were trimmed to remove low-quality reads and adaptors by TrimGalore (version 0.6.7) (-q 25 --length 20 --max_n 3 --stringency 3). Quality control for the data was performed with the FastQC3 (v0.11.5) tool. Trimmed reads were aligned to the human reference genome (GRCh38.106) with HISAT25 (version 2.2.1) at the default setting. The reference genome was downloaded from https://ftp.ensembl.org/pub/release-106/fasta/homo_sapiens/dna/Homo_sapiens.GRCh38.dna.primary_assembly.fa.gz. Output SAM files were converted to BAM files and sorted by means of SAMtools6 (v1.3.1). Transcriptome assembly and gene expression quantification were performed by using featureCounts (version 2.0.1) (-a Homo_sapiens.GRCh38.106.gtf.gz). The genome annotation file was downloaded from https://ftp.ensembl.org/pub/release-108/gtf/homo_sapiens/Homo_sapiens.GRCh38.108.gtf.gz. Individual mapped reads were adjusted to provide counts per million mapped fragments (CPM) based on the raw count number. The raw FASTQ files derived from analysis of extended cultured embryos are available at Gene Expression Omnibus (GEO) (https://www.ncbi.nlm.nih.gov/geo/) under the accession number GSE 130289. PCA and sample correlation were performed on the top regulated 1000 genes based on median absolute deviation (mad) with R package factoextra and corrplot respectively. Differential gene expression analysis was performed by using R package edgeR with default parameters. Genes were deemed differentially expressed if they provided a false discovery rate of <0.05 and fold change >2. Volcano plot of DEGs was performed by using R package ggplot2. Biological pathways (denoted as Gene Ontology terms and KEGG pathways) over-represented among up- and down-regulated genes were identified by using R package ClusterProfiler. FDR cutoff of

0.05 was used in selecting significant pathways. To further explore the function of DEGs in specific GO terms, GSEA was performed with the R package GSEABase.

Immunofluorescence and image acquisition

Monolayer cell cultures and extended culture 10 d. p. f. embryos were cultured on optical grade dishes (ibidi), fixed with 4 % paraformaldehyde (PFA) in PBS for 20 min, and washed three times for 5 min with wash buffer containing 0.1% (v/v) Tween 20 and 0.1 % (w/v) PVP in sterile PBS. Monolayer cell cultures were permeabilized for 30 min in 0.3% (v/v) Triton X-100 in sterile PBS, washed with wash buffer for 5 min, and non-specific binding of reagents were blocked in sterile blocking buffer containing 0.1% Tween 20, 0.1 M glycine, 10% (v/v) FCS with 1% bovine serum albumin (BSA, MP Probumin) in for 2 h. Following the blocking step, cells were washed once and stained with primary antibodies diluted 1:200 in antibody buffer containing 0.1% Tween 20 and 1.0% BSA overnight. Cells were washed with washing buffer three times for 5 min and incubated with secondary antibodies diluted 1:200 in antibody buffer for 1 h. Cells were washed three times with wash buffer for 5 min and mounted in ProLong Diamond antifade with DAPI (Fisher Scientific). Imaging for monolayer cell cultures were performed with an Olympus Fluoview FV10i confocal microscope.

Following fixation, extended culture embryos were washed three times with wash buffer containing 0.1% (v/v) Tween 20 in sterile PBS (PBST) for 10 min. Embryos were permeabilized with 0.5% (v/v) Triton X-100 in sterile PBS for 30 min and washed three times for 10 min in wash buffer. Embryos were then incubated in blocking buffer containing 10% (v/v) FCS with 3% BSA in PBST overnight. Embryos were stained with primary antibodies diluted 1:200 in blocking buffer overnight. The following day, embryos were washed three times with wash buffer for 10 min and incubated in secondary antibodies diluted 1:200 in blocking buffer for 6 h. Embryos were then washed three times with wash buffer for 10 min and mounted with ProLong Diamond

antifade with DAPI. Immunofluorescence imaging for peri-implantation embryos was completed using a 3i Marianas spinning disk confocal microscope.

The imaging experiments were performed in this manuscript were completed at the Advanced Light Microscopy Core at University of Colorado Anschutz Medical Campus.

Results

Trophoblast lineage marker expression in trophoblast cells derived from TSC, BAP and EEC models

Donated human embryos were warmed and cultured up to 7 days in EEC, i.e. 12 d. p. f. according to published protocols (3, 4, 25, Fig. 4.1A). Following extended culture, EEC embryos had clearly developed three apparent TB subpopulations; CTB positive for pan-TB transcription factor GATA3, STB positive for CGB, and a group of migratory cells that could be collected prior to dispersal of the conceptus and that were positive for the MTB marker HLA-G (Fig. 4.1B; Fig. 4.2). EEC embryos were then enzymatically digested into single cells and collected based on their morphologies prior to bulk RNA-sequencing (Fig. 4.1A, top row). BAP cells were generated as described previously (10) and showed positive staining for GATA3 in mononucleated CTB-like populations and positive CGB staining in large multinucleated plaques at d 8 following BAP treatment. At this stage of differentiation, BAP cells lacked apparent HLA-G expression (Fig. 4.1C) but clearly possess it at earlier stages of differentiation (6). BAP cells were enzymatically digested and filtered, to enrich CTB-like (<40 μm) and STB-like cell populations (>70 μm, Fig. 1A) as originally described by Yabe et al prior to collection. CTB from TSC also showed positive staining for transcription factor GATA3 (Fig. 4.1D). Following STB differentiation, TSC-STB was evident as multinucleated syncytial plaques that stained brightly for CGB (Fig. 4.1B), while differentiated TSC-MTB showed morphological elongation characteristic of MTB and also stained positively for HLA-G (Fig. 4.1D). Undifferentiated TSC-CTB and differentiated TSC-STB

and TSC-MTB were collected following enzymatic digestion and were used for bulk RNA-sequencing (Fig. 4.1A).

Trophoblast subtypes cluster together across cell models

Upon bulk RNA sequencing, principal component analysis (PCA), and unsupervised hierarchical clustering, EEC TB did not form discrete clusters and there was considerable overlap between TB sublineages (Fig. 4.7A). This was largely attributed to the method of collection for bulk RNA-sequencing for EEC TB. Small, round, presumably CTB on d 3 of EEC display a mix of differentiating TB; a multipotent CTB stem cell population contaminated with a “pre-STB” CTB population, and a “pre-MTB” CTB population (25). Because samples collected here were likely a mixed population, there was inappropriate grouping (Fig. 4.7A, B). For this reason, more distinct CTB, STB, and MTB single cell samples were used from our previously published dataset (25, accession number GSE 130289) and were purified by cell marker expression after single cell RNA sequencing (scRNA-seq) over three timepoints during the peri-implantation period (8, 10, and 12 d. p. f., 25). After re-analysis with the scRNA-seq TB dataset, distinct clusters of cells grouped according to cell type across all three models and, with the exception of the d 3 BAP cells, well separated from undifferentiated hESCs (H1, Fig. 4.1E). TB subpopulations showed the anticipated increase in marker gene expression, e.g. *TEAD4* and *CDH1* for CTB, *SDC1* and *CGB* for STB, and *HLA-G* and *MMP2* for MTB (Fig. 4.1F, G, H).

Cytotrophoblasts across trophoblast models display differences in stemness

The CTB in the TSC model and 8 d. p. f. EEC had the highest transcript abundance of putative CTB markers *TEAD4* and *CDH1* amongst all groups (Fig. 4.1F). We further examined CTB samples to tease out variations across models and found that CTB could be separated into two groups: CTB_subtype1 (including BAP CTB and 10/12 d. p. f. EEC CTB) and CTB_subtype2 (including TSC CTB and D8 EEC CTB, Fig. 4.2A, B). We then identified differentially expressed genes (DEGs) between these two CTB groups (Table 4.2) in which 2300 genes were upregulated in CTB_subtype1, while 1312 genes were upregulated in CTB_subtype2 (Fig. 4.3C,

D). Significantly enriched GO terms for CTB_subtype1 generally related to cell migration and invasiveness including extracellular matrix organization, wound healing, and integrin-mediated signaling pathways. In CTB_subtype2, Wnt signaling was a recurring theme amongst enriched GO terms including pattern specification process, embryonic placenta morphogenesis, and regionalization (Fig. 4.2E). Additionally, *FGFR2*, *WNT3*, *FZD5*, *CTNNB1*, *WNT7B*, *YAP1*, *RSPO4*, *JADE1*, *WLS*, and *KLF15* were among those that were significantly reduced in CTB_subtype1 compared to that in CTB_subtype2 whereas CTB_subtype1 DEGs, *ECH1* and *TFPI*, represent those of a slightly more differentiated CTB (Fig. 4.3C, F), indicating an increase in TB stem cell self-renewal abilities in CTB_subtype2 (18, 20, 21, 26). Other differentially expressed genes upregulated in CTB_subtype2 including *TP63*, *GATA4*, *GATA5*, and *DNMT3L* are also essential in maintaining CTB in a stem cell-like state and regulating placenta development (27-29).

Syncytiotrophoblasts across trophoblast models display differences in metabolic priorities

STB are multinucleated cells formed via fusion of CTB and mediate nutritional and gas exchange at the maternal-fetal interface (30). EEC STB from 8, 10, and 12 d. p. f. EEC were clearly grouped separately from both TSC STB and BAP STB following unsupervised hierarchical clustering and dimensional analysis (Fig. 4.3A, B). We specified STB derived from TSC and BAP models as STB_subtype1 and STB from extended cultured embryos at all three timepoints as STB_subtype2. By comparing DEGs between these two groups (Table 4.3), 3959 genes were enriched in STB_subtype1, while 1533 genes were enriched in STB_subtype2 (Fig. 4.3C, D). Enriched GO terms related to glycerophospholipid synthesis, phospholipid metabolic processes, and invasiveness were enriched in STB_subtype1 and upregulate DEGs including *PKP3* and *DGKZ* (Fig. 4.3 E, F), while GO terms enriched in STB_subtype2 were related to chromatin structure and cellular respiration and included DEGs *H2AZ1* and *CYCS* (Fig. 4.3E, F).

Migratory trophoblasts from peri-implantation embryos or trophoblast stem cells resemble different extra villous trophoblast subtypes

We compared MTB populations between EEC and TSC models, and found 1327 genes were upregulated in EEC, and 3827 genes were upregulated in TSC (Table 4.4, Fig. 4.4A, B). Extravillous TB populations in 8-week first trimester placenta segregate into 3 subtypes; the first with proliferative potential highly expressing *RRM2*, the second with increased receptor activity and increased immune response expressing *SERPINE1* and *SERPINE2*, and a third that displays similarities with both preceding two groups (31). Top GO terms enriched in TSC MTB were closely related to chromosome segregation and cell cycle, while MTB from EEC embryos were related to wound healing and collagen remodeling processes (Fig. 4.4C). Interestingly, DEGs of TSC and EEC MTB were reminiscent of two distinct extravillous TB subgroups from 8-week placentas. TSC MTB displayed increased expression of *RRM2* and *CCNB1*, while *SERPINE1* and *SERPINE2* expression was significantly increased in MTB from EEC (Fig. 4.4E). Furthermore, several transcripts from the family of metalloproteases (*MMP15*, *MMP2*, and *ADAMTS20*) were also increased in EEC MTB indicating their increased invasiveness compared to TSC MTB (Fig. 4.4E).

Novel trophoblast marker expression in peri-implantation human embryos

We next looked for new marker genes that were significantly upregulated (>4-fold) in a cell type-specific manner across each model (Fig. 4.5A). Among the 23 genes that were differentially expressed in all CTB models, we stained peri-implantation embryos with antibodies against *ANLN*. *ANLN* immunofluorescence expression was present in all TB populations and did not seem to be restricted to CGB-, GATA3+ CTB (Fig. 4.5B, Fig. 4.9A). Twenty-six genes were upregulated in STB across each cell model (Fig 4.5A). When we stained peri-implantation embryos with antibodies against *FIBCD1*, we found that flourescence intensity was increased in the peripheral CGB-positive regions of the embryo as well as some mononucleated CTB within the embryo (Fig. 4.5C, 4.9B). Both MTB and CTB near the very center of the embryo had

significantly reduced fluorescence compared to the GATA3-positive cells around the periphery of the embryo (Fig. 4.9B). Out of 28 upregulated genes in MTB, *MAMDC2* displayed significantly increased expression in *HLA-G*+ MTB in peri-implantation embryos compared to CTB or STB (Fig. 4.5D, 4.9C).

BAP and TSC marker expression in peri-implantation human embryos

RNA-sequencing results for both BAP and TSC TB models highlighted other potentially important TB marker genes from each model (18, 22). To further investigate their relevancy to peri-implantation stage human TB, we probed our RNA-sequencing and used immunofluorescence to detect the presence of each proposed marker gene. Indeed, EEC TB display increased transcript expression of BAP markers *VTCN1*, *WFDC2*, and *ACTC1* (Fig. 4.6A) in peri-implantation human embryos. Though *GABRP* transcripts were undetectable in TSC and EEC TB, *GABRP* protein was brightly localized in the nuclei of all TB populations increasingly up to d 7 in EEC (Fig. 4.10A-C). Cytoplasmic localization of *GABRP* began proximal to the epiblast by d 3 in EEC. A second localization pattern of *GABRP* also localized to the cell surface of a population of cells proximal to the *POU5F1*-positive epiblast by d 7 in EEC (Fig. 4.10D). Peri-implantation embryos also stained positive for BAP markers *VTCN1*, *WFDC2*, *ACTC1* (Fig. 4.6B-D). *VTCN1* did not localize in CGB+ areas on the periphery of the embryo, whereas *WFDC2* seem to be ubiquitous throughout the TB and *ACTC1* localized to the outer STB populations (Fig. 4.6B-D). EEC TB also expressed transcripts and stained positive for TB genes proposed in the original TSC manuscript with placenta-specific promoters, *CYP19A1*, *EDNRB*, *IL2RB*, and *PTN*. (Fig. 4.10A, E-H) though all markers seemed to be ubiquitous throughout TB populations.

Discussion

Preclinical pregnancy loss is the principal cause of low fecundity in humans (32). Because human embryos during this period are inaccessible, EEC is currently the best model to explore

events during the peri-implantation period. However, institutions that are reliant on federal grant funding mechanisms are unable to use human embryos for research, and many look to regenerative stem cell TB models for functional studies. Here, we performed RNA-seq to compare two widely used TB cell models (TSC and BAP) for each TB sublineage (CTB, STB, MTB) with TB from human embryos in EEC during the peri-implantation period. We show that TB meet the criteria of TB (33), group by TB sublineage regardless of model, and display subtle differences between models that resemble population subtypes found in first trimester placental tissues. Additionally, we identified several potential TB lineage markers conserved across each model that warrant further investigation, and validated BAP and TSC marker expression in peri-implantation embryos.

CTB are self-renewing TB stem cell progenitors that bifurcate terminally into STB or MTB (34). In peri-implantation human embryos, CTB are small, mononucleated cells that display transcriptional programs indicating their predisposition to develop into STB or MTB as early as 8 d. p. f. (25). Here, we found that our population of transcriptionally “purified” CTB. excluding “pre-STB” or “pre-MTB” cells. still exhibit subtle differences that indicate their level of TB stemness and self-renewal capability. Similar differences are also evident in CTB subgroups in 8-week first trimester placentas in which one subpopulation of CTB has increased proliferative capacity, and another upregulates transcripts related to extracellular matrix organization and invasiveness (31). Wnt signaling plays a critical role in the proliferation for TB and various other epithelial stem cells (18, 20, 21). We found that key Wnt signaling genes were significantly upregulated in CTB_subtype2 which was distinct from 10/12 d. p. f. EEC CTB and BAP CTB (CTB_subtype1) which display a transcriptional program geared more towards invasiveness and differentiation. Cells in the syncytium lose their proliferative capacity before they are able to upregulate fusogenic proteins necessary for cell fusion (35, 36). This invasive CTB group revealed DEGs including *TFPI*, *ECH1*, and *PSG4* among others which have demonstrated roles in the invasiveness and maturity of TB (19, 37, 38). Furthermore, many GO terms enriched in

10/12 d. p. f. EEC and BAP CTB were related to extracellular structure organization and migration which indicate a predisposition to develop further into another TB sublineage.

Functionally, the primitive STB differ in comparison to definitive STB (33). Primitive STB in the implanting conceptus prioritize proliferation and invasion as they help to invade and establish the framework for both an early form of nutrient sourcing (lacunae) and for a foundation for the future anchoring villous columns (42). When we probed for distinctions within the STB cluster, EEC STB at every time point grouped separate from both regenerative models TSC and BAP. EEC STB groups upregulated transcripts that were highly enriched in GO terms related to chromatin remodeling and oxygen-dependent metabolism. In general, CTB drive most of the ATP production in the placenta via oxidative phosphorylation as compared to STB (39, 43). But, in a nascent primitive syncytium, energy demands may be increased as the early embryo differentiates, proliferates, invades, and it is possible that this transitionary STB increases ATP production in order to keep up with energy requirements. GO terms also enriched in EEC STB included tissue migration, epithelial cell migration, extracellular matrix organization, and cell-substrate adhesion. These align with what we would expect to see in a primitive STB indicating that the primitive STB of EEC may have increased invasive and migratory capabilities as compared to a later stage TB.

Single nuclei RNA-sequencing reveals two subtypes of STB nuclei in the BAP model (44). In our bulk collection methods, we may have blurred the distinction between mixed populations within both BAP and TSC models as they both upregulate transcripts for both STB nuclei subtypes (*KRT8*, *S100P*, *XAGE2*, *ERVV-1*, *TBX3*, and *GRHL1*). We found that TSC and BAP STB DEGs placed heavy emphasis on glycerophospholipid synthesis. STB act as the primary barrier between mother and fetus and must maximize nutrient exchange by developing invaginations and increasing the surface area of STB at the maternal fetal interface (45). As STB develop invaginations, spread, invade, and increase vesicle mediated transport, new membranes must

be synthesized in accommodation. Glycerophospholipids are the main components of new membranes and are involved in other processes including cellular apoptosis (46). Glycerophospholipid metabolic pathways are also highly active in placental TB and a differentially regulated in pre-eclamptic placentas (47). We believe that early implanting embryos must place heavy emphasis on membrane synthesis in order to perform the highly specialized functions critical to fetal survival. Both TSC and BAP were also highly invasive compared to EEC STB. BAP are cultured on a Matrigel matrix while TSC are cultured on Collagen IV and EEC STB on fibronectin. Substrate differences may encourage invasiveness and cell spreading in the stem cell models compared to human embryos in extended culture.

During peri-implantation culture of human embryos, few groups have acknowledged the presence of MTB (25, 36). There is no villous column during this early point in development, begging the question of whether peri-implantation MTB are an artifact of the in vitro culture system, or if they represent a population of naturally occurring MTB before formation of the villous column. Early MTB may be early colonizers of the maternal spiral arteries and have a dual function in the immunomodulation responsibilities of the primitive placenta during implantation. Morphology of EEC MTB is quite different from the thin, stretched morphology of TSC MTB and suggests that though both cell types express extravillous TB markers, there may be differences between the two. First trimester human extravillous TB RNA-seq reveals three subpopulations of extravillous TB (31). Intriguingly, we found that the transcriptomes of EEC MTB and TSC MTB match closely with two of the first trimester extravillous TB subtypes. MTB in EEC closely resemble a subpopulation that upregulate pathways for receptor communication and immune signaling (31). EEC MTB express high levels of interferon stimulated genes and interferon receptors potentially responsible for immunomodulation during implantation (25). Alternatively, TSC MTB are more proliferative and upregulate pathways similar to the first trimester subgroup that is highly proliferative in nature (31). It is unclear whether or not MTB

from the TSC can faithfully replicate EEC MTB. Future studies will be needed to functionally test the usefulness of TSC MTB as they relate to modeling EEC MTB.

We used our transcriptomic data to identify new TB markers conserved across all models that may be significant to TB function. We identified 23-28 genes that were significantly upregulated in each cell type and validated some of their expression using immunofluorescence in extended culture human embryos. Several of these genes are known for their importance in TB function (*CGB1*, *CGB2*, and *HLA-G*), but many genes have not been considered for their significance to TB cells. *ANLN* plays a role in mediating nuclear division and is a prognostic marker in cancer cells (48, 49). Others have noted *ANLN* for its involvement in nuclear bridge formation in peri-implantation TB cytoplasmic bridges (36). Our results showed that *ANLN* was specifically expressed in CTB and most enriched in 8 d. p. f. EEC and TSC, which indicated that *ANLN* may promote cell proliferation and cell cycle. *FIBCD1* is an evolutionary-conserved myokine and is highly expressed in STB. *FIBCD1* plays an important role in regulating the cell size of cardiomyocytes (50). STB display similarities to cardiomyocytes in their multinucleated morphologies, and it is possible that *FIBCD1* may play a conserved role across these two cell types. Like *ANLN*, *FIBCD1* was also reported to be a prognostic factor by regulating inflammation and homeostasis (51, 52).

MAMDC2 was increased in MTB, particularly in EEC. *MAMDC2* acts as a tumor suppresser through inhibiting cell proliferation in cancer cells (53). Interestingly, *MAMDC2* mediates interferon responses downstream of viral entry (54). Peri-implantation EEC MTB also upregulate interferon stimulated genes during implantation and interferon may be involved in maternal tolerance of early pregnancy, though the exact mechanism is unknown (25). *MAMDC2* may mediate downstream interferon-stimulated gene expression in the presence of human endogenous retrovirus action while bypassing canonical interferon signaling mechanisms.

Future studies are needed to determine the potential role of *MAMDC2* in mediating interferon responses during the peri-implantation period.

Human peri-implantation embryos in extended culture also show positive immunofluorescent expression of markers upregulated in TSC with placental-specific promoters (*CYP19A1*, *EDNRB*, *IL2RB*, and *PTN*) implicating their role in the function of the primitive placenta. Because BAP TB like cells do not transcriptomically resemble later-stage TBs in the placenta, they have been proposed as a model for the primitive placenta (6). Proposed transcripts for four presumed markers of the primitive placenta (*GABRP*, *WFDC2*, *VTCN1*, and *ACTC1)* were significantly upregulated in the BAP model and in early placental tissues with negligible expression in term placental TB (22). We show that peri-implantation-stage human TB also upregulate transcript and protein expression of these markers. Though *GABRP* mRNA was undetected in several samples, immunoflourescent staining revealed bright localization in several areas throughout the embryo that increased over 7 d in extended culture. Transcripts for *VTCN1* and *ACTC1* were significantly increased in BAP and EEC compared to TSC suggesting that BAP may more closely resemble aspects of the primitive placenta than TSC.

Conclusion

The majority of human pregnancies are lost before clinical surveillance of an implanting embryo. Here, we validate two widely used regenerative TB models as they relate to the primitive placenta in vitro and describe subtle differences identified between each model. We show that CTB most closely resemble very early CTB in the implanting embryo whereas BAP CTB resemble a slightly later stage, more invasive CTB subtype at 10/12 d. p. f. STB from EEC are unique and most closely mimic what we would expect to see in the primitive placental transcriptional program. MTB from EEC and TSC are markedly different subtypes and the utility of TSC MTB will need to be validated in future functional studies. Furthermore, we validated the presence of 11 proteins of interest in EEC. In conclusion, both TSC and BAP are able to

recapitulate aspects of the primitive placenta during implantation. Our study will act as a powerful resource and reference to researchers to complete functional studies aimed to decipher events during implantation without the use of human embryos.

Table 4.1 Reads and mapping rate

Sample Name	% Aligned	Reads number				
SRR8952703	93.40%	8596413	GSM3735306	D10_E1_L1	SRR8952703	D10_E1_L
SRR8952704	93.80%	9898685	GSM3735307	D10_E1_L2	SRR8952704	D10_E1_L
SRR8952705	92.80%	9512642	GSM3735308	D10_E1_L3	SRR8952705	D10_E1_L
SRR8952706	95.50%	7299050	GSM3735309	D10_E1	SRR8952706	D10_E1_L
SRR8952707	93.10%	8420587	GSM3735310	D10_E1_S1	SRR8952707	D10_E1_S
SRR8952708	95.20%	7585880	GSM3735311	D10_E1_S2	SRR8952708	D10_E1_S
SRR8952709	94.20%	7909210	GSM3735312	D10_E1_S3	SRR8952709	D10_E1_S
SRR8952710	93.70%	1465483	GSM3735313	D10_E1_S4	SRR8952710	D10_E1_S
SRR8952711	95.20%	11499874	GSM3735314	D10_E1_S6	SRR8952711	D10_E1_S
SRR8952712	95.60%	7228973	GSM3735315	D10_E1_S7	SRR8952712	D10_E1_S
SRR8952713	94.30%	22891289	GSM3735316	D10_E1_S8	SRR8952713	D10_E1_S
SRR8952714	94.70%	8036833	GSM3735317	D10_E2_L10	SRR8952714	D10_E2_L
SRR8952715	93.50%	8408967	GSM3735318	D10_E2_L11	SRR8952715	D10_E2_L
SRR8952716	94.50%	6250180	GSM3735319	D10_E2_L1	SRR8952716	D10_E2_L
SRR8952717	92.00%	8472602	GSM3735320	D10_E2_L2	SRR8952717	D10_E2_L
SRR8952718	94.30%	7284695	GSM3735321	D10_E2_L3	SRR8952718	D10_E2_L
SRR8952719	94.00%	6510558	GSM3735322	D10_E2_L4	SRR8952719	D10_E2_L
SRR8952720	87.00%	6092800	GSM3735323	D10_E2_L5	SRR8952720	D10_E2_L
SRR8952721	92.90%	6965597	GSM3735324	D10_E2_L6	SRR8952721	D10_E2_L
SRR8952722	93.70%	5325537	GSM3735325	D10_E2_L7	SRR8952722	D10_E2_L
SRR8952723	93.60%	7620292	GSM3735326	D10_E2_L8	SRR8952723	D10_E2_L
SRR8952724	93.60%	7237066	GSM3735327	D10_E2_L9	SRR8952724	D10_E2_L
SRR8952725	94.10%	5054970	GSM3735328	D10_E2_S1	SRR8952725	D10_E2_S
SRR8952726	93.60%	6194481	GSM3735329	D10_E2_S2	SRR8952726	D10_E2_S
SRR8952727	96.40%	7523333	GSM3735330	D10_E2_S3	SRR8952727	D10_E2_S
SRR8952728	96.50%	6855838	GSM3735331	D10_E2_S4	SRR8952728	D10_E2_S
SRR8952729	95.50%	7798686	GSM3735332	D10_E2_S5	SRR8952729	D10_E2_S
SRR8952730	96.50%	8176716	GSM3735333	D10_E2_S6	SRR8952730	D10_E2_S
SRR8952731	96.80%	10078290	GSM3735334	D10_E2_S7	SRR8952731	D10_E2_S
SRR8952732	90.40%	12964451	GSM3735335	D10_E2_S8	SRR8952732	D10_E2_S
SRR8952733	95.80%	6345303	GSM3735336	D10_E3_S1	SRR8952733	D10_E3_S
SRR8952734	95.20%	7504765	GSM3735337	D10_E3_S2	SRR8952734	D10_E3_S
SRR8952735	96.00%	6938141	GSM3735338	D10_E3_S3	SRR8952735	D10_E3_S
SRR8952736	96.00%	5905482	GSM3735339	D10_E3_S4	SRR8952736	D10_E3_S

SRR8952737	96.40%	5230602	GSM3735340	D10_E3_S5	SRR8952737	D10_E3_S
SRR8952738	94.40%	4879572	GSM3735341	D10_E3_S6	SRR8952738	D10_E3_S
SRR8952739	96.10%	5064199	GSM3735342	D10_E3_S7	SRR8952739	D10_E3_S
SRR8952740	94.00%	9136764	GSM3735343	D10_E3_S8	SRR8952740	D10_E3_S
SRR8952741	90.50%	8138002	GSM3735344	D10_E4_L1	SRR8952741	D10_E4_L
SRR8952742	91.80%	8263717	GSM3735345	D10_E4_L2	SRR8952742	D10_E4_L
SRR8952743	90.80%	9083607	GSM3735346	D10_E4_L3	SRR8952743	D10_E4_L
SRR8952744	95.90%	7342117	GSM3735347	D10_E4_L4	SRR8952744	D10_E4_L
SRR8952745	90.30%	8854086	GSM3735348	D10_E4_L5	SRR8952745	D10_E4_L
SRR8952746	94.60%	9387246	GSM3735349	D10_E4_L6	SRR8952746	D10_E4_L
SRR8952747	94.40%	8230775	GSM3735350	D10_E4_S1	SRR8952747	D10_E4_S
SRR8952748	94.10%	5923126	GSM3735351	D10_E4_S2	SRR8952748	D10_E4_S
SRR8952749	91.70%	13462796	GSM3735352	D10_E4_S3	SRR8952749	D10_E4_S
SRR8952750	94.50%	8419271	GSM3735353	D10_E4_S4	SRR8952750	D10_E4_S
SRR8952751	96.20%	6378076	GSM3735354	D12_E3_S10	SRR8952751	D12_E3_S
SRR8952752	95.90%	7495034	GSM3735355	D12_E3_S11	SRR8952752	D12_E3_S
SRR8952753	94.70%	8576020	GSM3735356	D12_E3_S12	SRR8952753	D12_E3_S
SRR8952754	91.10%	38526	GSM3735357	D12_E3_S13	SRR8952754	D12_E3_S
SRR8952755	95.80%	7196557	GSM3735358	D12_E3_S14	SRR8952755	D12_E3_S
SRR8952756	95.50%	7687260	GSM3735359	D12_E3_S15	SRR8952756	D12_E3_S
SRR8952757	94.30%	8309106	GSM3735360	D12_E3_S16	SRR8952757	D12_E3_S
SRR8952758	96.60%	7099073	GSM3735361	D12_E3_S17	SRR8952758	D12_E3_S
SRR8952759	96.50%	9121694	GSM3735362	D12_E3_S18	SRR8952759	D12_E3_S
SRR8952760	96.50%	7020173	GSM3735363	D12_E3_S19	SRR8952760	D12_E3_S
SRR8952761	93.90%	8031614	GSM3735364	D12_E3_S1	SRR8952761	D12_E3_S
SRR8952762	96.50%	6636300	GSM3735365	D12_E3_S20	SRR8952762	D12_E3_S
SRR8952763	96.40%	14169433	GSM3735366	D12_E3_S21	SRR8952763	D12_E3_S
SRR8952764	96.50%	7085714	GSM3735367	D12_E3_S22	SRR8952764	D12_E3_S
SRR8952765	96.50%	8363848	GSM3735368	D12_E3_S23	SRR8952765	D12_E3_S
SRR8952766	96.60%	6627786	GSM3735369	D12_E3_S24	SRR8952766	D12_E3_S
SRR8952767	95.90%	8047829	GSM3735370	D12_E3_S2	SRR8952767	D12_E3_S
SRR8952768	96.10%	8358577	GSM3735371	D12_E3_S3	SRR8952768	D12_E3_S
SRR8952769	96.30%	6119895	GSM3735372	D12_E3_S4	SRR8952769	D12_E3_S
SRR8952770	95.50%	8567685	GSM3735373	D12_E3_S5	SRR8952770	D12_E3_S
SRR8952771	95.30%	6495861	GSM3735374	D12_E3_S6	SRR8952771	D12_E3_S

SRR8952772	95.60%	7569439	GSM3735375	D12_E3_S7	SRR8952772	D12_E3_S
SRR8952773	95.30%	8478756	GSM3735376	D12_E3_S8	SRR8952773	D12_E3_S
SRR8952774	93.80%	6645566	GSM3735377	D12_E3_S9	SRR8952774	D12_E3_S
SRR8952775	95.70%	7270245	GSM3735378	D12_E4_EVT10	SRR8952775	D12_E4_EVT
SRR8952776	96.00%	8174369	GSM3735379	D12_E4_EVT11	SRR8952776	D12_E4_EVT
SRR8952777	95.30%	5490346	GSM3735380	D12_E4_EVT12	SRR8952777	D12_E4_EVT
SRR8952778	96.30%	6262326	GSM3735381	D12_E4_EVT13	SRR8952778	D12_E4_EVT
SRR8952779	94.80%	9105202	GSM3735382	D12_E4_EVT1	SRR8952779	D12_E4_EVT
SRR8952780	96.20%	9617127	GSM3735383	D12_E4_EVT2	SRR8952780	D12_E4_EVT
SRR8952781	96.40%	9885444	GSM3735384	D12_E4_EVT3	SRR8952781	D12_E4_EVT
SRR8952782	95.80%	8431298	GSM3735385	D12_E4_EVT4	SRR8952782	D12_E4_EVT
SRR8952783	96.10%	8624450	GSM3735386	D12_E4_EVT5	SRR8952783	D12_E4_EVT
SRR8952784	96.20%	8688825	GSM3735387	D12_E4_EVT6	SRR8952784	D12_E4_EVT
SRR8952785	94.60%	7847667	GSM3735388	D12_E4_EVT7	SRR8952785	D12_E4_EVT
SRR8952786	96.10%	8765665	GSM3735389	D12_E4_EVT8	SRR8952786	D12_E4_EVT
SRR8952787	96.30%	7965308	GSM3735390	D12_E4_L1	SRR8952787	D12_E4_L
SRR8952788	94.50%	8204903	GSM3735391	D12_E4_L2	SRR8952788	D12_E4_L
SRR8952789	95.40%	8998275	GSM3735392	D12_E4_L3	SRR8952789	D12_E4_L
SRR8952790	96.10%	6887393	GSM3735393	D12_E4_L4	SRR8952790	D12_E4_L
SRR8952791	95.60%	8319181	GSM3735394	D12_E4_L5	SRR8952791	D12_E4_L
SRR8952792	96.30%	9307624	GSM3735395	D12_E4_L6	SRR8952792	D12_E4_L
SRR8952793	96.10%	8090547	GSM3735396	D12_E4_S1	SRR8952793	D12_E4_S
SRR8952794	96.50%	10046783	GSM3735397	D12_E4_S2	SRR8952794	D12_E4_S
SRR8952795	95.90%	8915944	GSM3735398	D12_E4_S3	SRR8952795	D12_E4_S
SRR8952796	96.30%	9376822	GSM3735399	D12_E4_S4	SRR8952796	D12_E4_S
SRR8952797	87.10%	7641755	GSM3735400	D12_E6_L1	SRR8952797	D12_E6_L
SRR8952798	69.00%	5964624	GSM3735401	D12_E6_L2	SRR8952798	D12_E6_L
SRR8952800	77.30%	4899946	GSM3735403	D12_E6_L4	SRR8952800	D12_E6_L
SRR8952801	89.10%	7926955	GSM3735404	D12_E6_L5	SRR8952801	D12_E6_L
SRR8952802	92.00%	7857383	GSM3735405	D12_E6_L6	SRR8952802	D12_E6_L
SRR8952803	96.50%	7864434	GSM3735406	D12_E6_S1	SRR8952803	D12_E6_S
SRR8952804	96.00%	8903070	GSM3735407	D12_E6_S2	SRR8952804	D12_E6_S
SRR8952805	96.10%	9065571	GSM3735408	D12_E6_S3	SRR8952805	D12_E6_S
SRR8952806	96.40%	8084656	GSM3735409	D12_E6_S4	SRR8952806	D12_E6_S
SRR8952807	96.20%	6953327	GSM3735410	D12_EVT2	SRR8952807	D12_EVT

SRR8952808	96.10%	7439458	GSM3735411	D12_EVT3	SRR8952808	D12_EVT
SRR8952809	96.00%	6714339	GSM3735412	D12_EVT4	SRR8952809	D12_EVT
SRR8952810	96.20%	8000180	GSM3735413	D12_EVT5	SRR8952810	D12_EVT
SRR8952811	96.80%	7380973	GSM3735414	D8_E1_S1	SRR8952811	D8_E1_S
SRR8952812	96.50%	5353845	GSM3735415	D8_E1_S2	SRR8952812	D8_E1_S
SRR8952813	96.20%	6024549	GSM3735416	D8_E1_S3	SRR8952813	D8_E1_S
SRR8952814	95.90%	6147204	GSM3735417	D8_E1_S4	SRR8952814	D8_E1_S
SRR8952815	96.10%	5922249	GSM3735418	D8_E1_S5	SRR8952815	D8_E1_S
SRR8952816	96.60%	6526278	GSM3735419	D8_E1_S6	SRR8952816	D8_E1_S
SRR8952817	96.70%	8315740	GSM3735420	D8_E1_S7	SRR8952817	D8_E1_S
SRR8952818	96.20%	7473363	GSM3735421	D8_E1_S8	SRR8952818	D8_E1_S
SRR8952819	96.50%	3414968	GSM3735422	D8_E2_S1	SRR8952819	D8_E2_S
SRR8952820	96.50%	6923348	GSM3735423	D8_E2_S2	SRR8952820	D8_E2_S
SRR8952821	97.10%	6247347	GSM3735424	D8_E2_S3	SRR8952821	D8_E2_S
SRR8952822	97.00%	6388755	GSM3735425	D8_E2_S4	SRR8952822	D8_E2_S
SRR8952823	96.70%	7549403	GSM3735426	D8_E2_S5	SRR8952823	D8_E2_S
SRR8952824	97.00%	6456780	GSM3735427	D8_E2_S6	SRR8952824	D8_E2_S
SRR8952825	97.00%	7261468	GSM3735428	D8_E2_S7	SRR8952825	D8_E2_S
SRR8952826	97.00%	7754509	GSM3735429	D8_E2_S8	SRR8952826	D8_E2_S
SRR8952827	94.80%	1616978	GSM3735430	D8_E3_L1	SRR8952827	D8_E3_L
SRR8952828	94.80%	7045379	GSM3735431	D8_E3_L2	SRR8952828	D8_E3_L
SRR8952829	94.40%	6730932	GSM3735432	D8_E3_L3	SRR8952829	D8_E3_L
SRR8952830	94.40%	6884676	GSM3735433	D8_E3_L4	SRR8952830	D8_E3_L
SRR8952831	96.70%	6668351	GSM3735434	D8_E3_S1	SRR8952831	D8_E3_S
SRR8952832	96.70%	7766811	GSM3735435	D8_E3_S2	SRR8952832	D8_E3_S
SRR8952833	96.70%	6236139	GSM3735436	D8_E3_S3	SRR8952833	D8_E3_S
SRR8952834	96.60%	4605993	GSM3735437	D8_E3_S4	SRR8952834	D8_E3_S
SRR8952835	96.50%	4987180	GSM3735438	D8_E3_S5	SRR8952835	D8_E3_S
SRR8952836	90.50%	4776822	GSM3735439	D8_E3_S6	SRR8952836	D8_E3_S
SRR8952837	96.90%	6911476	GSM3735440	D8_E3_S7	SRR8952837	D8_E3_S
SRR8952838	86.90%	6868793	GSM3735441	D8_E3_S8	SRR8952838	D8_E3_S
SRR8952839	95.80%	10719882	GSM3735442	D8_E4_S1	SRR8952839	D8_E4_S
SRR8952840	96.10%	7633814	GSM3735443	D8_E4_S2	SRR8952840	D8_E4_S
SRR8952841	95.80%	8308750	GSM3735444	D8_E4_S3	SRR8952841	D8_E4_S

Table 4.2 Differentially expressed genes between CTB subtypes. Subtype 2 vs. subtype 1

SYMBOL	logFC	logCPM	LR	PValue	FDR	regulated
TFPI	-4.3E+00	8.8E+00	2.1E+02	3.3E-47	7.7E-43	down
TUBB6	-2.0E+00	9.6E+00	1.4E+02	7.0E-33	8.2E-29	down
ECH1	-1.4E+00	7.3E+00	1.4E+02	2.5E-32	2.0E-28	down
PSG4	-3.8E+00	6.6E+00	1.3E+02	8.4E-30	4.9E-26	down
TPM1	-1.9E+00	1.1E+01	1.2E+02	1.9E-28	8.9E-25	down
PAPOLA	1.6E+00	9.9E+00	1.1E+02	1.1E-26	4.4E-23	up
SPARC	-2.6E+00	9.2E+00	1.1E+02	2.6E-26	8.7E-23	down
HINT1	-1.2E+00	9.0E+00	1.1E+02	6.5E-26	1.8E-22	down
CLTB	-2.1E+00	7.1E+00	1.1E+02	6.9E-26	1.8E-22	down
FERMT2	-1.5E+00	7.3E+00	1.1E+02	6.3E-25	1.4E-21	down
TFAP2C	2.0E+00	8.2E+00	1.1E+02	6.4E-25	1.4E-21	up
OSTF1	-1.3E+00	6.9E+00	9.8E+01	4.1E-23	8.0E-20	down
PDCD1LG2	-7.6E+00	3.5E+00	9.7E+01	5.8E-23	1.0E-19	down
ARL6IP5	-1.2E+00	8.0E+00	9.2E+01	7.4E-22	1.2E-18	down
MT1X	-5.3E+00	4.5E+00	9.2E+01	8.5E-22	1.3E-18	down
SLC7A8	3.1E+00	8.0E+00	9.2E+01	9.3E-22	1.4E-18	up
MT1H	-6.7E+00	4.4E+00	9.1E+01	1.8E-21	2.5E-18	down
SRI	-1.4E+00	7.6E+00	9.0E+01	2.2E-21	2.8E-18	down
TDRP	1.5E+00	7.9E+00	8.9E+01	3.3E-21	4.0E-18	up
MT1G	-5.9E+00	4.9E+00	8.9E+01	4.2E-21	4.8E-18	down
TMEM134	-1.7E+00	4.9E+00	8.8E+01	5.6E-21	6.1E-18	down
SLC25A15	-2.6E+00	6.9E+00	8.8E+01	5.7E-21	6.1E-18	down
GLIPR1	-5.7E+00	6.2E+00	8.8E+01	7.1E-21	7.2E-18	down
ATP6V1C2	2.2E+00	6.5E+00	8.7E+01	8.6E-21	8.3E-18	up
TFRC	1.7E+00	9.1E+00	8.7E+01	9.2E-21	8.5E-18	up
CASP4	-4.3E+00	5.5E+00	8.6E+01	1.8E-20	1.5E-17	down
DIO2	-6.1E+00	5.5E+00	8.4E+01	5.1E-20	4.2E-17	down
FABP5	1.8E+00	8.0E+00	8.4E+01	5.8E-20	4.7E-17	up
CALD1	-1.5E+00	8.1E+00	8.4E+01	6.3E-20	4.9E-17	down
ADAM12	-4.8E+00	4.9E+00	8.3E+01	7.2E-20	5.4E-17	down
S100A11	-1.3E+00	9.7E+00	8.2E+01	1.2E-19	8.6E-17	down
LYN	1.5E+00	8.3E+00	8.2E+01	1.7E-19	1.2E-16	up

TLE5	-1.7E+00	7.0E+00	8.1E+01	2.2E-19	1.5E-16	down
MYL6	-1.3E+00	9.8E+00	8.0E+01	3.4E-19	2.3E-16	down
RNF14	-1.2E+00	6.5E+00	7.9E+01	5.9E-19	3.6E-16	down
GTF2I-AS1	-6.7E+00	3.6E+00	7.8E+01	8.7E-19	5.0E-16	down
VGLL3	-4.2E+00	6.0E+00	7.8E+01	8.8E-19	5.0E-16	down
ABCC5	1.8E+00	6.6E+00	7.8E+01	1.2E-18	6.5E-16	up
ITGB1	-1.2E+00	9.6E+00	7.7E+01	1.7E-18	9.3E-16	down
PDLIM5	-1.8E+00	7.1E+00	7.7E+01	1.8E-18	9.8E-16	down
CTNNB1	1.5E+00	9.3E+00	7.6E+01	2.6E-18	1.3E-15	up
DNMT1	1.2E+00	7.4E+00	7.6E+01	3.2E-18	1.5E-15	up
SDCBP	-1.2E+00	9.7E+00	7.5E+01	3.8E-18	1.8E-15	down
BNIP3L	-1.3E+00	6.4E+00	7.5E+01	4.8E-18	2.2E-15	down
BCAT1	1.4E+00	7.9E+00	7.4E+01	9.0E-18	4.0E-15	up
SH3BGRL3	-1.8E+00	7.3E+00	7.3E+01	1.1E-17	5.0E-15	down
C12orf75	-2.0E+00	7.8E+00	7.3E+01	1.3E-17	5.7E-15	down
HNMT	-5.4E+00	3.5E+00	7.3E+01	1.5E-17	6.3E-15	down
S1PR2	1.8E+00	5.4E+00	7.2E+01	1.7E-17	7.3E-15	up
TRIM33	1.4E+00	7.2E+00	7.2E+01	2.0E-17	8.1E-15	up
SEC61G	-1.0E+00	6.8E+00	7.2E+01	2.5E-17	9.8E-15	down
STARD3NL	-1.2E+00	6.0E+00	7.1E+01	3.0E-17	1.2E-14	down
CNPY3	-1.1E+00	6.6E+00	7.0E+01	5.8E-17	2.2E-14	down
NUDT4	2.0E+00	6.0E+00	6.9E+01	8.6E-17	3.1E-14	up
MRPL4	1.2E+00	6.6E+00	6.9E+01	8.6E-17	3.1E-14	up
MFAP5	-2.9E+00	7.9E+00	6.9E+01	8.8E-17	3.1E-14	down
LAMA1	2.8E+00	7.9E+00	6.8E+01	1.3E-16	4.5E-14	up
MMP12	-7.1E+00	4.8E+00	6.8E+01	1.6E-16	5.5E-14	down
TAGLN2	-2.0E+00	9.1E+00	6.8E+01	2.0E-16	6.8E-14	down
TMSB10	-1.6E+00	1.0E+01	6.6E+01	3.8E-16	1.2E-13	down
GH2	-5.7E+00	3.7E+00	6.6E+01	4.5E-16	1.4E-13	down
FHOD3	-6.5E+00	1.1E+00	6.5E+01	6.1E-16	1.9E-13	down
S100P	-2.1E+00	7.0E+00	6.5E+01	7.3E-16	2.1E-13	down
LRRC32	-4.4E+00	6.7E+00	6.3E+01	1.6E-15	4.7E-13	down
RBM47	1.4E+00	7.8E+00	6.3E+01	1.8E-15	5.0E-13	up
COLEC12	2.9E+00	7.5E+00	6.3E+01	2.4E-15	6.5E-13	up
PNP	1.3E+00	7.1E+00	6.3E+01	2.4E-15	6.5E-13	up
CGB5	-3.0E+00	1.1E+01	6.2E+01	3.0E-15	7.9E-13	down
SCD	1.5E+00	1.0E+01	6.2E+01	3.4E-15	8.7E-13	up

CCKBR	3.4E+00	8.9E+00	6.2E+01	3.8E-15	9.7E-13	up
POLR3E	1.1E+00	6.2E+00	6.1E+01	5.3E-15	1.3E-12	up
FXYD5	-1.2E+00	6.7E+00	6.1E+01	5.8E-15	1.4E-12	down
COMT	-1.7E+00	6.2E+00	6.1E+01	6.0E-15	1.5E-12	down
APOA1	-8.7E+00	1.6E+00	6.0E+01	7.4E-15	1.8E-12	down
PDLIM7	-1.4E+00	6.5E+00	6.0E+01	8.0E-15	1.9E-12	down
CGB7	-2.7E+00	7.8E+00	6.0E+01	9.3E-15	2.2E-12	down
MEST	-2.5E+00	8.4E+00	6.0E+01	9.4E-15	2.2E-12	down
DNMT3B	2.8E+00	7.3E+00	6.0E+01	9.8E-15	2.3E-12	up
B4GALT4	-1.0E+00	7.1E+00	6.0E+01	1.0E-14	2.4E-12	down
MMP2	-3.2E+00	1.0E+01	6.0E+01	1.2E-14	2.6E-12	down
CGB8	-2.7E+00	1.0E+01	5.9E+01	1.6E-14	3.7E-12	down
EFNA1	-1.8E+00	8.0E+00	5.9E+01	2.0E-14	4.4E-12	down
MT2A	-4.0E+00	5.5E+00	5.8E+01	2.7E-14	6.0E-12	down
WIPF1	-3.4E+00	4.4E+00	5.8E+01	2.8E-14	6.1E-12	down
MTND2P28	-1.5E+00	5.5E+00	5.8E+01	2.9E-14	6.2E-12	down
ZNRF1	1.1E+00	6.3E+00	5.8E+01	2.9E-14	6.3E-12	up
KCNE5	-6.5E+00	1.1E+00	5.7E+01	3.9E-14	8.1E-12	down
PSME1	-1.9E+00	6.0E+00	5.7E+01	4.2E-14	8.6E-12	down
TPGS2	-1.1E+00	7.3E+00	5.7E+01	5.4E-14	1.1E-11	down
LAMA4	-7.0E+00	1.1E+00	5.6E+01	5.7E-14	1.1E-11	down
TET2	1.6E+00	7.2E+00	5.6E+01	6.8E-14	1.3E-11	up
PON2	-1.5E+00	6.6E+00	5.6E+01	7.6E-14	1.5E-11	down
TRIML1	5.4E+00	2.3E+00	5.6E+01	7.8E-14	1.5E-11	up
ATAD3B	1.0E+00	7.7E+00	5.5E+01	1.2E-13	2.2E-11	up
STS	1.4E+00	8.1E+00	5.5E+01	1.2E-13	2.2E-11	up
MYCN	1.5E+00	7.9E+00	5.5E+01	1.3E-13	2.4E-11	up
MED12L	2.1E+00	5.8E+00	5.4E+01	1.9E-13	3.3E-11	up
MYL7	-6.6E+00	3.3E+00	5.4E+01	1.9E-13	3.5E-11	down
PLOD1	-1.5E+00	8.2E+00	5.4E+01	2.1E-13	3.7E-11	down

Table 4.3 Differentially expressed genes between STB subtypes. Subtype 1 vs. subtype 2.

SYMBOL	logFC	logCPM	LR	PValue	FDR	regulated
AK6	-9.5E+00	2.7E+00	6.2E+02	9.2E-137	2.1E-132	down
BDP1	-9.4E+00	2.1E+00	5.3E+02	1.1E-116	1.2E-112	down
SMDT1	-9.9E+00	2.2E+00	4.8E+02	3.4E-106	2.7E-102	down
PKP3	2.9E+00	5.8E+00	4.1E+02	1.2E-90	6.9E-87	up
MIR22HG	-9.1E+00	1.7E+00	3.9E+02	1.3E-86	6.0E-83	down
ZNHIT3	-9.2E+00	1.5E+00	3.7E+02	1.1E-82	4.2E-79	down
TIMM22	-9.1E+00	1.4E+00	3.2E+02	1.6E-71	5.4E-68	down
AKAP17A	-9.4E+00	2.3E+00	3.1E+02	6.8E-69	2.0E-65	down
LENG1	-8.1E+00	7.3E-01	2.8E+02	1.8E-63	4.7E-60	down
PFDN6	-7.5E+00	1.7E-01	2.7E+02	1.7E-61	4.0E-58	down
DSEL	-8.8E+00	1.7E+00	2.7E+02	1.0E-60	2.1E-57	down
JUP	2.1E+00	8.1E+00	2.6E+02	2.9E-59	5.6E-56	up
CD99P1	-7.6E+00	5.7E-01	2.6E+02	5.0E-59	9.0E-56	down
CHCHD10	-7.6E+00	-4.6E-02	2.6E+02	6.3E-59	1.0E-55	down
C6orf136	-7.1E+00	-4.8E-01	2.6E+02	1.2E-58	1.8E-55	down
ZNF676	-8.2E+00	3.1E+00	2.6E+02	1.3E-58	1.8E-55	down
DGKZ	2.0E+00	5.4E+00	2.5E+02	8.4E-57	1.2E-53	up
RILP	-7.0E+00	-1.2E-02	2.5E+02	4.5E-56	5.8E-53	down
ATAT1	-6.8E+00	-4.8E-01	2.5E+02	8.6E-56	1.1E-52	down
ASMTL	-6.6E+00	-6.4E-01	2.5E+02	1.3E-55	1.6E-52	down
DHRSX	-7.7E+00	3.4E-01	2.5E+02	2.6E-55	2.9E-52	down
SMARCB1	-7.5E+00	8.1E-01	2.4E+02	1.3E-53	1.4E-50	down
MLLT6	-6.8E+00	-2.1E-01	2.3E+02	6.4E-53	6.2E-50	down
CISD3	-8.2E+00	5.2E-01	2.3E+02	1.0E-52	9.5E-50	down
DBNL	2.1E+00	6.1E+00	2.3E+02	3.5E-52	3.1E-49	up
NUAK2	2.8E+00	5.0E+00	2.2E+02	1.6E-50	1.4E-47	up
POMGNT1	2.0E+00	5.7E+00	2.2E+02	7.1E-49	5.9E-46	up
FKBPL	-6.5E+00	-7.8E-01	2.1E+02	4.6E-48	3.7E-45	down
FZD2	1.2E+01	3.2E+00	2.1E+02	1.2E-47	9.6E-45	up
FLOT2	2.3E+00	5.7E+00	2.1E+02	1.4E-47	1.0E-44	up
PIGW	-6.7E+00	-8.8E-01	2.1E+02	6.4E-47	4.7E-44	down
LY6G6C	-8.7E+00	1.3E+00	2.0E+02	1.9E-46	1.3E-43	down

DCTN1	2.1E+00	4.6E+00	2.0E+02	2.3E-45	1.6E-42	up
PPP6R1	2.4E+00	4.5E+00	2.0E+02	1.9E-44	1.2E-41	up
USP5	2.0E+00	5.2E+00	1.9E+02	1.4E-43	8.8E-41	up
SEC24C	3.0E+00	4.4E+00	1.9E+02	1.9E-43	1.2E-40	up
RIC8A	1.9E+00	5.6E+00	1.9E+02	7.8E-43	4.8E-40	up
TMEM259	1.9E+00	6.2E+00	1.9E+02	1.1E-42	6.6E-40	up
DUS1L	1.6E+00	6.3E+00	1.9E+02	3.0E-42	1.8E-39	up
PPP2R3B	-6.0E+00	-1.2E+00	1.8E+02	4.3E-42	2.4E-39	down
PFKL	1.9E+00	7.1E+00	1.8E+02	6.3E-42	3.5E-39	up
DPP3	2.7E+00	4.4E+00	1.8E+02	3.1E-41	1.7E-38	up
RPL4P5	-6.2E+00	-1.3E+00	1.8E+02	3.3E-41	1.7E-38	down
HGS	2.3E+00	5.5E+00	1.8E+02	6.0E-41	3.1E-38	up
GRN	2.6E+00	6.8E+00	1.8E+02	1.5E-40	7.7E-38	up
TOM1	1.5E+00	5.9E+00	1.8E+02	2.0E-40	1.0E-37	up
ITGB5	2.3E+00	5.1E+00	1.8E+02	3.0E-40	1.5E-37	up
IFIT2	6.1E+00	1.1E+00	1.7E+02	3.1E-39	1.5E-36	up
DLX5	-3.2E+00	6.0E+00	1.7E+02	5.1E-39	2.4E-36	down
WDR6	2.3E+00	5.1E+00	1.7E+02	1.2E-38	5.5E-36	up
RHOT2	2.1E+00	5.5E+00	1.7E+02	2.5E-38	1.1E-35	up
DNM2	1.9E+00	5.9E+00	1.7E+02	7.5E-38	3.3E-35	up
MED16	1.8E+00	5.5E+00	1.6E+02	1.4E-37	6.2E-35	up
STARD3	1.8E+00	5.0E+00	1.6E+02	2.1E-37	8.9E-35	up
POLD1	2.2E+00	3.8E+00	1.6E+02	2.9E-37	1.2E-34	up
DHCR24	2.4E+00	5.5E+00	1.6E+02	3.1E-37	1.3E-34	up
LRRC41	2.0E+00	6.0E+00	1.6E+02	7.3E-37	2.9E-34	up
SLC44A2	2.0E+00	7.6E+00	1.6E+02	1.8E-36	7.0E-34	up
ACTN1	2.3E+00	8.3E+00	1.6E+02	3.7E-36	1.4E-33	up
SERPINE1	2.2E+00	7.8E+00	1.5E+02	1.5E-35	5.4E-33	up
CERCAM	2.8E+00	5.2E+00	1.5E+02	1.5E-35	5.6E-33	up
MAN1B1	1.7E+00	5.3E+00	1.5E+02	1.8E-35	6.5E-33	up
CIZ1	2.0E+00	4.3E+00	1.5E+02	3.5E-35	1.2E-32	up
PIGO	2.1E+00	4.9E+00	1.5E+02	4.4E-35	1.5E-32	up
ELAC2	1.8E+00	5.5E+00	1.5E+02	8.8E-35	3.0E-32	up
SKA1	-6.2E+00	-1.3E+00	1.5E+02	2.8E-34	9.3E-32	down
ZNF723	-8.7E+00	1.3E+00	1.5E+02	7.6E-34	2.5E-31	down
LINC00221	-8.9E+00	1.2E+00	1.5E+02	1.1E-33	3.6E-31	down

PTRH2	-1.8E+00	6.9E+00	1.5E+02	1.1E-33	3.6E-31	down
CYFIP1	1.6E+00	6.2E+00	1.5E+02	1.3E-33	4.2E-31	up
PSAP	1.8E+00	9.8E+00	1.4E+02	3.0E-33	9.5E-31	up
C1orf115	2.4E+00	7.5E+00	1.4E+02	4.2E-33	1.3E-30	up
SPINT1	1.9E+00	7.7E+00	1.4E+02	7.2E-33	2.2E-30	up
VPS51	2.1E+00	5.6E+00	1.4E+02	1.1E-32	3.3E-30	up
APEH	1.4E+00	6.3E+00	1.4E+02	1.4E-32	4.1E-30	up
CHFR	1.8E+00	4.5E+00	1.4E+02	1.4E-32	4.2E-30	up
NECTIN2	3.0E+00	5.5E+00	1.4E+02	1.4E-32	4.2E-30	up
ZBTB8OS	-1.6E+00	6.6E+00	1.4E+02	1.5E-32	4.2E-30	down
FBXW5	1.7E+00	6.7E+00	1.4E+02	2.2E-32	6.1E-30	up
ITGA5	2.1E+00	8.1E+00	1.4E+02	2.8E-32	8.0E-30	up
SQSTM1	2.2E+00	7.9E+00	1.4E+02	5.4E-32	1.5E-29	up
NOC2L	1.9E+00	5.8E+00	1.4E+02	5.5E-32	1.5E-29	up
SELENOK	-1.7E+00	7.9E+00	1.4E+02	8.4E-32	2.3E-29	down
VPS16	1.9E+00	4.7E+00	1.4E+02	9.4E-32	2.5E-29	up
TNFRSF1A	1.6E+00	4.8E+00	1.4E+02	9.7E-32	2.6E-29	up
STK25	1.8E+00	6.3E+00	1.4E+02	1.1E-31	2.9E-29	up
C2	-7.1E+00	-5.3E-01	1.4E+02	1.5E-31	3.7E-29	down
ZYX	1.7E+00	6.1E+00	1.4E+02	1.5E-31	3.7E-29	up
GPAA1	1.6E+00	6.7E+00	1.4E+02	1.6E-31	4.0E-29	up
PLOD1	1.7E+00	7.2E+00	1.4E+02	1.6E-31	4.0E-29	up
CNP	2.2E+00	4.1E+00	1.4E+02	2.0E-31	5.0E-29	up
LRP10	1.5E+00	5.8E+00	1.4E+02	3.3E-31	8.0E-29	up
ARHGEF1	1.7E+00	4.6E+00	1.3E+02	6.1E-31	1.5E-28	up
MEST	2.0E+00	7.4E+00	1.3E+02	7.7E-31	1.8E-28	up
PRPF6	1.2E+00	6.0E+00	1.3E+02	8.6E-31	2.0E-28	up
CSH2	-6.9E+00	8.8E+00	1.3E+02	9.4E-31	2.2E-28	down
ACAD9	1.6E+00	4.7E+00	1.3E+02	1.4E-30	3.3E-28	up
AADACL2	-6.5E+00	-1.1E+00	1.3E+02	1.5E-30	3.6E-28	down
ARMC6	1.7E+00	4.2E+00	1.3E+02	2.4E-30	5.5E-28	up

Table 4.4 Differentially expressed genes between MTB models. EEC MTB vs. TSC MTB

SYMBOL	logFC	logCPM	LR	PValue	FDR	regulated
LAIR2	1.5E+01	7.5E+00	6.3E+02	6.3E-140	1.5E-135	up
ID1	5.0E+00	7.4E+00	2.5E+02	2.9E-55	3.4E-51	up
HAND1	1.2E+01	6.6E+00	2.4E+02	1.4E-53	1.1E-49	up
ETS2	4.5E+00	8.1E+00	2.1E+02	1.5E-46	8.7E-43	up
LITAF	8.0E+00	9.3E+00	1.8E+02	1.8E-40	7.1E-37	up
MMP12	1.1E+01	1.2E+01	1.6E+02	1.0E-35	3.5E-32	up
FST	7.6E+00	7.8E+00	1.4E+02	3.5E-33	1.0E-29	up
PSMB3	1.0E+01	3.3E+00	1.4E+02	3.2E-32	8.2E-29	up
CCN2	1.1E+01	1.1E+01	1.4E+02	7.9E-32	1.8E-28	up
GLIPR1	3.5E+00	7.5E+00	1.4E+02	1.0E-31	2.2E-28	up
EDNRB	5.0E+00	9.8E+00	1.3E+02	4.6E-30	8.9E-27	up
CLTB	3.9E+00	9.2E+00	1.3E+02	6.3E-30	1.1E-26	up
GLRX	6.2E+00	9.5E+00	1.2E+02	5.6E-29	9.4E-26	up
BAMBI	4.7E+00	6.5E+00	1.2E+02	1.1E-28	1.7E-25	up
RNF24	4.2E+00	6.4E+00	1.2E+02	6.3E-28	9.2E-25	up
PDCD1LG2	3.6E+00	7.1E+00	1.2E+02	1.2E-27	1.7E-24	up
ESAM	4.4E+00	1.0E+01	1.2E+02	3.0E-27	3.8E-24	up
GADD45B	4.1E+00	5.9E+00	1.2E+02	4.8E-27	5.9E-24	up
DHRS3	4.1E+00	6.6E+00	1.2E+02	5.3E-27	6.2E-24	up
SNN	4.4E+00	6.0E+00	1.1E+02	1.0E-26	1.1E-23	up
RAB32	5.0E+00	5.1E+00	1.1E+02	3.7E-25	3.9E-22	up
C1orf105	-1.1E+01	2.5E+00	1.1E+02	6.8E-25	6.9E-22	down
GPC1	-2.6E+00	7.2E+00	1.0E+02	2.0E-24	1.9E-21	down
ST14	-1.0E+01	2.9E+00	1.0E+02	3.0E-24	2.8E-21	down
TRIM61	9.5E+00	3.3E+00	1.0E+02	4.7E-24	4.2E-21	up
PAQR8	5.9E+00	6.3E+00	1.0E+02	5.6E-24	4.9E-21	up
ODAPH	7.9E+00	7.1E+00	1.0E+02	1.5E-23	1.2E-20	up
ASPHD2	4.1E+00	5.8E+00	1.0E+02	1.5E-23	1.2E-20	up
SLC52A1	-9.7E+00	2.6E+00	9.9E+01	2.6E-23	2.0E-20	down
CAB39L	3.9E+00	8.4E+00	9.4E+01	2.7E-22	2.1E-19	up
STAC	1.1E+01	5.1E+00	9.3E+01	5.0E-22	3.7E-19	up
MCM7	-2.4E+00	6.1E+00	9.2E+01	7.4E-22	5.3E-19	down

DSC2	-2.4E+00	8.4E+00	9.1E+01	1.2E-21	7.9E-19	down
PLEKHG5	5.7E+00	5.3E+00	8.9E+01	3.6E-21	2.4E-18	up
SLC4A8	7.7E+00	6.4E+00	8.8E+01	5.8E-21	3.8E-18	up
CLDN19	4.5E+00	5.7E+00	8.8E+01	7.4E-21	4.7E-18	up
SKIL	2.9E+00	6.6E+00	8.7E+01	8.4E-21	5.2E-18	up
TMPRSS2	-8.2E+00	2.3E+00	8.0E+01	3.0E-19	1.8E-16	down
PAK6	-1.1E+01	2.1E+00	7.9E+01	6.4E-19	3.8E-16	down
BUB1B-PAK6	-1.1E+01	2.1E+00	7.9E+01	6.4E-19	3.8E-16	down
DHRSX	9.2E+00	1.9E+00	7.9E+01	6.8E-19	3.9E-16	up
SMDT1	9.3E+00	1.3E+00	7.8E+01	8.6E-19	4.8E-16	up
MIR22HG	9.7E+00	2.4E+00	7.7E+01	1.4E-18	7.3E-16	up
ERBB3	-3.0E+00	7.7E+00	7.6E+01	2.6E-18	1.4E-15	down
PROS1	2.8E+00	6.9E+00	7.5E+01	4.2E-18	2.2E-15	up
CDC42EP5	1.0E+01	2.3E+00	7.4E+01	8.5E-18	4.3E-15	up
KCNK5	-9.0E+00	1.8E+00	7.4E+01	9.1E-18	4.5E-15	down
E2F1	-8.3E+00	2.0E+00	7.4E+01	9.4E-18	4.5E-15	down
AHCYL1	-1.8E+00	6.8E+00	7.3E+01	1.0E-17	4.9E-15	down
LINC00839	-1.0E+01	1.6E+00	7.3E+01	1.1E-17	5.0E-15	down
FAM83G	-3.2E+00	5.6E+00	7.3E+01	1.1E-17	5.2E-15	down
SEC14L1	2.8E+00	7.6E+00	7.3E+01	1.7E-17	7.5E-15	up
ANKRD13A	-1.9E+00	6.6E+00	7.2E+01	2.1E-17	9.2E-15	down
TIMM22	9.4E+00	1.5E+00	7.2E+01	2.6E-17	1.1E-14	up
TRIM33	-2.2E+00	6.3E+00	7.1E+01	3.7E-17	1.6E-14	down
CNEP1R1	2.4E+00	6.8E+00	7.0E+01	4.8E-17	2.0E-14	up
CCN1	3.7E+00	8.4E+00	7.0E+01	4.9E-17	2.0E-14	up
RAD54L	-1.0E+01	1.4E+00	7.0E+01	5.7E-17	2.3E-14	down
PLAUR	6.6E+00	8.2E+00	7.0E+01	6.3E-17	2.5E-14	up
SLC22A11	-7.0E+00	3.1E+00	7.0E+01	6.4E-17	2.5E-14	down
MMP11	1.0E+01	2.4E+00	6.9E+01	9.3E-17	3.5E-14	up
STARD8	-1.0E+01	1.3E+00	6.8E+01	1.3E-16	4.8E-14	down
SPSB1	3.4E+00	5.9E+00	6.8E+01	1.7E-16	6.1E-14	up
ASPM	-1.0E+01	1.3E+00	6.8E+01	1.9E-16	6.8E-14	down
CWC25	8.5E+00	1.2E+00	6.8E+01	2.0E-16	7.1E-14	up
ASF1B	-7.7E+00	1.8E+00	6.8E+01	2.1E-16	7.4E-14	down
TINAGL1	3.5E+00	1.0E+01	6.7E+01	2.3E-16	7.8E-14	up
CHST11	4.4E+00	6.8E+00	6.7E+01	2.3E-16	7.9E-14	up

PLCG2	-1.0E+01	1.2E+00	6.7E+01	3.0E-16	1.0E-13	down
FRMD3	-1.0E+01	1.5E+00	6.6E+01	5.3E-16	1.8E-13	down
BDP1	7.7E+00	1.3E+00	6.5E+01	6.7E-16	2.2E-13	up
TAGLN	5.8E+00	8.2E+00	6.5E+01	8.4E-16	2.7E-13	up
ST8SIA4	2.2E+00	7.4E+00	6.5E+01	8.5E-16	2.7E-13	up
KRT7	3.1E+00	1.2E+01	6.5E+01	9.0E-16	2.8E-13	up
LSM2	8.4E+00	4.4E-01	6.4E+01	1.1E-15	3.4E-13	up
PLS1	-1.0E+01	1.6E+00	6.4E+01	1.2E-15	3.7E-13	down
AKAP17A	9.0E+00	1.0E+00	6.4E+01	1.3E-15	3.9E-13	up
GTPBP6	8.3E+00	1.5E+00	6.4E+01	1.5E-15	4.4E-13	up
IER3	8.6E+00	1.8E+00	6.3E+01	1.9E-15	5.6E-13	up
SYBU	-9.7E+00	1.0E+00	6.3E+01	1.9E-15	5.6E-13	down
RPL4P5	6.2E+00	-1.5E+00	6.3E+01	2.2E-15	6.4E-13	up
PIGW	7.6E+00	-2.6E-01	6.3E+01	2.4E-15	6.7E-13	up
PDE3B	-9.7E+00	9.8E-01	6.3E+01	2.6E-15	7.1E-13	down
RHOBTB3	3.9E+00	6.8E+00	6.3E+01	2.6E-15	7.1E-13	up
ZNHIT3	8.5E+00	5.4E-01	6.2E+01	2.7E-15	7.4E-13	up
PFDN6	6.8E+00	-1.0E+00	6.2E+01	2.9E-15	7.8E-13	up
CHCHD10	7.3E+00	-5.7E-01	6.2E+01	3.0E-15	8.0E-13	up
ATP2C2	-9.6E+00	8.9E-01	6.2E+01	3.5E-15	9.2E-13	down
OCIAD2	4.2E+00	4.7E+00	6.2E+01	3.6E-15	9.5E-13	up
KRT81	6.3E+00	7.9E+00	6.2E+01	3.9E-15	1.0E-12	up
CFAP20	2.9E+00	8.6E+00	6.2E+01	4.2E-15	1.1E-12	up
STYXL2	-9.9E+00	1.2E+00	6.1E+01	4.8E-15	1.2E-12	down
GCN1	-1.7E+00	8.0E+00	6.1E+01	5.0E-15	1.3E-12	down
LOC728554	7.4E+00	9.6E-01	6.1E+01	5.2E-15	1.3E-12	up
HAP1	-9.7E+00	9.9E-01	6.0E+01	8.3E-15	2.0E-12	down
MYO7A	-1.0E+01	1.3E+00	6.0E+01	8.7E-15	2.1E-12	down
IFNAR1	1.9E+00	7.4E+00	6.0E+01	9.1E-15	2.2E-12	up
TGFB2	8.5E+00	7.2E+00	6.0E+01	9.6E-15	2.3E-12	up
GPC4	3.2E+00	9.3E+00	6.0E+01	1.1E-14	2.6E-12	up
LENG1	7.6E+00	-2.8E-01	5.9E+01	1.6E-14	3.8E-12	up

Table 4.5 Antibody information

Protein of interest	Host	Catalog number	Supplier
GATA3	Goat	AF2605	R&D SYSTEMS
HLA-G	mouse	sc-21799	santa cruz
CGB	Rabbit	ab 53087	abcam
CGB	Mouse	MS-1065-P1	FisherScientific
ANLN	Rabbit	PA5-84016	Invitrogen
FIBCD1	Rabbit	PA5-43502	Invitrogen
MAMDC2	Rabbit	PA5-54575	Invitrogen
VTCN1	Rabbit	ab209242	abcam
WFDC2	Rabbit	ab85179	abcam
ACTC1	Mouse	MABT823	Millipore Sigma
GABRP	Rabbit	AVARP13034_P050	Aviva Systems Biology
CYP19A1	Rabbit	PA5-120182	Invitrogen
EDNRB	Rabbit	PA3-066	Invitrogen
IL2RB	Rabbit	PA5-99398	Invitrogen
PTN	Rabbit	PA5-94984	Invitrogen

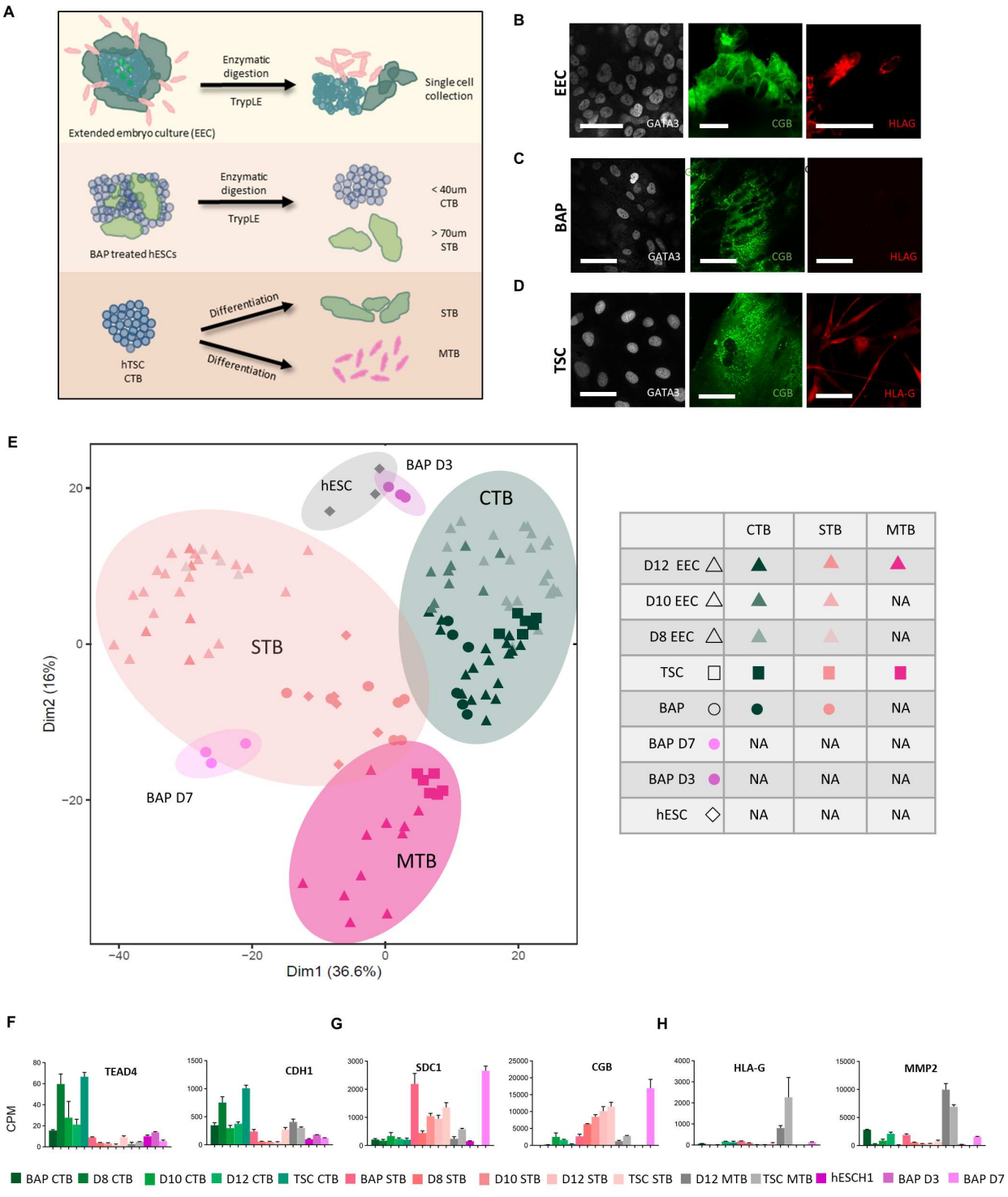

Figure 4.1. Trophoblast Models Express Putative Markers for cytotrophoblast (CTB), synctiotrophoblast, and extravillous trophoblast (EVTB) (also called migratory trophoblast, MTB, in extended embryo culture (EEC). A) Workflow for culturing and single-cell dispersal of CTB, STB, and EVTB/MTB from the three human trophoblast cell models. B) Positive staining for putative trophoblast markers for CTB (GATA binding protein, GATA3, left), STB (chorionic

gonadotropin subunit beta, CGB, middle), and EVTB marker human leukocyte antigen (HLA-G) in MTB (right) from in-tact human embryos cultured to embryonic d 12 in EEC. C) Human embryonic stem cells (hESC's) treated with BMP4, A83-01, and PD173074 (BAP) for 8 d showing marker staining for stem-state CTB-like cells (left) and differentiated STB-like cells (middle). At d 8 The colonies lack a definitive HLA-G component D) The trophoblast stem cell (TSC) model with positive marker staining for CTB (left), STB (middle), or EVTB/MTB (right). Scale bar= 50 μm E) Two-dimensional principal component analysis (PCA) representation of cell clusters by using the top 1000 genes for each cell based on median absolute deviation (mad) among all samples. CPM values of defined lineage marker genes for F) CTB, G) STB, and H) MTB presented as the mean ± SEM. NA= not applicable as no trophoblast sublineage (CTB, STB, MTB) is identified for each model.

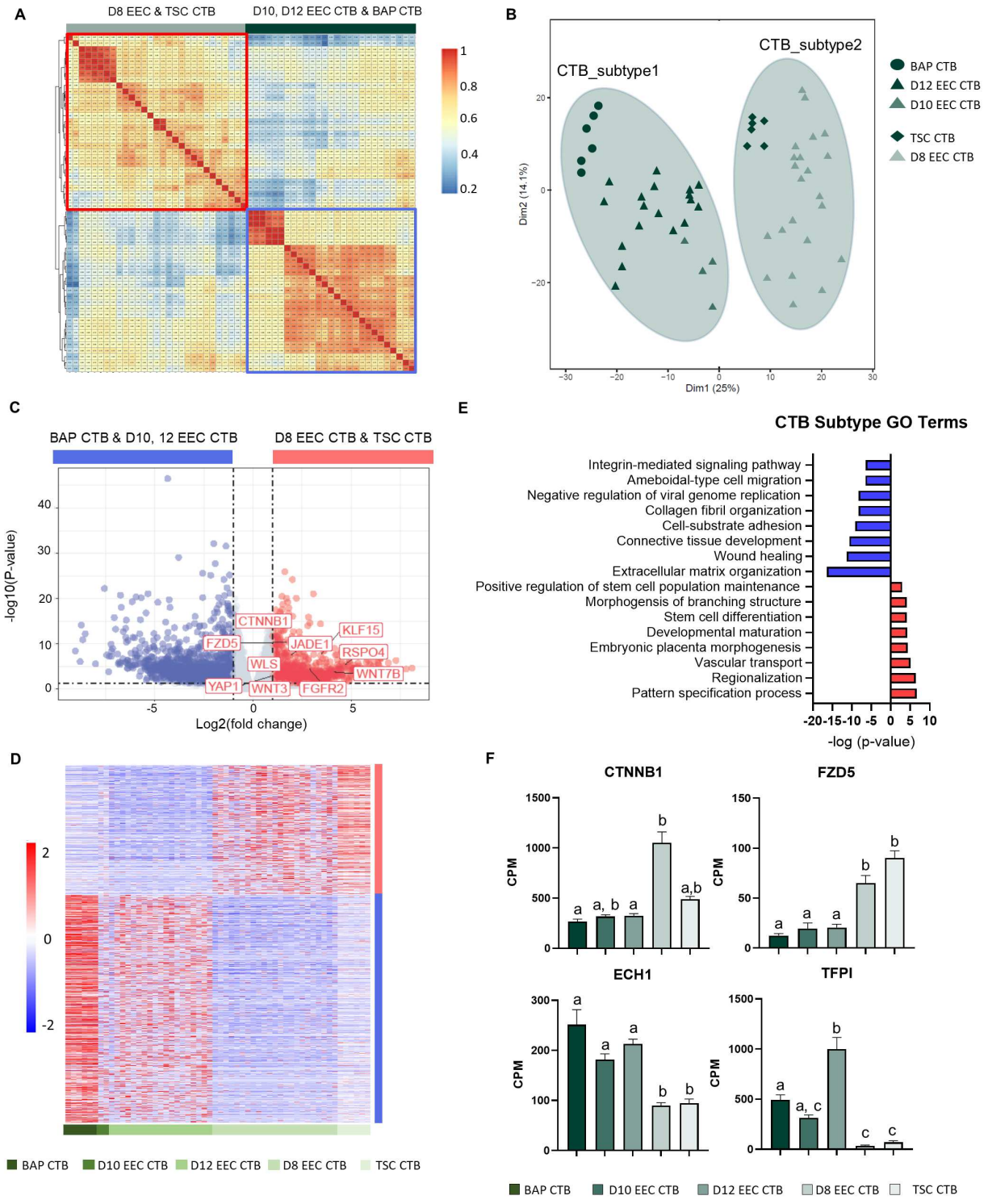

Figure 4.2. Cytotrophoblasts across trophoblast models display differences in stemness. A) Hierarchical clustering of all CTB samples, where the distance among samples was measured by the pairwise Pearson correlation. The color spectrum, ranging from red to blue, indicates correlation from high to low. B) Two-dimensional principal component analysis (PCA) representation of cell clusters using analysis from the top 1000 genes based on median

absolute deviation (mad) among all CTB samples. C) Volcano plot and D) heatmap showing differentially expressed genes (DEGs) between CTB_subtype1 and CTB_subtype2 E) Gene ontology (GO) term analysis of the DEGs. Red= enriched GO terms in CTB_subtype2, blue= enriched GO term in CTB_subtype1. DEGs were defined as $P < 0.01$, Foldchange > 2 F) CPM values of CTNNB1, FZD5, ECH1, and TFPI in CTB cells presented as the mean ± SEM. Different letters signify statistical differences after ANOVA or Kruskall Wallis rank based sum test where appropriate $p<0.05$.

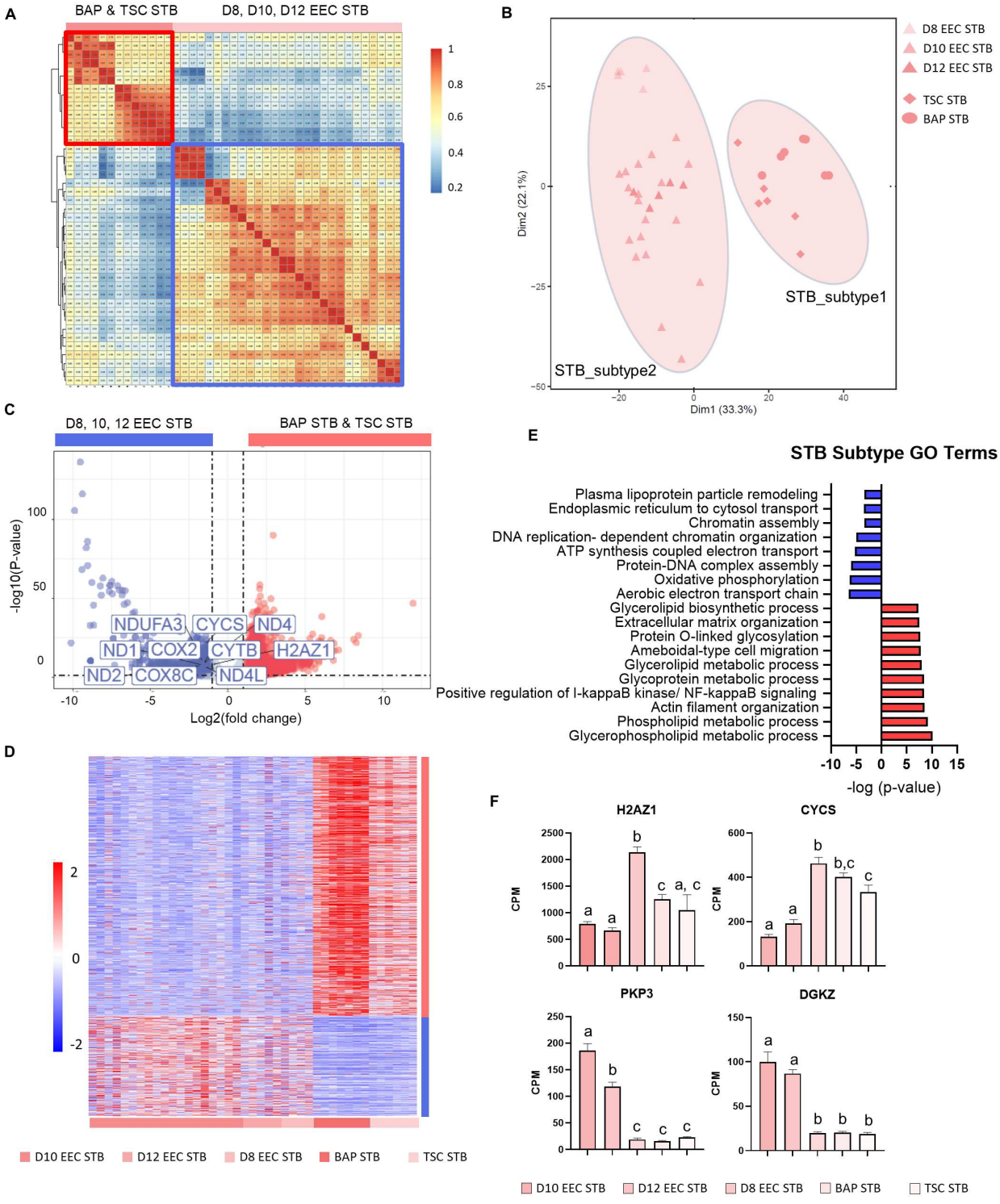

Figure 4.3. Syncytiotrophoblasts across trophoblast models display differences in metabolic priorities A) Hierarchical clustering of all STB samples, where the distance among samples was measured by the pairwise Pearson correlation. The color spectrum, ranging from red to blue, indicates correlation from high to low. B) Two-dimensional principal component analysis (PCA) representation of cell clusters analyzed top 1000 genes based on median absolute deviation

(mad) among all STB samples. C) Volcano plot and D) heatmap showing differentially expressed genes between STB_subtype1 and STB_subtype2, with gene ontology (GO) analysis of the DEGs. Differentially expressed genes were defined as P < 0.01, Foldchange > 2. E) Gene ontology (GO) term analysis of the DEGs. Red= enriched GO terms in STB_subtype1, blue= enriched GO term in STB_subtype2. DEGs were defined as P < 0.01, Foldchange > 2 F) CPM values of H2AZ1, CYCS, PKP3, and DGKZ in STB cells presented as the mean ± SEM. Different letters signify statistical differences after ANOVA or Kruskall Wallis rank based sum test where appropriate p<0.05.

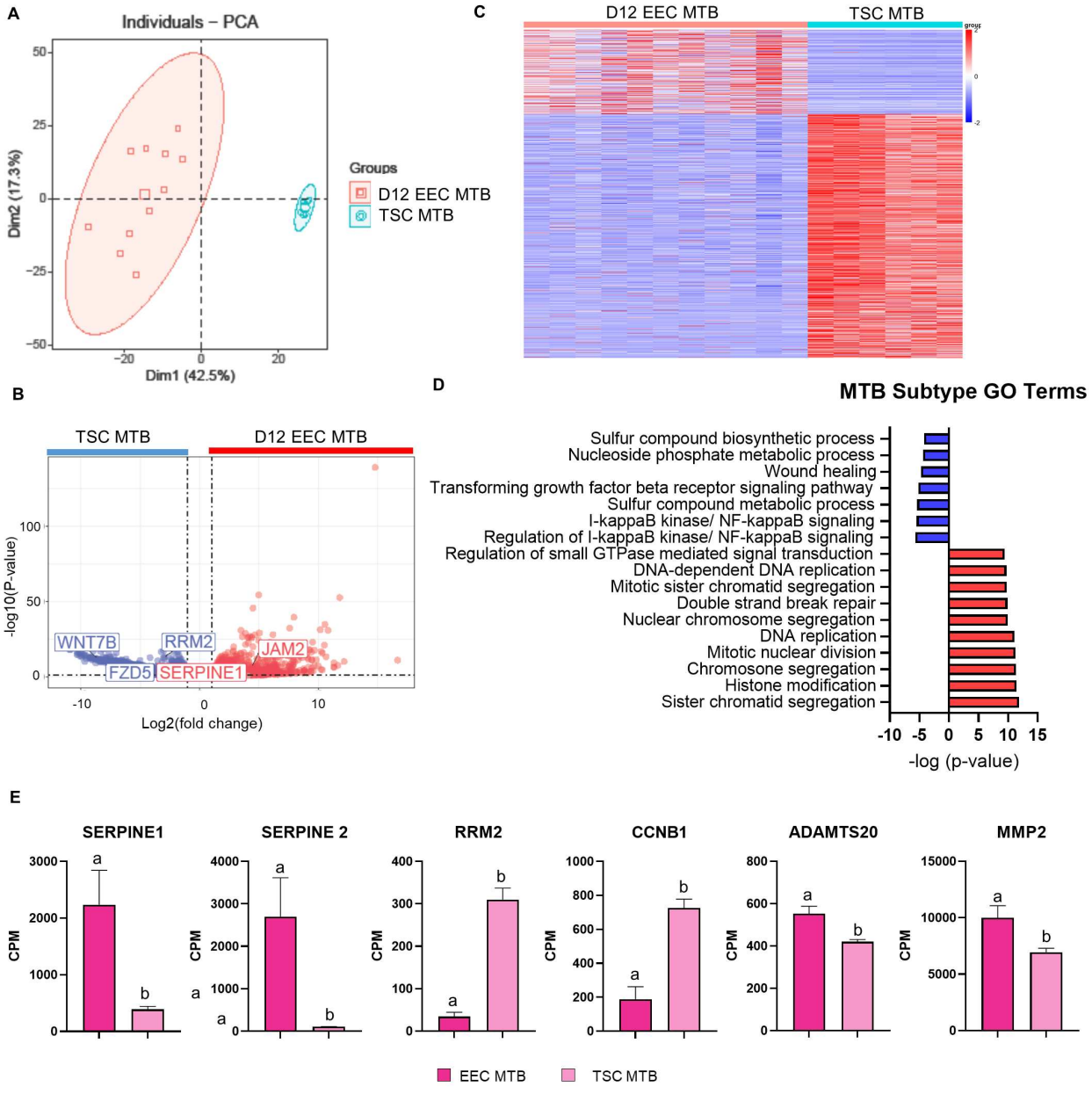

Figure 4.4. Migratory trophoblasts from peri-implantation embryos or trophoblast stem cells represent different extravillous trophoblast subtypes A) Two-dimensional principal component analysis (PCA) representation of cell clusters analyzed top 1000 genes based on median

absolute deviation (mad) among MTB samples. B) Volcano plot and C) heatmap showing differentially expressed genes between D12 EEC MTB and TSC MTB. Differentially expressed genes were defined as $P < 0.01$, Foldchange > 2. D) Gene ontology (GO) term analysis of the DEGs. Red= enriched GO terms in TSC MTB, blue= enriched GO term in EEC MTB. E) CPM values of SERPINE1, SERPINE2, RRM2, CCNB1, ADAMTS20, and MMP2 in MTB cells presented as the mean ± SEM. Different letters signify statistical differences after t. test or Mann Whitney rank based sum test where appropriate $p<0.05$.

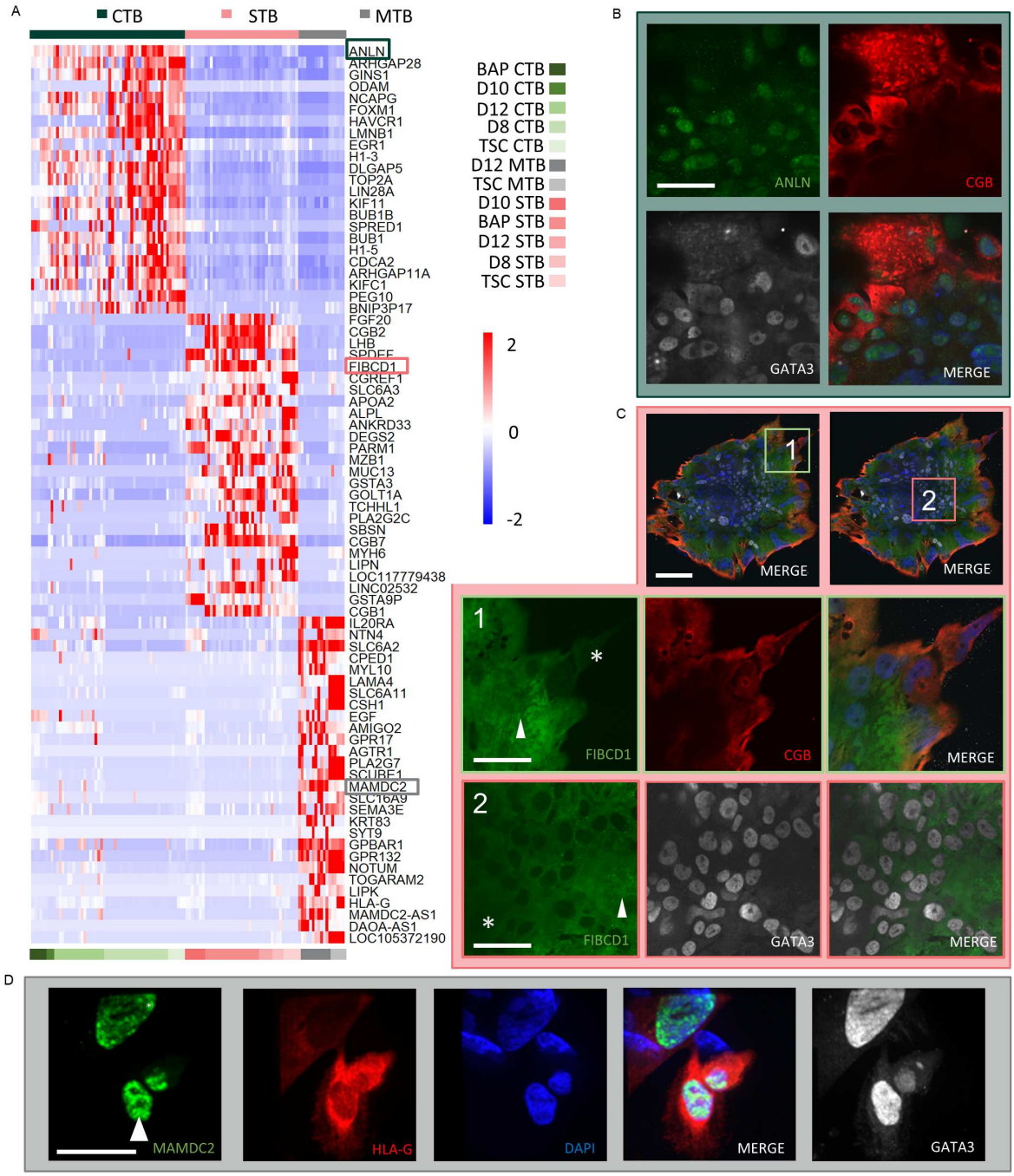

Figure 4.5. Novel trophoblast marker expression in peri-implantation human embryos A) Heatmap showing top highly expressed genes in each trophoblast cell lineage. The color spectrum, ranging from red to blue, indicates expression level from high to low. CTB= cytotrophoblasts, STB= sycytiotrophoblasts, MTB= migratory trophoblasts. B) Anillin (ANLN, green), human chorionic gonadotropin subunit beta (CGB, red), GATA binding protein (GATA3, grey) in peri-implantation human embryos. Scale bar= 50 µm. C) Fibrinogen C domain containing 1 (FIBCD1, green), CGB (red), GATA3 (grey) in peri-implantation human embryos. Scale bar= 100 µm (top row), 50 µm (middle and bottom rows) D) MAM domain containing 2 (green), major histocompatibility complex, class I, G, (HLA-G, red), GATA3 (grey) in peri-implantation human embryos. Scale bar=30 µm.

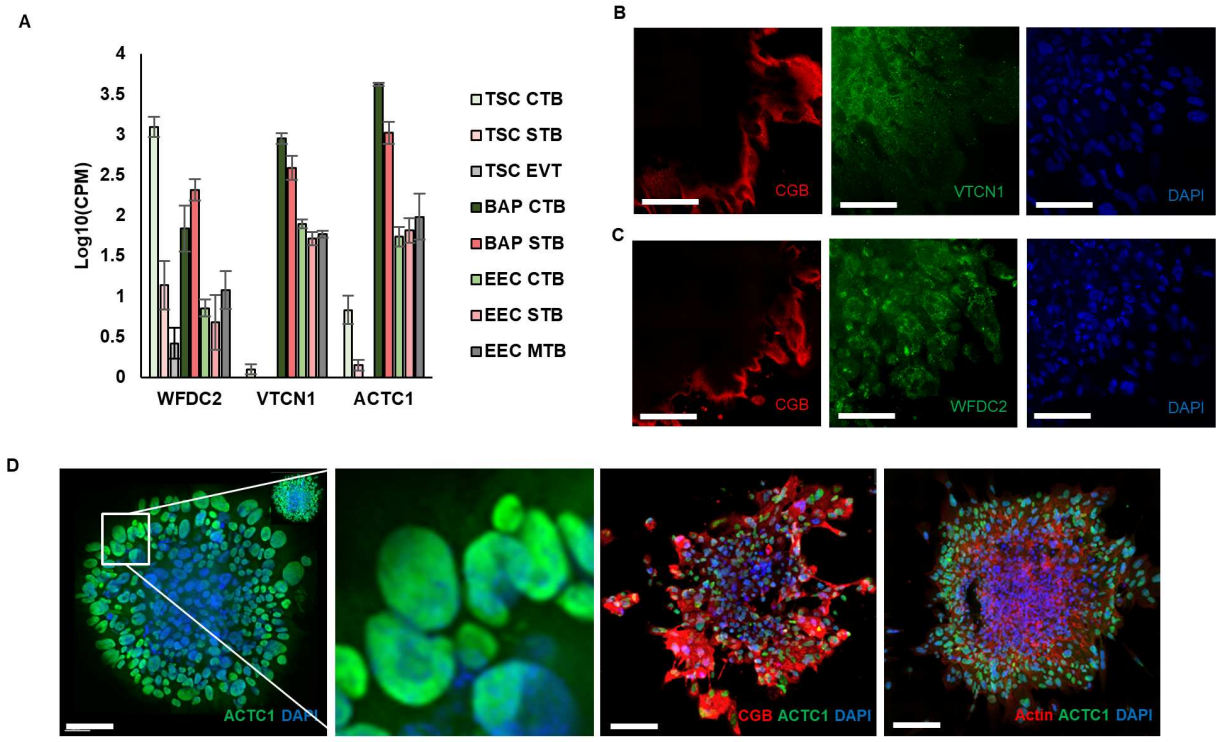

Figure 4.6. BAP marker expression in peri-implantation human embryos A) Transcript abundance in counts per million mapped reads (CPM) for BAP markers: WAP four disulfide core domain 2 (WFDC2), V-set domain containing T cell activation inhibitor 1 (VTCN1), and alpha actin cardiac muscle 1 (ACTC1). B) Immunofluorescence staining for human chorionic gonadotropin subunit beta (CGB, red), VTCN1 (green), and 4′,6-diamidino-2-phenylindole (DAPI, blue) in human embryos in extended culture on embryonic d 10. C) Immunofluorescence staining for CGB (red), WFDC2 (green), and DAPI (blue) in human embryos in extended culture on embryonic d 10. D) Immunofluorescence staining for ACTC1 (green) and DAPI (blue) in human embryos in extended culture on embryonic d 10 (left two panels) or on d 12 colocalized with CGB (red, third panel) or actin (far right panel). Scale bars= 50 μm.

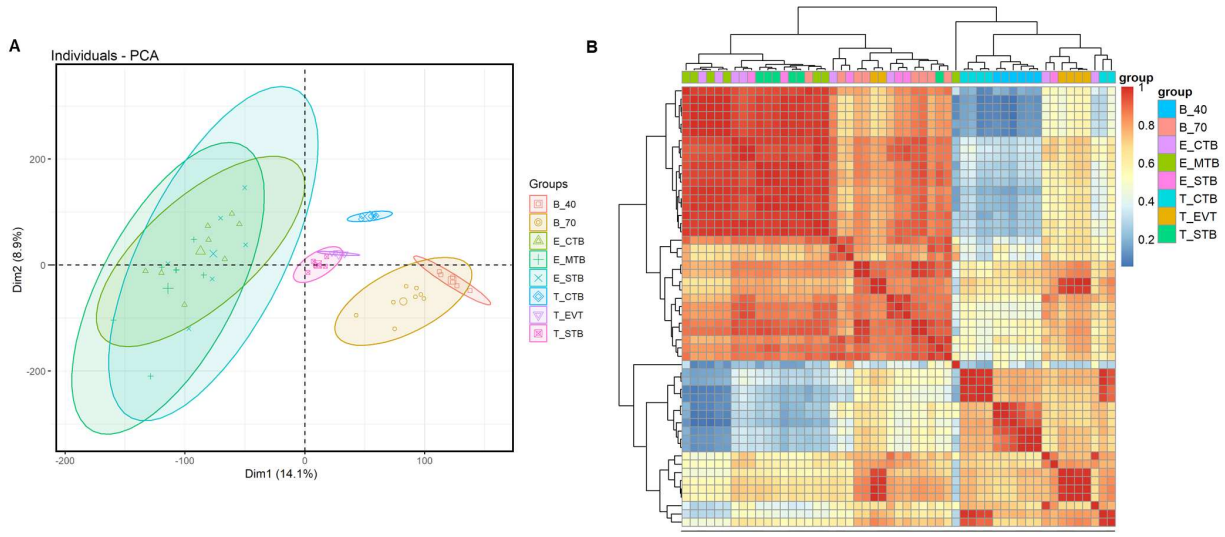

Figure 4.7. RNA sequencing results from bulk collection of extended culture embryos A) Principle component analysis (PCA) and B) unsupervised hierarchical clustering including extended embryo culture (EEC) trophoblasts) collected in bulk.

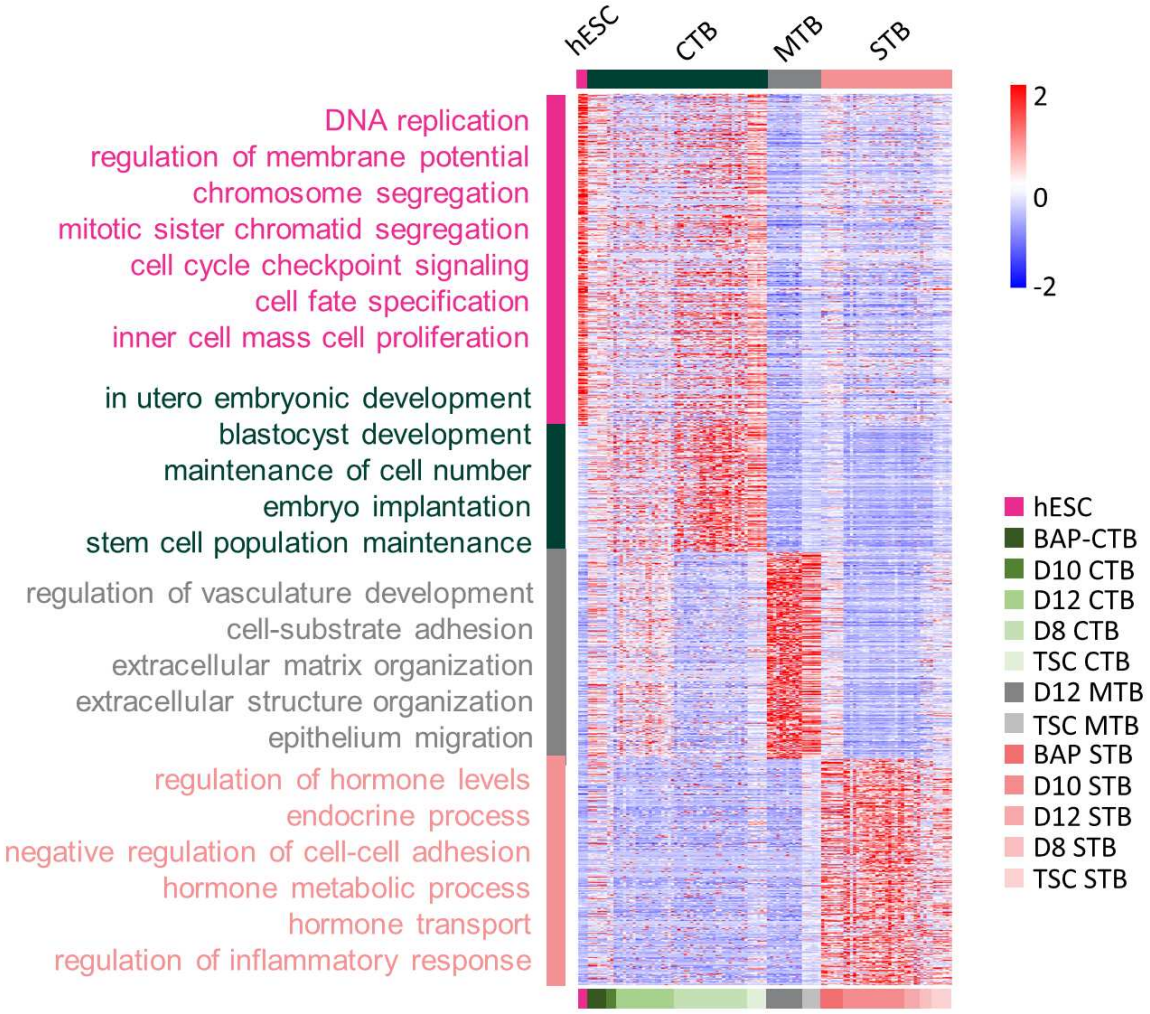

Figure 4.8. Heatmap showing expression of cell type specific expressed genes for human embryonic stem cells (hESC), cytotrophoblasts (CTB), syncytiotrophoblasts (STB), and migratory trophoblasts (MTB), with enriched GO terms in each gene set. The color spectrum, ranging from red to blue, indicates correlation from high to low expression.

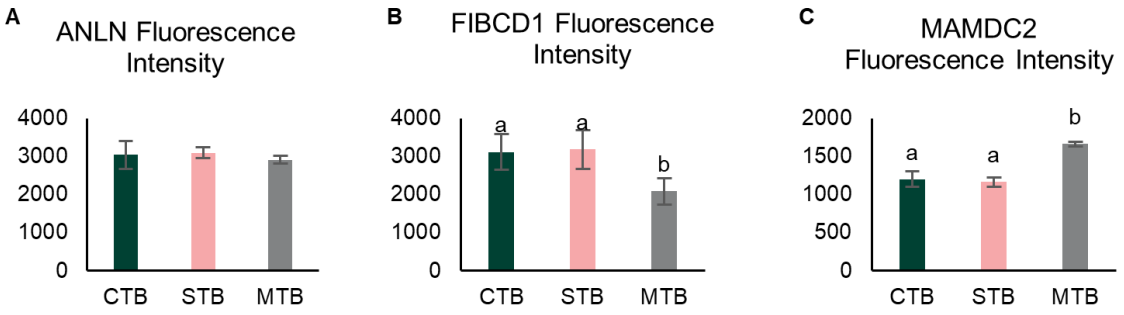

Figure 4.9. Trophoblast marker immunofluorescence intensity for A) Anillin (ANLN), B) Fibrinogen C domain containing 1 (FIBCD1), or MAM domain containing 2 (MAMDC2) in 10 d. p. f. human embryos in extended embryo culture. CTB= cytotrophoblasts, STB= syncytiotrophoblasts, MTB= migratory trophoblasts. Different letters signify statistical differences after ANOVA $p<0.05$.

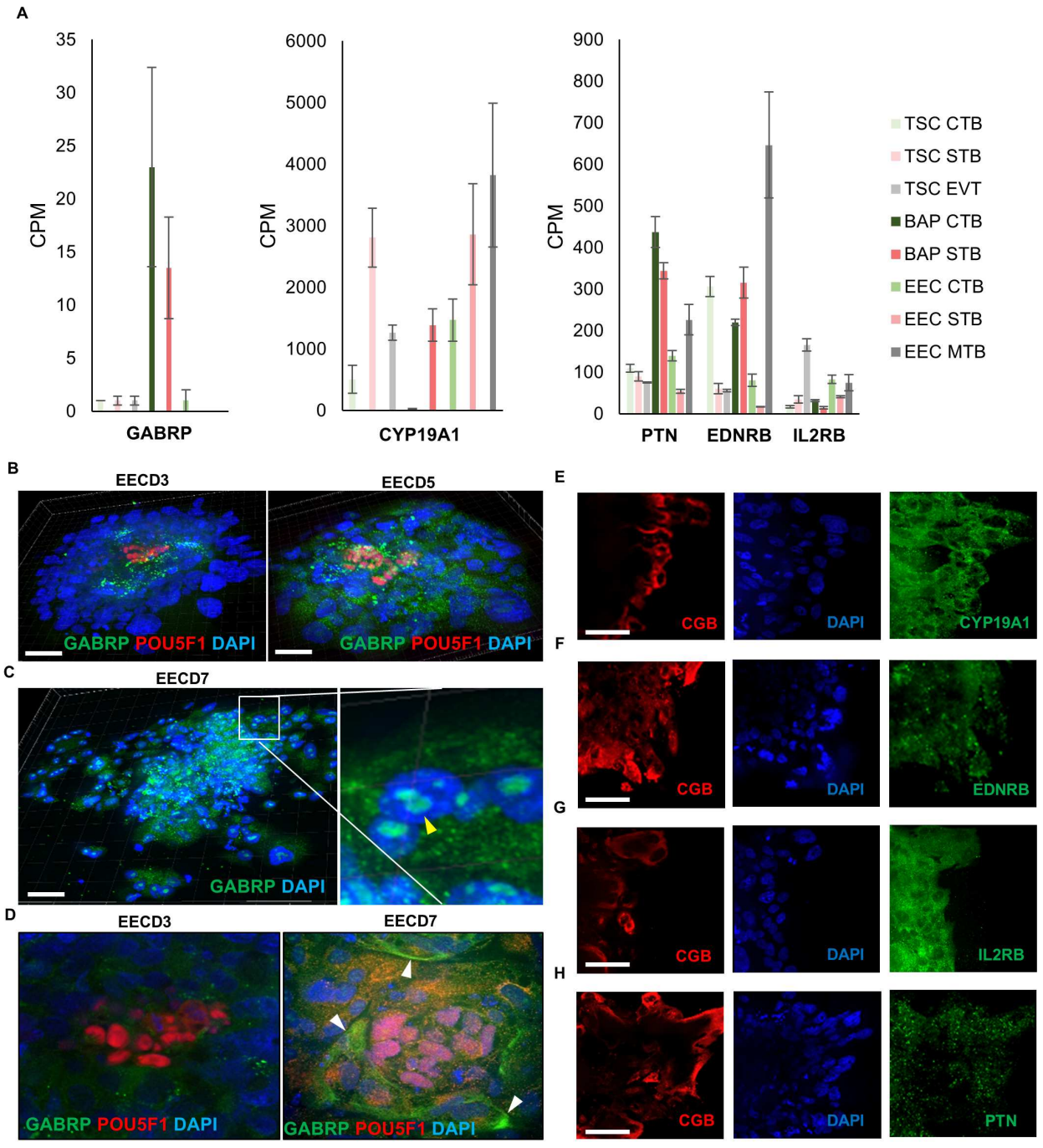

Figure 4.10. BAP and TSC marker expression in peri-implantation stage human embryos A) Transcript abundance in counts per million mapped read (CPM) for GABA receptor subunit pi (GABRP), cytochrome P450 family 19 subfamily A member 1 (CYP19A1), pleiotrophin (PTN), endothelin receptor type B (EDNRB), and interleukin 2 receptor subunit beta (IL2RB). B) Immunofluorescence staining for GABRP (green), pluripotency marker POU5F1 (red), and 4′,6-diamidino-2-phenylindole (DAPI, blue) in human embryos in extended culture for three days (EECD3, left) or 5 days (EECD5, right). C) Immunofluorescence staining for GABRP (green), POU5F1 (red), and DAPI (blue) in human embryos in extended culture for seven days (EECD7). Yellow arrow points to bright nucleolar localization in a zoomed in portion of the left image. D)

Immunofluorescence staining for GABRP (green), POU5F1 (red), and DAPI (blue) in human embryos at EECD3 or EECD7 showing the appearance of surface localization of GABRP near the pluripotent epiblast (white arrowheads). Immunofluorescence staining of CGB (red, left), DAPI (blue, center) and E) CYP19A1 (green), F) EDNRB (green), G)IL2RB (green), and I) PTN (green) in embryonic d 10 human embryos in extended culture. Scale bars= 50 μm.

REFERENCES

1. Khong TY, De Wolf F, Robertson WB, Brosens I. Inadequate maternal vascular response to placentation in pregnancies complicated by pre-eclampsia and by small-for-gestational age infants. Br J Obstet Gynaecol. 1986 Oct;93(10):1049-59. doi: 10.1111/j.1471-0528.1986.tb07830.x. PMID: 3790464.
2. Hertig AT, Rock J, Adams EC. A description of 34 human ova within the first 17 days of development. Am J Anat. 1956 May;98(3):435-93. doi: 10.1002/aja.1000980306. PMID: 13362122.
3. Shahbazi MN, Jedrusik A, Vuoristo S, Recher G, Hupalowska A, Bolton V, Fogarty NNM, Campbell A, Devito L, Ilic D, Khalaf Y, Niakan KK, Fishel S, Zernicka-Goetz M. Self-organization of the human embryo in the absence of maternal tissues. Nat Cell Biol. 2016 Jun;18(6):700-708. doi: 10.1038/ncb3347. Epub 2016 May 4. PMID: 27144686; PMCID: PMC5049689.
4. Deglincerti A, Croft GF, Pietila LN, Zernicka-Goetz M, Siggia ED, Brivanlou AH. Self-organization of the in vitro attached human embryo. Nature. 2016 May 12;533(7602):251-4. doi: 10.1038/nature17948. Epub 2016 May 4. PMID: 27144363.
5. Molè MA, Weberling A, Zernicka-Goetz M. Comparative analysis of human and mouse development: From zygote to pre-gastrulation. Curr Top Dev Biol. 2020;136:113-138. doi: 10.1016/bs.ctdb.2019.10.002. Epub 2019 Dec 26. PMID: 31959285.
6. Roberts, R. M., Ezashi, T., Sheridan, M. A., & Yang, Y. (2018). Specification of trophoblast from embryonic stem cells exposed to BMP4. *Biology of reproduction*, *99*(1), 212–224. https://doi.org/10.1093/biolre/ioy070
7. Xu RH, Chen X, Li DS, Li R, Addicks GC, Glennon C, Zwaka TP, Thomson JA. BMP4 initiates human embryonic stem cell differentiation to trophoblast. *Nat Biotechnol* 2002; 20(12):1261–1264.
8. Bernardo AS, Faial T, Gardner L, Niakan KK, Ortmann D, Senner CE, Callery EM, Trotter MW, Hemberger M, Smith JC, Bardwell L, Moffett A et al.. BRACHYURY and CDX2 mediate

BMP-induced differentiation of human and mouse pluripotent stem cells into embryonic and extraembryonic lineages. *Cell Stem Cell* 2011; 9(2):144–155.

9. Zhang P, Li J, Tan Z, Wang C, Liu T, Chen L, Yong J, Jiang W, Sun X, Du L, Ding M, Deng H. Short-term BMP-4 treatment initiates mesoderm induction in human embryonic stem cells. *Blood* 2008; 111(4):1933–1941.
10. Amita M, Adachi K, Alexenko AP, Sinha S, Schust DJ, Schulz LC, Roberts RM, Ezashi T. Complete and unidirectional conversion of human embryonic stem cells to trophoblast by BMP4. *Proc Natl Acad Sci USA* 2013; 110(13):E1212–E1221.
11. Jain A, Ezashi T, Roberts RM, Tuteja G. Deciphering transcriptional regulation in human embryonic stem cells specified towards a trophoblast fate. Sci Rep. 2017 Dec 8;7(1):17257. doi: 10.1038/s41598-017-17614-5. PMID: 29222466; PMCID: PMC5722916.
12. Seetharam AS, Vu HTH, Choi S, Khan T, Sheridan MA, Ezashi T, Roberts RM, Tuteja G. The product of BMP-directed differentiation protocols for human primed pluripotent stem cells is placental trophoblast and not amnion. Stem Cell Reports. 2022 Jun 14;17(6):1289-1302. doi: 10.1016/j.stemcr.2022.04.014. Epub 2022 May 19. PMID: 35594861; PMCID: PMC9214062.
13. Viukov S, Shani T, Bayerl J, Aguilera-Castrejon A, Oldak B, Sheban D, Tarazi S, Stelzer Y, Hanna JH, Novershtern N. Human primed and naïve PSCs are both able to differentiate into trophoblast stem cells. Stem Cell Reports. 2022 Nov 8;17(11):2484-2500. doi: 10.1016/j.stemcr.2022.09.008. Epub 2022 Oct 20. PMID: 36270280; PMCID: PMC9669397.
14. Sudheer S, Bhushan R, Fauler B, Lehrach H, Adjaye J. FGF inhibition directs BMP4-mediated differentiation of human embryonic stem cells to syncytiotrophoblast. *Stem Cells Dev* 2012; 21(16):2987–3000.
15. Ezashi T, Telugu BP, Roberts RM. Model systems for studying trophoblast differentiation from human pluripotent stem cells. *Cell Tissue Res* 2012; 349(3):809–824.
16. Io S, Kabata M, Iemura Y, Semi K, Morone N, Minagawa A, Wang B, Okamoto I, Nakamura T, Kojima Y, Iwatani C, Tsuchiya H, Kaswandy B, Kondoh E, Kaneko S, Woltjen K, Saitou M,

Yamamoto T, Mandai M, Takashima Y. Capturing human trophoblast development with naive pluripotent stem cells in vitro. Cell Stem Cell. 2021 Jun 3;28(6):1023-1039.e13. doi: 10.1016/j.stem.2021.03.013. Epub 2021 Apr 7. PMID: 33831365.

17. Guo G, Stirparo GG, Strawbridge SE, Spindlow D, Yang J, Clarke J, Dattani A, Yanagida A, Li MA, Myers S, Özel BN, Nichols J, Smith A. Human naive epiblast cells possess unrestricted lineage potential. Cell Stem Cell. 2021 Jun 3;28(6):1040-1056.e6. doi: 10.1016/j.stem.2021.02.025. Epub 2021 Apr 7. PMID: 33831366; PMCID: PMC8189439.
18. Okae H, Toh H, Sato T, Hiura H, Takahashi S, Shirane K, Kabayama Y, Suyama M, Sasaki H, Arima T. Derivation of human trophoblast stem cells. *Cell Stem Cell* 2018; 22(1):50–63.e6.
19. Yabe S, Alexenko AP, Amita M, Yang Y, Schust DJ, Sadovsky Y, Ezashi T, Roberts RM. Comparison of syncytiotrophoblast generated from human embryonic stem cells and from term placentas. Proc Natl Acad Sci U S A. 2016 May 10;113(19):E2598-607. doi: 10.1073/pnas.1601630113. Epub 2016 Apr 5. PMID: 27051068; PMCID: PMC4868474.
20. Fatehullah A, Tan SH, Barker N. Organoids as an in vitro model of human development and disease. Nat Cell Biol. 2016 Mar;18(3):246-54. doi: 10.1038/ncb3312. PMID: 26911908.
21. Hsu YC, Li L, Fuchs E. Emerging interactions between skin stem cells and their niches. Nat Med. 2014 Aug;20(8):847-56. doi: 10.1038/nm.3643. PMID: 25100530; PMCID: PMC4358898.
22. Karvas RM, McInturf S, Zhou J, Ezashi T, Schust DJ, Roberts RM, Schulz LC. Use of a human embryonic stem cell model to discover GABRP, WFDC2, VTCN1 and ACTC1 as markers of early first trimester human trophoblast. Mol Hum Reprod. 2020 Jun 1;26(6):425-440. doi: 10.1093/molehr/gaaa029. PMID: 32359161; PMCID: PMC7320820.
23. Parmegiani L, Minasi MG, Arnone A, Casciani V, Cognigni GE, Viñoles R, Varricchio MT, Quintero LA, Greco E, Filicori M. "Universal Warming" protocol for vitrified oocytes to streamline cell exchange for transnational donation programs: a multi-center study. J Assist

Reprod Genet. 2020 Jun;37(6):1379-1385. doi: 10.1007/s10815-020-01798-3. Epub 2020 May 3. PMID: 32363563; PMCID: PMC7311616.

24. Logsdon DM, Kile RA, Schoolcraft WB, Krisher RL, Yuan Y. Single Cell Collection of Trophoblast Cells in Peri-implantation Stage Human Embryos. J Vis Exp. 2020 Jun 12;(160). doi: 10.3791/61476. PMID: 32597868.
25. West RC, Ming H, Logsdon DM, Sun J, Rajput SK, Kile RA, Schoolcraft WB, Roberts RM, Krisher RL, Jiang Z, Yuan Y. Dynamics of trophoblast differentiation in peri-implantation-stage human embryos. Proc Natl Acad Sci U S A. 2019 Nov 5;116(45):22635-22644. doi: 10.1073/pnas.1911362116. Epub 2019 Oct 21. PMID: 31636193; PMCID: PMC6842583.
26. Meinhardt G, Haider S, Kunihs V, Saleh L, Pollheimer J, Fiala C, Hetey S, Feher Z, Szilagyi A, Than NG, Knöfler M. Pivotal role of the transcriptional co-activator YAP in trophoblast stemness of the developing human placenta. Proc Natl Acad Sci U S A. 2020 Jun 16;117(24):13562-13570. doi: 10.1073/pnas.2002630117. Epub 2020 Jun 1. PMID: 32482863; PMCID: PMC7306800.
27. Li Y, Moretto-Zita M, Leon-Garcia S, Parast MM. p63 inhibits extravillous trophoblast migration and maintains cells in a cytotrophoblast stem cell-like state. Am J Pathol. 2014 Dec;184(12):3332-43. doi: 10.1016/j.ajpath.2014.08.006. Epub 2014 Oct 7. PMID: 25307348; PMCID: PMC4258507.
28. Bai H, Sakurai T, Godkin JD, Imakawa K. Expression and potential role of GATA factors in trophoblast development. J Reprod Dev. 2013;59(1):1-6. doi: 10.1262/jrd.2012-100. PMID: 23428586; PMCID: PMC3943230.
29. Logan PC, Mitchell MD, Lobie PE. DNA methyltransferases and TETs in the regulation of differentiation and invasiveness of extra-villous trophoblasts. Front Genet. 2013 Dec 4;4:265. doi: 10.3389/fgene.2013.00265. PMID: 24363660; PMCID: PMC3849743.
30. Turco MY, Moffett A. Development of the human placenta. Development. 2019 Nov 27;146(22):dev163428. doi: 10.1242/dev.163428. PMID: 31776138.

31. Liu Y, Fan X, Wang R, Lu X, Dang YL, Wang H, Lin HY, Zhu C, Ge H, Cross JC, Wang H. Single-cell RNA-seq reveals the diversity of trophoblast subtypes and patterns of differentiation in the human placenta. Cell Res. 2018 Aug;28(8):819-832. doi: 10.1038/s41422-018-0066-y. Epub 2018 Jul 24. PMID: 30042384; PMCID: PMC6082907.
32. Macklon NS, Geraedts JP, Fauser BC. Conception to ongoing pregnancy: the 'black box' of early pregnancy loss. Hum Reprod Update. 2002 Jul-Aug;8(4):333-43. doi: 10.1093/humupd/8.4.333. PMID: 12206468.
33. Lee CQ, Gardner L, Turco M, Zhao N, Murray MJ, Coleman N, Rossant J, Hemberger M, Moffett A. What is trophoblast? a combination of criteria define human first-trimester trophoblast. *Stem Cell Rep* 2016; 6(2):257–272.
34. James JL, Carter AM, Chamley LW. Human placentation from nidation to 5 weeks of gestation. Part I: What do we know about formative placental development following implantation? Placenta. 2012 May;33(5):327-34. doi: 10.1016/j.placenta.2012.01.020. Epub 2012 Feb 26. PMID: 22374510.
35. Lu X, Wang R, Zhu C, Wang H, Lin HY, Gu Y, Cross JC, Wang H. Fine-Tuned and Cell-Cycle-Restricted Expression of Fusogenic Protein Syncytin-2 Maintains Functional Placental Syncytia. Cell Rep. 2017 Oct 31;21(5):1150-1159. doi: 10.1016/j.celrep.2017.10.019. Erratum in: Cell Rep. 2018 Jun 26;23(13):3979. PMID: 29091755.
36. Wang Y, Jiang X, Jia L, Wu X, Wu H, Wang Y, Li Q, Yu R, Wang H, Xiao Z, Liang X. A Single-Cell Characterization of Human Post-implantation Embryos Cultured *In Vitro* Delineates Morphogenesis in Primary Syncytialization. Front Cell Dev Biol. 2022 Jun 15;10:835445. doi: 10.3389/fcell.2022.835445. PMID: 35784461; PMCID: PMC9240912.
37. Muto M, Chakraborty D, Varberg KM, Moreno-Irusta A, Iqbal K, Scott RL, McNally RP, Choudhury RH, Aplin JD, Okae H, Arima T, Matsumoto S, Ema M, Mast AE, Grundberg E, Soares MJ. Intersection of regulatory pathways controlling hemostasis and hemochorial placentation. Proc Natl Acad Sci U S A. 2021 Dec 14;118(50):e2111267118. doi: 10.1073/pnas.2111267118. PMID: 34876522; PMCID: PMC8685669.

38. Khorami Sarvestani S, Shojaeian S, Vanaki N, Ghresi-Fard B, Amini M, Gilany K, Soltanghoraee H, Arefi S, Jeddi-Tehrani M, Zarnani AH. Proteome profiling of human placenta reveals developmental stage-dependent alterations in protein signature. Clin Proteomics. 2021 Aug 9;18(1):18. doi: 10.1186/s12014-021-09324-y. PMID: 34372761; PMCID: PMC8351416.
39. Kolahi KS, Valent AM, Thornburg KL. Cytotrophoblast, Not Syncytiotrophoblast, Dominates Glycolysis and Oxidative Phosphorylation in Human Term Placenta. Sci Rep. 2017 Feb 23;7:42941. doi: 10.1038/srep42941. PMID: 28230167; PMCID: PMC5322316.
40. Lindegaard ML, Olivecrona G, Christoffersen C, Kratky D, Hannibal J, Petersen BL, Zechner R, Damm P, Nielsen LB. Endothelial and lipoprotein lipases in human and mouse placenta. J Lipid Res. 2005 Nov;46(11):2339-46. doi: 10.1194/jlr.M500277-JLR200. Epub 2005 Sep 8. PMID: 16150822.
41. Dunn WB, Brown M, Worton SA *et al.* The metabolome of human placental tissue: investigation of first trimester tissue and changes related to preeclampsia in late pregnancy. *Metabolomics* **8**, 579–597 (2012). https://doi.org/10.1007/s11306-011-0348-6
42. Jaremek A, Jeyarajah MJ, Jaju Bhattad G, Renaud SJ. Omics Approaches to Study Formation and Function of Human Placental Syncytiotrophoblast. Front Cell Dev Biol. 2021 Jun 15;9:674162. doi: 10.3389/fcell.2021.674162. PMID: 34211975; PMCID: PMC8240757.
43. Fisher JJ, McKeating DR, Cuffe JS, Bianco-Miotto T, Holland OJ, Perkins AV. Proteomic Analysis of Placental Mitochondria Following Trophoblast Differentiation. Front Physiol. 2019 Dec 20;10:1536. doi: 10.3389/fphys.2019.01536. PMID: 31920727; PMCID: PMC6933824.
44. Khan T, Seetharam AS, Zhou J, Bivens NJ, Schust DJ, Ezashi T, Tuteja G, Roberts RM. Single Nucleus RNA Sequence (snRNAseq) Analysis of the Spectrum of Trophoblast Lineages Generated From Human Pluripotent Stem Cells *in vitro*. Front Cell Dev Biol. 2021 Jul 21;9:695248. doi: 10.3389/fcell.2021.695248. PMID: 34368143; PMCID: PMC8334858.
45. Tashev SA, Parsons D, Hillman C, Harris S, Lofthouse EM, Goggin P, Chatelet DS, Cleal JK, Smyth N, Palaiologou H, Page A, Lewis RM. Folding of the syncytiotrophoblast basal

plasma membrane increases the surface area available for exchange in human placenta. Placenta. 2022 Jan;117:57-63. doi: 10.1016/j.placenta.2021.11.002. Epub 2021 Nov 4. PMID: 34768170.

46. Hishikawa D, Hashidate T, Shimizu T, Shindou H. Diversity and function of membrane glycerophospholipids generated by the remodeling pathway in mammalian cells. J Lipid Res. 2014 May;55(5):799-807. doi: 10.1194/jlr.R046094. Epub 2014 Mar 19. Erratum in: J Lipid Res. 2014 Nov;55(11):2444. PMID: 24646950; PMCID: PMC3995458.
47. Zhang L, Bi S, Liang Y, Huang L, Li Y, Huang M, Huang B, Deng W, Liang J, Gu S, Chen J, Du L, Chen D, Wang Z. Integrated Metabolomic and Lipidomic Analysis in the Placenta of Preeclampsia. Front Physiol. 2022 Feb 4;13:807583. doi: 10.3389/fphys.2022.807583. PMID: 35185616; PMCID: PMC8854797.
48. Xia L, Su X, Shen J, Meng Q, Yan J, Zhang C, Chen Y, Wang H, Xu M. *ANLN* functions as a key candidate gene in cervical cancer as determined by integrated bioinformatic analysis. Cancer Manag Res. 2018 Apr 5;10:663-670. doi: 10.2147/CMAR.S162813. PMID: 29670400; PMCID: PMC5896649.
49. Long X, Zhou W, Wang Y, Liu S. Prognostic significance of ANLN in lung adenocarcinoma. Oncol Lett. 2018 Aug;16(2):1835-1840. doi: 10.3892/ol.2018.8858. Epub 2018 May 31. PMID: 30008873; PMCID: PMC6036425.
50. Graca FA, Rai M, Hunt LC, Stephan A, Wang YD, Gordon B, Wang R, Quarato G, Xu B, Fan Y, Labelle M, Demontis F. The myokine Fibcd1 is an endogenous determinant of myofiber size and mitigates cancer-induced myofiber atrophy. Nat Commun. 2022 May 2;13(1):2370. doi: 10.1038/s41467-022-30120-1. PMID: 35501350; PMCID: PMC9061726.
51. Jepsen CS, Dubey LK, Colmorten KB, Moeller JB, Hammond MA, Nielsen O, Schlosser A, Templeton SP, Sorensen GL, Holmskov U. FIBCD1 Binds *Aspergillus fumigatus* and Regulates Lung Epithelial Response to Cell Wall Components. Front Immunol. 2018 Sep 18;9:1967. doi: 10.3389/fimmu.2018.01967. PMID: 30279687; PMCID: PMC6153955.

52. Wang Y, Sun M, Liu J, Liu Y, Jiang C, Zhu H, Wang W, Wang Y. FIBCD1 overexpression predicts poor prognosis in patients with hepatocellular carcinoma. Oncol Lett. 2020 Jan;19(1):795-804. doi: 10.3892/ol.2019.11183. Epub 2019 Dec 4. PMID: 31897196; PMCID: PMC6924150.
53. Lee H, Park BC, Soon Kang J, Cheon Y, Lee S, Jae Maeng P. MAM domain containing 2 is a potential breast cancer biomarker that exhibits tumour-suppressive activity. Cell Prolif. 2020 Sep;53(9):e12883. doi: 10.1111/cpr.12883. Epub 2020 Jul 24. PMID: 32707597; PMCID: PMC7507446.
54. Wang Y, Luo W, Wang X, Ma Y, Huang L, Wang Y. MAMDC2, a gene highly expressed in microglia in experimental models of Alzheimers Disease, positively regulates the innate antiviral response during neurotropic virus infection. J Infect. 2022 Feb;84(2):187-204. doi: 10.1016/j.jinf.2021.12.004. Epub 2021 Dec 10. PMID: 34902449.

CHAPTER V: HUMAN BLASTOIDS MODEL HUMAN BLASTOCYST PERI-IMPLANTATION DEVELOPMENT AND RECAPITULATE MATERNAL-FETAL CROSSTALK

Summary

Proper implantation is critical to the establishment and maintenance of a healthy pregnancy, yet mechanisms surrounding human implantation remain elusive due to the delicate nature of human embryo research. Here, we compared blastoids with human embryos during the peri-implantation period to identify key similarities and differences and to determine if blastoids are capable of replicating maternal-fetal crosstalk events during implantation. First, we compared different medium formulations, blastoid criteria, and feeder conditions to optimize a model for human implantation. We noticed that GATA3+ trophoblast cells were able to fuse into multinucleate syncytiotrophoblast-like plaques when blastoids were co-cultured with immortalized endometrial stromal cells compared to fetal cord fibroblasts or fibronectin alone. To determine if stromal cell contact or secreted factors were responsible for syncytialization, we then cultured human embryos or blastoids on fibronectin, on fibronectin in stromal cell-conditioned medium, or on stromal cells directly. We then performed proteomics and phosphoproteomics analysis on the medium conditioned by stromal cells and used 10x genomics to identify similarities and differences between blastoids and blastocysts during implantation on stromal cells or fibronectin. Single cell RNA-sequencing revealed a population or trophoblast resembling early migratory trophoblasts when blastoids and blastocysts were co-cultured with endometrial stromal cells. Refining culture conditions of stem cell-derived blastoids will help to appropriately mimic human implantation in a way that has never been done before. Using this model, researchers can begin to tease apart mechanisms of early trophoblast differentiation and lineage segregation events during peri-implantation without the use of human embryos.

Introduction

During human pre-implantation development, a blastocyst forms approximately 5 days after fertilization. Historically, studies of pre- and peri-implantation human development have mainly relied on discarded blastocysts derived from in-vitro fertilization (IVF), which severely limit the reproducibility, scale, and types of experiments that can be performed. Human pluripotent stem cells (hPSCs) have an extended self-renewal ability and provide alternative means to study human development in a dish. Recent advances in naïve hPSC-derived blastocyst models, referred to as human blastoids, have broken new ground (1-3) and provide an invaluable ethical alternative to study the early stages of human development and implantation with reduced genetic heterogeneity between samples.

By modulating several signaling pathways, we first published a two-step three-dimensional culture strategy to generate blastoids from 5iLA-cultured naïve hPSCs (1, 4). Later, two independent studies reported methods to generate blastoids from PXGL-cultured naïve hPSCs (2, 3). Blastoids generated from both naïve conditions resembled human blastocysts in morphology, size, cell number and lineage composition, and demonstrated efficacies in studying mechanisms underlying cavity formation and first steps of human implantation (1-3). Despite the similarities, there are several notable differences among protocols in terms of efficiency, scalability, accessibility, and off-target cells. Although our previous protocol can easily be scaled-up and is more accessible due to the use of commercially available AggreWell™400 microwell plates, as opposed to the use of ultra-low attachment 96-well plates (2) and customized non-adherent hydrogel microwells (3), the derivation efficiency was lower and contained more off-target cells. Here, we used an optimized protocol that greatly improved the derivation efficiency and fidelity of blastoids generated from 5iLA-cultured naïve hPSCs (5iLA-blastoids). We then optimized culture conditions for extended blastoid culture (EBC) during the peri-implantation and

examined implantation dynamics side-by-side with human blastocysts. Finally, we used single cell RNA-sequencing (scRNA-seq) to compare transcriptional shifts from human embryos during co-culture with endometrial stromal cells to transcriptional shifts in blastoids in matching conditions.

Materials and Methods

Ethics statement

All human-embryo-related experiments were conducted at Colorado Center for Reproductive Medicine. Studies involving patient materials were performed following informed consent and were reviewed and approved by the WCG Institutional Review Board (WCG IRB) study no. 1179872 (blastocyst extended culture during the peri-implantation period), 20140449 (endometrial biopsies), 1332853 (blastocyst scRNA-Seq and data submission). Embryos were donated by couples undergoing in vitro fertilization (IVF). No embryos were cultured past embryonic day 12.

Human Embryo Warming and Recovery

Vitrified day 5 or 6 human embryos were donated with informed consent following successful IVF cycles at our clinic. Embryos were warmed according to manufacturer protocols (Kitazato, Shizuoka, Japan) and left to recover in 20 µL drops of an in-house single step culture medium supplemented with 20% Quinn's Advantage Serum Protein Substitute (SPS, Origio, Cooper Surgical, Trumbull, CT) under embryo grade culture oil (Spectrum, New Brunswick, NJ) for 2 h at 37°C and 6.5% O2 and 7.5% CO2 to mimic 5% O2 and 6% CO2 at sea level. Following a 2 h recovery, zonas were removed using a brief exposure to warmed acidic Tyrode's solution (Sigma Aldrich, St. Louis, MO) and returned to their recovery drops before single-cell dissociation or extended culture.

Endometrial Stromal Cell Isolation

Endometrial cells were obtained from patient biopsy during oocyte retrieval. biopsies were washed, minced, and enzymatically digested with 0.4mg/mL Collagenase V (Sigma) and 1.25 U/ mL Dispase II (Sigma). Digestion suspension was neutralized and passed through a 100 µm cell strainer to separate large glandular tissue fragments and then a 40 µm cell strainer. The filtrate from glandular fragment separation was further passed through a 10 µm cell strainer to separate stromal cells. Filtrate was centrifuged and resuspended in stromal culture 5 mL medium containing 10% fetal bovine serum (FBS, Gibco) and 1X ITS-X (ThermoFisher) in DMEM/F12, transferred to a T25 tissue flask, and incubated for 15 min. The medium suspension was then moved to a new T25 tissue flask to separate out contaminating epithelial cells.

Endometrial stromal cell culture and plating

The isolated stromal cells were immortalized by telomerase reverse transcriptase (TERT) overexpression. Early passage (p1) of primary stroma cells were infected with Lentivirus particles for hTERT overexpression driven by EEF1A1 promoter (GeneCopoeia, LP730-025) according to the manufacture's protocol. Cells infected with 5 MOI particles were used for the experiments within seven passages. Stromal cells were plated 3 days before extended culture for the cell expansion. On the day before extended culture, stromal cells were detached using TrypLE (ThermoFisher, Waltham, MA) and plated in ibidi dishes at 69,000 cells/ cm^2. Stromal cells were cultured in Advanced DMEM/F12 with 1X ITS-X (ThermoFisher), 1X GlutaMAX (ThermoFisher), and 5% fetal bovine serum (Sigma Aldrich).

Culturing of human naïve PSCs

Naive WIBR3 human ES cells were obtained from R. Jaenisch and T. Theunissen. Primed H9-hESCs, 46XX-hESCs, RC-hiPSCs and JB-hiPSCs were cultured in mTeSR Plus medium (Stemcell technologies). Primed human PSC lines were converted to the naïve state following a previously described protocol (4). All naive human PSCs were cultured on mitotically inactivated mouse embryonic fibroblast (MEF) feeders at 37 °C in 5% CO2 and 5% O2. In brief, around 2 × 10^5 cells were plated into 6-well plates pre-coated with MEFs in 5i/L/A medium. The cells were passaged with Accumax (Stemcell technologies). The 5i/L/A medium (500 ml) was prepared using the following: 250 ml DMEM/F12 (Invitrogen), 250 ml neurobasal medium (Invitrogen), 5 ml N2 supplement (Invitrogen), 10 ml B27 supplement (Invitrogen), 1× GlutaMAX (Gibco), 1× nonessential amino acids (Gibco), 0.1 mM β-mercaptoethanol (Gibco), 0.5% penicillin–streptomycin (Gibco), 50 mg/ml–1 bovine serum albumin (BSA, Sigma) and the following small molecules and cytokines: 1 μM PD0325901 (Stemgent), 0.5 μM IM-12 (Enzo), 0.5 μM SB590885 (R&D systems), 1 μM WH-4-023 (A Chemtek), 20 ng ml–1 recombinant human LIF (Peprotech), 10 ng ml–1 activin A (Peprotech) and 5 μM Y-27632 (Selleckchem).

Human blastoids generation

The protocol was optimized from our previous works (1). 5iLA naive human PSCs were dissociated into single cells by incubation with Accumax (Stemcell technologies) for 3 min at 37 °C. Cells were centrifugated at 200g for 5 min and collected in 5iLA medium. Then, the cell suspension was incubated in a 0.1% gelatin-coated tissue culture dish for 30 min at 37 °C in 5% CO_2 to remove MEF feeder cells. The supernatant containing naive human PSCs was collected and passed through a 40- μm cell strainer, and cells were counted. Meanwhile, an AggreWell-400 (STEMCELL Technologies) plate was prepared according to the manufacturer's

instructions. In brief, wells were rinsed with anti-adhesion rinsing solution (STEMCELL Technologies), centrifuged at max speed for 5 min, and then incubated at room temperature for 10 min. After incubation, wells were washed with eHDM once and 0.5 ml fresh eHDM was added. The corresponding number of cells (25 cells / microwell for WIBR3-hESCs, H9-hESCs. And YN-hESCs, 30 cells / microwell for RC-hiPSCs and YN-hiPSCs, and for other cell lines the starting number needs to be optimized) were resuspended in 1 mL eHDM and seeded into one well of a prepared AggreWell-400 24-well plate. The plate was centrifuged at 200g for 1 min and cultured at 37 °C in 5% CO_2 and 5% O_2, the day of cell plating was designated as day 0. The medium was half changed (1 mL old medium was removed and 1ml fresh medium were added) with eHDM on day 1 and day 2. On day 3, carefully remove as much eHDM as possible, and then add 1.5 ml of eTDM. Repeat this step one additional time to help completely remove the remaining eHDM. On the remaining days, the fresh eTDM was half changed every two days. The human blastoids usually formed after 5-6 d of culture in eTDM. All blastoids were manually isolated using a mouth pipette under a stereomicroscope for downstream experiments.

The eHDM was prepared using the following: 1:1 (v/v) mixture of DMEM/F12 and neurobasal medium, 1× N2 supplement, 1× B27 supplement, 1× GlutaMAX, 1× nonessential amino acids, 0.1 mM β-mercaptoethanol, 0.5% penicillin–streptomycin, 20 ng ml−1 bFGF (Peprotech), 20 ng ml−1 activin A, 3 μM CHIR99021 and CEPT cocktail [50 nM Chroman 1 (MedChem Express), 5 μM Emricasan (Selleckchem), 1X polyamine supplement (Sigma), and 0.7 μM TransISRIB (Tocris). The eTDM was prepared using the following: 1:1 (v/v) mixture of DMEM/F12 and neurobasal medium, 0.5× N2 supplement, 0.5× B27 supplement, 0.5% ITS-X, 0.5× GlutaMAX, 0.5× nonessential amino acids, 0.1 mM β-mercaptoethanol, 0.5% knockout serum replacement

(KSR, Gibco), 0.5% penicillin–streptomycin, 2 μ M PD0325901, 1 μM A83-01, 0.5 μM SB590885, 1 μM LPA. 20 μM WH-4-023, 10 ng ml−1 recombinant human LIF, and 0.5

Human blastocyst and blastoid extended culture

Embryos and blastocysts were placed into 300 μL of EBC medium containing DMEM/F12 and Neurobasal (Thermo Fisher, 21103049) with N2 supplement (Thermo Fisher, 17502048), B27 supplement (ThermoFisher, 17504044), GlutaMAX (Gibco, 35050061), non-essential amino acids (ThermoFisher, 11140050), 0.1 mM β-mercaptoethanol, 15% fetal bovine serum (Hyclone, SH30070.02), 8 nM water-soluble estradiol (E4389), 200 ng/mL progesterone (P7556), 1 mM sodium pyruvate (SigmaP4562), 10 ug/mL Gentamicin (Cellgro, 30-005-CR), 50 nM Chroman 1 (MedChem Express, HY-15392), 5 μM Emricasan (Selleckchem, S7775), 1X polyamine supplement (P8483), and 0.7 μM TransISRIB (Tocris, 5284). All extended culture experiments were completed in 8-well ibi-Treat dishes (Ibidi, Martinsried, Germany) coated in fibronectin from human plasma (F0895). Embryos and blastoids were cultured for 72 h in the extended culture system (5, 6) on either fibronectin-coated ibidi dishes (7) or ibidi dishes seeded with, fetal cord fibroblasts, or immortalized endometrial stromal cells. After 48 h, 1⁄2 medium volume was exchanged with fresh EBC. After 72 h, samples were fixed with 4% paraformaldehyde (Electron Microscopy Sciences, 30525-89-4). For stromal cell conditioned medium, EBC was conditioned overnight on immortalized endometrial stromal cells without the presence of a blastocyst or blastoid.

Human Chorionic Gonadotropin Quantification

150 μL of spent medium was collected and snap frozen in LN_2 upon the conclusion of culture and stored in -80°C. Samples were analyzed for human chorionic gonadotropin (CGB) using electrochemiluminescence on a Roche Cobas e601 analyzer and is reported in mIU/mL.

Outgrowth Area Measurement

Images of peri-implantation blastoids and embryos were captured using an Olympus DP22 (Olympus, Melville, NY) camera fixed to a stereomicroscope. In ImageJ, trophectoderm outgrowth was measured with the freehand selection tool and areas were calculated using the scale bar as a reference (8).

Immunofluorescence Staining

Human blastocysts and blastoids were fixed with 4% paraformaldehyde (PFA) in PBS for 20 min at room temperature and permeabilized with 0.5% Triton X-100 in PBS for 1 h. Samples were then blocked with blocking buffer (PBS containing 5% FBS, 4% BSA and 0.1% Tween-20) at room temperature for 1 h, or overnight at 4 °C. Primary antibodies diluted in blocking buffer were applied to samples and incubated overnight at 4 °C. Samples were washed three times with PBS containing 0.1% Tween-20 (PBS-T), followed by incubation with fluorescently conjugated secondary antibodies diluted in blocking buffer for overnight at 4 °C. Samples were washed three times with PBS-T. Finally, cells were counterstained with 300 nM 4,6-diamidino-2-′ phenylindole (DAPI) solution at room temperature for 10 mins. Phalloidin was directly stained along with other secondary antibodies in the blocking buffer. Samples were imaged using a fluorescence (Revolve, Echo) or a confocal microscope (A1R, Nikon; 3i Marianas spinning disk confocal). The cell numbers were counted manually using the Imaris surface tool for GATA3+ positive nuclei.

scRNA-seq library preparation

To characterize extended culture, 23 and 27 human blastocysts, or 120 and 80 blastoids were seeded on fibronectin-coated ibidi dishes or ibidi dishes seeded with immortalized endometrial stromal cells, respectively. After three days of culture in EBC medium, all implantation sites were

manually picked up using a mouth pipette during a 10 min incubation in TrypLE at 37 °C. For the co-culture, surrounding stromal cells were also collected. Harvested aggregates were rigorously pipetted to make the single-cell suspension, followed by dissociated cell isolation with a 30 µm filter (130-041-407, Miltenyi Biotec, Germany). Cell number and viability were examined via trypan blue assay on an automatic cell counter (Eve, NanoEntek). Single cell suspensions (500-1000 cells/mL) were loaded into a 10x Genomics Chromium Chip following the manufacturer's instruction 1. (10x Genomics, Pleasanton, CA, Chromium Next GEM Single Cell 3′ GEM, Library & Gel Bead Kit v3.1, catalog number 1000121).

Sequencing, base calling and fastq demultiplexing

Single cell libraries were sequenced using Illumina NextSeq 500/550 and NovaSeq 6000 sequencing systems (Illumina, San Diego, CA). The generated binary base call (BCL) files were demultiplexed and converted to standard FASTQ files using the mkfastq function from 10x Genomics' Cell Ranger pipeline (version 6.1.2).

Preprocessing single-cell data

Fastq files were mapped to the human GRCh38 reference (version 3.0.0, downloaded from 10x website) using 10x Genomics' Cell Ranger pipeline (version 6.1.2) with default parameters. For blastoid samples, the number of cells expected was set to 10,000. For human blastocyst samples, cell-associated barcodes were determined based on the inflection point of the UMI saturation curves. Scrublet was used to detect multiplets for blastoid samples (version 0.2.1). Cells with more than 20% of UMIs from mitochondrial genomes and less than 200 genes detected were discarded.

Raw fastq files of public datasets were downloaded and re-processed to minimize platform and processing differences as described in Yu et al. (1). The cell lineage annotations of the public

datasets were derived from their perspective publications (see https://github.com/jlduan/replica for details).

Genotyping

To separate the mix-sequenced blastocyst and blastoid cells, two approaches were used. First, the genotypic variant calling of the 3,202 samples from the 1000 Genomes Project was downloaded and only SNPs with more than 10% allelic frequency on chromosomes 1 to 22 and X were kept (9). This SNP list served as the reference genotype. Individual cells from separately sequenced blastoid samples were compared against the reference genotype, and a consensus genotype of the blastoid cells was summarized. Then the cells from the mix-sequenced sample were compared against the blastoid consensus genotype and scored based on the percentage of SNPs that agree with it. For the second approach, instead of using the genotypes from the 1000 Genomes Project, the reference genotype of blastoid cells was called using HaplotypeCaller module from GATK (version 4.2.4.1) and homogeneous SNPs with more than 3 reads support were kept as blastoid consensus genotypes (10). Prior to the variant calling, reads contributing to real cells from the alignment file generated by 10x Genomics' Cell Ranger were processed with GATK's SplitNCigarReads module with default parameters.

The distribution of genotype scores was plotted, and the cutoff was determined using Gaussian mixture distribution model from scikit-learn (version 1.0.2) with likelihood set to 0.9.

Single cell genotype clustering was performed using souporcell (version 2.4) with a range of different numbers of clusters. And the total log likelihood of each run was recorded, and an elbow plot was generated (11). The number of major genotypes was determined based on the inflection point of the elbow curve. The separation of blastocysts and blastoids co-cultured with IESCs was performed in the similar fashion, with separably sequenced IESCs as the reference genotype.

Dimensionality reduction

Reprocessed single cell data from selected public and our previous studies were combined with newly generated data (1-3, 12-14). The combined expression matrix was median-normalized, natural-log-transformed with the addition of a pseudocount of 1 and standardized per gene prior to principal component analysis (PCA). sc.tl.pca from Scanpy package (version 1.9.1) was used to compute the first 100 components (15).

Batch correction

The python implementation harmonypy (version 0.0.5, https://github.com/slowkow/harmonypy) of Harmony algorithm was used to remove the batch effect (16). Each 10x Genomics run was considered as one batch, Smart-Seq2 libraries from individual studies were treated as individual batches.

Uniform Manifold Approximation and Projection (UMAP)

Batch corrected principal components were used as input for UMAP (version 0.5.3) with default parameters (17).

Clustering

Single cells were clustered using the leiden algorithm implemented in the Scanpy package (version 1.9.1, 10). Briefly, the batch corrected principal components were used as input for sc.pp.neighbors function from Scanpy package to compute a neighborhood graph of observations (n_neighbors=30). Then, leiden algorithm was used to cluster single cells with default parameters.

Functional enrichment

Gene Ontology (GO) enrichment

Fisher's exact test implemented in topGO (version 2.48.0; org.hs.eg.db version 3.15.0) was used for GO term enrichment tests (algorithm = "classic").

KEGG pathway enrichment

KEGG pathway enrichment was performed using clusterProfiler (version 4.4.4) with default parameters.

Proteomics data analysis

Processed proteomics datasets were analyzed with R package DEP (18). Only proteins identified in at least two replicates of the same condition were kept. Blastoids were normalized through the function normalize_vsn. Due to great differences in total protein levels between conditioned stromal medium and control, normalization of this dataset was based on albumin levels. Missing values were imputed by funcion impute, with parameter fun="QRILC". Functions test_diff and add_rejections were employed for differential enrichment test, with alpha=0.05.

Blastoid scRNA-seq and proteomics integrated analysis

Data was processed using base Python. Venn diagrams were plotted with the matplotlib_venn package (19). Genes detected by both scRNA-seq and mass spectrometry were ordered based on mean abundance across samples, and scatter plots were generated with package Seaborn (20).

Proteomics

Stromal cells cultures in 100mm dishes were cultured to 80% confluency, media was changed for a FBS free, 0.1xITSX, 0.01%BSA stroma cell culture media and cells where cultured for 48h. Then media was recovered, and cell debris was removed via centrifugation, supernatant was

filtered in 0.22µm syringe filters. TCA-DOC protein precipitation was performed as described by Par, et al, with slight modifications. Briefly supernatant was brought to 1% (v/v) of a 2% sodium deoxycholate solution to the supernatants and incubate don ice for 30 minutes under gentle mixing. Then 100% trichloroacetic acid was added to a final concentration of 7,5% (v/v) and incubated on ice for 60 minutes under gentle mixing. Proteins were precipitated by centrifugation (10,000 rpm for 60 minutes at 4°C) and supernatant were carefully discarded. Protein pellets were washed and vortex with 20 ml of 1cold 00% acetone (-20°C) and incubated at acetone at -20°C for 5 minutes. Samples where centrifuged (15,000g for 5 minutes at 4°C) and the supernatants were discarded. Pellets where washed a second time with 5 ml of 100% cold acetone (-20°C), vortex, and centrifuged (15,000g for 5 minutes at 4°C) and discard the supernatants. Protein pellets where air-dry in a chemical hood for 30 minutes and dissolve in 500 µl of RIPA buffer with 1x protease and 1x phosphatase inhibitor cocktail. Samples where snap frozen in liquid nitrogen and submitted to the UT Southwestern proteomics core for tandem mass tag (TMT) labeling followed by liquid chromatography with tandem mass spectrometry (LC-MS/MS) and phosphopeptide enrichment.

Phosphopeptide enrichment and signaling

Genes present in both scRNA-seq and mass spectrometry datasets were selected for phosphopeptide enrichment analysis. Detected phosphopeptides were tested against curated kinase datasets from PTMsigDB (21) by Fisher exact test, with significance level of 0.05. Results were plotted with Python package Seaborn.

Code availability

The code used in this project is provided at https://github.com/jlduan/blastoidverse.

Data availability

Single cell RNA-seq data generated in this study have been deposited in the Gene Expression Omnibus (GEO) with accession number GSE210962.

Results

Extended Blastoid Medium Supports Both Blastoid and Blastocyst Growth

We found that moving blastoids from eTDM medium directly to IVC medium for extended culture was detrimental to their health, and the majority would disassemble gradually over the course of a few days. To mitigate this detriment, we developed an extended blastoid culture medium (EBC) to incorporate components of eTDM with IVC to better support their growth during peri-implantation. We found that when blastoids were cultured during peri-implantation in either IVC or EBC, those in EBC were healthier as evidence by their continued growth and did not exhibit the extensive damage that we noticed in IVC alone (Fig. 5.2A). Additionally, EBC medium was able to support the growth of human blastocysts during the peri-implantation period (Fig. 5.2A), and both blastoids and blastocysts displayed significantly increased trophectoderm outgrowth areas compared to those cultured in IVC (Fig. 5.2B).

Blastoids Produced From an 8-day Protocol Show Increased Growth in Extended Culture

The majority of blastoid cavities are produced after 5 d in eTDM medium (D8). However, some blastocoele cavities form or persist after an additional day in eTDM medium (D9). D8 blastoids had significantly increased outgrowth areas in extended culture compared to those that persisted or formed after D9 (Fig. 5.2C). We then stained for trophoblast lineage markers and found that D9 blastoids did not express pluripotent marker POU5F1 whereas D8 blastoids expressed POU5F1 brightly localized to the ICM (Fig. 5.2D), similar to 6 d. p. f. human pre-implantation blastocysts (Fig. 5.1G).

Endometrial cells promote trophoblast proliferation and differentiation.

During human implantation, the polar TE of a blastocyst attaches to the endometrial lining of the uterus, invades the endometrial epithelium, stroma, and the maternal circulation to form the placenta (22). Implantation is a complex process in which several cell types interact. Endometrial epithelium is the first maternal contact for an implanting embryo and only serves as a transient gateway for embryo implantation (23). Following the penetration through epithelium, the differentiation and invasion of the early human trophoblast occur in endometrial stroma in a controlled manner that ultimately result in a functional placenta (24). A recent study established an in vitro implantation model by co-culturing human blastoids with endometrial epithelial cells (3). To date, however, how endometrial stromal cells influence the growth and differentiation of implanting blastoids remains elusive. To fill this gap, we established a co-culture system by growing human blastoids on immortalized primary endometrial stromal cells (IESCs) to study their crosstalk. We first established primary cultures of endometrial stromal cells (see Methods) from patient uterine biopsies, which exhibited typical fibroblast-like morphology. Because primary endometrial stromal cells have limited self-renewal ability in culture, we subjected them to immortalization by forced expression of telomerase reverse transcriptase (TERT, 25). We plated human blastoids on a hormone-stimulated monolayer of IESCs in EBC medium and compared their growth to those grown on female umbilical cord fibroblasts (herein referred to as fibroblasts) or fibronectin-coated dishes. After plating, we found human blastoids quickly attached to the IESCs and readily grew outward, similar to what were observed on fibronectin-coated plates. After staining with the trophoblast marker GATA3, we found significantly more GATA3+ nuclei in blastoid outgrowths on both fibroblasts and IESCs than on fibronectin (Figure 5.2E, F). Interestingly, we found a significantly increased number of multinucleated syncytiotrophoblast (ST)-like cells (STLCs) from blastoid outgrowths on IESCs than on fibroblasts or fibronectin alone (Figure 5.2E, G).

We then compared blastoid attachment dynamics to human blastocysts on fibronectin or IESCs. We found that most human blastocysts exhibited a 24-48h delay in attachment compared to the blastoids (Figure 5.3A). Following a 72h growth period in extended culture, blastoids and blastocyst both attached and readily outgrew (Figure 5.3B). Late-attached blastocysts retained a large blastocoele cavity that reduced in size gradually and concurrently with trophoblast differentiation at the cell interface. After 72 h, these late-attached blastocysts were largely proliferative but with reduced syncytialization and fewer CGB+ syncytiotrophoblast (ST) cells (Figure 5.3C). Approximately 30% of human blastocysts were able to attach to fibronectin-coated plates or IESCs early within 24h and exhibited reduced proliferation and early blastocoele collapse with more accelerated ST differentiation and increased number of CGB+ cells (Figure 5.3A, C). Though trophectoderm outgrowth area was similar amongst human blastocysts and blastoids during extended culture (data not shown), blastoids exhibited an attachment and outgrowth dynamic similar to the early-attached human embryos (Figure 5.3A). Following 72h growth in extended culture on fibronectin, blastoids secrete comparable amounts of CGB into spent medium (Figure 5.3D), and show development of epiblast cells, a proamniotic cavity (Figure 5.3E), and peripheral syncytiotrophoblast cells (Figure 5.3F) similar to human blastocysts.

We then studied the effects of IESCs on blastoids and blastocysts and asked if direct contact and/or secreted factors were responsible for the proliferation and fusion of trophoblast (GATA3+) cells. To this end, we cultured blastoids/blastocysts on fibronectin-coated dishes in EBC or in IESC-conditioned EBC (IESC-CM), or together with IESCs. Blastoids/blastocysts in IESC-CM or co-cultured with IESCs developed more GATA3+ nuclei compared to those grown on fibronectin in fresh EBC (Figures 5.4 A-D). However, the number of GATA3+ nuclei that were fused into multinucleated ST-like cells (STLCs) was increased only in blastoid/blastocyst-IESC co-cultures (Figure 5.4C, F). This suggests that direct contact with IESCs encourages trophoblast syncytialization. We also observed CGB levels in spent medium increased in

blastoid/blastocyst-IESC co-cultures (Figure 5.4F). To identify the secreted factors in IESC-CM that may be responsible for increased trophoblast cell proliferation, we performed LC-MS/MS proteomic analysis. We identified 398 proteins from IESC-CM over unconditioned EBC medium control among which 182 were annotated as secreted proteins by SPR proteome and the human protein atlas databases. Among the enriched Pfam domains were Calcium binding EGF like domains (e.g., BMP1, FBN2), IGF binding proteins (IGFBP3,4,5,7), and Follistatin-N-terminal domain-like (FOLN) (e.g., SPARC, FSTL1, Figure 5.4G, H, Table 5.1) .

Collectively, our results demonstrate IESCs promote trophoblast cell proliferation, syncytialization, and CGB secretion when co-cultured with human blastoids and blastocysts. Extended culture of human blastoids model a population of early-attached blastocysts, but not the late-attached majority of human blastocyst, suggesting more room for improvements.

Single cell transcriptomes of human blastocysts/blastoids and endometrial co-cultures

To further explore whether blastoids are suitable to model peri-implantation development, we compared single-cell transcriptomes between blastoids and blastocysts attached on fibronectin-coated dishes or IESCs and cultured for 3 days in EBC (Figure 5.5A). We also sequenced IESCs separately as a control to help deconvolute IESCs in co-culture samples (Figure 5.6A, B). Unbiased clustering identified 16 distinct transcriptomic clusters (Figure 5.5A). Separately sequenced IESCs are preeminently clustered in clusters 1, 2, 6, 11, 12, 13 (Figure 5.5A), mirroring the results of genotypic deconvolution of IESCs in co-culture samples (Supplementary Figure 5.1B). Marker genes for EPI (SOX2) and HYP (SOX17) are significantly enriched in clusters 8 and 14, respectively, while genes for trophoblasts (TB) (GATA3 and CYP19A1) are enriched in clusters 0, 3, 4, 5, 7, 9, 10 (Figure 5.5B). These clusters have distinct expression patterns. For instance, NANOG is highly expressed in clusters 8 and 15, while CCNA1 is only highly expressed in cluster 15 (Figure 5.5C). To identify blastoid cell states that respond to IESCs, we calculated cluster composition (Figure 5.5D, 5.6C). We observed that blastoids co-

cultured with IESCs were enriched in TB clusters 3 and 5, as compared to those cultured on fibronectin (Figure 5.5D, cluster 3: 1.7-fold, cluster 5: 1.3-fold), in a similar trend to blastocysts (Figure 5.5D, cluster 3: 13.1-fold, cluster 5: 1.9-fold). In contrast, we observed little to no differences in EPI and HYP clusters among different samples (Figure 5.5D). To gain a better understanding of TB clusters 3 and 5, we compared gene expression patterns with TB clusters 0, 7 and 9, which are enriched with cells grown on fibronectin (Figure 5.5D, E). We observed that *MMP10, MMP3, CTGF, KRT17, CNN1, SERPINE2, FN1, and DBP,* all of which are implicated in TB migratory and extracellular remodeling activities were highly enriched in clusters 3 and 5 vs clusters 0, 7, and 9 (Figure 5.5E, F, 26-32). Consistent with this result, Gene Ontology analysis revealed that cluster 3 and 5 were enriched in terms related to extracellular matrix organization (Figure 5.5G). In contrast, genes in clusters 0, 7, and 9 were enriched in GO terms related to chromosome organization, nucleic acid metabolic process (Figure 5.5H). To annotate distinct TB clusters, we used top marker genes identified from single-cell RNA-sequencing of human peri-implantation culture (33). Clusters 9, 0, and 7 were significantly enriched for cytotrophoblast markers including RRM1 (Figure 5.6D). Clusters 4 and 10 expressed ST-specific markers including the CGB family and NUCB2 (Figure 5.6D). Cluster 3 was highly enriched in transcripts for migratory TB including TIMP2 (Figure 5.6D). Compared to cluster 3, cluster 5 expresses DEGs corresponding to both proliferative cytotrophoblasts and invasive extravillous TB (*LIN28B, PEG10, LMNB1, and PLK2*). We therefore hypothesize that clusters 3 and 5 correspond to two subtypes of migratory TB corresponding to two distinct extravillous subtypes similarly noted in the 8-week placenta (31, 34-37).

We also pooled ELCs, HLCs and TLCs from each sample and compared their transcriptome profiles between blastoids and blastocysts cultured on fibronectin, as well as co-cultured with IESCs. KEGG pathway analyses based on the DEGs revealed: 1) For IESC-cultured samples, ECM-receptor interaction and focal adhesion were enriched in blastocysts while blastoids showed increased transcription of p53 and FoxO signaling (Figure 5.5I). 2) For fibronectin

cultured samples, Necroptosis, ferroptosis and apoptosis (EPI), cholesterol metabolism, fat and vitamin digestion and absorption (HYP), and Hippo signaling pathway (TB) were among the top pathways in blastocyst cells; And HIF-1 signaling pathways and diabetic cardiomyopathy related genes were among the upregulated DEGs in blastoid cells (Figure 5.6E).

Taken together, our results show that IESCs encourage differentiation of a more invasive trophoblast population in both blastoids and blastocysts and human blastoids are able to stimulate transcriptomic changes in IESCs resembling those from human blastocysts.

Discussion

During the peri-implantation period, TB of the embryo attach, penetrate through the uterine epithelium, and come in direct contact with the decidualized endometrial stromal cells. Rapid proliferation of the progenitor cytotrophoblast around embryonic day 8 is followed by the formation of the invasive primitive ST that burrow into the endometrial stroma and secret sufficient CGB, both of which are prerequisites for establishing early pregnancy (34). TB proliferation, differentiation, and invasion within endometrial stroma are the early events that establish the maternal-fetal crosstalk before the formation of mature placenta. By using human blastoids, we demonstrated that IESCs facilitated TLC differentiation into multi-nucleated STLCs while simultaneously promoting proliferation and mitigating apoptosis. These results are consistent with our observations and other studies performed using human blastocysts demonstrating the utility of human blastoids in modeling maternal-fetal crosstalk (38-40). Using blastoids, we were also able to detect significant differences among different treatment conditions, likely due to the reduced variability between samples. Furthermore, we show that blastoids can respond to IESCs in a similar fashion to human blastocysts. Co-culture with IESCs encouraged differentiation of a TB population resembling early migratory TB (33) which significantly upregulated transcripts necessary for vascular development and cell migration.

Future studies using co-culture of patient-specific blastoids and/or endometrial stromal cells will be instrumental to understanding developmental defects and early pregnancy loss.

In sum, our study showcases a robust, reproducible, and efficient method for large-scale production of high-fidelity human blastocyst-like structures from naïve hPSCs. The newly optimized protocol will facilitate broad adoption of human blastoids as an accessible, perturbable, scalable, tractable, and ethical model for human blastocysts. In this study we also identified key signaling pathways underlying blastoid formation and uncovered pro-survival and pro-differentiation effects of endometrium stromal cells on trophoblast outgrowth. Finally, we demonstrate that human blastoids are able to recapitulate maternal-fetal crosstalk events during the peri-implantation period. These findings may help develop strategies to enhance blastoid function, thereby promoting more robust post-implantation development.

Limitations of the study

It should be noted that, human blastoids generated from all existing protocols (including this study) do not fully recapitulate human blastocysts. To generate blastoids, naïve hPSCs need to be induced into TE- and HYP- like cells under non-physiological conditions with different chemicals and growth factors, which is in sharp contrast to the development of human blastocysts. In addition, both 5iLA and PXGL cultured naïve hPSCs more resemble E6-7 EPI cells than E3-4 blastomeres. They are also genetically and epigenetically unstable, and consistently show loss of imprinting (41, 42). Thus, it's not appropriate to use the human blastocyst developmental sequence and timing as criteria to evaluate blastoid models. In this study, we performed side-by-side scRNA-seq between blastoids and blastocysts, as well as post-implantation cultures, to better understand the differences between blastoids and blastocysts, which can sever as important resource for further improving human blastoid models in the future.

Conclusion

We have optimized extended culture conditions to accommodate blastoids and found that blastoids mimic a population of human embryos that attach and differentiate within 24h. Additionally, we show that stromal cells encourage TB proliferation and differentiation into multinucleate syncytial plaques and that blastoids are capable of recapitulating these events. Finally, we used scRNA-seq to tease apart transcriptomic differences between human embryos and blastoids during the peri-implantation period and show that stromal cells encourage differentiation of an invasive migratory TB population. Though blastoids are able to mimic aspects of human peri-implantation development, continued optimization of blastoid production methods and extended blastoid culture conditions are needed to make blastoids more physiologically relevant.

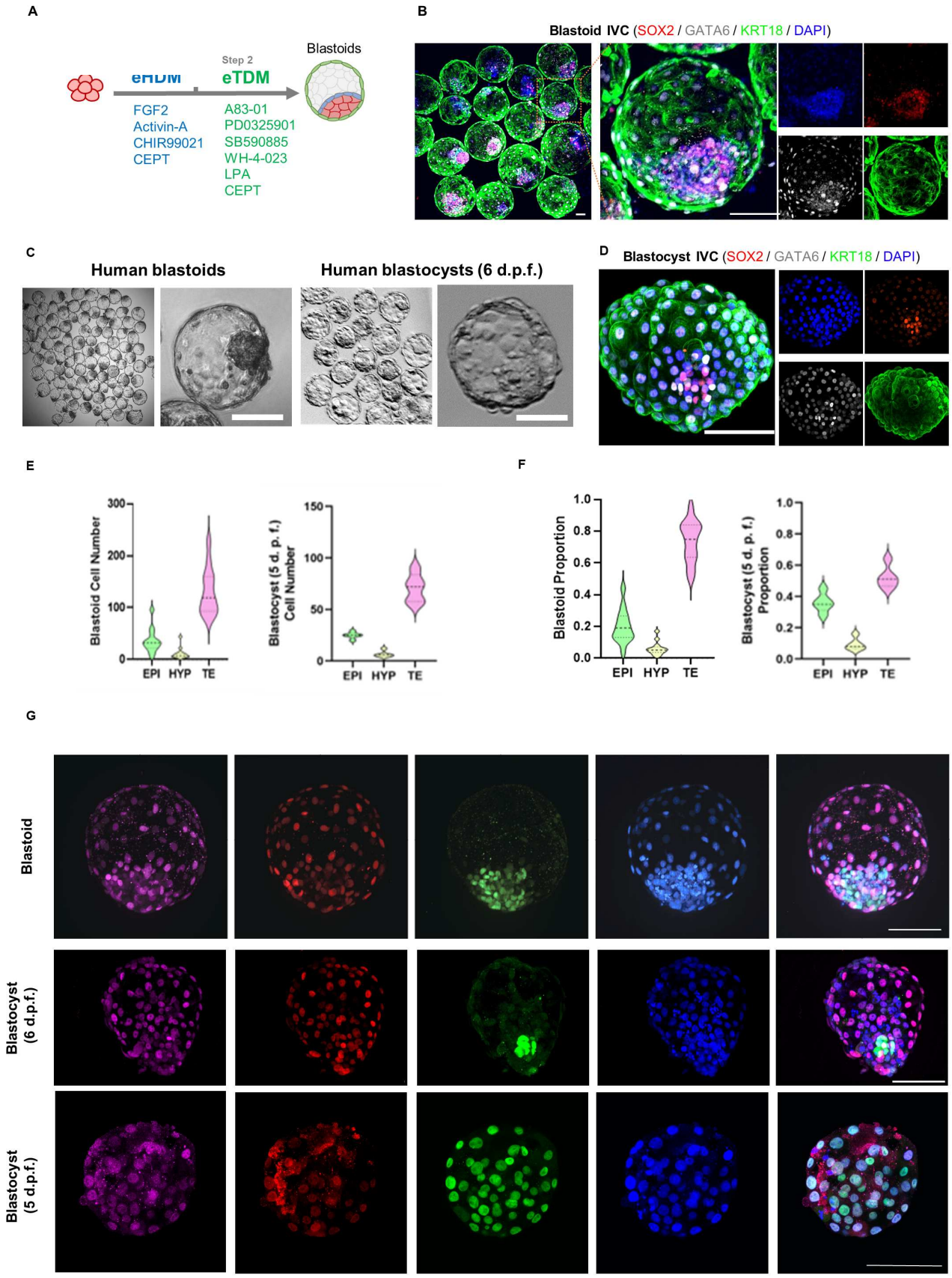
A
Step 2
eTDM
Blastoids
FGF2
Activin-A
CHIR99021
CEPT
A83-01
PD0325901
SB590885
WH-4-023
LPA
CEPT
B
Blastoid IVC (SOX2 / GATA6 / KRT18 / DAPI)
C
Human blastoids
Human blastocysts (6 d.p.f.)
D
Blastocyst IVC (SOX2 / GATA6 / KRT18 / DAPI)
E
Blastoid Cell Number
Blastocyst (5 d. p. f.) Cell Number
EPI HYP TE
F
Blastoid Proportion
Blastocyst (5 d. p. f.) Proportion
EPI HYP TE
G
Blastoid
Blastocyst (6 d.p.f.)
Blastocyst (5 d.p.f.)

Figure 5.1. Characterization of human blastoids. (A) Schematic of the optimized blastoid formation protocol. (B) Representative immunofluorescence co-staining images of SOX2, GATA6, and KRT8 in blastoids. (C) Representative phase-contrast images of human blastoids (left) and 5 d.p.f. human blastocysts (right). Scale bars, 100 μm. (D) Representative immunofluorescence co-staining images of SOX2, GATA6, and KRT8 in a 6 d.p.f. blastocyst. Scale bar, 100 μm. Quantification of the number (E) and proportion (F) of epiblast (EPI), hypoblast (HYP) and trophectoderm (TE) cells in human blastoids (n=13; EPI=35.69 ± 6.39, HYP= 11.31 ± 11.10, TE= 130.8 ± 44.56) and blastocysts (5 d.p.f.) (n=5; EPI= 24.80 ± 3.19, HYP= 6.60 ± 3.13, TE= 70.80 ± 13.85). (G) Representative immunofluorescence staining image of GATA3 and GATA6, OCT4 in human blastoid(upper), 6 d.p.f blastocyst (middle), and 5 d.p.f. blastocyst (bottom). Scale bars, 100 μm.

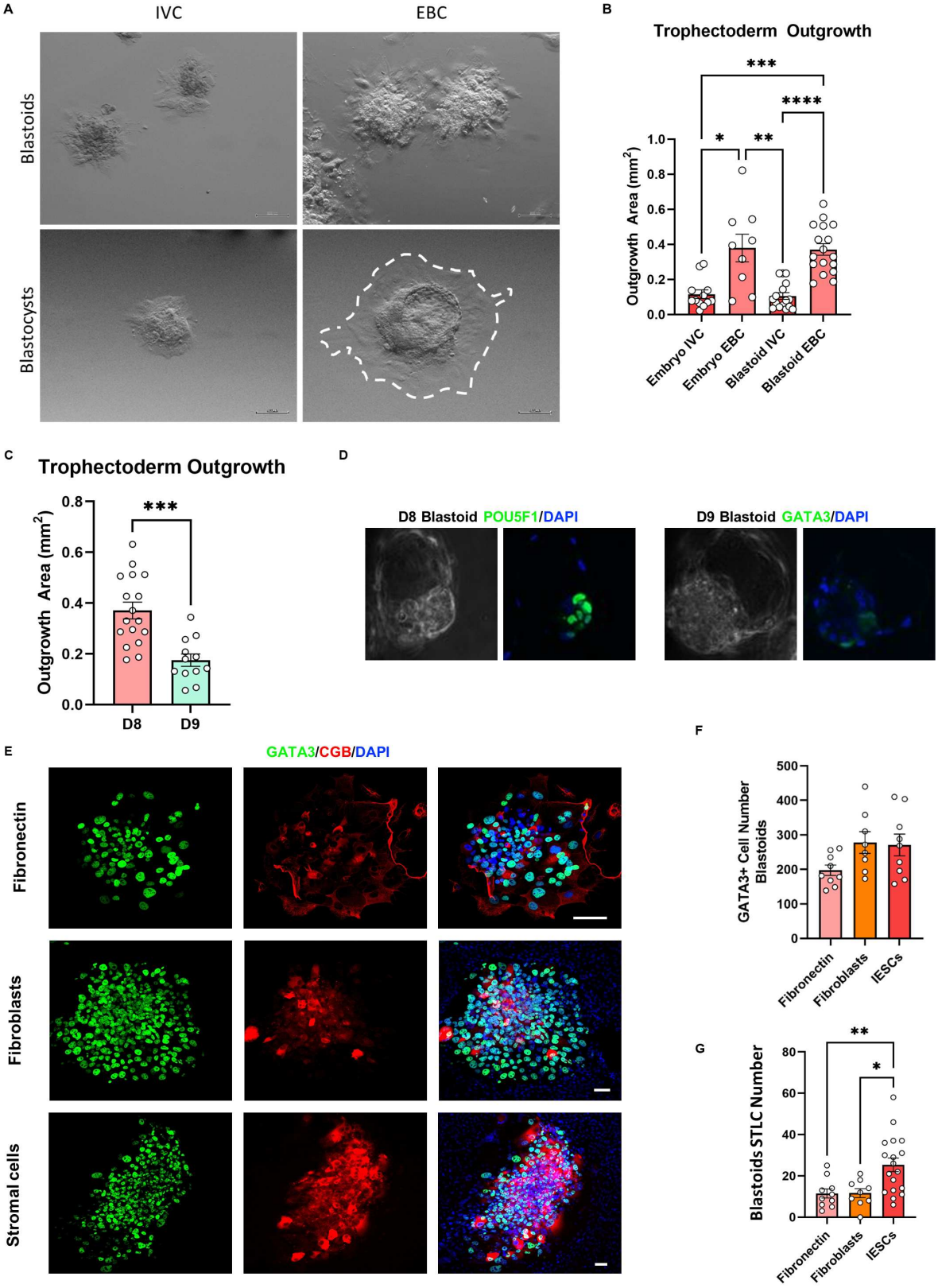
A
IVC
EBC
Blastoids
Blastocysts
B
Trophectoderm Outgrowth
Outgrowth Area (mm2)
Embryo IVC
Embryo EBC
Blastoid IVC
Blastoid EBC
C
Trophectoderm Outgrowth
Outgrowth Area (mm2)
D8
D9
D
D8 Blastoid POU5F1/DAPI
D9 Blastoid GATA3/DAPI
E
GATA3/CGB/DAPI
Fibronectin
Fibroblasts
Stromal cells
F
GATA3+ Cell Number Blastoids
Fibronectin
Fibroblasts
IESCs
G
Blastoids STLC Number
Fibronectin
Fibroblasts
IESCs

Figure 5.2. Optimizing extended blastoid culture conditions A) Representative brightfield images of extended culture of human blastocysts and blastoids in EBC or IVC medium. Scale bar= 200 μM. B)Trophoblast outgrowth area measurements of in vitro cultured human blastocysts and blastoids in EBC or IVC medium after 72 h in extended culture. Kruskal-Wallis rank sum test *p<0.05, **p<0.01, ***p<0.001, ***p<0.0001. (C) Trophoblast outgrowth area measurements of in vitro cultured human blastoids after 8 (D8) or 9 (D9) days of differentiation in eHDM/eTDM. Student t. test ***p<0.001. (D) Representative confocal images of in vitro cultured human blastoids after 8 (D8) or 9 (D9) days of differentiation in eHDM/eTDM. POU5F1=green, DAPI=blue. (E) Representative immunofluorescence co-staining image of CGB (red) and GATA3 (green) in EBC-cultured blastoids grown on fibronectin (top), fetal cord fibroblasts (middle), or immortalized endometrial stromal cells (bottom). Scale bar, 100 μm. (F) GATA3+ cell number in blastoids on fibronectin, fibroblasts, or endometrial stromal cells after 72 h in extended culture. G) Percentage of the multi-nucleated STLCs of total GATA3+ cells in EBC-cultured blastoids. One way ANOVA *p<0.05, **p<0.01.

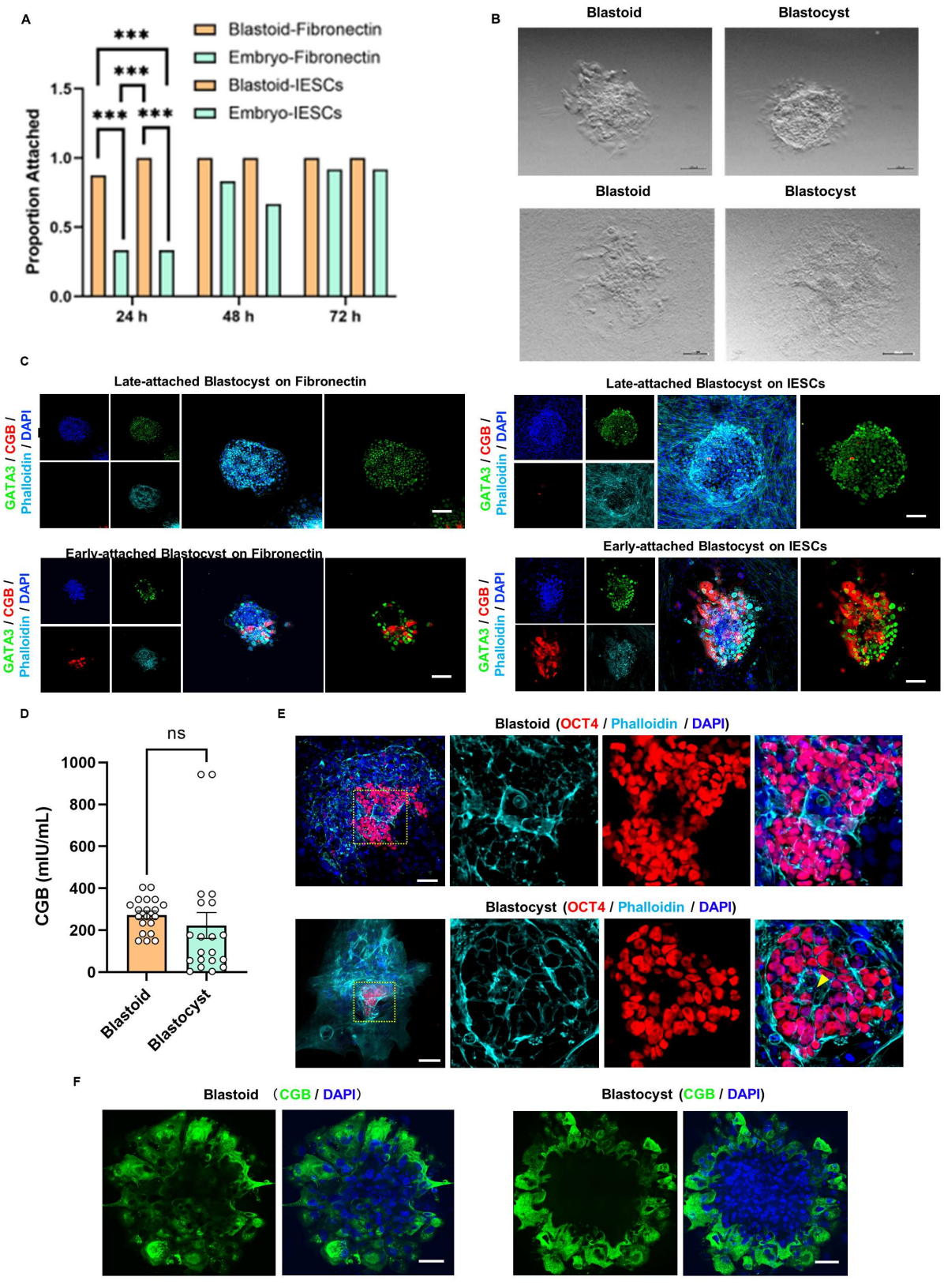
A
Blastoid-Fibronectin
Embryo-Fibronectin
Blastoid-IESCs
Embryo-IESCs
Proportion Attached
1.5
1.0
0.5
0.0
***
***
***
***
24 h
48 h
72 h
B
Blastoid
Blastocyst
Blastoid
Blastocyst
C
Late-attached Blastocyst on Fibronectin
Late-attached Blastocyst on IESCs
Early-attached Blastocyst on Fibronectin
Early-attached Blastocyst on IESCs
GATA3 / CGB / Phalloidin / DAPI
D
ns
CGB (mIU/mL)
1000
800
600
400
200
0
Blastoid
Blastocyst
E
Blastoid (OCT4 / Phalloidin / DAPI)
Blastocyst (OCT4 / Phalloidin / DAPI)
F
Blastoid （CGB / DAPI）
Blastocyst (CGB / DAPI)

Figure 5.3. Blastoids resemble human embryos during the peri-implantation period. (A) Attachment rates of human blastocysts and blastoids plated on fibronectin coated plates or on endometrial stromal cells over 72 h in extended culture. Fishers Exact test ***p<0.001. (B) Representative brightfield images of blastoids (left) and blastocysts (right) cultured on fibronectin coated plates (top) or co-cultured with endometrial stromal cells (bottom). Scale bars, 200 μm. (C) Representative immunofluorescence co-staining image of CGB and GATA3 in late-attached (top panels) or early-attached (bottom panels) human blastocysts cultured on fibronectin coated plates (left panels) or co-cultured with endometrial stromal cells (right panels). Scale bars, 100 μm. (D) The CGB levels in spent media were collected from EBC-cultured human blastocysts (n=20) and blastoids (n=20) after 5 d in extended culture. ns, not significant. (E) Representative immunofluorescence co-staining images of OCT4 and phalloidin in EBC-cultured human blastoids (upper) and blastocysts (bottom). Higher-magnification images of the boxed areas are shown on the right. The yellow arrowheads indicate the amniotic-cavity-like structures. Scale bar, 100 μm. (F) Representative immunofluorescence co-staining images of CGB in EBC-cultured human blastoids (left) and blastocysts (right) after 3 d in extended culture. Scale bar, 200 μm.

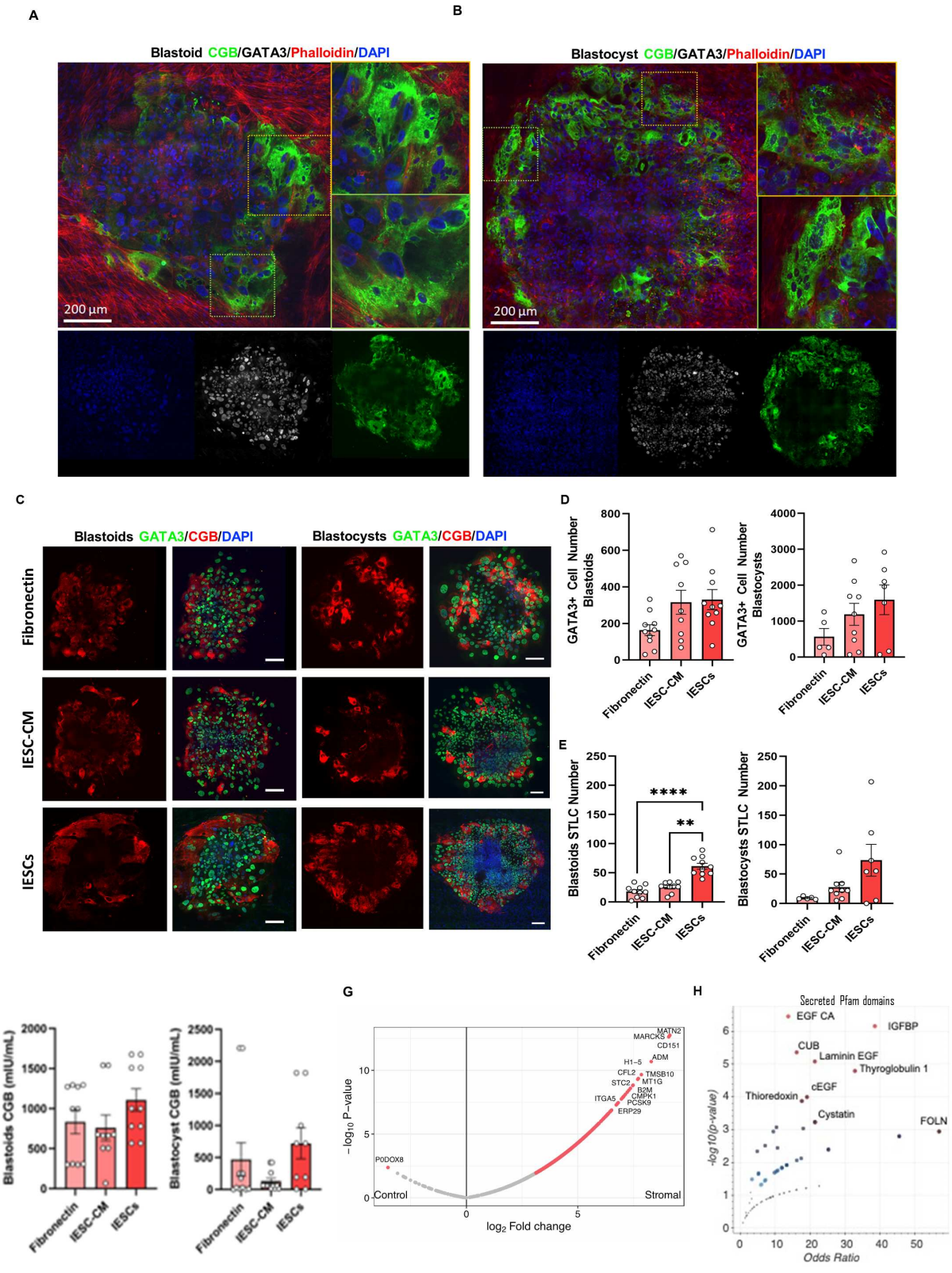
A
B
Blastoid CGB/GATA3/Phalloidin/DAPI
Blastocyst CGB/GATA3/Phalloidin/DAPI
200 µm
200 µm
C
Blastoids GATA3/CGB/DAPI
Blastocysts GATA3/CGB/DAPI
Fibronectin
IESC-CM
IESCs
D
GATA3+ Cell Number Blastoids
GATA3+ Cell Number Blastocysts
Fibronectin
IESC-CM
IESCs
E
Blastoids STLC Number
Blastocysts STLC Number
****
**
F
Blastoids CGB (mIU/mL)
Blastocyst CGB (mIU/mL)
G
MATN2
MARCKS
CD151
ADM
H1-5
CFL2
TMSB10
STC2
MT1G
B2M
CMPK1
ITGA5
PCSK9
ERP29
P0DQX8
Control
Stromal
log2 Fold change
H
Secreted Pfam domains
EGF CA
IGFBP
CUB
Laminin EGF
Thyroglobulin 1
cEGF
Thioredoxin
Cystatin
FOLN
Odds Ratio

Figure 5.4. Endometrial cells promote blastoid trophoblast proliferation and differentiation. Representative confocal images of a blastoid (A) and blastocyst (B) co-cultured on IESCs. Colored boxes are magnified to the right of each merged image. Blue= DAPI, red= Phalloidin, green= CGB, white= GATA3. Scale bars= 200 μm. (C) Representative confocal images on blastoids (left) and blastocysts (right) cultured for 72 h on fibronectin (top row), fibronectin in IESC-conditioned medium (IESC-CM, middle row), or directly on IESCs (bottom row). Scale bars= 100 μm. (D) Cell number of GATA3+ cells in EBC-cultured blastoids (left) or early attached (within 48 h) blastocysts (right) on fibronectin, fibronectin with IESC-CM, or IESCs after 72 h in extended culture. (E) Number of multi-nucleated STLCs of total GATA3+ cells in EBC-cultured blastoids (left) and early attached blastocysts (right). One-way ANOVA **p<0.01, ****p<0.0001. (F) CGB secretion in the spent medium (mIU/mL) of blastocysts (left) and blastoids (right) cultured on fibronectin coated plates, on fibronectin plates in stromal cell conditioned medium (IESC-CM), or co-cultured on IESCs. (F). Principal component analysis of conditioned stromal cell media and control. (G). Volcano plot depicting Log2 fold change vs -log10 of P-value, all significant detected proteins are in red. (H) Stroma cell proteins annotated as secreted Pfam domains colored by p-value.

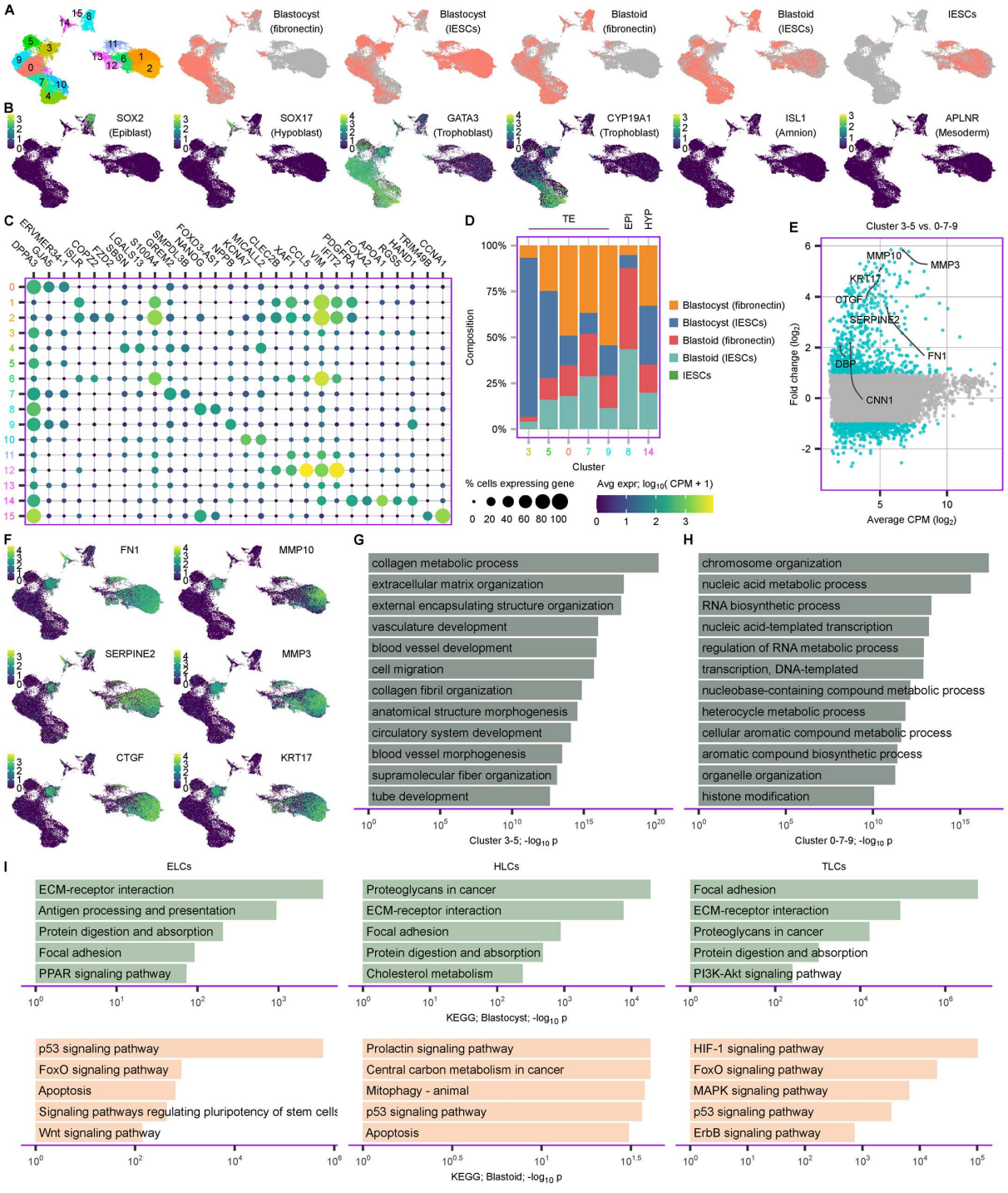

Figure 5.5. Blastoids are capable of recapitulating human embryo implantation events. (A) Co-embedding of blastoids and blastocysts implanted on fibronectin-coated dishes or IESCs. Left panel, colors indicate different transcriptomic clusters. (B) Gene expression patterns of lineage markers: SOX2 (EPI), SOX17 (HYP), GATA3 and CYP19A1 (trophoblast), ISL1 (amnion), and APLNR (mesoderm). (C) Expression patterns across different clusters. (D) Cellular compositions of selected clusters. (E) Differentially expressed genes between clusters 3, 5 and

0, 7, 9. (F) Gene expression patterns of LRRC75A, S100A14, c1orf56, MMP11, APOA1 and MGP. (G-H) Gene oncology enrichment analysis of genes highly expressed in cluster 3 comparing to the rest of TE clusters and clusters 0, 7, 9 comparing to clusters 3, 5. (I) KEGG enrichment analysis of differentially expressed genes from each lineage between blastocysts and blastoids grown on IESCs.

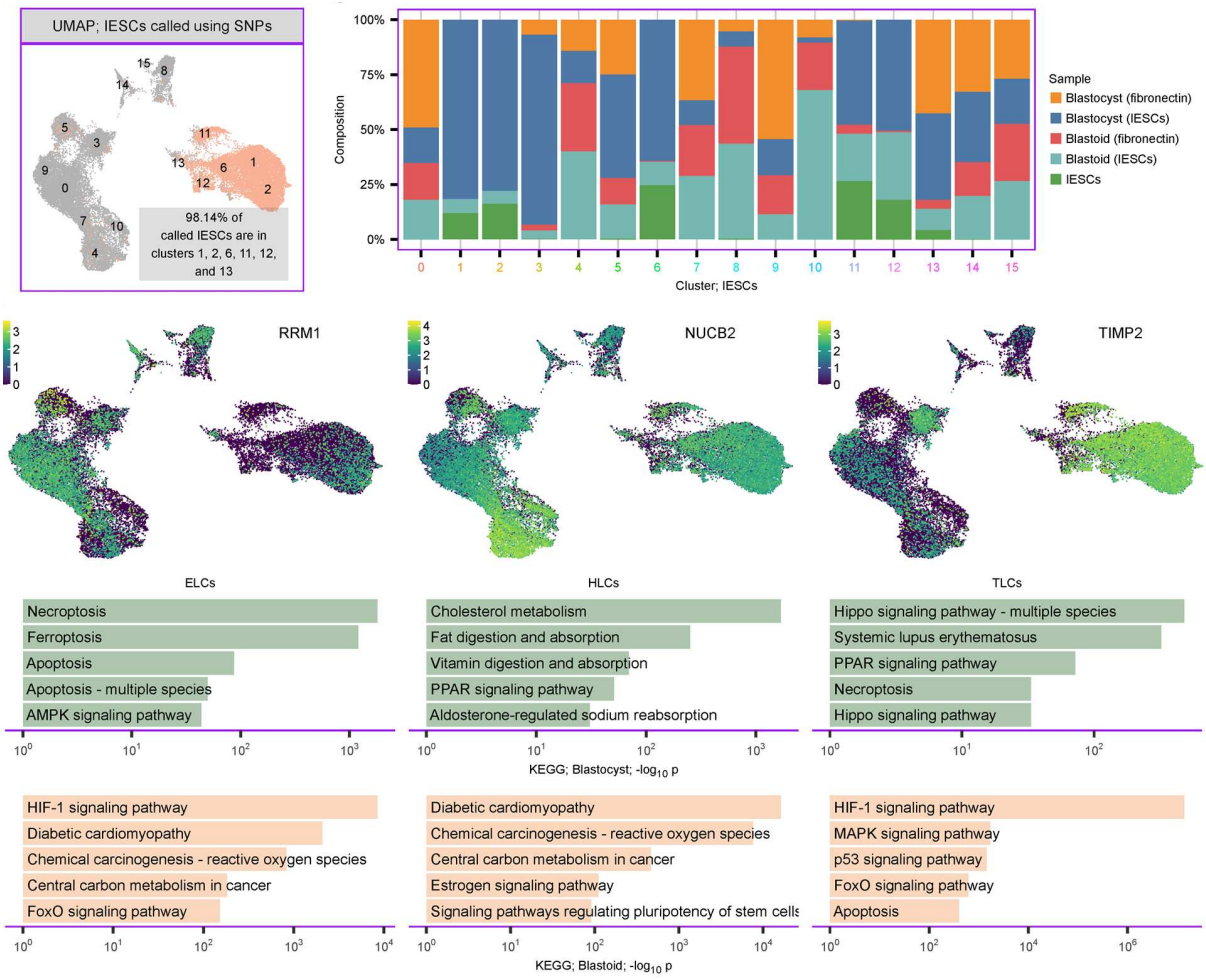

Figure 5.6. (A) Visualization of IESCs called from reference SNPs. The SNP reference is derived from de novo variant calling of IESCs. (B) Percentage of cells in each cluster derived from different sources. (C) Gene expression patterns of RRM1, NUCB2 and TIMP2. (D) KEGG enrichment analysis of differentially expressed genes between blastocysts and blastoids grown on fibronectin of each lineage.

Table 5.1 Pfam domains in stromal cell conditioned medium.

Term	P-value	Odds Ratio	Genes	
EGF CA	4.58E-07	13.32	FBN2;CCBE1;EFEMP2;BMP1;PROS1;FBLN1;THBS2;FBLN2	
IGFBP	6.71E-07	39.29	IGFBP5;IGFBP4;IGFBP3;CRIM1;IGFBP7	
CUB	5.13E-06	15.78	BMP1;C1S;TNFAIP6;C1R;PCOLCE;MASP1	
Laminin EGF	8.97E-06	21.14	LAMA4;NTN4;LAMC2;LAMB1;HSPG2	
Thyroglobulin 1	1.53E-05	33.66	IGFBP5;IGFBP4;IGFBP3;IGFBP6	
cEGF	1.05E-04	19.02	FBN2;EFEMP2;FBLN1;FBLN2	
Thioredoxin	1.40E-04	17.49	PDIA3;QSOX1;PDIA6;PDIA4	
NTR	5.74E-04	21.76	C4A;NTN4;PCOLCE	
Cystatin	5.74E-04	21.76	CST3;CSTB;AHSG	
FOLN	8.36E-04	72.17	SPARC;FSTL1	
EF-hand 5	9.16E-04	18.13	RCN3;PRKCSH;CALU	
VWA	9.27E-04	10.16	COL6A2;COL12A1;COL6A1;COL6A3	
ANATO	1.25E-03	54.13	C4A;FBLN2	
EFhand Ca insen	1.25E-03	54.13	ACTN1;ACTN4	
Sushi	1.26E-03	9.29	C1S;C1R;PAPPA;MASP1	
EGF	3.45E-03	6.93	PROS1;FAT1;MFGE8;HSPG2	
Laminin G 1	3.65E-03	27.06	PROS1;HSPG2	
Cofilin ADF	3.65E-03	27.06	CFL2;CFL1	
Laminin G 2	3.77E-03	10.52	LAMA4;PROS1;FAT1	
Trypsin	5.38E-03	4.72	CFD;C1S;C1R;MASP1;PRSS23	
Xlink	7.20E-03	18.04	TNFAIP6;CD44	
EGF 2	8.26E-03	16.65	TNXB;TNC	
Kunitz BPTI	1.18E-02	13.52	APP;COL6A3	
SRCR	1.18E-02	13.52	LGALS3BP;LOXL2	
PG binding 1	1.45E-02	12.02	MMP2;MMP3	
Disintegrin	1.45E-02	12.02	ADAM19;ADAM9	
Spectrin	1.74E-02	10.82	ACTN1;ACTN4	
Peptidase M10	1.90E-02	10.30	MMP2;MMP3	
Fibrinogen C	2.06E-02	9.83	TNXB;TNC	
CH	2.33E-02	5.17	ACTN1;ACTN4;CNN3	
DEAD	2.42E-02	5.09	DDX6;DDX39B;DDX1	
Kazal 2	3.52E-02	7.21	IGFBP7;FSTL1	
fn3	3.68E-02	3.32	TNXB;AXL;COL12A1;TNC	
Lipocalin	3.72E-02	6.97	CRABP2;PTGDS	
ICAM N	4.54E-02	26.92	ICAM1	
M20 dimer	4.54E-02	26.92	CNDP2	
Reprolysin	4.81E-02	6.00	ADAM19;ADAM9	
EF-hand 8	5.04E-02	5.84	RCN3;CALU	
Thiolase C	5.42E-02	21.53	ACAT2	
Thiolase N	5.42E-02	21.53	ACAT2	

Thiolase N	5.42E-02	21.53	ACAT2	
Astacin	5.42E-02	21.53	BMP1	
C4	5.42E-02	21.53	COL4A1	
DUF1899	6.30E-02	17.94	CORO1C	
SPARC Ca bdg	6.30E-02	17.94	SPARC	
Cadherin pro	6.30E-02	17.94	CDH2	
Glyco hydro 18	6.30E-02	17.94	CHID1	
Glyco transf 7N	6.30E-02	17.94	B4GALT4	
ERAP1 C	7.17E-02	15.38	ANPEP	
CSD	7.17E-02	15.38	CARHSP1	
EMI	8.03E-02	13.46	EMILIN2	
Methyltransf 11	8.03E-02	13.46	CIAPIN1	
Peptidase S8	8.88E-02	11.96	PCSK9	
MG2	8.88E-02	11.96	C4A	
Cadherin	8.92E-02	2.93	CDH6;CDH2;FAT1	
A2M BRD	1.06E-01	9.78	C4A	
A2M recep	1.06E-01	9.78	C4A	
Pentaxin	1.06E-01	9.78	PTX3	
EGF 3	1.06E-01	9.78	THBS2	
Gla	1.06E-01	9.78	PROS1	
Peptidase C1	1.14E-01	8.97	CTSB	
Peptidase M1	1.14E-01	8.97	ANPEP	
Kazal 1	1.14E-01	8.97	SPARC	
fn2	1.14E-01	8.97	MMP2	
TED complement	1.14E-01	8.97	C4A	
Gelsolin	1.22E-01	8.28	CAPG	
ADH N	1.30E-01	7.69	ADH5	
WAP	1.30E-01	7.69	WFDC1	
Clat adaptor s	1.30E-01	7.69	ARCN1	
LIM	1.34E-01	3.22	CSRP2;CSRP1	
UPAR LY6	1.54E-01	6.33	CD59	
Aldo ket red	1.54E-01	6.33	AKR1B1	
MHC I	1.62E-01	5.98	ULBP2	
EF-hand 7	1.82E-01	2.63	NUCB1;NUCB2	
F5 F8 type C	1.93E-01	4.89	MFGE8	
Pro isomerase	2.00E-01	4.68	PPIB	
hEGF	2.29E-01	3.98	FBN2	
C2-set 2	2.29E-01	3.98	ALCAM	
zf-CCHC	2.29E-01	3.98	CNBP	
C1q	2.50E-01	3.58	EMILIN2	
Sulfotransfer 1	2.64E-01	3.36	CHST3	
Serpin	2.98E-01	2.91	SERPINF1	
IL8	3.48E-01	2.39	CXCL12	
I-set	3.52E-01	1.63	IGFBP7;HSPG2	
TSP 1	4.06E-01	1.95	THBS2	
BACK	4.28E-01	1.82	LGALS3BP	
C1-set	4.44E-01	1.73	B2M	
Ig 2	5.03E-01	1.45	HSPG2	
Pkinase Tyr	6.97E-01	0.84	AXL	

REFERENCES

1. Yu, L., Wei, Y., Duan, J., Schmitz, D.A., Sakurai, M., Wang, L., Wang, K., Zhao, S., Hon, G.C., and Wu, J. (2021). Blastocyst-like structures generated from human pluripotent stem cells. Nature *591*, 620–626. 10.1038/s41586-021-03356-y.

2. Yanagida, A., Spindlow, D., Nichols, J., Dattani, A., Smith, A., and Guo, G. (2021). Naive stem cell blastocyst model captures human embryo lineage segregation. Cell Stem Cell *28*, 1016-1022.e4. 10.1016/j.stem.2021.04.031.

3. Kagawa, H., Javali, A., Khoei, H.H., Sommer, T.M., Sestini, G., Novatchkova, M., Reimer, Y.S. op, Castel, G., Bruneau, A., Maenhoudt, N., et al. (2022). Human blastoids model blastocyst development and implantation. Nature *601*, 600–605. 10.1038/s41586-021-04267-8.

4. Theunissen, T.W., Powell, B.E., Wang, H., Mitalipova, M., Faddah, D.A., Reddy, J., Fan, Z.P., Maetzel, D., Ganz, K., Shi, L., et al. (2014). Systematic Identification of Culture Conditions for Induction and Maintenance of Naive Human Pluripotency. Cell Stem Cell *15*, 471–487. 10.1016/j.stem.2014.07.002.

5. Deglincerti, A., Croft, G.F., Pietila, L.N., Zernicka-Goetz, M., Siggia, E.D., and Brivanlou, A.H. (2016). Self-organization of the in vitro attached human embryo. Nature *533*, 251–254. 10.1038/nature17948.

6. Shahbazi, M.N., Jedrusik, A., Vuoristo, S., Recher, G., Hupalowska, A., Bolton, V., Fogarty, N.M.E., Campbell, A., Devito, L.G., Ilic, D., et al. (2016). Self-organization of the human embryo in the absence of maternal tissues. Nat Cell Biol *18*, 700–708. 10.1038/ncb3347.

7. Logsdon, D.M., Grimm, C.K., West, R.C., Engelhorn, H.J., Kile, R., Reed, L.C., Swain, J.E., Katz-Jaffe, M., Schoolcraft, W.B., Krisher, R.L., et al. (2022). Maternal physiology and blastocyst morphology are correlated with an inherent difference in peri-implantation human embryo development. Fertil Steril *117*, 1311–1321. 10.1016/j.fertnstert.2022.02.018.

8. Schindelin, J., Arganda-Carreras, I., Frise, E., Kaynig, V., Longair, M., Pietzsch, T., Preibisch, S., Rueden, C., Saalfeld, S., Schmid, B., et al. (2012). Fiji: an open-source platform for biological-image analysis. Nat Methods *9*, 676–682. 10.1038/nmeth.2019.

9. Byrska-Bishop, M., Evani, U.S., Zhao, X., Basile, A.O., Abel, H.J., Regier, A.A., Corvelo, A., Clarke, W.E., Musunuri, R., Nagulapalli, K., et al. (2021). High coverage whole genome sequencing of the expanded 1000 Genomes Project cohort including 602 trios. Biorxiv, 2021.02.06.430068. 10.1101/2021.02.06.430068.

10. Poplin, R., Ruano-Rubio, V., DePristo, M.A., Fennell, T.J., Carneiro, M.O., Auwera, G.A.V. der, Kling, D.E., Gauthier, L.D., Levy-Moonshine, A., Roazen, D., et al. (2018). Scaling accurate genetic variant discovery to tens of thousands of samples. Biorxiv, 201178. 10.1101/201178.

7. Heaton, H., Talman, A.M., Knights, A., Imaz, M., Gaffney, D.J., Durbin, R., Hemberg, M., and Lawniczak, M.K.N. (2020). Souporcell: robust clustering of single-cell RNA-seq data by genotype without reference genotypes. Nat Methods *17*, 615–620. 10.1038/s41592-020-0820-1.

8. Xiang, L., Yin, Y., Zheng, Y., Ma, Y., Li, Y., Zhao, Z., Guo, J., Ai, Z., Niu, Y., Duan, K., et al. (2020). A developmental landscape of 3D-cultured human pre-gastrulation embryos. Nature *577*, 537–542. 10.1038/s41586-019-1875-y.

9. Petropoulos, S., Edsgärd, D., Reinius, B., Deng, Q., Panula, S.P., Codeluppi, S., Plaza Reyes, A., Linnarsson, S., Sandberg, R., and Lanner, F. (2016). Single-Cell RNA-Seq Reveals Lineage and X Chromosome Dynamics in Human Preimplantation Embryos. Cell *165*, 1012–1026. 10.1016/j.cell.2016.03.023.

10. Tyser, R.C.V., Mahammadov, E., Nakanoh, S., Vallier, L., Scialdone, A., and Srinivas, S. (2021). Single-cell transcriptomic characterization of a gastrulating human embryo. Nature *600*, 285–289. 10.1038/s41586-021-04158-y.

11. Wolf, F.A., Angerer, P., and Theis, F.J. (2018). SCANPY: large-scale single-cell gene expression data analysis. Genome Biol *19*, 15. 10.1186/s13059-017-1382-0.

12. Korsunsky, I., Millard, N., Fan, J., Slowikowski, K., Zhang, F., Wei, K., Baglaenko, Y., Brenner, M., Loh, P., and Raychaudhuri, S. (2019). Fast, sensitive and accurate integration of single-cell data with Harmony. Nat Methods *16*, 1289–1296. 10.1038/s41592-019-0619-0.

13. McInnes, L., Healy, J., and Melville, J. (2018). UMAP: Uniform Manifold Approximation and Projection for Dimension Reduction. Arxiv.

14. Zhang X, Smits A, van Tilburg G, Ovaa H, Huber W, Vermeulen M (2018). “Proteome-wide identification of ubiquitin interactions using UbIA-MS.” *Nature Protocols*, **13**, 530–550.

15. JD. "Matplotlib: A 2D Graphics Environment", Computing in Science & Engineering, vol. 9, no. 3, pp. 90-95, 2007

16. Waskom, M. L., (2021). seaborn: statistical data visualization. Journal of Open Source Software, 6(60), 3021, https://doi.org/10.21105/joss.03021

17. Krug K, Mertins P, Zhang B, Hornbeck P, Raju R, Ahmad R, Szucs M, Mundt F, Forestier D, Jane-Valbuena J, Keshishian H, Gillette MA, Tamayo P, Mesirov JP, Jaffe JD, Carr SA, Mani DR. A Curated Resource for Phosphosite-specific Signature Analysis. Mol Cell Proteomics. 2019 Mar;18(3):576-593. doi: 10.1074/mcp.TIR118.000943. Epub 2018 Dec 18. PMID: 30563849; PMCID: PMC6398202.

18. Hustin, J., and Schaaps, J.-P. (1987). Echocardiograhic and anatomic studies of the maternotrophoblastic border during the first trimester of pregnancy. Am J Obstet Gynecol *157*, 162–168. 10.1016/s0002-9378(87)80371-x.

19. Ye, X. (2020). Uterine Luminal Epithelium as the Transient Gateway for Embryo Implantation. Trends Endocrinol Metabolism *31*, 165–180. 10.1016/j.tem.2019.11.008.

20. Grewal, S., Carver, J.G., Ridley, A.J., and Mardon, H.J. (2008). Implantation of the human embryo requires Rac1-dependent endometrial stromal cell migration. Proc National Acad Sci *105*, 16189–16194. 10.1073/pnas.0806219105.

21. Harada, H., Nakagawa, H., Oyama, K., Takaoka, M., Andl, C.D., Jacobmeier, B., Werder, A. von, Enders, G.H., Opitz, O.G., and Rustgi, A.K. (2003). Telomerase induces immortalization of

human esophageal keratinocytes without p16INK4a inactivation. Mol Cancer Res Mcr *1*, 729–738.

22. Anacker, J., Segerer, S.E., Hagemann, C., Feix, S., Kapp, M., Bausch, R., and Kämmerer, U. (2011). Human decidua and invasive trophoblasts are rich sources of nearly all human matrix metalloproteinases. Mhr Basic Sci Reproductive Medicine *17*, 637–652. 10.1093/molehr/gar033.

23. Chen, A., Liao, S., Cheng, M., Ma, K., Wu, L., Lai, Y., Qiu, X., Yang, J., Xu, J., Hao, S., et al. (2022). Spatiotemporal transcriptomic atlas of mouse organogenesis using DNA nanoball-patterned arrays. Cell *185*, 1777-1792.e21. 10.1016/j.cell.2022.04.003.

24. Ji, J., Chen, L., Zhuang, Y., Han, Y., Tang, W., and Xia, F. (2020). Fibronectin 1 inhibits the apoptosis of human trophoblasts by activating the PI3K/Akt signaling pathway. Int J Mol Med *46*, 1908–1922. 10.3892/ijmm.2020.4735.

25. Ganguly, A., Tamblyn, J.A., Shattock, A., Joseph, A., Larner, D.P., Jenkinson, C., Gupta, J., Gross, S.R., and Hewison, M. (2021). Trophoblast uptake of DBP regulates intracellular actin and promotes matrix invasion. J Endocrinol *249*, 43–55. 10.1530/joe-20-0626.

26. Kipkeew, F., Kirsch, M., Klein, D., Wuelling, M., Winterhager, E., and Gellhaus, A. (2016). CCN1 (CYR61) and CCN3 (NOV) signaling drives human trophoblast cells into senescence and stimulates migration properties. Cell Adhes Migr *10*, 163–178. 10.1080/19336918.2016.1139265.

27. Liu, Y., Fan, X., Wang, R., Lu, X., Dang, Y.-L., Wang, H., Lin, H.-Y., Zhu, C., Ge, H., Cross, J.C., et al. (2018). Single-cell RNA-seq reveals the diversity of trophoblast subtypes and patterns of differentiation in the human placenta. Cell Res *28*, 819–832. 10.1038/s41422-018-0066-y.

28. Wang, Y., Sun, L., Wang, L., Yu, H., Yu, X., and Zou, Y. (2021). PUM1 modulates trophoblast cell proliferation and migration through LRP6. Biochem Cell Biol *99*, 735–740. 10.1139/bcb-2021-0044.

29. West, R.C., Ming, H., Logsdon, D.M., Sun, J., Rajput, S.K., Kile, R.A., Schoolcraft, W.B., Roberts, R.M., Krisher, R.L., Jiang, Z., et al. (2019). Dynamics of trophoblast differentiation in

peri-implantation–stage human embryos. Proc National Acad Sci *116*, 22635–22644. 10.1073/pnas.1911362116.

30. Canfield, J., Arlier, S., Mong, E.F., Lockhart, J., Wye, J.V., Guzeloglu-Kayisli, O., Schatz, F., Magness, R.R., Lockwood, C.J., Tsibris, J.C.M., et al. (2019). Decreased LIN28B in preeclampsia impairs human trophoblast differentiation and migration. Faseb J *33*, 2759–2769. 10.1096/fj.201801163r.

31. Chen, H., Sun, M., Liu, J., Tong, C., and Meng, T. (2015). Silencing of Paternally Expressed Gene 10 Inhibits Trophoblast Proliferation and Invasion. Plos One *10*, e0144845. 10.1371/journal.pone.0144845.

32. Gamage, T.K., Chamley, L.W., and James, J.L. (2016). Stem cell insights into human trophoblast lineage differentiation. Hum Reprod Update *23*, 77–103. 10.1093/humupd/dmw026.

33. Aghajanova, L., Shen, S., Rojas, A.M., Fisher, S.J., Irwin, J.C., and Giudice, L.C. (2012). Comparative Transcriptome Analysis of Human Trophectoderm and Embryonic Stem Cell-Derived Trophoblasts Reveal Key Participants in Early Implantation. Biol Reprod *86*, Article 11, 1-21. 10.1095/biolreprod.111.092775.

34. Arjmand, F., Khanmohammadi, M., Arasteh, S., Mohammadzadeh, A., Kazemnejad, S., and Akhondi, M.-M. (2016). Extended Culture of Encapsulated Human Blastocysts in Alginate Hydrogel Containing Decidualized Endometrial Stromal Cells in the Presence of Melatonin. Mol Biotechnol *58*, 684–694. 10.1007/s12033-016-9968-4.

35. Aberkane, A., Essahib, W., Spits, C., Paepe, C.D., Sermon, K., Adriaenssens, T., Mackens, S., Tournaye, H., Brosens, J.J., and Velde, H.V. de (2018). Expression of adhesion and extracellular matrix genes in human blastocysts upon attachment in a 2D co-culture system. Mhr Basic Sci Reproductive Medicine *24*, 375–387. 10.1093/molehr/gay024.

36. Ruane, P.T., Garner, T., Parsons, L., Babbington, P.A., Wangsaputra, I., Kimber, S.J., Stevens, A., Westwood, M., Brison, D.R., and Aplin, J.D. (2022). Trophectoderm differentiation to invasive syncytiotrophoblast is promoted by endometrial epithelial cells during human embryo implantation. Hum Reprod. 10.1093/humrep/deac008.

37. Keshet, G., and Benvenisty, N. (2021). Large-scale analysis of imprinting in naive human pluripotent stem cells reveals recurrent aberrations and a potential link to FGF signaling. Stem Cell Rep *16*, 2520–2533. 10.1016/j.stemcr.2021.09.002.

38. Guo, G., Meyenn, F. von, Rostovskaya, M., Clarke, J., Dietmann, S., Baker, D., Sahakyan, A., Myers, S., Bertone, P., Reik, W., et al. (2017). Epigenetic resetting of human pluripotency. Development *144*, 2748–2763. 10.1242/dev.146811.

CHAPTER VI: SUMMARY

In this dissertation, we validate the relevance and demonstrate the utility of five contemporary models of peri-implantation stage human trophoblast development. These are the first studies to validate widely available models as they relate to peri-implantation human embryos during extended embryo culture. Additionally, each chapter highlights a novel insight to trophoblast development.

Access to human one-cell zygotes is extremely limited, and mouse embryos share many similarities to humans during cell specification events up to the blastocyst stage. Here, we demonstrated how mouse embryos can be used to interrogate the affect of estradiol supplementation on trophoblast development and implantation in vitro. At the blastocyst stage, human and mouse embryos have remarkably similar localization patterns of estrogen receptor alpha. In the mouse embryo, low levels of estradiol supplementation encourages blastocyst development and development during extended embryo culture. It is likely that if human embryos maintain a conserved mechanism, estradiol supplementation into IVF culture medium may improve blastocyst development.

Human embryos cultured for an extended time in the IVC culture system during peri-implantation is the current gold standard for studying implantation events in vitro. It is almost impossible to validate this model without comparative data from in vivo pregnancies. Because in vivo monitoring of implanting human embryos is impossible, we compared clinical live birth data for patient demographic information with growth in extended culture for embryos from similar demographic parameters. We found that development during extended culture mirrors several live birth trends that we expect to see clinically. Most notably, embryos from advanced maternal age mothers had reduced trophoblast outgrowth areas and epiblast cell number compared to their young counterparts.

We are the only group that has directly compared human peri-implantation trophoblasts to the most commonly used regenerative models, BMP4/A83-01/PD173074 (BAP) -treated

embryonic stem cells and trophoblast stem cells from a first trimester villous column. We showed that each cell the clustered according to their trophoblast subtype across each model. Additionally, we validated the presence of 4 proposed markers of peri-implantation trophoblasts from the BAP model and describe the presence of novel genes *ANLN, FIBCD1, and MAMDC2.*

Finally, we explore the relevance of newly emerging stem cell-derived blastocyst-like structures termed blastoids in modeling human embryos during implantation. At the pre-implantation stage, blastoids contain the three cell lineages found in human embryos (hypoblast, epiblast, and trophectoderm) in similar proportions. During implantation, blastoids are able to self-direct their trophoblast differentiation to stem-cell progenitor cytotrophoblasts and fused, multinucleate syncytiotrophoblasts that secrete human chorionic gonadotropin as the signal for maternal recognition of pregnancy in humans. Remarkably, we found that endometrial stromal cells not only encourage proliferation of trophoblast, but they also encourage differentiation into the syncytiotrophoblast lineage in both human embryos and blastoids. At the transcriptional level, we can see that both embryos and blastoids also begin to direct differentiation towards a migratory trophoblast subtype in the presence of endometrial stromal cells.

Taken together, these data provide a valuable resource for those interested in studying early trophoblast development during peri-implantation. Functional and descriptional comparisons with human embryos are almost impossible for those reliant on federal funding mechanisms. Our studies validate the appropriate use of mouse embryos, regenerative contemporary cell models, and stem cell-derived blastoids as a surrogate for studying human implantation.

APPENDIX

APPENDIX I: EGG CYLINDER DEVELOPMENT DURING IN VITRO EXTENDED EMBRYO CULTURE PREDICTS THE POST TRANSFER DEVELOPMENTAL POTENTIAL OF MOUSE BLASTOCYSTS

This work was published in the Journal of Assisted Reproduction and Genetics April 2020

Introduction

Identifying parameters indicative of a blastocyst's developmental potential is highly desirable for human in vitro fertilization (IVF), agricultural production, and biomedical research. Human IVF requires the selection of the most viable embryo prior to transfer to improve clinical outcomes. Numerous approaches developed to assess embryo viability have had varying degrees of success in clinical application. These include morphological assessment by standard and novel optical methods, preimplantation genetic testing (PGT), morphokinetics, metabolomics, and proteomics profiling of embryo culture media, gene expression in the cumulus cells, and even the oxygen consumption of individual embryos (reviewed in [1–3]). For basic research, additional methods of assessment are available since embryo transfer and pregnancy is not the goal. These include analysis of blastocyst cell number, analysis of inner cell mass (ICM), and trophectoderm (TE) cell allocation, mitochondrial DNA content, mitochondrial activity, levels of reactive oxygen species, and examination of the expression of competence-related genes at the blastocyst stage. Some of these parameters, such as mtDNA, PGT, and blastocyst gene expression, can also be assessed clinically with an embryo biopsy. However, it is generally accepted that current methods for evaluating blastocyst quality for clinical use may not accurately reflect an embryo's likelihood of producing a live birth [1]. Currently, morphological assessment remains the most frequently used method for selection of an embryo for transfer in the clinical setting. In the research setting, embryo transfer is, of course, the most direct and

accurate approach to determine the ability of a blastocyst to implant and give rise to a fetus; however, this method is technically demanding, time consuming, and the results may be confounded with maternal effects. Furthermore, it is not possible to use embryo transfer to examine the developmental potential of a human embryo outside of a clinical treatment cycle. More recently, an extended in vitro embryo culture system has been developed in both mouse and human that supports embryo self-organization and key developmental milestones beyond the blastocyst stage without any maternal communication [4–6]. This system allows us to monitor development during peri- and even post-implantation periods and offers an opportunity to find new parameters that may be useful in predicting embryo developmental potential more accurately. Thus, our aim was to establish parameters during mouse extended embryo culture that accurately predict fetal developmental potential of a blastocyst without the complications of performing ET.

During extended culture in vitro, the distal trophectoderm (TE) of the mouse blastocyst attaches to the bottom of the plate, the blastocoel collapses, and the TE begins to differentiate into trophoblast giant cells. The inner cell mass (ICM) and remaining TE form an emerging egg cylinder with a distinctive cluster of epiblast cells that express the pluripotency marker POU5F1. These epiblast cells become polarized into a rosette structure and upon the formation of a nascent lumen, create the pro-amniotic cavity lined by a cup-shaped layer of columnar epithelial epiblast cells [4, 5]. We hypothesized that an embryo with increased developmental potential would not only attach and form TE outgrowth, but would also form a more organized fetus proper and extra embryonic structures during this peri-implantation period.

Materials and methods

All chemicals were purchased from Sigma-Aldrich (St. Louis, MO) unless otherwise stated.

Animals

All procedures were approved by the Fertility Laboratories of Colorado Ethics in Research Committee and followed animal care and use guidelines, as described by the Guide for the Care and Use of Laboratory Animals [7]. Healthy female outbred mice (CF1; Envigo, Indianapolis, IN) were selected between 4 and 8 weeks of age for superovulation. Mice were kept in 14:10 light:dark group housing for females or individual housing for males (BDF1 strain; Envigo, Indianapolis, IN), and were offered food and water ad libitum.

Blastocyst production

Embryos of varying quality inferred by the duration of their time in vitro were produced. For the in vitro maturation (IVM) group, immature oocytes were collected from mouse ovaries in 3-(N-morpholino)-propanesulfonic acid (MOPS)-buffered medium with 5% (v/v) fetal calf serum (FCS) (Hyclone, Waltham, MA) 48 h post intraperitoneal injection of 5 I.U. pregnant mare serum gonadotropin (PMSG) (Calbiochem, Billerica, MA). Oocytes with even layers of unexpanded cumulus cells were matured in an in-house prepared maturation medium [8] for 18 h in 50 µl drops under mineral oil (OvOil, Vitrolife, Englewood, CO). For the in vitro fertilization (IVF) group, in vivo matured oocytes were collected from the ampulla in MOPS-buffered medium with 5% FCS 18 h post 5 I.U. human chorionic gonadotropin (hCG) (Calbiochem, Billerica, MA) administration and 66 h post PMSG stimulation. All IVM and IVF oocytes were moved to fertilization medium [8] and co-cultured with 1 × 106 spermatozoa/ml collected from a BDF1 male (10 oocytes/50 µl drop) for 6 h. Prospective zygotes with two pronuclei were selected and cultured in a sequential culture system for 84 h (D 3.5) before extended culture or embryo transfer, and embryos were cultured for 115 h (D 5) before fixation for blastocyst cell number. In vitro culture was performed under 37 °C in 6.5% O2 and 7.5% CO2 to compensate for the high altitude of our laboratory (equivalent to 5% O2 and 6% CO2 at sea level) and maintain a pH between 7.2 and 7.3.

For the in vivo produced (VIVO) group, embryonic day (E) 3.5 blastocysts were flushed directly from the uterine horns in MOPS-buffered medium approximately 138 h post PMSG and 90 h post hCG administration/mating. All females were checked for mating plugs 16 h post mating with an intact BDF1 male (> 10 weeks old).

Blastocyst cell number analysis

Hatching or hatched blastocysts from each group were fixed using 4% paraformaldehyde (PFA, Electron Microscopy Sciences, Hatfield, PA) and stained for antibodies against CDX2 (1:200; MU392A-UC, Biogenex, Freemont, CA) for TE and SOX2 (1:200; AN579, Biogenex, Freemont, CA) for ICM, as described previously [9]. Blastocysts were imaged under × 400 magnification on an Olympus BX52 microscope with the Photometrics CoolSnap HQ camera (Fig. 6.1a). Images were analyzed using the hand-count tool on Metamorph Advanced software version 7.7.0.0.

Surgical embryo transfers and analysis

On D 3.5, expanded blastocysts from each treatment group (IVM, IVF, and VIVO) were surgically transferred as previously described [10] to pseudo-pregnant recipient Swiss Webster mice approximately 82 h post coitum. Pseudo-pregnancy was induced by mating females in estrus or proestrus with vasectomized CF1 males (Envigo, Indianapolis, IN) and was confirmed by the identification of a vaginal plug after mating [11]. Following ET, on E 17.5, females were euthanized and the number of fetuses and resorptions were noted. Implantation (sum of resorptions and viable fetuses) and fetal development were assessed, and the fetus and the placenta were weighed. Fetal crown-rump-lengths and placental diameters were measured using a Whitworth digital caliper.

Blastocyst extended culture

Blastocyst extended culture was performed as described earlier [4, 5] with minor modifications. The zona pellucida of E 3.5 expanded blastocysts was removed using acidic Tyrode's solution

and cultured in IVC1 medium (Cell Guidance Systems, Cambridge, UK) in µ-Slide 8 Well chambered coverslips (Ibidi, Martinsried, Germany) coated with 30 µg/cm2 fibronectin. After 72 h, 50% of the IVC1 medium was replaced by the same volume of IVC2 medium (Cell Guidance Systems, Cambridge UK) and embryos were cultured for an additional 48 h until E 8.5. All extended culture was carried out at 37 °C in 7.5% CO2 and atmospheric O2.

Extended culture immunofluorescence staining

Embryos were washed once with sterile PBS and fixed in 4% PFA in PBS for 30 min. Fixed embryos were permeabilized with 0.5% (v/v) Triton X-100 in PBS for 30 min and blocked in blocking buffer containing 10% (v/v) FCS (Hyclone), 3% BSA (MP Biomedicals, Solon, Ohio) and 0.1% Tween 20 (Fisher Scientific, Fair Lawn, NJ) in PBS overnight at 4 °C. Embryos were then stained with a primary antibody against POU5F1 (1:200; Santa Cruz Biotechnology, Dallas, TX) in the blocking buffer overnight in 4 °C. After three washes in 0.1% (v/v) Tween 20 in PBS (PBST), embryos were incubated with secondary antibody Alexa Fluor 488 (1:200; Invitrogen), NucBlue (Hoechst33342, R37605, Life Technologies, Carlsbad, CA) and rhodamine phalloidin (1:200; Cytoskeleton, Denver, CO) in the blocking buffer overnight in 4 °C. Embryos were washed three times in PBST and then coated in ProLong Gold Antifade with DAPI (Life Technologies) before confocal imaging.

3D confocal imaging and analysis

Confocal images were obtained using the 3i Marianas inverted spinning disk confocal microscope at the Advanced Light Microscopy Core Facility at the University of Colorado Anschutz Medical Campus (https://lightmicroscopy.ucdenver.edu/). Egg cylinders were captured in a 3D montage with 0.75 µM Z steps on Slidebook software version 6.0.16 (Fig. 6.1c). The entire outgrowth area was not imaged with confocal microscopy. Egg cylinder volume included any embryonic tissues above a height of approximately 10 µM from the bottom of the well. Each image was deconvoluted using Slidebook before further quantitative and qualitative analysis.

Confocal images were analyzed using Imaris × 64 9.20. Using the surface tool, surfaces were created for F-actin, DAPI, and POU5F1 channels. Total surface volume for both actin and DAPI channels were summed to represent total egg cylinder volume (Fig. 6.1c). The POU5F1 channel surface was specified to identify objects approximately 5–10 μM in diameter within the positively stained surface for a total epiblast cell number (Fig. 6.1c). Egg cylinder morphology was qualitatively noted for each embryo upon visual confirmation of advanced structures including the ectoplacental cone, proamniotic cavity, and the morphological characterization of epiblast cells to a columnar shape surrounding the proamniotic cavity [5].

TE outgrowth area measurement

Before fixation on E 8.5, embryos were imaged using the Olympus DP22 camera on a stereomicroscope. ImageJ2 [12] was used to outline and quantify TE outgrowth area, as indicated in pink in Fig. 6.1c (right panel).

Statistical analysis

Results for ICM/TE cell number, epiblast cell number, egg cylinder volume, outgrowth area, and outgrowth morphologies were analyzed using one-way ANOVA by Graphpad Prism 8.2.0 and significance was noted at $P \leq 0.05$. Statistical significance for surgical embryo transfers was determined using Pearson's chi square analysis and significance was noted at $P \leq 0.05$.

Results and discussion

The amount of time spent in vivo during the preimplantation period directly correl207ates with embryo quality. Poor quality mouse blastocysts were produced from in vitro matured (IVM) oocytes followed by IVF and in vitro culture (IVC), and were defined as the "IVM" group in this study. Intermediate quality blastocysts were produced from in vivo matured oocytes followed by IVF/IVC, defined as the "IVF" group. High quality blastocysts developed in vivo were flushed directly from the uterine horns and defined as the "VIVO" group. At embryonic day (E) 3.5,

embryos from these three experimental groups were morphologically similar (Fig. 6.1b). When fixed to examine ICM and TE cell distribution at E 5, IVM embryos had significantly less ICM and TE cells compared with the other groups, suggesting their compromised developmental potential. IVF embryos had similar numbers of ICM cells but significantly more TE cells compared with the VIVO embryos (Fig. 6.2a).

At E 17.5 after embryo transfer, the IVM group had significantly reduced implantation compared with the VIVO group, and both IVM and IVF groups had significantly reduced fetal development compared with the VIVO group (Fig. 6.2b, left panel). For the embryos that developed into fetuses, the IVM embryos again had reduced fetal length, fetal weight, and placental weight, suggesting that the health of the fetuses resulting from IVM embryos may have also been compromised (Fig. 6.2b, middle and right panels). In humans, low fetal weight for gestational age, often defined as the intrauterine growth restriction, is associated with increased morbidity and mortality [13]. IVF embryos had normal fetal weight, but increased placenta weight (Fig. 6.2b, right panel). The overgrowth of placenta is a phenomenon that was observed in maternally aged mice and has been associated with developmental abnormalities [14]. It may be also correlated with the higher number of TE cells found in the IVF blastocysts. These results confirmed that mouse blastocysts from IVM, IVF, and VIVO groups had distinct implantation and fetal developmental potential, which cannot be accurately predicted by morphology alone. We then used the same model to study parameters during extended embryo culture that could be indicative of blastocyst developmental potential.

Embryos at E 3.5 from each group were placed into extended culture until E 8.5. The surface area covered by TE was obtained and defined as the outgrowth area (Fig. 6.1c) [15]. Embryos from the IVM and IVF groups had significantly smaller outgrowth area compared with those from the VIVO group (Fig. 6.2c, left panel). When we examined the average epiblast cell number, again, VIVO embryos had significantly more epiblast cells (Fig. 6.2c right panel). More

interestingly, the proportional differences in epiblast cell number are strikingly similar to fetal development following embryo transfer, suggesting that this parameter may be indicative of the potential of an embryo to successfully develop into a fetus (Fig. 6.2b, left panel). The measurement of other advanced morphological structures (egg cylinder volume, formation of proamniotic cavity, ectoplacental cone, and epiblast cell polarization) also suggested that VIVO embryos had higher developmental potential than both IVM and IVF embryos (Fig. 6.2c, d, Fig. 6.3), although the proportional differences do not closely approximate fetal development.

Obviously, extended embryo culture cannot be used in clinical assisted reproductive technology (ART) to predict implantation and fetal developmental potential prior to transfer to produce a pregnancy. However, this technique can still prove quite valuable for research assessment of human embryos and improvement of ART methodology. Either abnormally fertilized 3PN zygotes that would normally be discarded, or blastocysts donated for research, could be cultured in novel media or culture environments prior to extended embryo culture. Currently, after treatment, such embryos would be assessed morphologically and possibly for cell number and allocation or gene expression, as a means to decipher the effectiveness of the novel culture method. Using extended embryo culture, these embryos can be evaluated in a manner that accurately predicts embryo quality. Thus, decisions about new culture medium, supplements, or devices can be based on outcomes known to correlate with post transfer success. These new treatments can then be applied in clinical trials with a higher degree of confidence, less risk, and a better chance of success, leading to faster implementation of innovative culture techniques for human embryos and better clinical outcomes for ART patients.

Ethical approval

All procedures were approved by the Fertility Laboratories of Colorado Ethics in Research Committee and followed animal care and use guidelines, as described by the Guide for the Care and Use of Laboratory Animals.

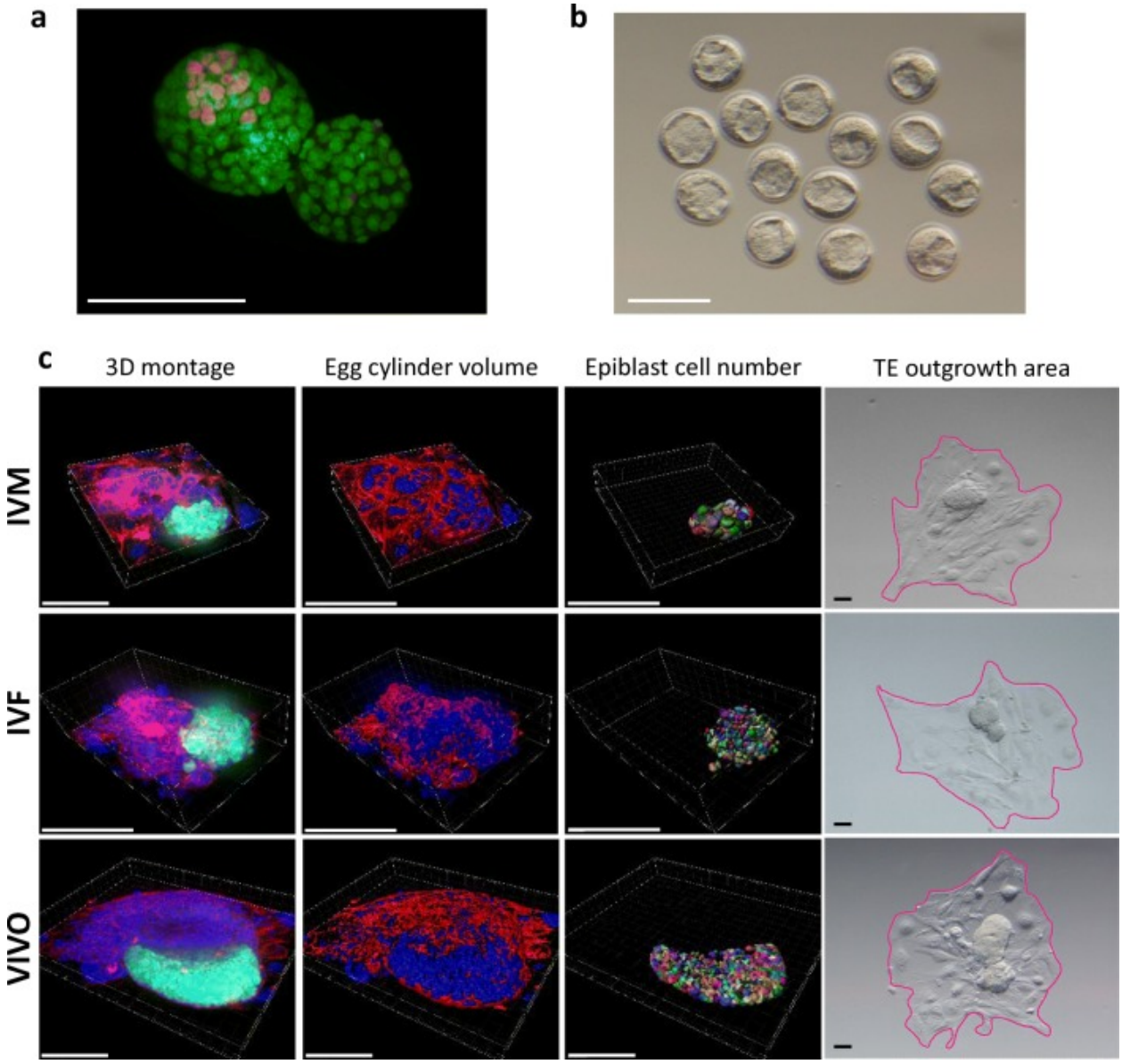

Figure 6.1. A) A representative immunofluorescence image of blastocyst cell number and allocation. Embryos were stained with SOX2 (red) for ICM and CDX2 (green) for TE. Scale bar, 100 μM. B) A representative image of E 3.5 expanded embryos of similar quality prior to zona removal and embryo extended culture. Scale bar, 100 μM. C) Representative 3D confocal images, images for egg cylinder volume analyses, epiblast cell number analysis, and TE outgrowth area for IVM (top row), IVF (center row), and VIVO (bottom row) embryos. Embryos were stained with DAPI for nuclei (blue), rhodamine phalloidin for F-actin (red), and antibody against POU5F1 (green). Scale bars, 100 μM

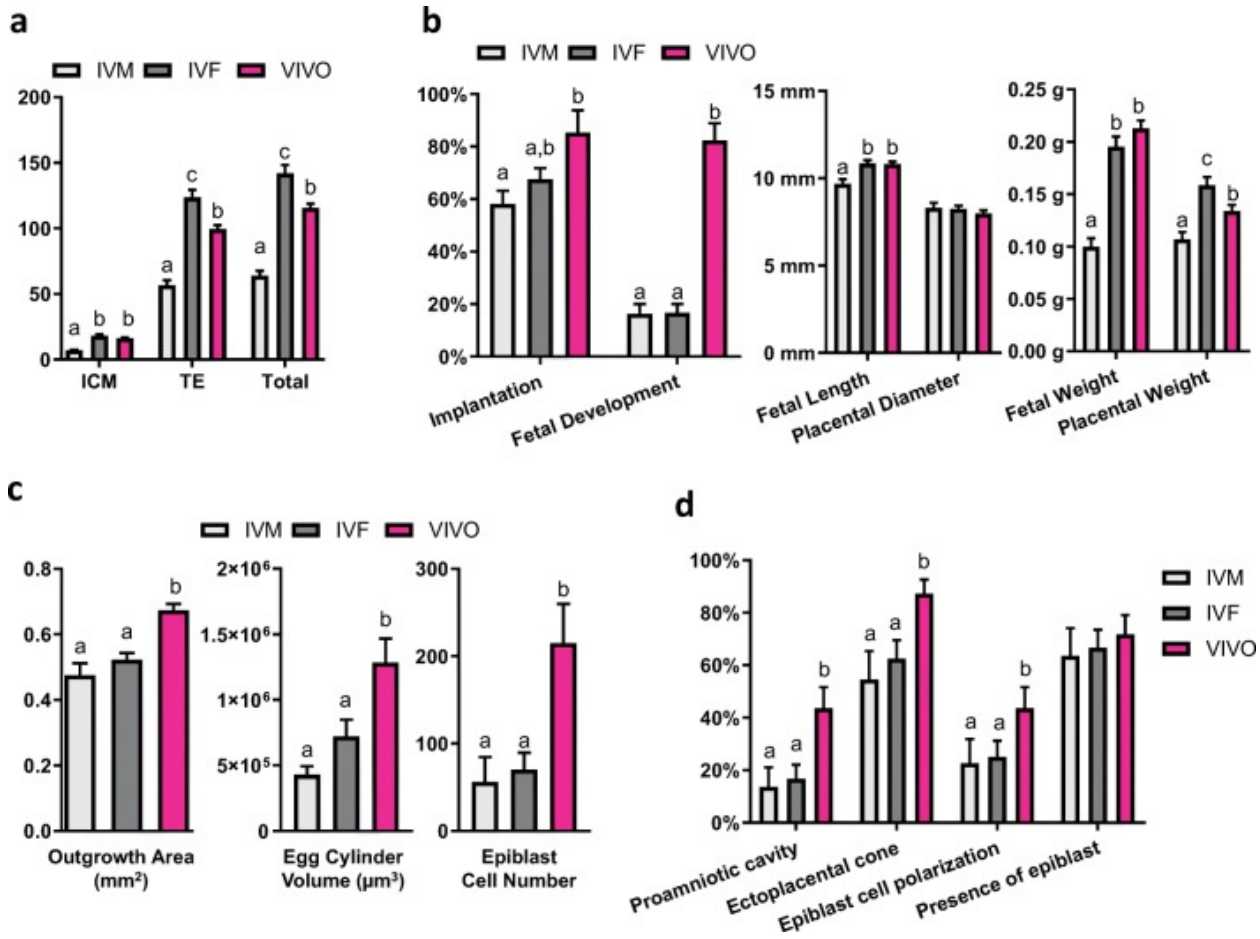

Figure 6.2. A) ICM, TE, and total cell number in hatching or hatched blastocysts produced from in vitro matured oocytes (IVM) and in vivo matured oocytes (IVF) after 115 h in culture, and in vivo flushed blastocysts (VIVO) at E 4. This experiment was replicated three times with 116 embryos. B) Implantation and fetal development after surgical embryo transfer (left), fetal and placental length and diameter, respectively (center), and fetal and placental weights for IVM, IVF, and VIVO fetuses. A total of 279 embryos and 31 recipient animals were used. C) Outgrowth areas (left), egg cylinder volume (center), epiblast cell number (right), and D) incidences of proamniotic cavity, ectoplacental cone formation, epiblast cell polarization, and presence of epiblast cells in IVM, IVF, and VIVO embryos during in vitro extended culture. Experiments in c and d were replicated three times with 109 embryos. Different letters (a, b, and c) indicate significant different ($P < 0.05$) value between treatment groups.

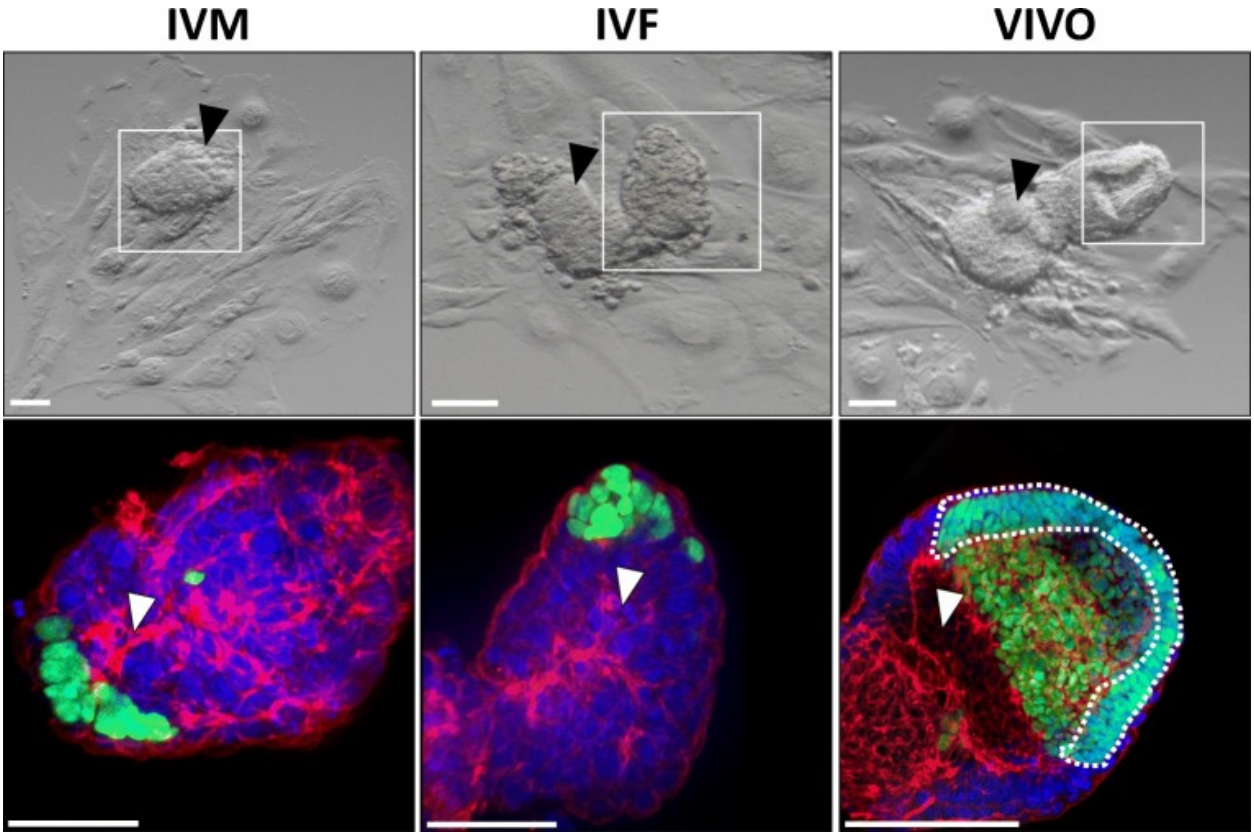

Figure 6.3. Representative morphological (top) and confocal immunofluorescence (bottom) images for IVM (left), IVF (center), and VIVO (right) embryos. The white box on top panels delineates the area of the confocal image below. Black arrows indicate an emerging ectoplacental cone. White arrows indicate formation of a proamniotic cavity. The dashed white line in bottom right image indicates polarized epiblast cells. Embryos were stained with DAPI for nuclei (blue), rhodamine phalloidin for F-actin (red), and antibody against POU5F1 (green), and the maximum intensity projection of the 3D montage images are presented. Scale bars, 100 μM Our results demonstrate that extended embryo culture provides more accurate information regarding developmental potential than blastocyst morphological assessment. Specifically, epiblast cell number is valuable in predicting fetal developmental potential. Outgrowth area, formation of the proamniotic cavity, ectoplacental cone, and epiblast cell polarization may also provide valuable information about embryo quality, although they are not as predictive of fetal developmental potential as is epiblast cell number. Both the presence of an organized egg cylinder with a proliferative epiblast cell population in conjunction with a proliferative TE during extended embryo culture reflects blastocyst viability. Thus, extended embryo culture offers a means to sensitively and accurately measure embryo viability without the use of embryo transfer.

REFERENCES

1. Sallam HN, Sallam NH, Sallam SH. Non-invasive methods for embryo selection. Facts Views Vis Obgyn. 2016;8:87–100.

2. Gardner DK, Meseguer M, Rubio C, Treff NR. Diagnosis of human preimplantation embryo viability. Hum Reprod Update. 2015;21: 727–47.

3. Sanchez T, Seidler EA, Gardner DK, Needleman D, Sakkas D. Will noninvasive methods surpass invasive for assessing gametes and embryos? Fertil Steril. 2017;108:730–7.

4. Bedzhov I, Leung CY, Bialecka M, Zernicka-Goetz M. In vitro culture of mouse blastocysts beyond the implantation stages. Nat Protoc. 2014;9:2732–9.

5. Bedzhov I, Zernicka-Goetz M. Self-organizing properties of mouse pluripotent cells initiate morphogenesis upon implantation. Cell. 2014;156:1032–44.

6. Shahbazi MN, Jedrusik A, Vuoristo S, Recher G, Hupalowska A, Bolton V, et al. Self-organization of the human embryo in the absence of maternal tissues. Nat Cell Biol. 2016:1–8.

7. National Research Council (US) Committee for the update of the guide for the care and use of laboratory animals. In: guide for the care and use of laboratory animals. Washington (DC): National Academies Press (US) National Academy of Sciences. 2011.

8. Herrick JR, Strauss KJ, Schneiderman A, Rawlins M, Stevens J, Schoolcraft WB, et al. The beneficial effects of reduced magnesium during the oocyte-to-embryo transition are conserved in mice, domestic cats, and humans. Reprod Fertil Dev. 2015;27:323–31.

9. Bakhtari A, Ross PJ. DPPA3 prevents cytosine hydroxymethylation of the maternal pronucleus and is required for normal development in bovine embryos. Epigenetics. 2014;9:1271–9.

10. Nagy A, Gertsenstein M, Vintersten K, Behringer R. Manipulating the mouse embryo: a laboratory manual. 3rd ed. Cold Spring Harbor (NY): Cold Spring Harbor Laboratory Press; 2003.

11. Byers SL, Wiles MV, Dunn SL, Taft RA. Mouse estrous cycle identification tool and images. PLoS One 2012; 7:9.

12. Schindelin J, Arganda-Carreras I, Frise E, Kaynig V, Longair M, Pietzsch T, et al. Fiji: an open source platform for biological-image analysis. Nat Methods. 2012;9:676–82.
13. Garite TJ, Clark R, Thorp JA. Intrauterine growth restriction increases morbidity and mortality among premature neonates. Am J Obstet Gynecol. 2004;191:481–7.
14. Paczkowski M, Schoolcraft WB, Krisher RL. Dysregulation of methylation and expression of imprinted genes in oocytes and reproductive tissues in mice of advanced maternal age. J Assist Reprod Genet. 2015;32:713–23.
15. Hannan NJ, Paiva P, Meehan KL, Rombauts LJ, Gardner DK, Salamonsen LA. Analysis of fertility-related soluble mediators in human uterine fluid identifies VEGF as a key regulator of embryo implantation. Endocrinology. 2011;152:4948–56.

APPENDIX II: FATTY ACIDS PRESENT IN COMMERCIAL ALBUMIN PREPARATIONS DIFFERENTIALLY AFFECT DEVELOPMENT OF MURINE EMBRYOS BEFORE AND DURING IMPLANTATION

This work was published in the journal F & S Science in February 2021

Summary

Objective:To characterize fatty acid (FA) profile of commercially available albumin products and determine their effect on embryonic development.

Design:Research study.

Setting:Private research facility.

Animal(s): Outbred mice aged 4–8 weeks.

Intervention(s): Gas chromatography-mass spectrometry was used to quantify the FA content of 15 commercial albumins. Embryos were produced in media containing different albumin products, with or without carnitine or exogenous FA supplementation, to determine their effect on embryo development in vitro.

Main Outcome Measure(s): Total micrograms of FA per milligram of albumin for the 15 albumin products, blastocyst development, cell number, allocation to the trophectoderm (TE) or inner cell mass (ICM), and evaluation of morphology during implantation.

Result(s): The albumin products contained 0.07–16.77 μg total FA/mg albumin. Compared to media with with >1.4 μg FA/mg albumin, media with <0.5 μg FA/mg albumin supported improved blastocyst development, and addition of carnitine mitigated this difference. Addition of palmitoleic acid or oleic acid individually did not improve blastocyst development and decreased ICM:TE ratio. However, in the presence of carnitine, there was improved blastocyst development and maintenance of the ICM:TE ratio. Embryos cultured in Vitrolife human serum

albumin with supplementation of carnitine, palmitoleic acid, and oleic acid were more likely to develop cells positive for POU5F1 in an extended embryo culture than embryos cultured in Origio serum protein substitute.

Conclusion(s): Commercial albumin products contain FAs, which vary in abundance. These FAs have different effects on embryo development and quality before and during the implantation stage. Several of these albumin preparations are routinely used for human-assisted reproductive technologies; therefore, serious consideration is warranted when selecting a product for clinical use.

Key Words: Albumin, blastocyst, culture medium, epiblast, fatty acid

Introduction

Media for in vitro culture (IVC) of embryos contain a balance of carbohydrates, amino acids, vitamins, antibiotics, and macromolecules. An improper balance of these nutrients, among a myriad of other culture system components, may lead to cellular fragmentation, developmental delay or arrest, and embryonic death (1, 2). Although most of the components of culture media are present in specific, empirically derived concentrations, macromolecules, including blood-derived albumin and other serum proteins, are complex molecules that often contain a significant number of unspecified biologically active compounds (3, 4, 5, 6, 7). Today, many human-assisted reproductive technology clinics use commercial fractionated human serum albumin (HSA) products to support embryo growth (5, 8). Yet, despite improvements in culture conditions over the past decade, the percentage of live births per in vitro fertilization cycle is approximately 24% in the United States (9). Further refinement of culture conditions, including quantifying and controlling types and concentrations of contaminants in commercially available albumin preparations, will ultimately lead to real advances in embryo culture efficiency and improved clinical outcomes.

Albumin supports embryo growth by buffering pH, stabilizing the cell membrane, acting as a surfactant, scavenging for heavy metals, providing amino acids as a nutrient source, and carrying a variety of elements and compounds necessary for survival (amino acids, vitamins, fatty acids [FAs], hormones, growth factors, and others) of the cell (8, 10). Numerous studies have highlighted the variability in albumin products with respect to their associated amino acids, organic acids, transferrin, and elements that interact with the albumin molecule (3, 4, 5, 6, 11). However, to date, none have examined the specific FA content of various albumin products. FAs are known to affect embryo growth and survival. Supplementation of an embryo culture medium with 100 μM palmitic acid affects gene expression and metabolism in embryos and has a detrimental effect on embryonic development in mice (12). Furthermore, supplementation of a culture medium with palmitic acid alters epigenetic landscape of bovine embryos (13, 14), and combinations of palmitic, stearic, and oleic acids increase apoptosis and decrease cell numbers in bovine blastocysts in vitro (15, 16). Thus, it is imperative to define and study FAs introduced into a microenvironment containing albumin. In this study, our objective was to elucidate various types and quantities of long-chain FAs present in different commercial albumin sources. We hypothesized that differences in the types and concentrations of attached FAs differentially affects embryo development and that carnitine supplementation influences these developmental effects. Finally, we investigated whether supplementation of an embryo culture medium with specific FAs impacts embryo development before and during implantation in mice.

Materials and methods

All products were purchased from Sigma Aldrich (St. Louis, MO) unless otherwise stated.

Albumin sources

Fifteen albumin products were purchased from 8 different suppliers, including 7 bovine serum albumins (BSAs) (Sigma Fraction V [FrV] BSA, Albumax, knockout serum replacement [KOSR], Sigma fatty acid-free [FAF] BSA, Millipore Probumin, MP Biomedical FAF BSA, and MP

Biomedical FrV BSA), 3 recombinant human albumins (Albumin Biosciences Albagen, Novozymes AlbIX, and Vitrolife G-MM), and 5 HSAs (Origio serum protein substitute [SPS], Origio HSA, Sigma FAF HSA, Sigma FrV HSA, and Vitrolife HSA), and analyzed.

Table 6.1 Product information for fifteen commercial albumin products analyzed for their fatty acid profile, including name of the product, supplier, protein source, and catalog number. FAF=fatty acid free, FrV= fraction V, BSA= bovine serum albumin, HSA= human serum albumin.

Sample	Supplier	Source	Catalog #
MP Bio FrV BSA	MP Bio	Bovine Serum	180542
Albumax (lipid rich)	ThermoFisher	Bovine Serum	11020021
Sigma FrV BSA	Sigma	Bovine Serum	A7511
KOSR (lipid rich)	ThermoFisher	Bovine Serum	10828010
Sigma FrV HSA	Sigma	Human Serum	A1653
Origio HSA	Origio	Human Serum	ART-3001
Albagen	Albumin Bio	Recombinant Human	1001
SPS	Origio	Human Serum	ART-3011
GMM	Vitrolife	Recombinant Human	10038
AlbIX	Albumedix	Recombinant Human	205-005
Vitrolife HSA	Vitrolife	Human Serum	10064
Sigma FAF BSA	Sigma	Bovine Serum	A7511
MP Bio FAF BSA	MP Bio	Bovine Serum	219989980
Sigma FAF HSA	Sigma	Human Serum	A3782
Millipore Probumin	Millipore	Bovine Serum	820473

Analysis of FA composition

Samples (50–100 mg) from each albumin source (liquid or lyophilized powder) were blinded and sent to Colorado State University Analytical Resources Core - Bioanalysis and Omics (https://www.research.colostate.edu/pmf/) for quantitative analysis of the FA content by gas chromatography-mass spectrometry. FAs were extracted using the Folch method with modifications (17). Briefly, solid albumin samples (approximately 30 mg) were first mixed with

350 µL of water, which together with liquid albumin samples (350 µL) were acidified with 20 µL of concentrated HCl and then extracted with 6 mL of chloroform-methanol (2:1 by volume) containing 10 µg of nonadecanoic acid as an internal standard. Then, 1.15 mL of 0.88% (wt%) KCl in water was added to induce phase separation. The mixture was centrifuged at 3,000 × *g* for 10 minutes. Chloroform extract was recovered from the lower phase, and the solvent was removed using nitrogen. To the dried extracts, 50 µL of toluene and 200 µL of 3 M methanolic HCl were added, and the samples were incubated at 60°C for 2 hours. After derivatization, the sample was cooled to an ambient temperature, added to 500 µL of hexane and 700 µL of water, vortexed for 1 minute, and centrifuged at 3,000 × *g* for 1 minute. The hexane layer on the top was recovered and reconstituted in 70 µL of hexane. Calibration curves were prepared based on a series of dilutions of authentic standards of FAs in methanol before derivatization. The extracted samples were injected onto a Thermo Trace 1310 gas chromatograph coupled to an ISQ-LT mass spectrometer (Thermo Fisher, Waltham, MA). Fatty acid methyl ester separation was achieved on a DB-WAXUI column (J&W, Agilent, Santa Clara, CA) (30 m × 0.25 mm, 0.25-µm film thickness). The injector was held at 250°C and a 10:1 split ratio. The oven temperature was held at 180°C for 0.5 minutes, ramped to 250°C at 10°C per minute, and held for 6 minutes. The mass detector was operated in a full-scan mode (50–650 m/z, 5 scans per second) with electron impact ionization. The mass spectrometer transfer line and ion source temperature were kept at 250°C. The quantities reported are averages for all replicates (n = 2–10) of each albumin product. Lot-to-lot variation was not analyzed because of the number of albumin products tested and overall costs of processing.

Animals

All protocols followed animal care and use guidelines as described by the Guide for the Care and Use of Laboratory Animals (18) and were approved by the fertility laboratories of Colorado Ethics in Research Committee. Healthy outbred female mice (Swiss Websters for comparison 1 and CF1 for all other experiments; Envigo, Indianapolis, IN) between 4 and 8 weeks of age were

selected for superovulation. The mice were kept in a 14:10 ratio of light-dark hour cycle (group housing for females and individual housing for males [B6D2F1, 3–4 months of age; Envigo]) and provided with food and water ad libitum.

Blastocyst production and assessment of development

Injections of pregnant mare serum gonadotropin (Calbiochem, Billerica, MA) (5 IU, intraperitoneal) were given to the female mice, followed by human chorionic gonadotropin (Calbiochem) (5 IU, intraperitoneal) 48 hours later to induce ovulation. Approximately 17 hours after the human chorionic gonadotropin injection, the mice were euthanized and immediately dissected to isolate in vivo matured cumulus oocyte complexes (COCs) from the ampullae of the oviducts. All COCs were collected into a 3-(N-morpholino)-propanesulfonic acid-buffered medium prepared in house, supplemented with 5% (vol/vol) fetal calf serum (Hyclone, Waltham, MA) at 37°C.

Fresh spermatozoa were collected from the caudae epididymides and vasa deferentia of the male BDF1 mice and capacitated for 1 hour in 1 mL of an optimized fertilization medium (19). After capacitation, the spermatozoa were diluted in the optimized fertilization medium and allocated into 50-μL culture drops in 8 mL of mineral oil (OvOil; Vitrolife, Englewood, CO). The spermatozoa (1 × 106 spermatozoa/mL) and COCs (1 COC mass per drop) were cocultured for 6 hours.

After 6 hours of coincubation with the spermatozoa, zygotes with 2 visible pronuclei (PN) were cultured in groups of 10 in 20-μL drops of optimized embryo culture medium 1 (2.5 mg albumin/mL culture medium), the first step of a 2-step sequential culture system (19), in mineral oil. At approximately 22–24 hours after insemination, the embryos were evaluated for cleavage to reach the 2-cell stage. Uncleaved zygotes and degenerate embryos were removed from the culture drops at this time. After 48 hours of culture, the embryos were moved to 20-μL drops of

optimized embryo culture medium 2 (2.5 mg albumin/mL culture media) in mineral oil (19). After 96 hours (day 4) and 114 hours (day 5) of the culture, the embryos were evaluated for blastocyst development and classified as morula, early blastocyst, blastocyst, hatching blastocyst, fully hatched blastocyst, or nondeveloped. The oocytes, embryos, and spermatozoa were incubated in the presence of 6.5% O2 and 7.5% CO2 to account for the elevation of our laboratory (equal to 5% O2 and 6% CO2 at sea level) and maintain the media's pH between 7.2 and 7.3.

Analysis of blastocyst cell number

After 114 hours in culture, the hatching and hatched blastocysts were fixed with 4% paraformaldehyde (PFA) (Electron Microscopy Sciences, Hatfield, PA) in phosphate-buffered saline and imaged with immunofluorescence as previously described (20). Antibodies against SOX2 (1:200; rabbit polyclonal, AN833; BioGenex, Fremont, CA) were used to identify the inner cell mass (ICM), and antibodies against CDX2 (1:200; mouse monoclonal, MU392A-UC; BioGenex) were used to identify the trophectoderm (TE). Secondary antibodies Alexafluor 488 (1:200; donkey anti-rabbit IgG, A-21206; Invitrogen, Carlsbad, CA) and Alexafluor 555 (1:200; goat anti-mouse IgG, A-21424; Invitrogen) were used to identify the primary antibodies for ICM and TE, respectively. Differential staining was imaged using an Olympus BX52 (Olympus, Melville, NY) microscope with ultraviolet illumination filters for each secondary antibody. Images were captured using a Photometrics CoolSnap HQ camera (Photometrics, Tucson, AZ), and individual cells were counted using the hand-count tool of the MetaMorph Advanced software, version 7.7.0.0 (MetaMorph, Nashville, TN).

Blastocyst extended culture and analysis

Extended culture of the mouse blastocysts till embryonic day-8.5 was performed as previously described (21, 22, 23), with minor modifications. Day-3.5 blastocysts (84 hours in culture with 5 mg albumin/mL of the culture medium) with a fully expanded blastocoel without any evidence of

hatching from the zona pellucida (ZP) were briefly exposed to acidic Tyrode solution for ZP removal and cultured in IVC-1 medium (Cell Guidance Systems, Cambridge, United Kingdom). All the embryos were cultured on optical-grade µ-Slide 8-well chambered coverslips (Ibidi, Martinsried, Germany) coated with 30 µg/cm2 of fibronectin from human plasma. One half of the 300-µL well volume was exchanged with IVC-2 (Cell Guidance Systems) after 72 hours in culture, and the embryos were left to grow for an additional 48 hours before fixation. All the extended cultures were performed in the presence of atmospheric oxygen and 7.5% CO2 at 37°C. The extended-culture embryos were imaged using an Olympus DP22 camera (Olympus) on a stereomicroscope before fixation in 4% PFA. Images were imported to ImageJ2 software (24), and embryo outgrowth areas were outlined at the outer edge of TE using the freehand selection tool and quantified.

Immunofluorescent staining of the extended-culture embryos was performed as described previously (23). After fixation in 4% PFA in phosphate-buffered saline, the embryos were treated with primary antibodies against POU5F1 (1:200; sc-5279, Santa Cruz Biotechnology, Dallas, TX) and secondary antibody Alexa Fluor 488 (1:200; donkey anti-mouse IgG A-21202, Invitrogen) for identification of epiblast cells, NucBlue (Hoechst 33342, R37605; Life Technologies, Carlsbad, CA) for identification of cell nuclei, and rhodamine phalloidin (1:200; PHDR1; Cytoskeleton, Denver, CO) for visualization of F-actin.

The imaging was performed in the Advanced Light Microscopy Core Facility, which is a part of the NeuroTechnology Center at the University of Colorado Anschutz Medical Campus. The content is the authors' sole responsibility and does not necessarily represent official views of the National Institutes of Health. Images of egg cylinders were obtained using a 3i Marianas (3i, Denver, CO) inverted spinning-disk confocal microscope. Egg cylinders (0.75 µM) with positive expression of POU5F1 were captured in a 3-dimensional montage using Z steps in Slidebook 6.0.16 software (3i). Confocal 3-dimensional images were captured using Imaris x64 9.20, and

using the surface tool, a surface was created for POU5F1. Algorithm preferences were adjusted so that objects of approximately 5–10 μM diameter would be counted as individual nuclei. The total number of objects calculated on the POU5F1 surface was used as the number of epiblast cells for the analysis. Visual identification of advanced morphological structures was performed as previously described (23).

Statistical analysis

Statistical analyses of embryonic development, cell number, outgrowth area, epiblast cell number, and development of the advanced morphological structures in the extended culture were performed using a 1-way analysis of variance with Bonferroni multiple comparison correction. All the analyses were completed using NCSS software (NCSS, Kaysville, UT) (25). Significance was noted at $P \leq .05$.

Results

Individual and total FA compositions

In a blind screening analysis, the total FA concentration and weight percentage of individual FAs were evaluated. The long-chain FAs present were palmitic acid (16:0), stearic acid (18:0), oleic acid (18:1), linoleic acid (18:2), alpha-linolenic acid (18:3), palmitoleic acid (16:1), myristic acid (14:0), and magaric acid (17:0). The total average FA concentration ranged from 0.07 μg/mg albumin (Millipore Probumin) to as high as 16.77 μg/mg albumin (MP Bio FrV BSA) (Fig. 7.1A). Sources that contained a high concentration of total FAs tended to contain higher fractions of palmitic acid, stearic acid, oleic acid, linoleic acid, and alpha-linolenic acid (Table 6.2).

Table 6.2 Long chain fatty acid profiles for different commercial albumin products. Albumin products are listed in descending order by total fatty acid content. Fatty acid concentrations are given in μg fatty acid per mg albumin. ND= non-detected.

Sample	Palmitic acid	Stearic acid	Oleic acid	Linoleic acid	alpha-Linolenic acid	Palmitoleic acid	Myristic acid	Margaric acid
MP Bio								
FrV BSA	3.105	3.684	3.333	3.895	2.111	0.291	0.162	0.195
Albumax	1.690	2.104	2.044	0.976	0.606	0.153	0.112	0.104
Sigma								
FrV BSA	1.212	1.132	1.286	1.186	0.809	0.227	0.103	0.129
KOSR	1.261	1.262	1.494	0.537	0.367	0.148	0.108	0.074
Sigma								
FrV HSA	1.263	0.269	1.195	1.891	0.067	0.164	0.099	0.012
Origio								
HSA	0.758	0.193	0.871	0.764	0.043	0.074	0.043	0.006
Albagen	0.318	0.086	0.730	0.626	0.160	0.165	0.019	0.018
SPS	0.552	0.169	0.305	0.334	0.009	0.017	0.017	ND
GMM	0.073	0.009	0.041	ND	ND	0.320	0.035	ND
AlbIX	0.074	0.016	0.080	0.003	0.002	0.320	0.021	0.005
Vitrolife								
HSA	0.120	0.031	0.058	0.085	0.003	0.004	0.007	0.002
Sigma								
FAF BSA	0.055	0.026	0.048	0.015	0.009	0.003	0.001	0.004
MP Bio								
FAF BSA	0.042	0.038	0.035	ND	ND	ND	0.017	0.008
Sigma								
FAF HSA	0.029	0.020	0.016	0.006	0.001	0.001	0.007	0.004
Millipore								
Probumin	0.022	0.008	0.005	0.029	ND	ND	0.003	0.002

Note: Albumin products are listed in descending order of total FA content. FA concentrations are given in micrograms of FA per milligram of albumin. BSA = bovine serum albumin; FA = fatty acid; FAF = fatty acid-free; FrV = fraction V; GMM = Vitrolife G-MM; HSA = human serum

albumin; KOSR = knockout serum replacement; MP Bio= MP Biomedicals; ND = not detected; SPS = serum protein substitute.

Effect of different albumin products on blastocyst development

In comparison 1, fertilized zygotes with 2 PN were cultured till the blastocyst stage in Sigma FAF HSA (n = 56), AlbIX (n = 57), SPS (n = 55), or Sigma FrV HSA (n = 56). The total FA concentrations in Sigma FAF HSA, AlbIX, SPS, and Sigma FrV HSA were 0.16 µg/mg albumin, 0.47 µg/mg albumin, 1.40 µg/mg albumin, and 4.96 µg/mg albumin, respectively (Fig. 7.1A). The proportion of embryos that began to hatch from ZP on day 4 was significantly higher when they were cultured in AlbIX (<0.50 µg/mg albumin) compared to when they were cultured in SPS or Sigma FrV HSA (>0.50 µg/mg albumin) (Fig. 7.1B). The proportion of embryos that began to hatch from ZP on day 4 was also higher when they were cultured in Sigma FAF HSA (<0.50 µg/mg albumin) compared to when they were cultured in Sigma FrV HSA (>0.50 µg/mg albumin) (Fig. 7.1B). The proportion of embryos that developed until the blastocyst stage on day 4 tended to be higher when they were cultured in AlbIX compared to when they were cultured in SPS or Sigma FrV HSA (*P* = .07) (Fig. 7.1B).

For comparison 2, embryo development data collected in our laboratory over 2 years using different albumin products were pooled. Fertilized zygotes with 2 PN were cultured till the blastocyst stage in Millipore Probumin (n = 314, 7 biologic replicates), Vitrolife HSA (VLHSA) (n = 147, 4 biologic replicates), AlbIX (n = 867, 8 biologic replicates), or Albagen (n = 133, 4 biologic replicates). The total FA concentrations in Millipore Probumin, VLHSA, AlbIX, and Albagen were 0.07 µg/mg albumin, 0.32 µg/mg albumin, 0.47 µg/mg albumin, and 2.15 µg/mg albumin, respectively (Fig. 7.1A). The proportion of embryos that were hatching from ZP on day 5 was significantly lower when they were cultured in Albagen (2.15 µg/mg albumin) than when they were cultured in AlbIX or VLHSA (both <0.5 µg/mg albumin; *P*<.001) (Fig. 7.1C). The proportion of embryos that developed till the blastocyst stage on day 4 tended to be lower when

they were cultured in Millipore Probumin than when they were cultured in AlbIX (P = .053) (Fig. 7.1C).

Effect of carnitine on blastocyst development

To examine the effect of carnitine with albumins of differing FA content, the embryo development data collected in our laboratory over 2 years were pooled again. Zygotes with 2 PN were cultured till the blastocyst stage in 2 recombinant human albumin products with different levels of FA contaminants: AlbIX (0.32 μg FA/mg albumin, n = 61, 3 biologic replicates) or Albagen (2.15 μg FA/mg albumin, n = 130, 4 biologic replicates), with and without the addition of carnitine (1 mM; AlbIX + carnitine, n = 74, 3 biologic replicates; Albagen + carnitine, n = 73, 3 biologic replicates). Carnitine significantly increased the proportion of embryos that developed till the blastocyst stage on day 4 when they were cultured in only Albagen (P<.001) (Fig. 7.1D). The addition of carnitine also increased the proportion of hatching blastocysts on day 5 when the embryos were cultured in only Albagen (P<.001) (Fig. 7.1D). The proportion of embryos that reached the blastocyst stage on day 4 or began hatching on day 4 or 5 was significantly lower when they were cultured in Albagen compared to when they were cultured in either AlbIX or AlbIX + carnitine (Fig. 7.1D).

Effect of palmitoleic acid, oleic acid, and carnitine on embryo development and quality before implantation

The embryos developed successfully with AlbIX supplementation, and this protein supplement was regularly used in our mouse embryo research. As described, the AlbIX supplementation involved the addition of 0.8 μg/mL of palmitoleic acid and 0.2 μg/mL of oleic acid to the embryo culture medium. To approximate the FA composition of AlbIX (Table 6.1), we supplemented VLHSA, which contains low levels of FAs (0.32 μg/mg albumin) (Table 6.1) and is FDA-approved for use in human embryo culture, with oleic acid (VLHSA + O, 0.3 μg/mL, n = 156) or palmitoleic acid (VLHSA + P, 0.75 μg/mL, n = 154). We also cultured embryos in VLHSA with

carnitine (VLHSA + C, 1 mM, n = 62); without carnitine (VLHSA, n = 147); or with a combination of carnitine (1 mM), oleic acid (0.3 μg/mL), and palmitoleic acid (0.75 μg/mL) (VLHSA + COP, n = 73). There were no differences in embryonic development before implantation between the embryos cultured in VLHSA, VLHSA + O, and VLHSA + P. However, the addition of carnitine, with or without oleic and palmitoleic acids (VLHSA + C, VLHSA + COP), improved blastocyst development on day 4 (P<.001) (Fig. 7.2A). Carnitine alone improved day-4 blastocyst hatching compared with VLHSA alone, and VLHSA + COP improved day-5 blastocyst hatching compared with VLHSA alone or VLHSA with oleic acid or palmitoleic acid (P<.001) (Fig. 7.2A). The addition of carnitine alone to VLHSA decreased the total blastocyst cell number compared with VLHSA + P (P<.001) (Fig. 7.2B), and the addition of oleic acid or carnitine to VLHSA significantly reduced the number of ICM cells (P<.001) (Fig. 7.2B) compared with VLHSA alone. Although VLHSA + P did increase the total cell number, this resulted in a decreased ICM:TE ratio (P<.001) (Fig. 7.2C). VLHSA + O and VLHSA + C also decreased the ICM:TE ratio compared with VLHSA (P<.001) (Fig. 7.2C). VLHSA + COP was the only treatment that maintained the ICM:TE ratio similar to that maintained by the control (VLHSA).

Effect of different albumins on embryonic development during implantation

We used an extended embryo culture system to model the implantation and fetal developmental potential of embryos (22) following culture till day 3.5 in several common albumin supplements (GMM, AlbIX, VLHSA, SPS) and VLHSA + COP. There were no significant differences in the proportion of embryos that developed an ectoplacental cone, a proamniotic cavity, or columnar epiblast cells (Fig. 7.3A). However, the proportion of embryos with at least 1 cell with positive POU5F1 expression (epiblast) was significantly lower when the embryos were cultured till day 3.5 in SPS compared to when they were cultured in VLHSA + COP ($P \leq .05$) (Fig. 7.3B). There were no significant differences in the average outgrowth areas (Fig. 7.3C and D) or total epiblast cell number (Fig. 7.3E and F), as verified by the POU5F1-positive expression.

Discussion

Much of the lot-to-lot variability observed in albumin products is due to the variation of contaminants, including FAs, bound to the albumin protein (3, 4, 5, 6, 7, 8, 10, 11). FAs in the microenvironment impact not only embryonic development in vitro but also developmental competence of oocytes and the self-renewal capabilities of human embryonic stem cells (12, 26, 27, 28). Similarly, BSA may directly contribute to an aberrant cell lineage specification in an early mouse embryo (29) as a result of the molecular structure and function of albumin as a carrier for small molecules, including FAs. However, neither are there published studies that define the FA profiles of commercial albumin products, nor are they provided to consumers. On the basis of our analysis, commercial albumin preparations vary significantly in their long-chain FA profiles, and this variation impacts the ability of albumin supplements to support embryo development before and during implantation.

Our work demonstrated that the murine embryos thrived in the culture medium that contained reduced concentrations (<0.50 µg FA/mg albumin) of exogenous FA bound to albumin added as a protein supplement. The addition of carnitine, a cofactor necessary for FA oxidation, significantly improved murine embryo development when added to a culture medium containing albumin with relatively high levels of FAs. During beta oxidation, transport of FAs into the mitochondria by carnitine palmitoyltransferase is a rate-limiting step (30). Consistent with our results, stimulation of this pathway by the addition of L-carnitine to the culture medium significantly improved blastocyst development and oocyte quality (12, 31, 32, 33). Although carnitine alone was not able to improve embryo quality, as measured by the blastocyst cell allocation, additional supplementation of palmitoleic and oleic acids (VLHSA + COP) rescued the ICM:TE ratio while maintaining significantly improved blastocyst development compared with VLHSA alone. In the extended culture, the proportion of embryos with at least 1 epiblast cell cultured in VLHSA+ COP was higher than the proportion of those cultured in SPS, suggesting that VLHSA + COP supports high blastocyst development and good blastocyst

quality in mouse embryos. Suppliers should perhaps consider the addition of carnitine to either mitigate the harmful effects of FA species or potentially enhance the performance of therapeutic FAs in their media products.

It is worth noting that our assessments of embryo quality, as determined by the blastocyst development, cell number, allocation to ICM or TE, and development of advanced morphological structures in the extended culture, were not directly compared with in vivo flushed blastocysts, which is a limitation of our study. It is of particular concern that many of the FA profiles of commercial albumin products contain FA species that are detrimental for embryo development. For example, 8 of the 15 albumin sources, 2 of which are commonly used in human-assisted reproductive technology, contain relatively high levels of palmitic acid (0.55–3.10 μg/mg albumin) (Fig. 7.1A). Exogenous palmitic acid significantly increases intracellular lipid content in murine oocytes, which decreases subsequent embryo cleavage and blastocyst development (12). Lipotoxicity also occurs in several nonadipose cells because of addition of palmitic acid to the microenvironment, resulting in insulin resistance, mitochondrial dysfunction, and apoptosis (34, 35). These effects can be reversed with the addition of palmitoleic acid to skeletal muscle cells (36). Oleic acid also mitigates the negative effects of saturated palmitic and stearic acids on the developmental potential of bovine oocytes (37). Our data demonstrate that oleic and palmitoleic acids, when supplemented with carnitine, improve blastocyst development and quality even in the absence of high levels of palmitic acid.

FAs are generally thought of as an energy source rather than biologically active molecules that can influence cell behavior. However, free FAs have the capability to act as transcriptional regulators by altering the epigenetic landscape of bovine embryos (13), and some long-chain FAs can even act as ligands that promote cell proliferation (38, 39). With abnormally high levels of FAs, embryonic and extraembryonic cell lineages may be epigenetically altered in an unfavorable and unintended way, negatively impacting embryo quality and even offspring health

(13). Negative impacts of excess free FAs can not only result in their accumulation in nonadipose tissues but also induce cellular apoptosis (35). Thus, we would suggest that because FAs are biologically active molecules affecting embryo metabolism and other physiologically important processes that impact development, suppliers should provide information to consumers about dominant FA species that are found in each lot of their albumin products. We encourage suppliers to perform a simple FA profile analysis, as we have reported here, and that this be a component of albumin product quality-control measures that are included in the Certificate of Analysis and package insert accompanying albumin products.

In conclusion, given the variety of FA contaminants in commercially available albumin used in human in vitro fertilization, it is important to investigate the consequences of FAs that are inadvertently added to the culture environment and ultimately set guidelines for FA species and their amounts in albumin for optimal embryo development. When using protein supplements for embryo culture, scientists and embryologists should be mindful that albumins have variable FA profiles, among other contaminants, that can differentially affect embryonic development before and during implantation.

Acknowledgments

The authors thank Kati Wright, our Animal Care Supervisor, and Caitlyn Graham, our former Animal Care Technician, for their contributions to the care and welfare of the animals used in these studies.

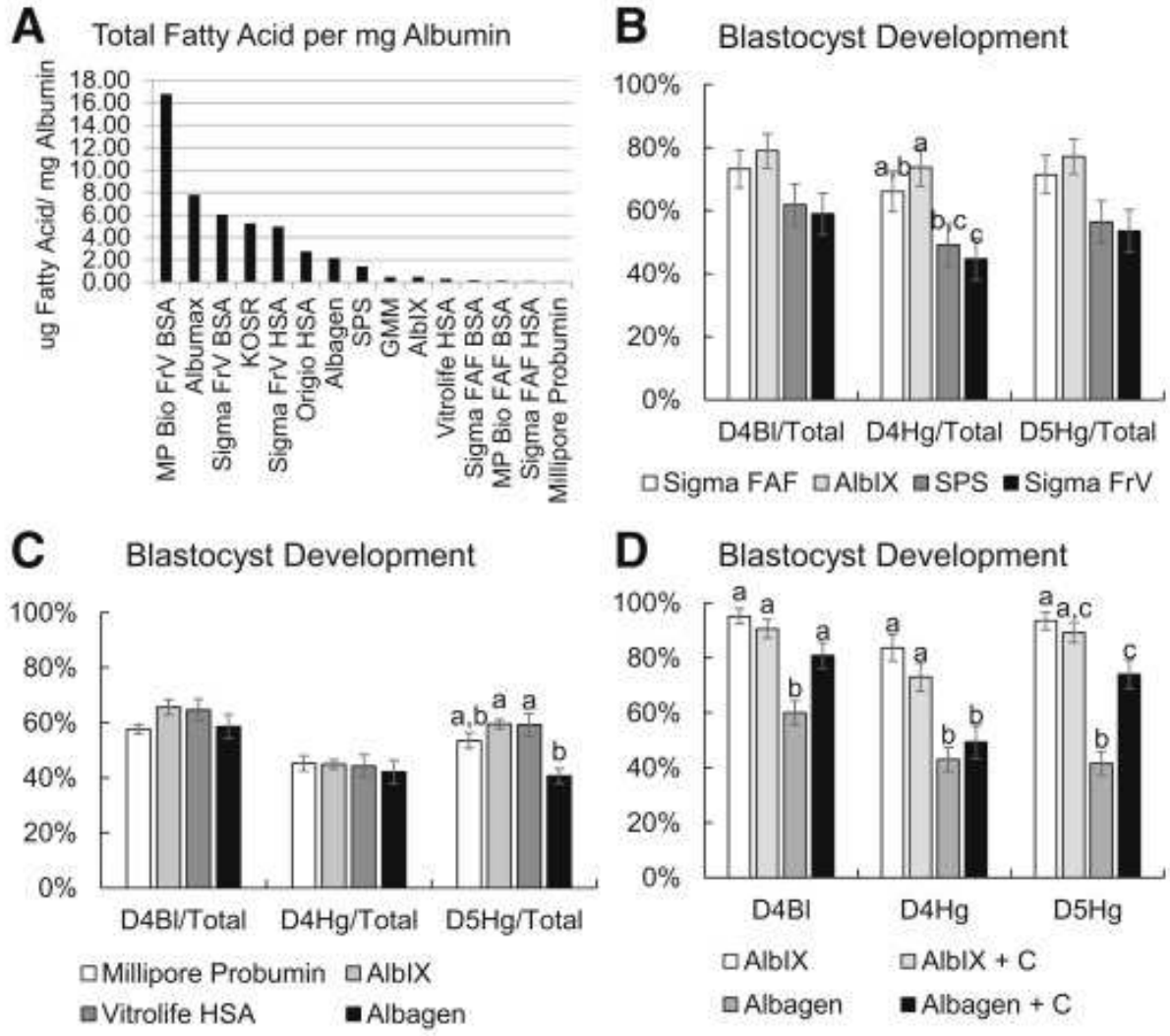

Figure 7.1(A) Total amount of long-chain FAs in 15 different albumin sources, presented as micrograms of FA per milligram of albumin. Total concentrations of FAs were determined by gas chromatography-mass-spectrometry. (B) Mouse embryonic development following culture in 4 different albumin sources (2.5 mg/mL: Sigma FAF HSA, n = 56; AlbIX, n = 57; SPS, n = 55; and Sigma FrV HSA, n = 56) with varying FA content. The total FA concentrations of Sigma FAF HSA, AlbIX, SPS, and Sigma FrV HSA were 0.16 µg/mg albumin, 0.47 µg/mg albumin, 1.40 µg/mg albumin, and 4.96 µg/mg albumin, respectively. (C) Mouse embryonic development following culture in 4 different albumin sources (2.5 mg/mL: Millipore Probumin, n = 314; VLHSA, n = 147; AlbIX, n = 867; and Albagen, n = 133) with varying FA content. The total FA concentrations in Millipore Probumin, VLHSA, AlbIX, and Albagen were 0.07 µg/mg albumin, 0.32 µg/mg albumin, 0.47 µg/mg albumin, and 2.15 µg/mg albumin, respectively. (D) Mouse embryonic development following culture in 2 recombinant human albumin sources (2.5 mg/mL: AlbIX, 0.47 µg/mg albumin; Albagen, 2.15 µg/mg albumin) with and without 1 mM carnitine (AlbIX, n = 61; AlbIX + carnitine, n = 74; Albagen, n = 130; Albagen + carnitine, n = 73). Data are presented as mean ± SEM. Embryonic day-4 Bl and Hg Bl development per total number of zygotes in culture and embryonic day 5 Hg Bl development per total number of oocytes in culture are shown for each treatment. Different superscripts indicate statistically different treatments based on 1-way

ANOVA and Bonferroni's test for multiple comparisons ($P \leq .05$). ANOVA = analysis of variance; Bl = blastocyst; FAs = fatty acids; FAF HSA = fatty acid-free human serum albumin; FrV HSA = fraction V human serum albumin; Hg = hatching; SEM = standard error of mean; SPS = serum protein substitute; VLHSA = Vitrolife human serum albumin.

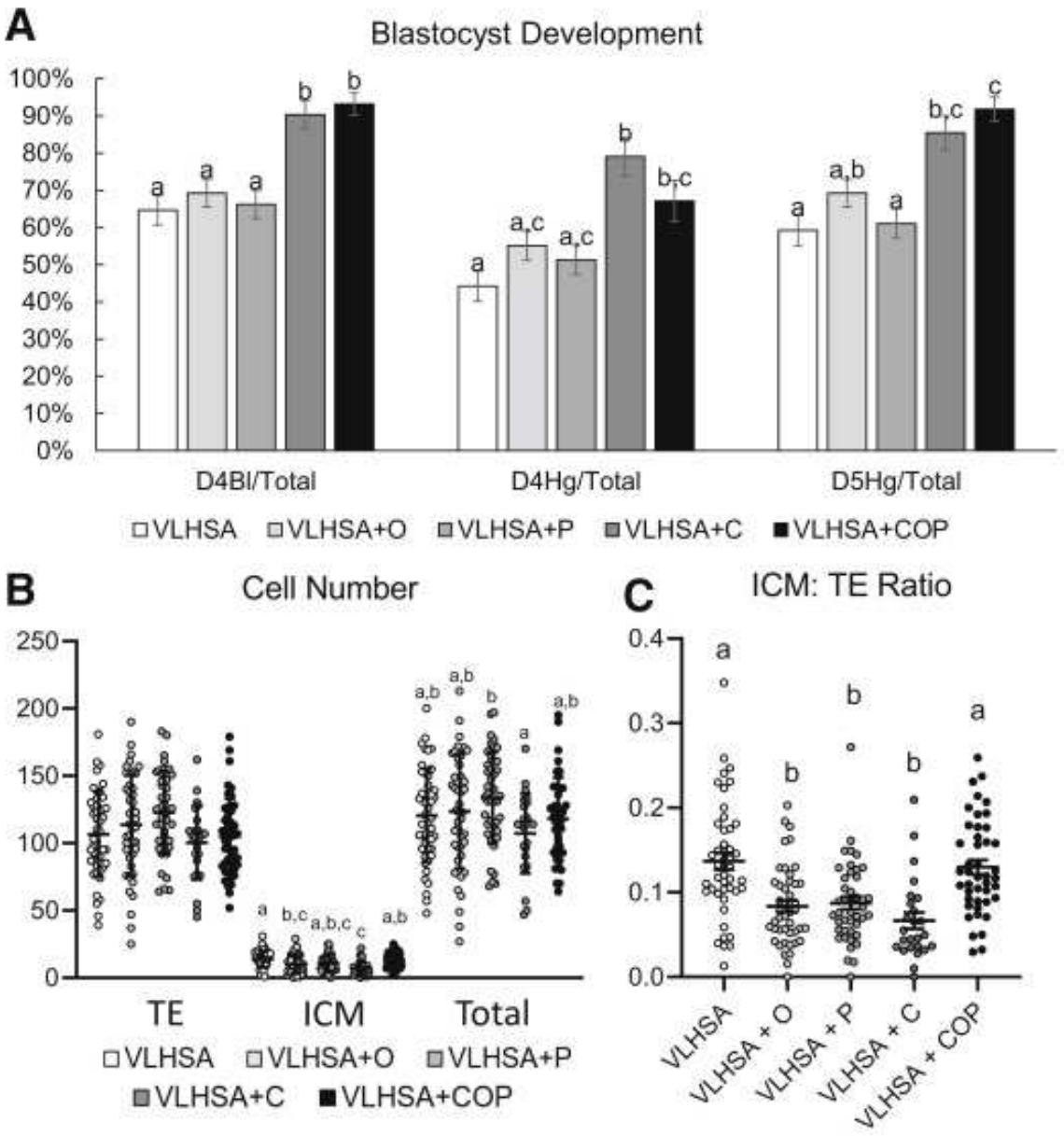

Figure 7.2 (A) Mouse embryonic development following culture in VLHSA alone or supplemented with oleic acid (VLHSA + O), palmitoleic acid (VLHSA + P), carnitine (VLHSA + C), or all 3 in combination (VLHSA + COP). Embryonic day-4 Bl and Hg Bl development and embryonic day-5 Hg Bl development are shown for each treatment. Data are presented as mean ± SEM. (B) Mean cell allocation ± SEM and (C) mean ICM (SOX2-positive):TE (CDX2-positive) ratio ± SEM as determined by immunofluorescent staining of hatching and hatched blastocysts from development replicates in panel A on day 5. Different superscripts indicate

statistically different treatments based on 1-way ANOVA and Bonferroni's test for multiple comparisons ($P \leq .05$). ANOVA = analysis of variance; BI = blastocyst; C = carnitine; Hg = hatching; ICM = inner cell mass; O = oleic acid; P = palmitoleic acid; SEM = standard error of mean; TE = trophectoderm; VLHSA = Vitrolife human serum albumin.

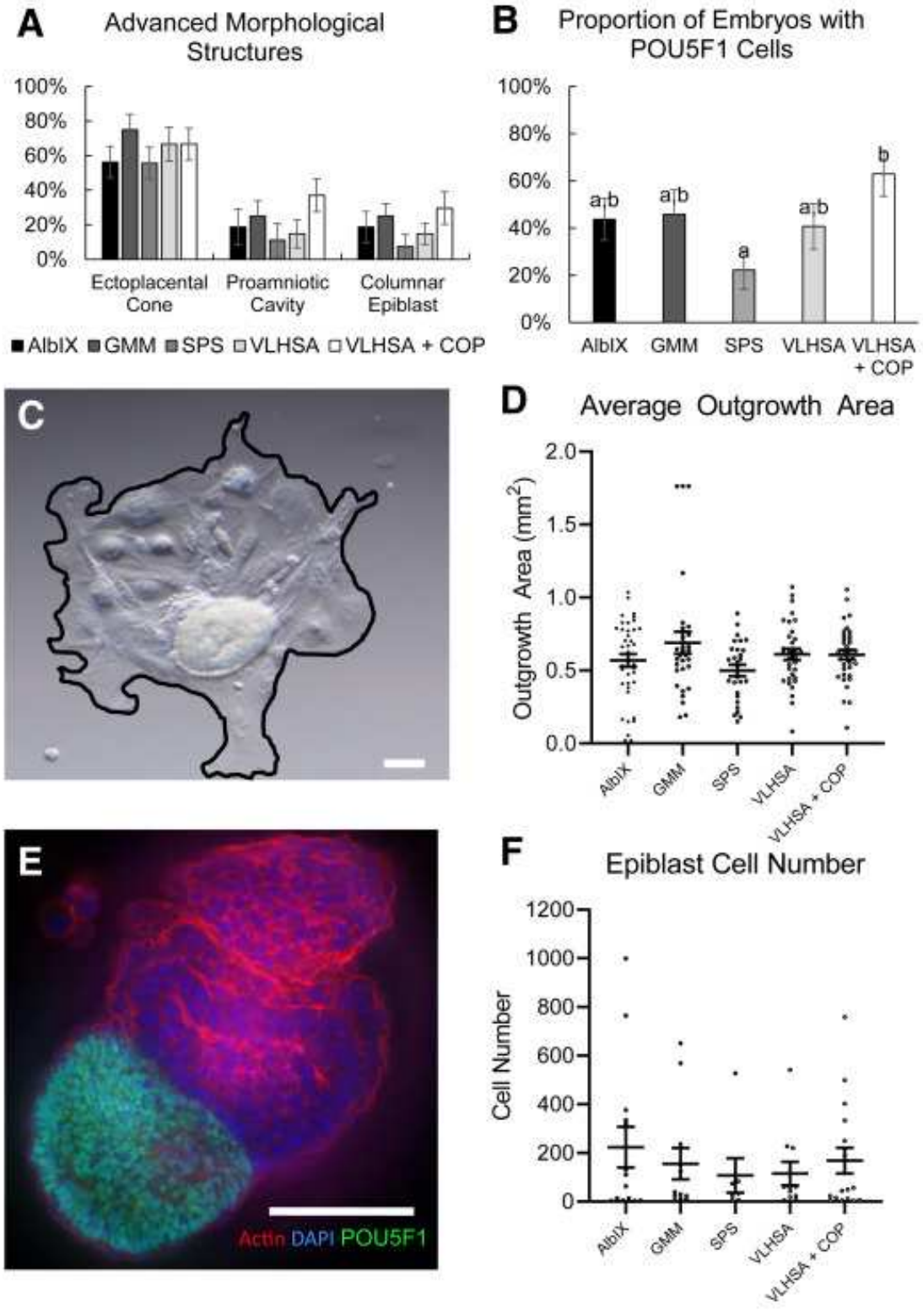

Figure 7.3(A) Proportion of day-8.5 embryos with advanced morphological structures in an extended-culture system following in vitro embryo culture till day 3.5 with Novozymes AlbIX (AlbIX), Vitrolife G-MM (GMM), Origio Quinn's Advantage serum protein substitute (SPS),

VLHSA alone, or Vitrolife FAF HSA with 1 mM carnitine, oleic acid (0.3 μg/mL), and palmitoleic acid (0.75 μg/mL) (VLHSA + COP) supplementation. (B) Proportion of embryos with at least 1 POU5F1 cell for embryos fixed at embryonic day-8.5 in an extended-culture system after in vitro embryo culture. (C) Representative image of an embryonic day-8.5 mouse embryo in the extended culture. The *black* line indicates area of TE outgrowth area. Scale bar = 100 μm. (D) Outgrowth area (mm2) of day-8.5 mouse embryos in an extended-culture system after in vitro embryo culture. (E) Representative confocal image of a fixed embryonic day-8.5 egg cylinder stained with DAPI in blue, rhodamine phalloidin in red, and antibodies against POU5F1 in green. Scale bar = 100 μm. (F) Epiblast cell number as determined by positive staining for pluripotency factor POU5F1 using Imaris software x64 9.20. Data are presented as mean ± SEM. Different superscripts indicate statistically different treatments based on 1-way ANOVA and Bonferroni's test for multiple comparisons ($P \leq .05$). ANOVA = analysis of variance; DAPI = 4′,6-diamidino-2-phenylindole; FAF HSA = fatty acid-free human serum albumin; SEM = standard error of mean; TE = trophectoderm; VLHSA = Vitrolife human serum albumin.

REFERENCES

1. Quinn P. Culture Media, Solutions, and Systems in Human ART. Cambridge: Cambridge University Press, 2014.

2. Bavister BD. Early history of in vitro fertilization. Reproduction 2002;124:181-96.

3. Dyrlund TF, Kirkegaard K, Poulsen ET, Sanggaard KW, Hindkjaer JJ, Kjems J *et al.* Unconditioned commercial embryo culture media contain a large variety of non-declared proteins: a comprehensive proteomics analysis. Human Reproduction 2014;29:2421-30.

4. Leonard PH, Charlesworth MC, Benson L, Walker DL, Fredrickson JR, Morbeck DE. Variability in protein quality used for embryo culture: embryotoxicity of the stabilizer octanoic acid. Fertility and sterility 2013;100:544-9.

5. Morbeck DE, Paczkowski M, Fredrickson JR, Krisher RL, Hoff HS, Baumann NA *et al.* Composition of protein supplements used for human embryo culture. Journal of Assisted Reproduction and Genetics 2014;31:1703-11.

6. Fredrickson J, Krisher RL, Morbeck DE. The impact of the protein stabilzer octanoic acid on embryonic development and fetal growth in a murine model. J Assist Reprod Genet 2015;32:1517-24.

7. Kane MT. Culture of Preimplantation Rabbit Embryos. In: Herrick J, ed. Comparative Embryo Culture Vol. 2006. Humana, New York, New York: Springer Protocols, 2019:63-91.

8. Blake D, Svalander P, Jin M, Silversand C, Hamberger L. Protein supplementation of human IVF culture media. Journal of Assisted Reproduction and Genetics 2002;19:137-43.

9. CDC. Fertility Clinic Success Rates Report. In: National Center for Chronic Disease Prevention and Health Promtion DoRH, ed., 2018.

10. van der Vusse GJ. Albumin as fatty acid transporter. Drug Metab Pharmacokinet 2009;24:300-7.

11. Bar-Or D, Bar-Or R, Rael LT, Gardner DK, Slone DS, Craun ML. Heterogeneity and oxidation status of commercial human albumin preparations in clinical use.[see comment]. Critical Care Medicine 2005;33:1638-41.

12. Paczkowski M, Schoolcraft WB, Krisher RL. Fatty acid metabolism during maturation affects glucose uptake and is essential to oocyte competence. Reproduction 2014;148:429-39.

13. Desmet KLJ, Van Hoeck V, Gagné D, Fournier E, Thakur A, O'Doherty AM *et al.* Exposure of bovine oocytes and embryos to elevated non-esterified fatty acid concentrations: integration of epigenetic and transcriptomic signatures in resultant blastocysts. BMC Genomics 2016;17:1004.

14. Van Hoeck V, Rizos D, Gutierrez-Adan A, Pintelon I, Jorssen E, Dufort I *et al.* Interaction between differntial gene expression profile and phenotype in bovine blastocysts originating from oocytes exposed to elevated non-esterified fatty acid concentrations. Reprod Fertil Dev 2015;27:372-84.

15. Van Hoeck V, Sturmey RG, Bermejo-Alvarez P, Rizos D, Gutierrez-Adan A, Leese HJ *et al.* Elevated non-esterified fatty acid concentrations during bovine oocyte maturation compromise early embryo physiology. PLoS ONE [Electronic Resource] 2011;6:e23183.

16. Leroy JLMR, Vanholder T, Mateusen B, Christophe A, Opsomer G, de Kruif A *et al.* Non-esterified fatty acids in follicular fluid of dairy cows and their effect on developmental capacity of bovine oocytes in vitro. Reproduction 2005;130:485-95.

17. J Folch, M Lees, Sloane GHS. A simple method for the isolation and purification of total lipides from animal tissues. J Biol Chem 1957;226:497-509.

18. Institute of Laboratory Animal Resources (ILAR). Guide for the care and use of laboratory animals. [8th] ed. Washington, D.C.: National Academy Press, 2011.

19. Herrick JR, Strauss KJ, Schneiderman A, Rawlins M, Stevens J, Schoolcraft WB *et al.* The beneficial effects of reduced magnesium during the oocyte-to-embryo transition are conserved in mice, domestic cats and humans. Reproduction, Fertility and Development 2015;27:323-31.

20. Bakhtari A, Ross PJ. DPPA3 prevents cytosine hydroxymethylation of the maternal pronucleus and is required for normal development in bovine embryos. Epigenetics 2014;9:1271-9.

21. Ivan Bedzhov CYL, Monika Bialecka, Magdalena Zernicka-Goetz. In vitro culture of mouse blastocysts beyond the implantation stages. Nature Protocols 2014;9:2732-9.

22. Zernicka-Goetz IBaM. Self-Organizing Properties of Mouse Pluripotent Cells Initiate Morphogenesis upon Implantation. Cell 2014; 156: 1032–44.

23. Logsdon DM, Ermisch AF, Kile R, Schoolcraft WB, Krisher RL, Yuan Y. Egg cylinder development during in vitro embryo culture predicts the post transfer developmental potential of mouse blastocysts. J Assist Reprod Genet 2020;37:747-52.

24. Schindelin J, Arganda-Carreras I, Frise E, Kaynig V, Longair M, Pietzsch T *et al.* Fiji: an open-source platform for biological-image analysis. Nature Methods 2012;9:676-82.

25. NCSS 11 Statistical Software In. Kaysville, Utah, USA: NCSS, LLC, 2016.

26. Sakurai M, Suzuki C, Koji Y. Effect of knockout serum replacement supplementation to culture medium on porcine blastocyst development and piglet production. Theriogenology 2015;83:679-86.

27. Suzuki C, Sakaguchi Y, Hoshi H, Yoshioka K. Lipid-rich bovine serum albumin improves the viabiltiy and htching ability of porcine blastocysts produced in vitro. J Reprod Dev 2016;62:79-86.

28. Garcia-Gonzalo FR, Izpisúa Belmonte JC. Albumin-associated lipids regulate human embryonic stem cell self-renewal. PLoS ONE 2008;3.

29. Frum T, Ralston A. Culture conditions antagonize lineage-promoting signaling in the mouse blastocyst. Reproduction 2020;160:V5-V7.

30. McGarry JD, Brown NF. The mitochondrial carnitine palmitoyltransferase system-from concept to molecular analysis. European Journal of Biochemistry 1997;244:1-14.

31. Dunning KR, Cashman K, Russell DL, Thompson JG, Norman RJ, Robker RL. Beta-oxidation is essential for mouse oocyte developmental competence and early embryo development. Biology of Reproduction 2010;83:909-18.

32. Dunning KR, Russell DL, Robker RL. Lipids and oocyte developmental competence: the role of fatty acids and beta-oxidation. Reproduction 2014;148:13-0251.

33. Dunning KR, Robker RL. Promoting lipid utilization with l-carnitine to improve oocyte quality. Anim Reprod Sci 2012;134:69-75.

34. El-Assaad W, Buteau J, Peyot M, Nolan C, Roduit R, Hardy S *et al.* Saturated fatty acids synergize with elevated glucose to cause pancreatic β-cell death. Endocrinology 2003;144:4154-63.

35. Listenberger LL, Schaffer JE. Mechanisms of lioapoptosis: implications for human heart disease. Trends in Cardiovascular Medicine 2002;12:134-8.

36. Talbot NA, Wheeler- Jones CP, Cleasby ME. Palmitoleic acid prevents palmitic acid-induced macrophage activation and consequent p38 MAPK-mediated skeletal muscle insulin resistance. Mol Cell Endocrinol 2014;393:129-42.

37. Aardema H, Vos PLAM, Lolicato F, Roelen BAJ, Knijn HM, Vaandrager AB *et al.* Oleic acid prevents detrimental effects of saturated fatty acids on bovine oocyte developmental competence. Biology of Reproduction 2011;85:62-9.

38. Hardy S, St-Onge GG, Joly E, Langelier Y, Prentki M. Oleate promtoes the proliferation of breast cancer cells via the G protein-coupled receptor GPR40. J Biol Chem 2005;280:13285-91.

39. Brown AJ, Jupe S, Briscoe C. A family of fatty acid binding receptors. DNA Cell Biol 2005;24:54-61.

APPENDIX III: DYNAMICS OF TROPHOBLAST DIFFERENTIATION IN PERI-IMPLANTATION STAGE HUMAN EMBRYOS

This work was published in the Proceedings of the National Academy of Sciences journal in October 2019

Significance

The mechanisms that lead to establishment of pregnancy and formation of a functional placenta during early human development are poorly understood due to ethical and technical constraints limiting research, yet this period is when many pregnancies fail and placental pathologies are most likely initiated. We cultured donated human embryos to days 8, 10, and 12 postfertilization and, for each stage, performed single-cell RNA sequencing on the trophoblast cells that compose the early placenta and enclose the embryo proper as it implants. Over the 5 d of culture, 2 cell lineages emerged from a progenitor stem cell population. One was syncytial and produced placental hormones. The second became motile and expressed genes associated with the innate immune system and invasion.

Summary

Single-cell RNA sequencing of cells from cultured human blastocysts has enabled us to define the transcriptomic landscape of placental trophoblast (TB) that surrounds the epiblast and associated embryonic tissues during the enigmatic day 8 (D8) to D12 peri-implantation period before the villous placenta forms. We analyzed the transcriptomes of 3 early placental cell types, cytoTB (CTB), syncytioTB (STB), and migratoryTB (MTB), picked manually from cultured embryos dissociated with trypsin and were able to follow sublineages that emerged from proliferating CTB at the periphery of the conceptus. A unique form of CTB with some features of

STB was detectable at D8, while mature STB was at its zenith at D10. A form of MTB with a mixed MTB/CTB phenotype arose around D10. By D12, STB generation was in decline, CTB had entered a new phase of proliferation, and mature MTB cells had begun to move from the main body of the conceptus. Notably, the MTB transcriptome at D12 indicated enrichment of transcripts associated with IFN signaling, migration, and invasion and up-regulation of HLA-C, HLA-E, and HLA-G. The STB, which is distinct from the STB of later villous STB, had a phenotype consistent with intense protein export and placental hormone production, as well as migration and invasion. The studies show that TB associated with human embryos is in rapid developmental flux during peri-implantation period when it must invade, signal robustly to the mother to ensure that the pregnancy continues, and make first contact with the maternal immune system.

Keywords: single-cell RNA sequencing, transcriptome, interferon, human endogenous retroviruses

Introduction

Implantation of the human embryo into the uterine wall is poorly understood and not closely paralleled in model organisms, such as the mouse. It is estimated that 40 to 60% of human conceptions fail, with the majority of the losses occurring just prior to or during implantation (1, 2), a process that is initiated soon after the blastocyst attaches to the uterine wall at about day 6 (D6) postconception. What little is known of early human embryo development and emergence of the earliest form of the placenta (3, 4) has come from histological studies performed more than 50 y ago (5–7), archived material (8), and parallels with nonhuman primates (8–10). The generally accepted view is that soon after the polar trophectoderm of the D6 to D7 blastocyst adheres to the uterine wall, a zone of invasive syncytiotrophoblast (STB) forms at the implantation site where it locally displaces uterine epithelial cells, thereby allowing the conceptus to penetrate the underlying stroma. The STB soon surrounds the conceptus and, as

it advances into the decidualized endometrium, hollows out lacunae, which become filled with blood and uterine secretions that likely provision the conceptus (11–14). The trophoblasts of this tiny conceptus must also release sufficient human chorionic gonadotropin (hCG) to rescue the corpus luteum; otherwise, the pregnancy fails. By D12, columns of cytotrophoblast (CTB) begin to penetrate the STB to form primary villi, which will eventually branch, acquire cores of blood vessels and connective tissue, and form the emerging villous placenta, while the fate of the original STB layer remains unclear. All these events occur prior to the time that a new menstrual cycle would normally begin in a nonpregnant woman.

The above histological studies have only provided a glimpse of events that occur during the second week of pregnancy and have been unable to provide insights into the dynamic process of implantation and what can go wrong. Some models for understanding placental trophoblast emergence have shown promise. For example, human pluripotent stem cells exposed to BMP4 can be driven efficiently to what has been proposed to be trophoblast analogous to that encountered around the periphery of an implanting conceptus (15, 16). Trophoblast stem cells derived from either preimplantation blastocysts or first trimester villi (17) and from trophoblast organoids (18, 19) also can be induced to differentiate along trophoblast sublineages. Recently, a system has been described that allows human embryos to be cultured in vitro for up to 14 d (20, 21). Here we have used such a system to compare trophoblast lineages from embryos at increasing days in culture, primarily through use of single-cell RNA sequencing (RNA-seq) to gain insights into events driving early placental emergence. It should be noted that there have been 3 previous papers that explored the nature of trophoblast in cultured human embryos by using the single-cell RNA-seq approach (22–24), but these studies were confined to the preimplantation period.

Results

Embryo Extended Culture and Single-Cell Collection

Vitrified and warmed D5 donated human blastocysts were cultured to embryonic D8, D10, and D12 according to a published protocol (20, 21) (Fig. 8.1 *A* and *B* and Table 7.1). By D8, most embryos attached to the bottom of the dish and possessed a peripherally located, apparently syncytial region that was positive for CG subunit beta (CGB) (Fig. 8.1*C*), a definitive STB marker, and had initiated secretion of hCG into the medium (Fig. 8.1*D*). Syncytial areas expanded over time and stained more intensely for CGB at D10 and D12 than at D8 (Fig. 8.1*C* and Fig. 8.6*A*). Daily release of hCG increased 41-fold by D10 compared to D8 (Fig. 8.1*D*). The expression of epiblast marker, POU5F1, was confined to a central area that represents the formation of the embryonic disk (Fig. 8.6 *A* and *B*). The commonly used trophoblast markers, KRT7 and GATA3, were also confirmed in these outer regions by immunofluorescence staining (Fig. 8.6*B*). In some D10 cultures, it was possible to observe a few cells migrating away from the embryo. By D12, these migrating cells had become more numerous. A time-lapse video that followed development between D8 and D12 was consistent with these patterns of cell fusion and migration during extended culture.

Finally, after treating D8, D10, and D12 embryos with trypsin, 3 different classes of placental cells were selected and individually picked, based on their size and location, for RNA-seq. The smallest, round cells (Fig. 8.1*E*) were inferred to be mononucleated CTB and possibly also similarly sized cells from other lineages. The multinucleated STB (*Fig. 8.6A*) were easily identified as irregular shaped structures significantly larger than the small cells (Fig. 8.1*E*). The migratory trophoblast cells (MTB) recognized as seemingly moving away from the main body of the embryo were collected before the embryos had been fully dissociated by the trypsin (Fig. 8.1 *B* and *E*). Although we were able to pick populations of CTB and STB at D8, D10, and D12, MTB cells were solely from D12 because of their scarcity at earlier times (Fig. 8.1 *A* and *B*).

RNA was extracted from 139 samples derived from 11 embryos (Table 7.2) and, upon sequencing, generated ~1.4 billion reads (~10 million reads per individual cell). To ensure we were only analyzing the transcriptomes of trophoblast cells and not other cell types, cell lineages were first predicted based on reported expression of lineage markers derived from human blastocysts (24) by Spearman correlation algorithm. Initially, 7 single-cell samples were considered to be nontrophoblast by these criteria. However, when additional known lineage marker genes (*POU5F1*, *GATA6*, *KRT7*, *GATA3*, *SOX2*, *NANOG*, and *CD24*) (20) were used to check these 7 cells, 5 were considered to be trophoblast because of their high expression of *KRT7* and *GATA3.* The remaining 2 were confirmed as epiblast (high expression of *POU5F1*, *SOX2*, and *NANOG* and low in *KRT7* and *GATA3*) and were excluded from the extended analysis (Table 7.3). Principal component analysis (PCA) and clustering analyses identified 9 cells as outliers, while 3 cells had low read counts (<8,000 genes detected). These were also discarded. In the final analysis of the remaining 125 cells (78 CTB, 31 STB, and 16 MTB), there were 14,105 genes with a maximum FPKM ≥ 1 and 15,420 genes with a maximum FPKM ≥ 0.3 in at least 4 cells (Fig. 8.7*A*). These genes remained in the analysis, while all others were excluded. In general, the CTB expressed the highest number of expressed genes per cell, but there was no significant difference in number within any grouping between D8, D10, and D12 (Fig. 8.7*B*).

Cell Type Specific Marker Expression and Pathway Analysis

PCA was performed to show transcriptional profiles of all 3 cell populations at the different collection time points (Fig. 8.2*A*). The transcriptomic profiles clustered better according to cell type (CTB, STB, and MTB) than by day, i.e., developmental stage (Fig. 8.8 *A* and *B*). Unsupervised clustering analysis (K-means) further revealed 17 small cells (CTB) had a partial MTB signature and were classified as Pre-MTB, while 15 small cells had a partial STB signature and were designated Pre-STB (Fig. 8.2*B*). We infer that these intermediate-stage cells were in the process of differentiating from CTB to either the MTB or STB sublineages. Cells considered

to be in these 2 intermediate classes were removed from the remainder of the CTB group in order to identify the unique transcriptome signature for CTB. We also identified genes that were enriched in each cell type. Specifically, 2932, 592, and 569 genes were identified as enriched marker genes for CTB, STB, and MTB, respectively (Fig. 8.2 *C* and *D* and Table 7.7). Based on such gene panels, each main cell type could be clearly separated by hierarchical clustering analysis (Fig. 8.2*E*), which indicated strong correlations to their corresponding cell type specific genes (Fig. 8.2*F*) and demonstrated the robustness of each panel to identify each respective cell lineage.

Next, gene ontology (GO) and pathway analysis was performed to identify pathways most strongly associated with each cell type. The top GO terms for CTB were ones linked to cell proliferation, transcription, and energy metabolism (Fig. 8.9), consistent with the inferred role of CTB in supplying cells to the other trophoblast lineages and ultimately the placenta as a whole. For STB, the top terms were protein folding, transport, and hormone processing (Fig. 8.9), which are again consistent with known functions of syncytial trophoblast, whether in the villous placenta or the primitive placenta encountered in very early pregnancy (16). Pathways involved in protein export and uptake, steroidogenesis, and migration were also up-regulated. The latter term may reflect the suspected invasive as well as endocrine nature of early STB during the implantation phase of pregnancy (25). As anticipated, MTB-enriched pathways underscored roles in cell migration and invasion into the extracellular matrix. More surprising was the presence of terms and pathways associated with type I and type II IFN signaling, innate immune responses, and antigen processing (Fig. 8.9).

Dynamics of Trophoblast Differentiation

While the transcriptomic profiles of the STB remained relatively stable between D8 and D12, those of the CTB showed considerable change, possibly reflecting the developmental plasticity of the CTB as the cells prepare for differentiation (Fig. 8.3 *A* and *B*). A comparison of the

transcriptomes of CTB between D8 and D10, for example, reflected a switch from a proliferative phenotype at D8 to one with a greater emphasis on syncytialization, protein processing, and steroidogenesis at D10, suggesting that differentiation toward STB had become an emphasis. Additionally, several MTB-related GO pathways, including angiogenesis, response to hypoxia, and response to cytokines and hormones, had also become active at D10 (Fig. 8.3*D* and Fig. 8.10). These data suggest that there are 2 distinct differentiation routes ongoing for CTB at D10, one to STB and the other to MTB. This inference is supported by the fact that the majority of small cells collected at D10 were either Pre-STB (12 out of 23) or Pre-MTB (6 out of 23), and only 5 (21.7%) possessed the phenotype of bona fide undifferentiated CTB (Fig. 8.3*C*). By D12, there was evidence of a more emphatic shift toward a Pre-MTB phenotype, as evidenced by an up-regulation of pathways related to IFN signaling, hypoxia, cell migration, and vascular remodeling, while genes associated with syncytium formation had become less dominant than in D10 CTB (Fig. 8.3*D* and Fig. 8.10). Additionally, more Pre-MTB (10 out of 30 small cells) and fewer Pre-STB (2 out of 30 small cells) were present in the population of CTB collected at D12 (Fig. 8.3*C*). There also appeared to be a partial restoration of undifferentiated CTB numbers at D12, as well as the appearance of a possible new phenotype in the form of 2 cells with a mixed STB/MTB signature (Fig. 8.3*C*).

We then compared the transcriptomes of Pre-STB and Pre-MTB, with undifferentiated CTB and differentiated STB and MTB regardless of their collection day. While Pre-STB had up-regulated genes associated with syncytium formation (Fig. 8.3*E* and Fig. 8.11*A*), they also had retained high mitotic activity as suggested by their expression levels of the cell proliferation markers *PCNA* and *MCM* genes (26, 27) (Fig. 8.12). By contrast, the differentiated STB showed evidence for departure from the cell cycle and possessed gene networks linked to protein transport and hormone production that were largely absent from Pre-STB (Fig. 8.3*E* and Fig. 8.11*A*). We conclude that the Pre-STB represent a population of dividing CTB primed to fuse to form syncytium but that had not yet up-regulated the machinery required for hormone

production and cell fusion (Fig. 8.3*E* and Fig. 8.11*A*). The Pre-MTB existed in an analogous state to the Pre-STB, i.e., committed to differentiation but lacking the full-blown phenotype of MTB. For example, they appeared to be continuing to proliferate, although the pathways related to RNA processing had begun to decline (Fig. 8.3*E* and Fig. 8.11*B*). GO terms related to IFN signaling and antigen processing that had been strongly represented in mature MTB had apparently not been acquired by the Pre-MTB.

Gene Networks Linked to IFN Responses.

Closer analysis of the RNA-seq data revealed that several IFN response genes were expressed as early as D8 in trophoblast cells and increased in expression as development proceeded (Fig. 8.4*A*). GO pathway analysis indicated that D12 CTB (Fig. 8.10) and MTB (Fig. 8.9) had several terms associated with type I and type II IFN signaling pathways. To confirm these findings, we immunostained embryos for type I IFN receptor subunits 1 (IFNAR1), type II IFN receptor subunit 2 (IFNGR2), and ISG20 (Fig. 8.4*B*). We found expression of INFAR1 and ISG20 as early as D8, with IFNAR1 and ISG20 mainly located to the periphery of the colonies where differentiation occurs (Fig. 8.4*B*). All of the IFN-related markers became positive by D12. The increase in expression of IFNAR2 and ISG15 were also confirmed by Western blotting (Fig. 8.4*C*).

An IFN response triggered by type I and type II IFN is mediated by the JAK-STAT pathway (28). Although total STAT1 increased over time, we found no evidence for the presence of its phosphorylated form, indicating the JAK-STAT pathway was probably not activated (Fig. 8.4*D*). In addition, mTOR signaling activity, a mechanism that has been considered to mediate IFN-induced mRNA translation (28), remained unchanged over time, also suggesting that the classical JAK-STAT mediated IFN signaling pathway was inactive (Fig. 8.4*D*). Although increased concentrations of phosphorylated AKT and ERK1/2 were detected, these factors play more general roles in metabolism, rather than up-regulating type I and type II IFN responses.

We also found no evidence for either bacterial contamination or endotoxin in the medium that might have triggered a type II IFN response, nor were IFNG or IFNA/B detectable in the medium by immunoassay. Finally, FPKM values for *IFNA* subtypes and *IFNB* were extremely low (Fig. 8.4*A*), while *IFNG* transcripts were undetectable. These data suggest that the up-regulation of IFN receptors and downstream IFN response genes were not triggered by exogenous factors but were components of a constitutive developmental process associated with normal development.

About 8% of the human genome (29) consists of human endogenous retroviruses (HERV) capable of producing virus-like particles competent to induce an IFN response. The placenta expresses several HERV that have been implicated in trophoblast differentiation and syncytialization (30, 31). Eight HERV were expressed in cultured human embryos (Fig. 8.5*A*). Of these, 5 (*ERV3-1*, *ERVFRD-1*, *ERVV-1*, *ERVV-2*, and *ERVW-1*) were more abundantly expressed in differentiated trophoblast cells (Pre-STB, Pre-MTB, STB, and MTB) than in CTB. *ERVV-1*, *ERV-2*, and *ERVW-1* had the highest transcript levels, with the highest expression at D10 when the presence of ERVW-1 could be confirmed by immunofluorescence (Fig. 8.5*B*). By contrast, expression of *ERVH48-1* and *ERVMER34-1* was higher in undifferentiated CTB than in the more differentiated cell populations. ERVH48-1 is known to inhibit rather than promote cell fusion, which it accomplishes by competing with ERVW-1 for binding to its cell surface receptor (32). ERVMER34-1 has barely been studied, but its presence in CTB rather than STB suggests that it, too, might be an inhibitor of cell fusion.

Discussion

Here we have employed an extended culture system for human embryos, combined it with single-cell RNA-seq, and successfully captured transcriptome dynamics in trophoblast cells occurring within the primitive placenta between D8 and D12 postfertilization, a time that in vivo corresponds to the first 5 d after the embryo begins to implant into the uterine wall. It is important to note that during this period, the familiar villous placenta, with its characteristic thin

outer syncytialized epithelium overlaying a mitotic population of CTB stem cells has not yet emerged. Instead, the embryo proper is surrounded by a mass of trophoblast, with STB and, as demonstrated here, a population of migratory cells (here called MTB) toward the exterior. Our data are consistent with the hypothesis that STB and MTB are replenished from below by a progenitor population of CTB. However, several facts should be born in mind about this early placental structure. First, unlike villous STB (33), it has invasive/migratory features that are probably responsible for its ability to burrow into the endometrium and place the conceptus within a hollowed-out niche where it can gain nutritional support from close proximity with surrounding maternal decidual cells, capillaries, and glands. Second, the conceptus must produce sufficient hCG and possibly other supporting factors to prevent a decline in progesterone resulting from regression of the corpus luteum as would occur in a nonfertile cycle. Third, this early placenta, although functional, is short lived. Columns of CTB begin to penetrate the STB layer beginning around D12 and ultimately give rise to the villous placenta while the fate of the initial STB remains unclear. It is mistaken to believe, as others have done, that the STB associated with the D8 to 12 placenta is equivalent to villous STB, which it clearly is not, although it may have an analogous function in supplying the embryo proper with nutrient support. Additionally, the migratory cells (called MTB here) should probably not be referred to as extravillous TB, since there are no villous structures at this stage from which MTB could arise. In terms of marker gene expression, the transcriptome profiles of the MTB, including the expression of HLA-G, do appear to resemble those of first trimester EVT arising from the tips of anchoring villi, but whether the latter are of the same lineage as MTB is not clear.

At D8, when implantation in vivo would have just begun, the majority of TB cells in the embryos were small and apparently mitotically active and had a predominantly CTB phenotype, although some STB and 1 or 2 Pre-STB and Pre-MTB cells were also present in the CTB population (Fig. 8.3*C*) and were probably responsible for the small amount of hCG produced at this time (Fig. 8.1*D*). Trophectoderm, a simple epithelium, may provide the progenitors for trophoblast

outgrowth from cells at the polar end of the blastocyst (24) but is clearly functionally distinct from the trophoblast associated with implantation. Additionally, our transcriptomic data reveal that the small cell population, while appearing morphologically homogeneous, contained a subset of mitotically active intermediate cytotrophoblast cells already transcriptionally preparing either to fuse to form syncytium, particularly apparent at D10, or to differentiate toward MTB (Figs. 8.2*B* and 8.3C). This lineage bifurcation seemed to initiate around D8 but was most apparent at D10, when commitment to STB was at a maximum and production of hCG was rising sharply (Figs. 8.1*D* and 8.3C). By D12, STB differentiation was in decline, but MTB production was on the upswing (Fig. 8.3*C*). At D12, there was also an indication of an upsurge in the proportion of undifferentiated, mitotically active CTB (Fig. 8.3*C*), possibly reflecting the beginning of villous formation and the demise of the early placenta. Together these data suggest that the early placenta is distinct from trophectoderm and, although short-lived, is able to prioritize highly specialized cell functions at very specific time points throughout the implantation period.

The transcriptomic data also provided some surprises. One was the identification of several genes and GO pathways associated with IFN signaling and partial activation of antiviral responses in the MTB. Although the production of type I and type II IFN by trophoblast has been demonstrated in some ungulates (34), and is especially important in ruminants where IFN-tau (IFNT) plays a critical role in maternal recognition of pregnancy (35, 36), no homologous role for IFN was evident here for the human, where neither type I nor type II IFN genes were being transcribed (Fig. 8.4*A*). Rather, the MTB seemed poised to respond to IFN, having both the receptors and some component effectors already in place. Conceivably, IFN released by cells resident in the endometrium would be able to trigger an IFN response in trophoblast and provide some survival advantage to the embryo in addition to serving as a first line of defense against viral and bacterial infections. For example, in vitro fertilization (IVF) patients with recurrent implantation failure have significantly lower concentrations of intrauterine IFNG than controls (37). Of course, overstimulation of IFN may desensitize IFN pathways, a mechanism that

contributes to unresponsiveness of type I IFN in HIV disease (38). In human embryos, a high level of IFN exposure as a result of uterine infection or inflammation could lead to desensitization of IFN pathways and blockage of trophoblast differentiation, resulting in embryo loss, thereby sparing maternal costs associated with continuation of a blighted pregnancy. Thus, IFN response pathways may act as a safety switch that determines the success of implantation in vivo.

As anticipated, expression of transcripts for classical MHC class I molecules, *HLA-A* and *HLA-B* (39), as well as MHC class II molecules (40), illustrated here by *HLA-DOB* and *HLA-DRB1* (Fig. 8.13*C*), were poorly expressed in each class of trophoblast cell at each developmental time point. By contrast, *HLA-C*, and the nonclassical *HLA-E*, and *HLA-G* genes were robustly expressed by D12 (Fig. 8.13 *A* and *B*), especially in MTB. These human versions of the major histocompatibility complex (MHC) molecules have been proposed to be responsible for creating an in vivo immunomodulatory environment that favors extravillous trophoblast invasion (41). Such features of the MHC system, like the IFN signaling pathway discussed previously, may be critical for early conceptus survival prior to formation of the villous placenta at a perilous time in pregnancy when embryonic wastage is high. A deeper investigation of these transcriptomic data will likely elucidate additional insights into mechanisms that facilitate human implantation.

It should be recognized that the embryos used in our experiments were cultured in a medium in absence of maternal decidual cells and on a substratum, namely, fibronectin, that would only be a single component of the mixed matrix encountered in the endometrium during implantation. For example, both substrate composition and stiffness can influence transcriptomes of stem cells (42, 43). Thus, the developmental trajectory observed here in vitro might be somewhat different from that occurring in vivo in a normal pregnancy. As demonstrated in Fig. 8.5, however, major metabolism pathways remained active at D12, and there was an apparent increase of mitotically active CTB and a rise of MTB. Nonetheless, it would be overly optimistic

to believe that the embryos were not losing viability by this stage. As the technology for extended embryo culture improves, it is likely that a system more reflective of endometrium–conceptus interactions as they occur in vivo will emerge. Therefore, even though the data provided in the present paper can only be an incomplete indication of what goes on in vivo, we suspect that they still provide insight into the functioning of the early placenta, a structure essential for pregnancy maintenance prior to the time that the villous placenta emerges. Our results are consistent with the inference that initial implantation events and endocrine support of ovarian progesterone production by the mother are a function of the STB surrounding the conceptus as it invades, while the motile MTB is responsible for initiating additional colonization of the uterine endometrium prior to the outgrowth of placental villi.

Materials and Methods

Ethics Statement

This research was approved by the Western Institutional Review Board (study no. 1179872) and followed international guidelines for extended embryo culture. Embryos were donated for research with patients' informed consent. Once a patient has completed treatment and has no further medical need for their frozen embryos and no longer wants to retain them, they have several options: discard and thus destroy their embryos, donate their embryos to another couple for embryo adoption, or donate them to research. This choice is certified by a signed and notarized disposition document. This process is completed by nonresearch personnel. Once a patient has chosen and finalized "donation to research" and their decision has been confirmed, those embryos become available for research.

Human Embryo Thawing and Zona Pellucida Removal

Human embryos (see *SI Appendix* for further details) were voluntarily donated by patients at the Colorado Center for Reproductive Medicine. D5 and D6 vitrified human blastocysts were thawed in prewarmed solution for 1 min and transferred to modified Kitazato dilution solution (Kitazato)

for 3 min prior to washing solution (WS) for 5 min (44). Individual blastocysts were placed in individual culture drops of IVC1 medium (Cell Guidance Systems, M11 25) overlaid in mineral oil and left for 2 h at 37 °C under 20% O2 and 7.5% CO2 to adjust for the high elevation where these studies have been performed. After 2 h, embryos were moved to 3-(*N*-morpholino)propanesulfonic acid (Mops) buffered medium before removal of the zona pellucida by 3 sequential washes in Acidic Tyrode's solution (Millipore Sigma, T1788) followed by 3 sequential washes in Mops.

Extended Embryo Culture

The extended embryo culture procedure was performed as previously described (20, 21). Briefly, blastocysts immediately after zona removal were washed in a 60-mm center-well organ culture dish (Corning, 353037) containing warmed IVC1 medium before transfer into 8-well chamber dishes (Ibidi, 80841). Each chamber had been coated with sterile fibronectin (Millipore Sigma, F0895) diluted in PBS at a 3:100 dilution. Plates were coated overnight, and remaining soluble fibronectin were then removed before addition of 300 µL equilibrated IVC1 medium. After at least 1 h, embryos lacking zonas were placed in the medium and cultured for a further 48 h. On extended embryo culture day 2, embryo attachment was assessed for all embryos. For embryos that had attached, half the IVC1 medium was removed and replaced with fresh IVC2 medium (Cell Guidance Systems, M12-25). After day 2, a 50% media change with IVC2 media was performed daily on all attached embryos.

Isolation of Single Cells

Single cells were isolated from embryos at embryonic D8, D10, and D12; incubated with TrypLE Express reagent for 10 min; and dissociated into single cells. For D12 embryos, migratory TB (MTB) that were located outside the main colony were collected before the main colony had been dissociated. After gentle pipetting, rounded, single mononucleated cytoTB (CTB) and

multinucleated syncytioTB (STB) were collected. Each cell was transferred into a 0.2-mL PCR tube (Eppendorf) containing cell lysis buffer and kept at −80 °C until library preparation.

Single-Cell RNA-Seq Library Preparation

The RNA-seq libraries were generated from individual cells by using the Smart-seq2 v4 kit with minor modification from manufacturer's instructions. Briefly, individual cells were lysed, and mRNA was captured and amplified with the Smart-seq2 v4 kit (Clontech). After AMPure XP beads purification, amplified RNAs were quality checked by using Agilent High Sensitivity D5000 kit (Agilent Technologies). High-quality amplified RNAs were subject to library preparation (Nextera XT DNA Library Preparation Kit; Illumina) and multiplexed by Nextera XT Indexes (Illumina). The concentration of sequencing libraries was determined by using Qubit dsDNA HS Assay Kit (Life Technologies) and KAPA Library Quantification Kits (KAPA Biosystems). The size of sequencing libraries was determined by means of High Sensitivity D5000 Assay in at Tapestation 4200 system (Agilent). Pooled indexed libraries were then sequenced on the Illumina HiSeq X platform with 100-bp pair-end reads.

Single-Cell RNA-Seq Data Filtration and Processing

Multiplexed sequencing reads that passed filters were trimmed to remove low-quality reads and adaptors by TrimGalore-0.4.3. The quality of reads after filtering was assessed by fastQC, followed by alignment to the human genome (hg38) by STAR (2.5.3a) with default parameters. Approximately 10 million reads per individual cell were generated. Individual mapped reads were adjusted to provide FPKM (fragments per kilobase of exon model per million mapped fragments) values with RefSeq genes as reference. The raw FASTQ files and normalized gene expression profiles (FPKM) are available at Gene Expression Omnibus (GEO) (https://www.ncbi.nlm.nih.gov/geo/) under the accession number GSE 130289. Differential gene expression analysis was performed by a Partek Flow GSA algorithm with default parameters. The genes were deemed differentially expressed if they provided a false discovery rate of <0.05

and fold change >2. DAVID (https://david.ncifcrf.gov) and IPA (Ingenuity Pathway Analysis) were used to reveal the Gene Ontology (GO) and pathways, respectively. Cells with more than 8,000 detected genes, each with FPKM values >0.3, were used for downstream analysis for lineage specification. Lineage specification was performed by Spearman correlation. PCA and cluster analysis were performed by using R. Identification of cell type and stage-specific genes was performed as previously described (45). Briefly, to identify cell type and stage-specific genes, a unit vector was constructed for each cell type (stage), followed by the calculation of the Pearson correlation between the vector and individual genes. This unit vector was designed to represent cell type (stage)-specific gene expression patterns. More specifically, the entries of the vector corresponding to samples of a cell type (or at a stage) were set to 1, with all others being 0. Genes with *P* value (after Bonferroni correction for multiple testing) less than 0.05 were labeled as cell type (stage) specific.

Immunofluorescence and Image Acquisition

Embryos were washed 3 times in warmed, filtered PBS and fixed in 4% paraformaldehyde (PFA) for 20 min. They were then washed in 0.1% Tween20 (Millipore Sigma, P1379) in PBS (PBS-T) 3 times and permeabilized by 0.5% Triton X-100 (Millipore Sigma, X100) in PBS for 30 min. Embryos were washed again in PBS-T and exposed to 10% vol/vol FBS and 3% wt/vol BSA in PBS-T overnight at 4 °C. Primary antibodies (*SI Appendix*, Table S4) were added at a 1:200 dilution in blocking buffer (10% FBS/3% BSA/PBS-T) and incubated at 4 °C overnight. Samples were then washed in PBS-T 3 times and incubated with secondary antibodies overnight at 4 °C. After incubation, embryos were washed again in PBS-T and then mounted in ProLong Gold antifade reagent with DAPI (ThermoFisher Scientific, P36931) mounting medium. Embryos were imaged on a 3I Marianas inverted spinning disk microscope. Z-stack images were captured by using a 40x/1.52 numerical aperture oil-immersion objective. The lasers 405, 488, and 561 were used to capture DAPI, Alexa Fluor 488, and Alexa Fluor 594, respectively. Laser intensity and exposure time was manually adjusted for each sample to avoid

oversaturation or photobleaching of samples. After image capture, images were immediately deconvoluted by means of Slidebook software (3i) set to the “Nearest Neighbors” setting. Images were rendered and processed with Imaris microscopy image analysis software (Bitplane) to generate maximum intensity projections.

Other methods including Western blotting, ELISA and ECLIA analyses, and statistical analysis are summarized in *SI Appendix*. Antibodies used for immunofluorescence and Western blotting are listed in *SI Appendix*, Tables S4 and S5.

Notes

We thank Karen Maruniak and the Colorado Center for Reproductive Medicine (CCRM) Clinical Laboratory for processing hCG samples and Sue McCormick and the CCRM IVF Laboratory for embryo collection. We thank Dr. Radu Moldovan and Dr. Dominik Stich at the University of Colorado Advanced Light Microscopy Core for their help with the confocal image acquisition and image processing. We also thank Dr. Thomas Hansen, Dr. Gerrit Bouma at Colorado State University, Dr. Danny Schust, Dr. Laura Schultz, and Dr. Jie Zhou at University of Missouri for their critical inputs. This project was funded by internal research funds provided by the CCRM. The microscopy and imaging services provided by the Advanced Light Microscopy Core Facility at the University of Colorado Anschutz School of Medicine to the CCRM were billed at the nonacademic (non-NIH funded user) rate.

Footnotes

The authors declare no competing interest.

Data deposition: Data have been deposited in the Gene Expression Omnibus (GEO) database, https://www.ncbi.nlm.nih.gov/geo/ (accession no. GSE 130289).

This article contains supporting information online at www.pnas.org/lookup/suppl/doi:10.1073/pnas.1911362116/-/DCSupplemental.

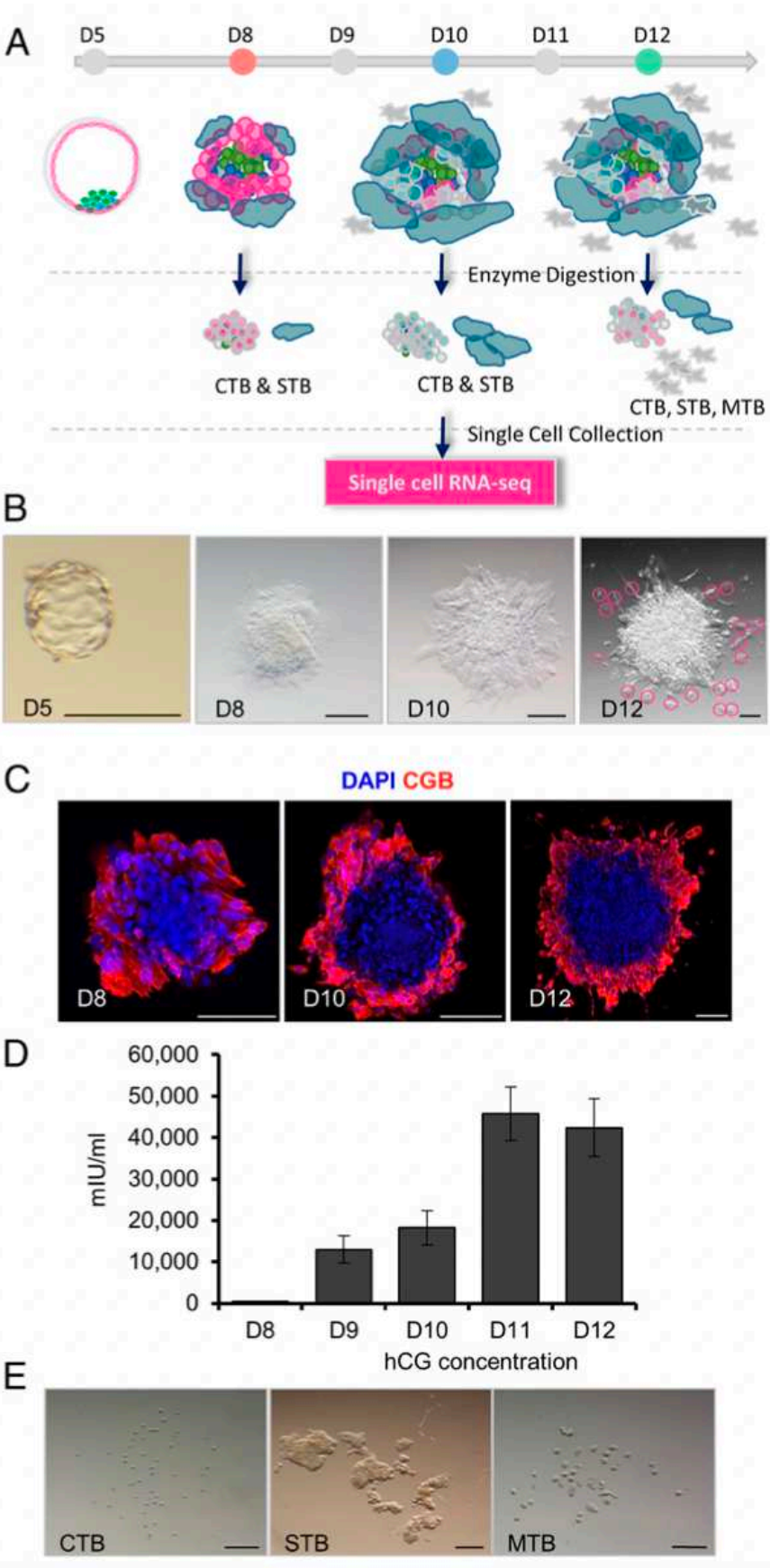
A
D5
D8
D9
D10
D11
D12
Enzyme Digestion
CTB & STB
CTB & STB
CTB, STB, MTB
Single Cell Collection
Single cell RNA-seq
B
D5
D8
D10
D12
C
DAPI CGB
D8
D10
D12
D
60,000
50,000
40,000
30,000
20,000
10,000
0
mIU/ml
D8
D9
D10
D11
D12
hCG concentration
E
CTB
STB
MTB

Figure 8.1. Isolation of single cells from extended cultured human embryos. (*A*) Workflow for culturing human embryos and isolating cytotrophoblast (CTB), syncytiotrophoblast (STB), and migratory trophoblast (MTB) for single-cell RNA-seq. (*B*) Morphologies of a D5 human blastocyst after zona pellucida removal and embryos at embryonic D8, D10, and D12. Pink circles outline MTB seen at D12 but rarely earlier. (Scale bar, 200 μm.) (*C*) Beta-human CG (CGB) immunofluorescence at embryonic D8, D10, and D12 ($n = 3$). (Scale bar, 200 μm.) (*D*) Levels of hCG in cell culture medium at embryonic D8 to D12 (mean ± SEM) ($n = 13$). (*E*) Morphologies of CTB, STB, and MTB after single-cell enzyme digestion. (Scale bar, 200 μm.)

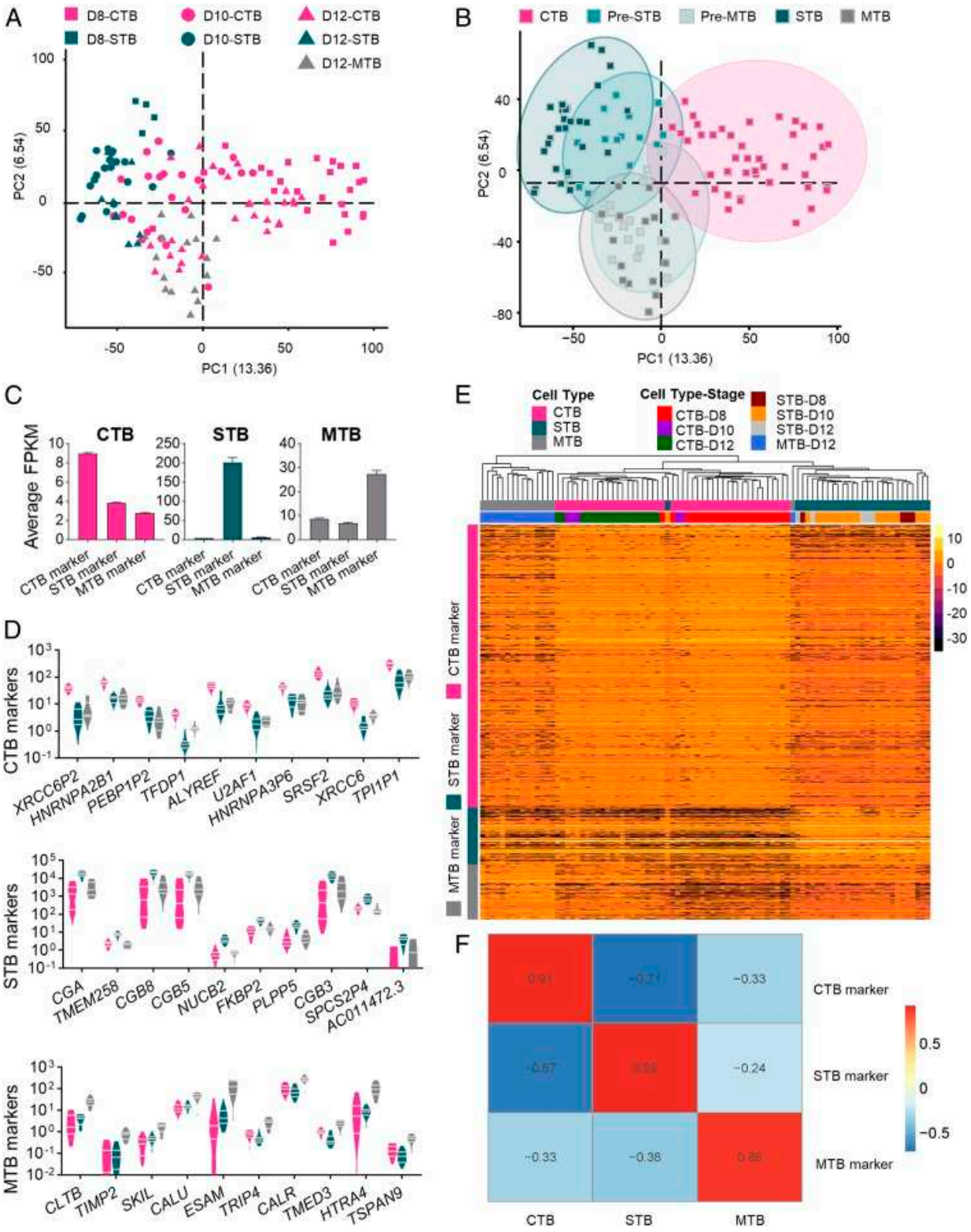
A
D8-CTB
D10-CTB
D12-CTB
D8-STB
D10-STB
D12-STB
D12-MTB
PC2 (6.54)
PC1 (13.36)
B
CTB
Pre-STB
Pre-MTB
STB
MTB
PC2 (6.54)
PC1 (13.36)
C
Average FPKM
CTB
STB
MTB
CTB marker
STB marker
MTB marker
D
CTB markers
XRCC6P2
HNRNPA2B1
PEBP1P2
TFDP1
ALYREF
U2AF1
HNRNPA3P6
SRSF2
XRCC6
TPI1P1
STB markers
CGA
TMEM258
CGB8
CGB5
NUCB2
FKBP2
PLPP5
CGB3
SPCS2P4
AC011472.3
MTB markers
CLTB
TIMP2
SKIL
CALU
ESAM
TRIP4
CALR
TMED3
HTRA4
TSPAN9
E
Cell Type
CTB
STB
MTB
Cell Type-Stage
CTB-D8
CTB-D10
CTB-D12
STB-D8
STB-D10
STB-D12
MTB-D12
CTB marker
STB marker
MTB marker
F
CTB marker
STB marker
MTB marker
CTB
STB
MTB

Figure 8.2. Identification of cell type specific markers for CTB, STB, and MTB. (*A*) PCA of trophoblast cells showing discrete clusters based on cell type. (*B*) PCA analysis reveals subsets of CTB that had partial STB and MTB signatures, classified as Pre-STB and Pre-MTB, respectively. (*C*) Average FPKM for CTB, STB, and MTB marker gene expression in each cell type. (*D*) Expression, based on least likelihood of false discovery of the top 10 marker genes for CTB, STB, and MTB in each cell type. (*E*) Hierarchical clustering analysis of cell type marker genes in trophoblast cells. These 3 panels of marker genes clearly partitioned each major TE cell type. Three panels of marker genes specifically for CTB, STB, and MTB are presented in the *y* axis, and cell types with different developmental stages are presented in the *x* axis. The color spectrum, ranging from yellow to black, indicates high to low normalized levels of gene expression. (*F*) Spearman correlation map indicating strong correlations between each cell type and their marker genes. The color spectrum, ranging from red to blue, indicates the correlation from high to low.

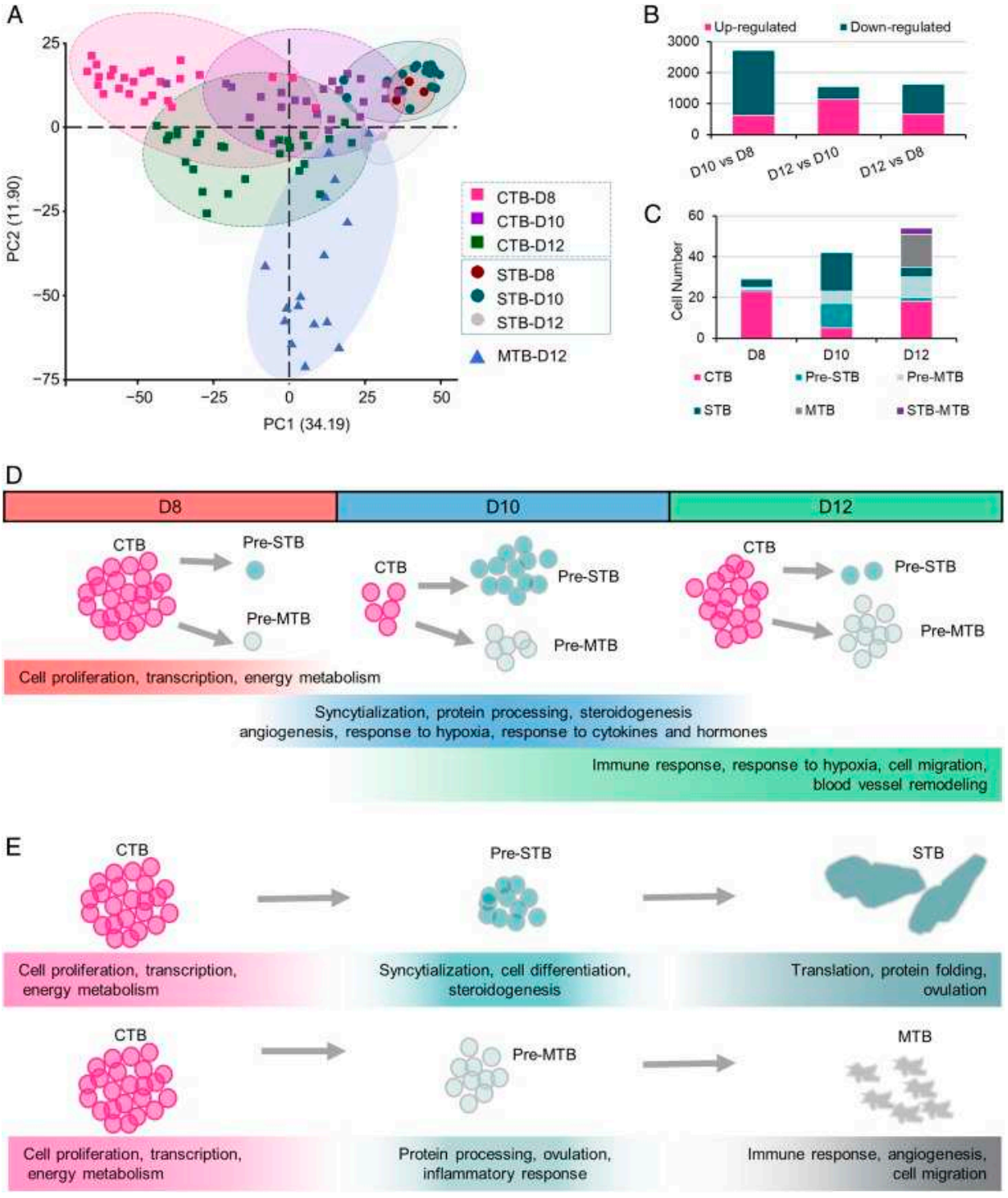
A
PC2 (11.90)
PC1 (34.19)
CTB-D8
CTB-D10
CTB-D12
STB-D8
STB-D10
STB-D12
MTB-D12
B
Up-regulated
Down-regulated
D10 vs D8
D12 vs D10
D12 vs D8
C
Cell Number
D8
D10
D12
CTB
Pre-STB
Pre-MTB
STB
MTB
STB-MTB
D
D8
D10
D12
CTB
Pre-STB
Pre-MTB
Cell proliferation, transcription, energy metabolism
Syncytialization, protein processing, steroidogenesis
angiogenesis, response to hypoxia, response to cytokines and hormones
Immune response, response to hypoxia, cell migration,
blood vessel remodeling
E
CTB
Pre-STB
STB
Cell proliferation, transcription,
energy metabolism
Syncytialization, cell differentiation,
steroidogenesis
Translation, protein folding,
ovulation
CTB
Pre-MTB
MTB
Cell proliferation, transcription,
energy metabolism
Protein processing, ovulation,
inflammatory response
Immune response, angiogenesis,
cell migration

Figure 8.3. Dynamics of CTB differentiation. (*A*) PCA of trophoblast cells clustered by cell type and developmental stages. Data suggest that CTB cells are considerably more dynamic than STB in different developmental stages. (*B*) Numbers of differentially expressed genes in CTB from different developmental stages. (*C*) The number of cells in each cell type collected at different developmental stages. (*D*) Diagram to illustrate the switch of cell functions of CTB at different developmental stages as revealed by GO terms and pathway analysis. (*E*) Diagram to illustrate the switch of cell functions of CTB as they undergo differentiation to STB (*Upper*) and MTB (*Lower*) as revealed by GO terms and pathway analysis.

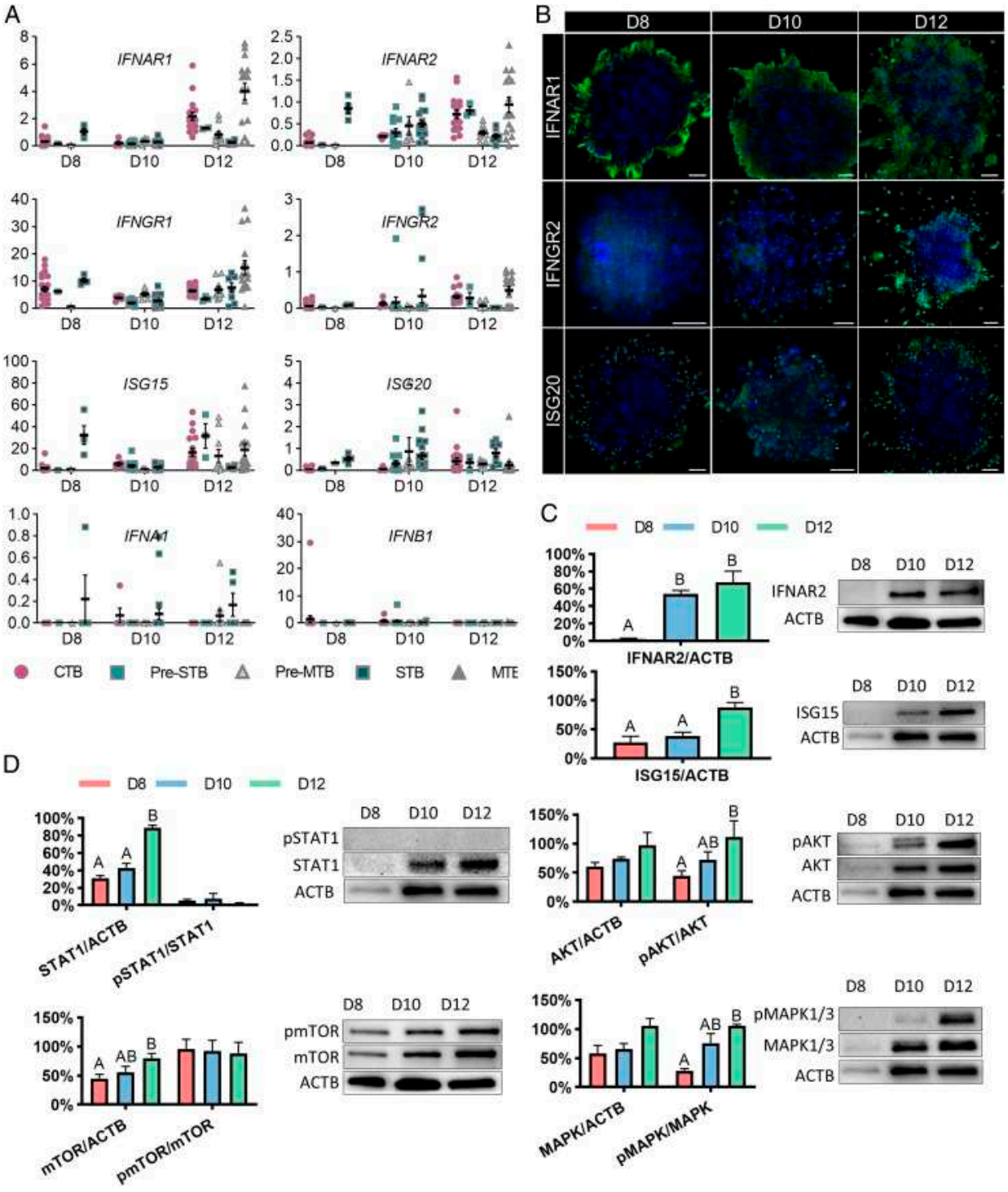

Figure 8.4. IFN response pathways in early pregnancy. (*A*) FPKM values of the IFN-related genes: type I and type II IFN receptors (IFNAR1, IFNAR2, IFNGR1, and IFNGR2), type I IFN (IFNA1 and IFNB1), and IFN-stimulated genes (ISG15 and ISG20). (*B*) Immunofluorescent localization of proteins implicated in potential IFN responses in human embryos between D8 and D12 (n = 3). (Scale bar, 100 μm.) (*C*) Western blot analysis of IFNAR2 and ISG15 (n = 3) and (*D*) phosphorylation of STAT1 (n = 3), mTOR (n = 3), AKT (n = 3), and MAPK1/3 (n = 3) in

human embryos between D8 and D12. The expression of protein levels was normalized to ACTB (actin beta). The ratio of phosphorylated (p) and total protein abundance was used to determine the phosphorylation level of target proteins. All data are presented as the mean ± SEM.

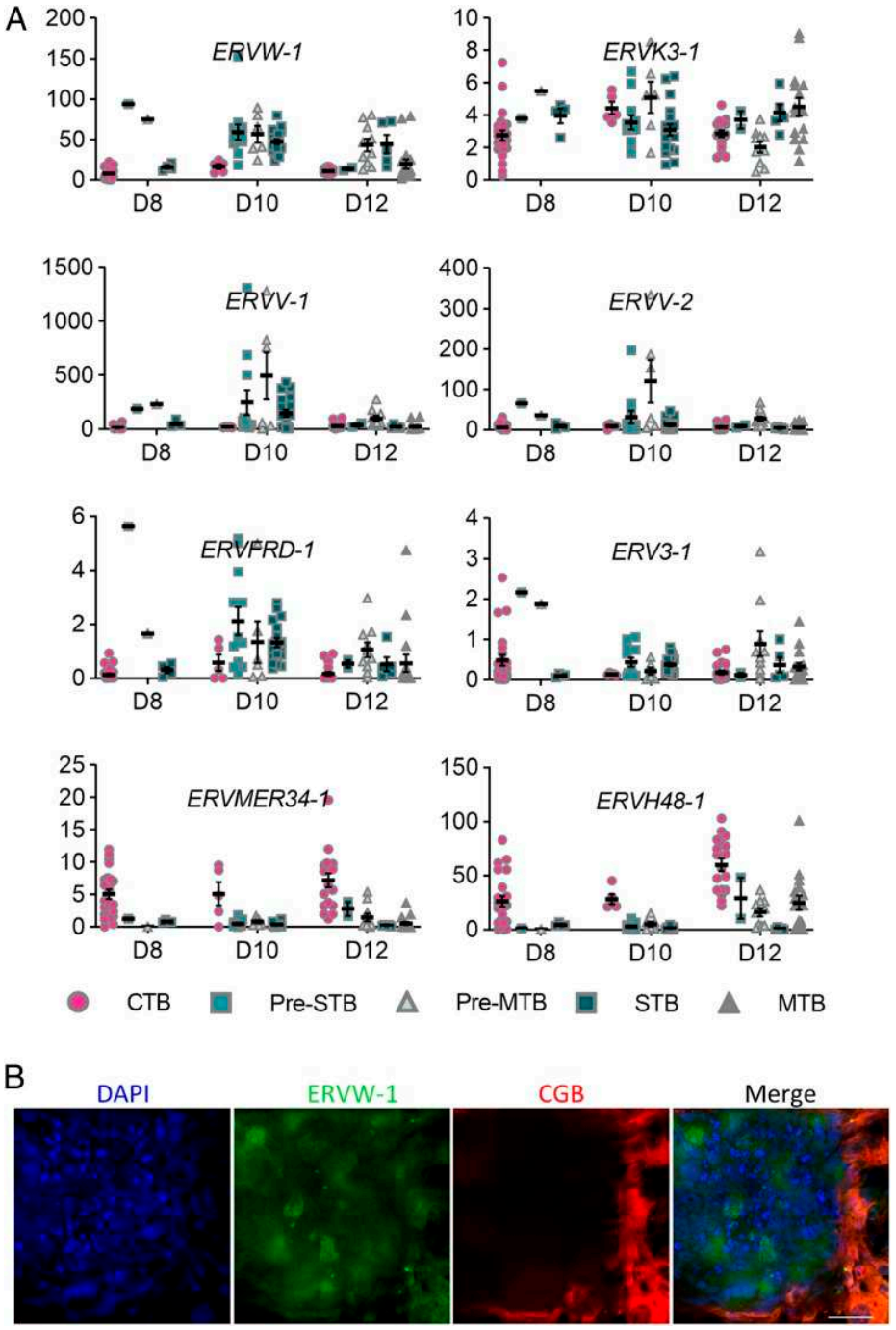

Figure 8.5. Human endogenous retroviruses in peri-implantation embryos. (*A*) FPKM values (mean ± SEM) of several *HERV* in human embryos between D8 and D12. (*B*) Immunofluorescence of ERVW-1 in D10 human embryos (*n* = 3). (Scale bar, 100 μm.)

Materials and Methods

Western blotting. Western blot analysis was used to determine the expression and phosphorylation level of target proteins. Embryos were manually removed from culture plates and washed in 0.01% polyvinyl alcohol (PVA) in PBS. Embryos were lysed in 20 µL of RIPA buffer (Sigma; #R0278) containing a phosphatase inhibitor and protease inhibitor cocktail. Lysate was mixed with 4X Laemmli buffer and incubated for 5 min at room temperature (RT) before boiling at 100°C for 10 min. Samples were cooled to RT and then analyzed on 4-20% Mini-Protean TGX Precast gels (Bio-Rad, #4561093) at 150V for 70 min. After running, protein-SDS complexes were transferred onto a PVDF membrane (Millipore; #IPVH00010) at 95V for 65 min. The membrane was then incubated in blocking buffer (3 % w/v BSA in 1X TBST) at room temperature for 1 h and probed with primary antibodies (Table S5) at a 1:5000 dilution in blocking buffer at 4°C overnight. Membranes were washed 3-4 times for 3 min in 1X TBST and incubated with corresponding secondary antibody (also at a 1:5000 dilution in blocking buffer) at RT for 1 h. Membranes were again washed 3 times in 1 X TBST then incubated in SuperSignal West Dura Chemiluminescent substrate (Thermo Scientific; #34076) for 2 min. Protein band images were captured by using ChemiDoc XRS (Bio-Rad Laboratories). Quantitative densitometry analysis was performed with ImageJ software (http://imagej.nih.gov/ij/) and expression normalized relative to actin (ACTB). The ratio of phosphorylated and total protein abundance was used to determine the phosphorylation level of target proteins. www.pnas.org/cgi/doi/10.1073/pnas.1911362116

Enzyme-Linked Immunosorbent Assay (ELISA). Medium was collected at D8, D10, and D12 and frozen at -80°C until assays (n = 5). iIFNA was measured with an Affymetrix eBiosciences ELISA kit (ThermoFisher Scientific, BMS216) according to manufacturer's directions with an Epoch Microplate spectrophotometer (BioTek) used to measure absorbance.

Endotoxin Assay. To determine if embryo culture medium had been contaminated by exogenous endotoxins, a Limulus ameobocyte lysate (LAL) assay was performed with the Endosafe Cartridge system (Charles River). Randomly selected samples of medium from 9 different time points were analyzed. All samples had the same (undetectable) endotoxin levels as fresh IVC1 and IVC2 medium (Table S6).

Electrochemiluminescence Assay (ECLIA). Human hCG in the embryo culture medium was measured daily with the Elecsys HCG STAT kit (Roche Diagnostics), beginning at 24 h post-attachment (embryo D7) until embryo D12. Samples (n = 13) were immediately frozen and stored at -80°C. After thawing, 10 µL aliquots were added to a biotinylated hCG antibody and another monocolonal hCG-specific antibody labeled with a ruthenium complex to create a sandwich complex. After incubating, streptavidin-coated microparticles were added to the mixture. The mixture was added to the measuring cell of the Cobas system, and results calculated. Raw results were normalized and, to account for daily medium changes, raw values were multiplied by 2. Then the previous day's measured concentration was subtracted from the value, i.e. D9 actual concentration = (D9 measure concentration x 2) – D8 concentration.
Statistical Analysis. Statistical analysis was performed with One-Way ANOVA followed by Tukey's test with the Prism8 Software (Graphpad). P-values less than 0.05 were considered likely to represent a significant difference between entities.

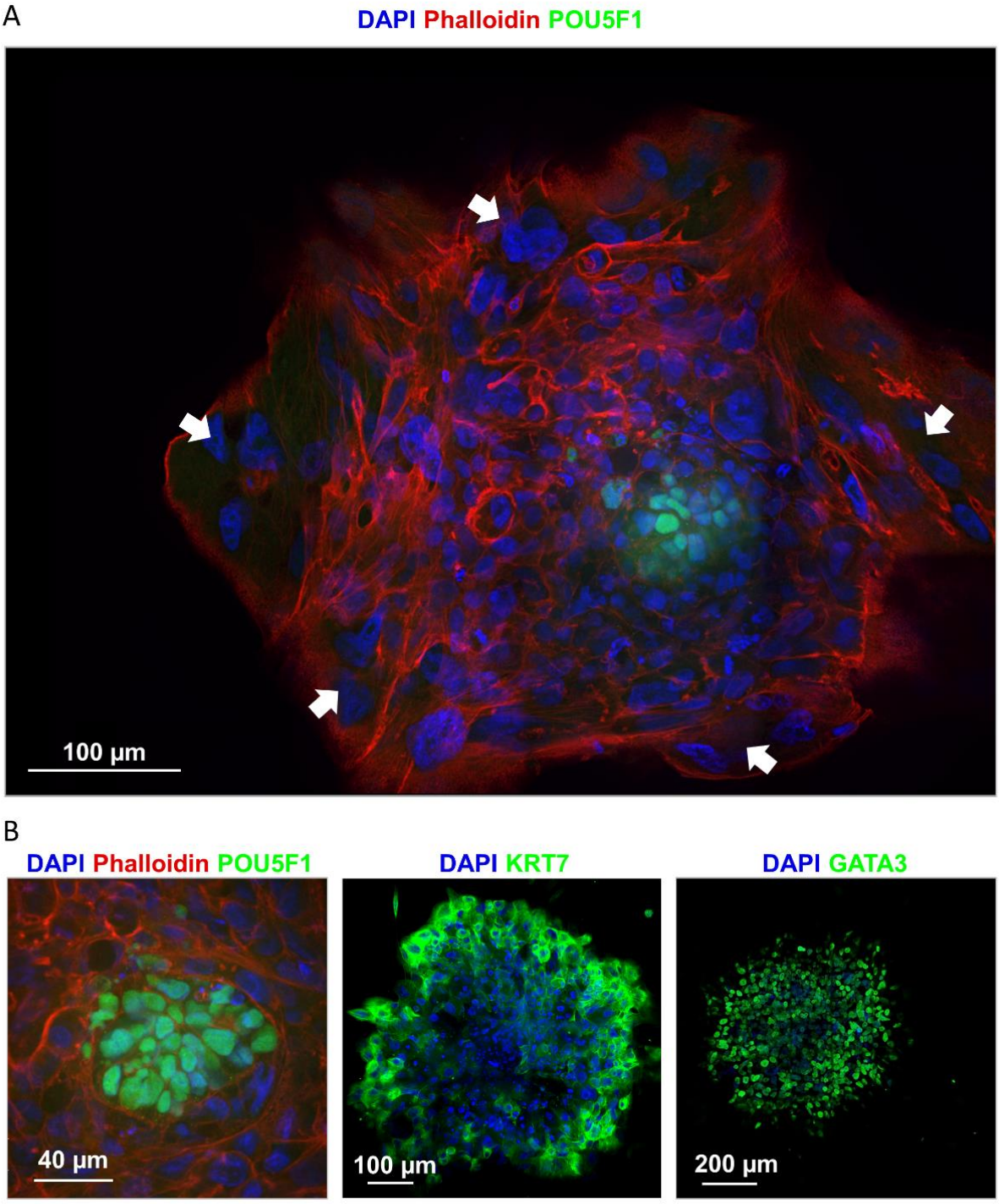

Figure 8.6. Expression of epiblast marker POU5F1, TB markers KRT7 and GATA3 in human D10 embryos. (A) A 3D montage of a D10 human embryo demonstrating the multi-nucleated syncytium located on the periphery (indicated by arrows), and POU5F1 positive epiblast cells confined to the central area of the embryo. (B) POU5F1 positive epiblast cells formed the

embryonic disc (Left panel) (experiment performed on three separate embryos); Expression of KRT7 and GATA3 in human D10 embryos (Middle and right panel, respectively) (experiment performed on three separate embryos).

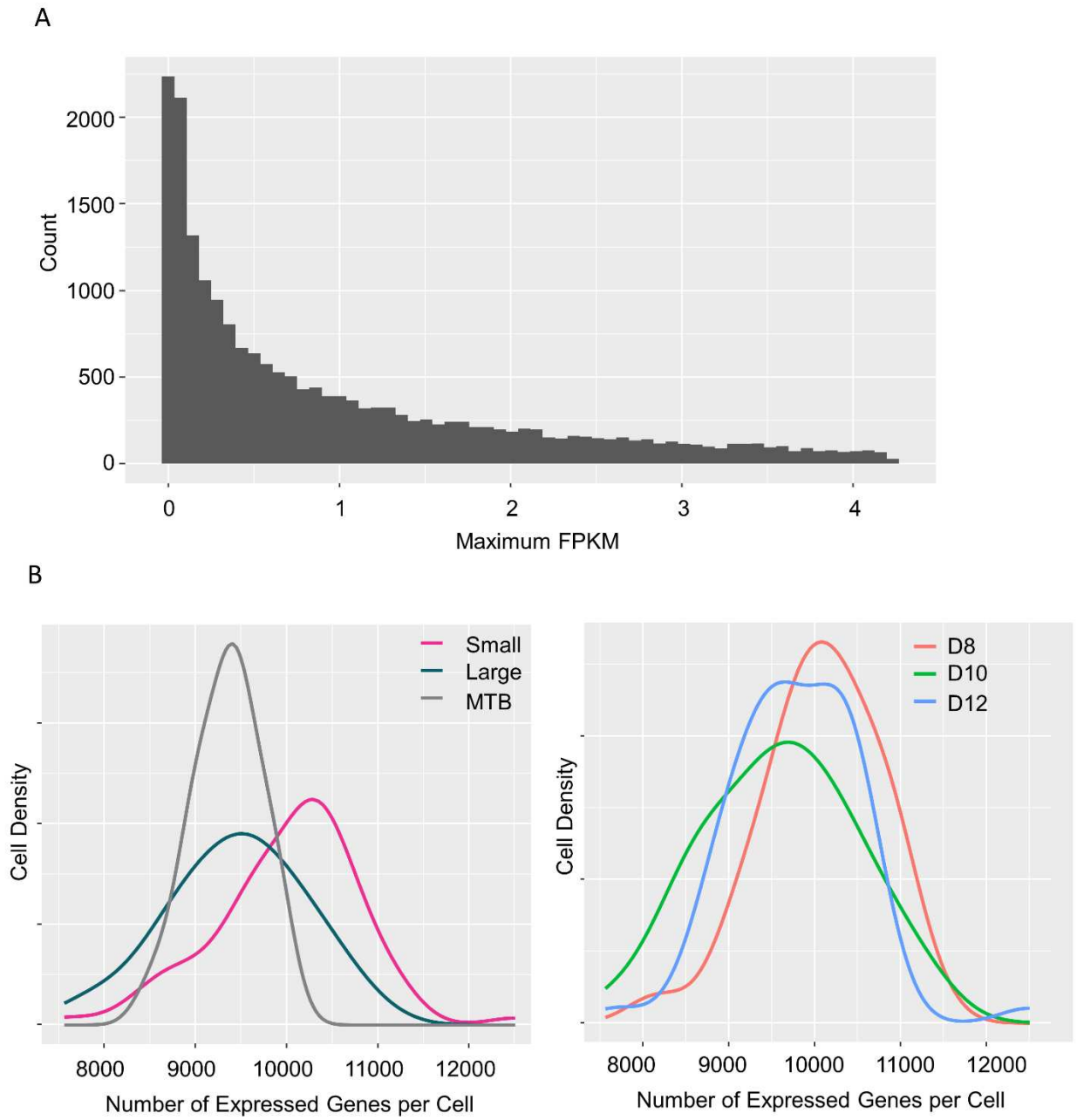

Figure 8.7. Filtration of sequencing data. (A) 14,105 genes had maximum FPKM values of at least 1, and 15,420 genes had FPKM values of at least 0.3 in at least 4 cells. Genes with FPKM values of less than 0.3 in at least 4 cells were removed from analysis. (B) CTB cells expressed more genes than STB and MTB cells. However, there was no significant increase in number of expressed genes between D8, D10, and D12.

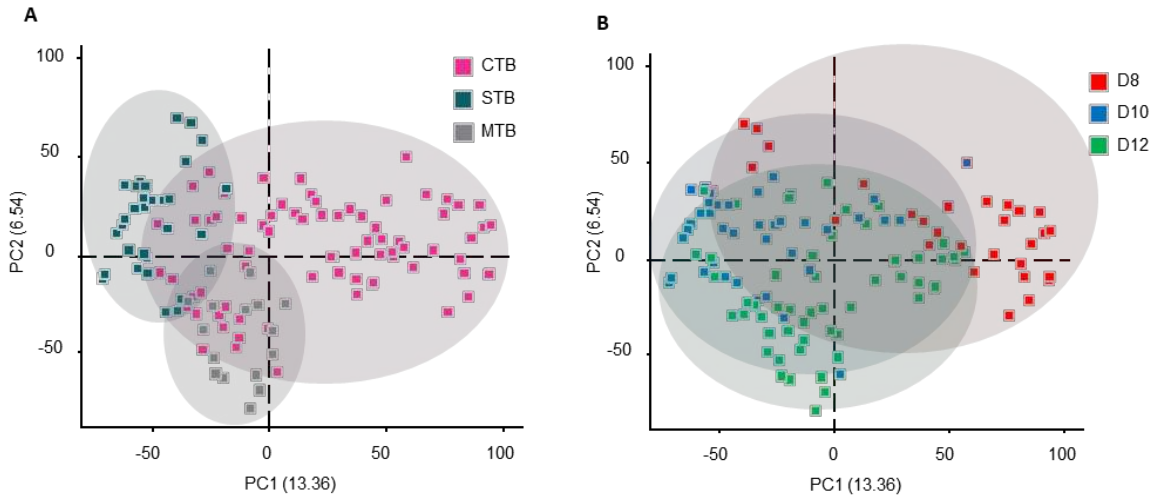

Figure 8.8. Principal component analysis of TB cells clustered by cell type (A) or developmental stage (B).

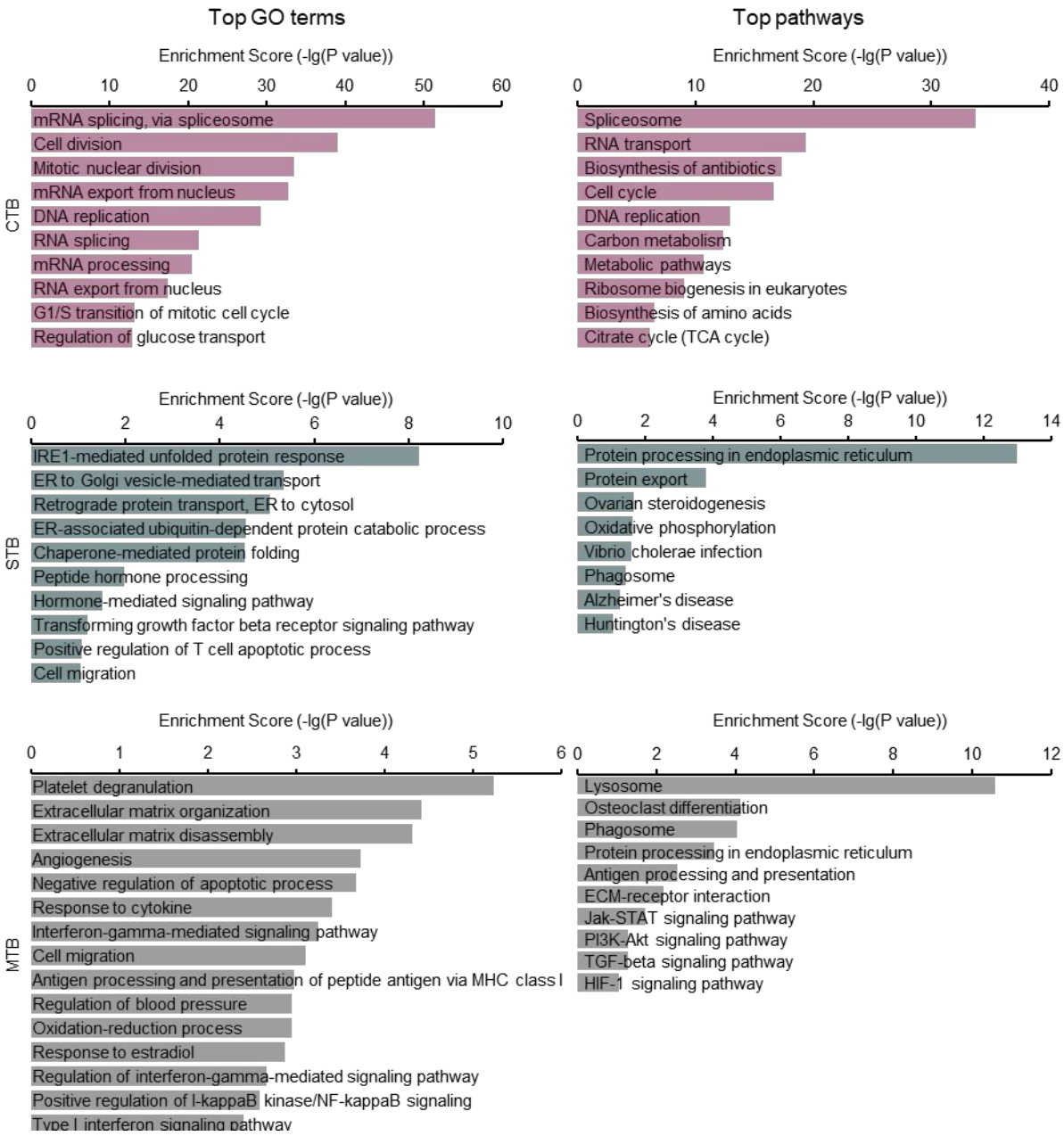

Figure 8.9. Gene ontology and pathway analysis of cell type specific genes for CTB, STB, and MTB.
Top GO terms and pathways for CTB involved cell division, RNA processing and transport, and energy metabolism. GO terms and pathways for STB involved protein folding, transport, and hormone production. GO terms and pathways for MTB revealed upregulation of genes necessary of cell migration, invasion, vasculature remodeling, and immune response.

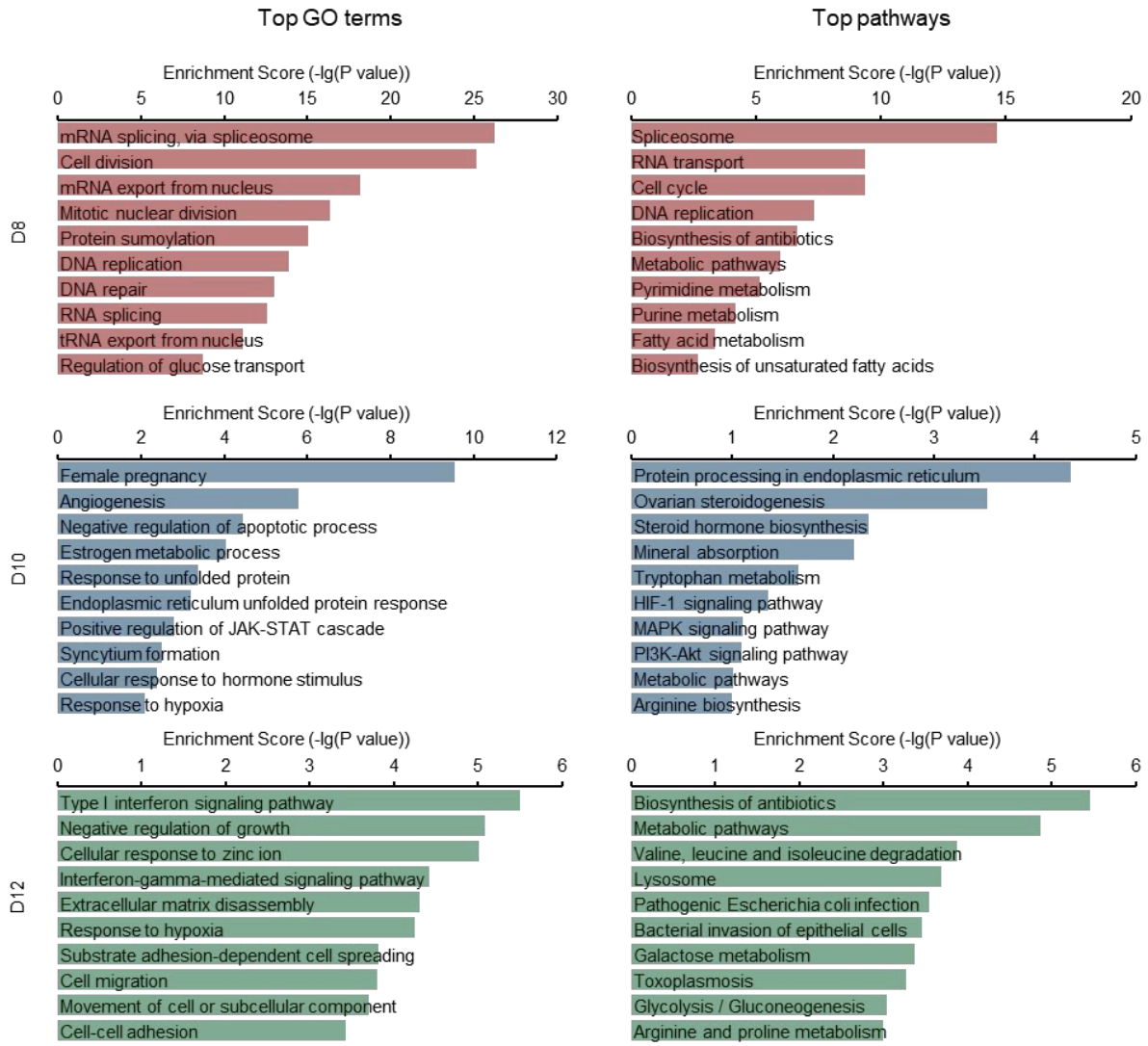

Figure 8.10. Gene ontology and pathway analysis of D8, D10, and D12 CTB. Top GO terms and pathways for D8 CTB include cell proliferation, transcription, and energy metabolism, whereas by D10, the focus had shifted to hormone production, syncytialization, and protein processing. At D12, top pathways have further shifted towards angiogenesis, hypoxia, and interferon signaling.

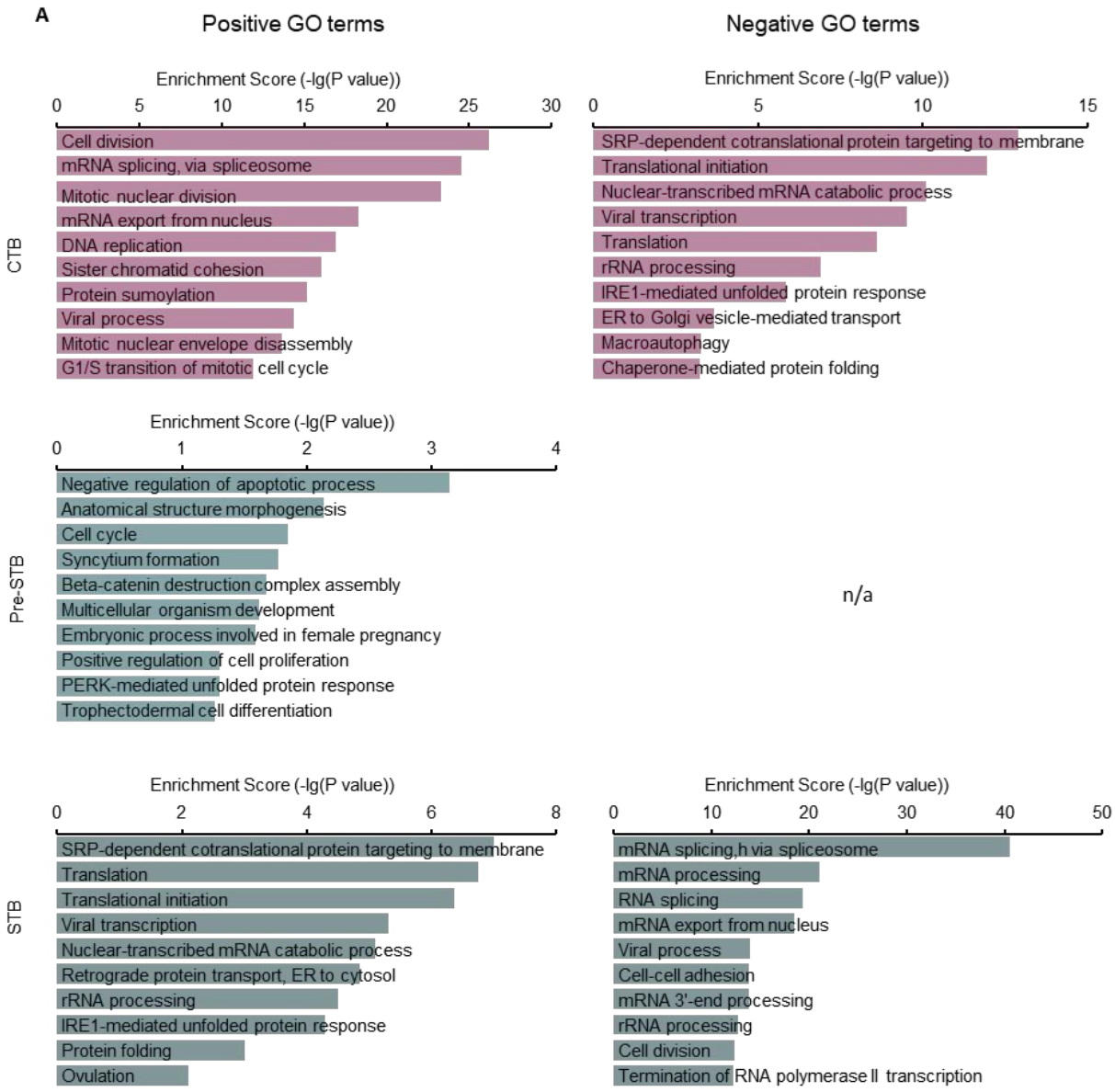

Fig. 8.11. Comparing GO terms and pathway analysis between (A) CTB, pre-STB, and STB and (B) CTB, pre-MTB, and MTB. The GO terms and pathway analysis of pre-STB cells showed a mix of CTB and STB processes. Pre-STB cells still have evidence for mitosis while also demonstrating GO terms important for STB function such as syncytium formation, cell differentiation, and protein processing. An analogous phenomenon also holds true for pre-MTB cells, since these cells have pathways linked to proliferation as well as migration and invasion, immunomodulation etc.

Table 7.1 Embryo donor age, body mass index (BMI), embryo grade and infertility diagnosis

	Age	BMI	Embryo Grade	Diagnosis
D8 E1	35	23.33	4AB	Unexplained infertility
D8 E2	32	18.2	3BB	Unexplained infertility
D8 E3	37	23.81	4AB	Secondary infertility-history of ectopic pregnancy
D8 E4	32	18.2	3BA	Unexplained infertility
D10 E1	35	20.59	3BB	Recurrent pregnancy loss - history of ectopic pregnancy
D10 E2	34	18.91	4AB	Habitual abortion
D10 E3	32	18.2	5AB	Unexplained infertility
D10 E4	41	19.76	4AA	Infertility-AMA & history of endometriosis
D12 E3	40	22.22	4BB	Advanced maternal age
D12 E4	36	27.89	3BB	Recurrent pregnancy loss
D12 E6	36	28.54	4AB	Advanced maternal age

All embryos were donated at the conclusion of completed fertility treatment with patients' informed consent.

Table 7.2 Cell sample information

	CTB	STB	MTB
D8 E1	8	0	0
D8 E2	8	0	0
D8 E3	8	4	0
D8 E4	3	0	0
D10 E1	8	3	0
D10 E2	8	11	0
D10 E3	8	0	0
D10 E4	4	6	0
D12 E3	24	0	4
D12 E4	4	6	12
D12 E6	4	6	0

Table 7.3 FPKM values of gene markers used to determine cell lineages

	Sample ID						
	D10_E3_C1	**D12_E4_C3**	**D12_E6_S6**	**D8_E3_S1**	**D8_E4_C1**	**D8_E4_C2**	**D8_E4_C3**
POU5F1	1.89	0.03	0	0.26	37.26	0	0
GATA6	0.35	0.04	0.08	0	0.28	0	0.20
KRT7	0.52	17.69	3.41	12.03	5.24	9.86	12.96
GATA3	3.40	3.98	2.16	1.70	2.86	23.25	12.00
CDX2	0	0	0	0	0	0	0
SOX2	2.39	0	0.06	0	21.03	0	0
NANOG	0.03	0.01	0.02	0.36	39.65	0.01	0.02
CD24	9.34	0.31	3.92	5.60	11.20	0.05	0.88

*'D10_E3_C1' and 'D8_E4_C1' were considered as epiblast cells and excluded from the analysis. The others were considered as TB and remained in the analysis. The Sample ID "D10_E3_C1" indicates CTB from D10 Embryo 3.

Table 7.4 Primary antibodies for immunofluorescence

Protein	**Antibody**	**Host**	**Dilution**
IFNAR1	Santa Cruz, sc-7391	Mouse	1:200
IFNGR1	Abcam, Ab200327	Rabbit	1:200
ISG15	Santa Cruz, sc-166755	Mouse	1:200
ISG20	Abcam, ab198801	Rabbit	1:200
HLA-G	Santa Cruz, sc-21799	Mouse	1:200
ERVW1	Abcam, Ab234850	Rabbit	1:200

Table 7.5 Sources of primary antibodies for Western Blotting

Protein	Antibody	Host
STAT1	Cell Signaling, #9172	Rabbit
Phospho-STAT1	Cell Signaling, #9177	Rabbit
AKT	Cell Signaling, #4691S	Rabbit
Phospho-AKT	Cell Signaling, #4060S	Rabbit
MAPK1/3	Cell Signaling, #4695S	Rabbit
Phospho-MAPK1/3	Cell Signaling, #4370S	Rabbit
HRP Anti-Rabbit IgG	Thermo Scientific, #PA1-74421	Mouse

Table 7.6 Endotoxin levels in culture medium

Medium	Concentration (EU/mL)
IVC1	0.006
IVC2	0.009
24h Post-Attachment	0.005
48h Post-Attachment	0.006
74h Post-Attachment	0.006

Table 7.7 Top 100 marker genes for CTB, STB, and MTB ranked by p-value

CTB Markers		STB Markers		MTB Markers	
gene	P-value	gene	P-value	gene	P-value
XRCC6P2	1.12E-31	CGA	1.44E-29	CLTB	1.79E-24
HNRNPA2B1	8.28E-30	TMEM258	1.61E-28	TIMP2	2.06E-22
PEBP1P2	1.03E-29	CGB8	2.32E-27	SKIL	1.35E-21
TFDP1	8.03E-29	CGB5	4.43E-27	CALU	6.63E-21
ALYREF	1.72E-28	NUCB2	2.11E-26	ESAM	9.24E-21
U2AF1	2.14E-28	FKBP2	5.34E-26	TRIP4	9.37E-21
HNRNPA3P6	2.31E-28	PLPP5	3.07E-25	CALR	1.01E-19
SRSF2	5.87E-28	CGB3	2.02E-22	TMED3	1.13E-19
XRCC6	1.02E-27	SPCS2P4	7.68E-22	HTRA4	1.22E-19
TPI1P1	1.95E-27	AC011472.3	1.37E-21	TSPAN9	1.33E-19
HNRNPA1P7	2.88E-27	POLR2K	1.81E-21	CD59	3.29E-19
RRM1	6.54E-27	DAD1	2.21E-21	LGMN	4.24E-19
YWHAQ	9.55E-27	TPT1	4.01E-21	FN1	9.34E-19
AC106795.1	1.07E-26	ZBTB8OSP2	4.45E-21	ADGRG6	2.78E-18
AC078819.1	1.20E-26	SEC11C	1.92E-20	AC011497.2	4.72E-18
HNRNPCP2	1.38E-26	SEC61B	5.2E-20	FBLN1	6.08E-18
THOC6	1.69E-26	LHB	9.97E-20	TES	1.02E-17
PGAM1	4.24E-26	CRIPT	1.06E-19	ITM2B	1.64E-17
HSPD1P4	5.55E-26	EIF1	1.69E-19	CPVL	2.07E-17
TPI1	5.61E-26	EXOSC1	2.35E-19	ZFAND5	2.13E-17
ATIC	7.91E-26	S100P	2.48E-19	SERINC1	2.40E-17
BX842568.2	1.14E-25	SAP18	2.65E-19	LAIR2	7.44E-17
ENO1	1.21E-25	MANF	3E-19	AP001189.1	1.08E-16
ENO1P1	1.30E-25	CGB7	4.02E-19	TFPI	1.69E-16
VDAC1P1	1.42E-25	TAF13	4.72E-19	DAPP1	2.70E-16
CCT4	1.68E-25	SPCS3	5.07E-19	RSU1	3.72E-16
HSPD1	2.60E-25	C12orf57	5.36E-19	CTSL	5.23E-16
TUBA1B	3.81E-25	AL139260.3	7.51E-19	MMP12	7.65E-16
KHDRBS1	4.36E-25	MCEE	9.68E-19	YIPF3	1.16E-15
MRPL38	5.69E-25	ATP5G1	1.18E-18	DAP	1.21E-15
HNRNPA1P48	6.27E-25	NDUFA3	1.23E-18	LAPTM4A	1.31E-15

CCT3	6.31E-25	PTRH2	1.24E-18	AC022306.1	1.33E-15
HSP90AB3P	7.61E-25	SAR1B	2.06E-18	COTL1	1.40E-15
HSPD1P1	8.01E-25	NDUFA6	2.22E-18	ITGA1	1.54E-15
THOC3	8.49E-25	LARP1B	4.42E-18	DHRS3	1.70E-15
CHCHD3P3	8.95E-25	CGB1	5.51E-18	SERPING1	2.00E-15
CCT7	1.42E-24	MSMB	6.86E-18	GSTK1	2.14E-15
AC245052.4	1.62E-24	CGB2	8.75E-18	ETHE1	2.50E-15
POLD2	1.68E-24	SOCS7	1.97E-17	MFAP2	2.67E-15
RNPS1P1	2.04E-24	AC012254.2	3.22E-17	MAOA	3.66E-15
ACTL6A	2.69E-24	IL20RB	4.43E-17	TRIM16	3.99E-15
TYMS	2.97E-24	MAST4-AS1	4.82E-17	MMP2	4.02E-15
CCT5	3.59E-24	SPCS2P1	5.35E-17	TSNAX	4.77E-15
TUBAP2	3.77E-24	SSR1	5.65E-17	PRDX6	5.36E-15
AC021224.1	3.89E-24	MAP1LC3B2	5.75E-17	HIST2H2BE	8.01E-15
SERBP1P1	4.45E-24	RPS11	7.03E-17	EDNRB	8.92E-15
PRMT1	4.47E-24	AP002387.1	7.33E-17	CPM	1.11E-14
HNRNPA1P10	4.92E-24	EIF2S2	8.23E-17	RALB	1.12E-14
HDAC1	7.90E-24	IFT20	1.1E-16	GALNT2	1.16E-14
HNRNPF	7.93E-24	XAGE2	1.37E-16	PROS1	1.32E-14
AC092115.1	9.69E-24	RNF181	1.65E-16	TIMP1	1.35E-14
HNRNPA1	1.01E-23	AL450306.1	1.91E-16	NDEL1	1.66E-14
CHCHD3	1.41E-23	AL513497.1	2.26E-16	ITGB1	1.77E-14
SUPT16HP1	1.67E-23	ORMDL2	2.44E-16	ANXA2P2	1.81E-14
PTMA	3.76E-23	INSL4	2.62E-16	QSOX1	1.82E-14
HSP90AB1	4.65E-23	LGALS16	3.27E-16	VGLL3	1.87E-14
CSE1L	5.50E-23	AL671710.1	3.81E-16	HM13	2.18E-14
HNRNPKP2	5.52E-23	NECTIN3	3.99E-16	MCAM	2.70E-14
CHPT1	5.54E-23	SERP1	4.41E-16	CSF2RB	2.76E-14
GLO1	7.36E-23	SSR4	4.7E-16	SEC14L1	3.25E-14
KPNA2	8.32E-23	RAD51C	6.66E-16	SNN	3.28E-14
CCT5P2	1.05E-22	FKBP11	7.42E-16	LITAF	3.67E-14
TCP1	1.21E-22	RPS24	8.21E-16	PDCD1LG2	4.80E-14
SKP2	1.34E-22	FAM120A	1.46E-15	FSTL3	5.22E-14
ZWINT	1.91E-22	UBALD2	2.34E-15	AL139002.1	5.32E-14
HNRNPAB	2.01E-22	ATPIF1	3.09E-15	JAK1	5.50E-14
LDHAP4	2.02E-22	FIBCD1	3.76E-15	ABHD8	7.00E-14
SETP14	2.48E-22	RYBP	5.27E-15	CSF2RA	7.11E-14

CCT2	5.13E-22	CBX3P9	9.75E-15	ADAMTS20	7.82E-14
NUDT15	5.22E-22	AC025259.1	1.03E-14	CFAP20	9.31E-14
PIPSL	6.14E-22	DERL2	1.11E-14	TINAGL1	1.31E-13
RNPS1	6.19E-22	AC008738.3	1.13E-14	SLC23A2	1.41E-13
EIF4A1P4	6.43E-22	SELENOK	1.16E-14	HPGD	1.43E-13
SNRPB	6.75E-22	TPT1P9	1.21E-14	ASPHD2	1.52E-13
PTMAP2	8.46E-22	BOLA2B	1.23E-14	ITGB1P1	1.55E-13
NCL	9.45E-22	BOLA2	1.89E-14	HLA-E	1.82E-13
HNRNPD	1.00E-21	MALAT1	1.92E-14	EVA1A	1.92E-13
XRCC5	1.17E-21	AP005019.1	2.13E-14	GNPTG	2.07E-13
ZNF511	1.49E-21	COX5B	2.34E-14	PDXK	3.24E-13
SERBP1P6	1.91E-21	AL392046.2	2.5E-14	CHPF	3.88E-13
UBE2I	1.99E-21	RPS25	3.33E-14	RNF24	4.23E-13
G3BP1	2.14E-21	MT-ND4	4.4E-14	GLRX	4.94E-13
KLHDC3	2.24E-21	AC008687.1	4.61E-14	LIPA	4.95E-13
ICMT	2.57E-21	AL158206.1	5.12E-14	IFNAR1	5.34E-13
NONO	2.79E-21	MUCL1	5.37E-14	P4HB	5.40E-13
HNRNPRP1	3.70E-21	LGALS13	5.55E-14	CD46	5.46E-13
ADSL	3.71E-21	CAMK2N1	7.2E-14	KRT7	6.07E-13
CCT8P1	3.74E-21	USMG5	7.29E-14	MAPK3	6.36E-13
CDK2	4.25E-21	ATP2B4	8.75E-14	EVA1B	7.60E-13
PRPF40A	4.93E-21	SNORA59B	1.22E-13	PDIA3	1.41E-12
NAP1L4	5.82E-21	CHP1	1.72E-13	SH3BGRL3	1.45E-12
CCNE1	5.83E-21	C6orf203	2.21E-13	GNG4	1.56E-12
DDX39A	7.41E-21	MT-ND1	2.96E-13	TMEM87B	1.73E-12
AC009948.2	8.17E-21	AP003068.1	3.36E-13	TNFRSF25	1.92E-12
TRIP13	9.84E-21	NCF4-AS1	3.55E-13	JPT1	1.98E-12
ANP32E	1.05E-20	MRPL57	3.96E-13	AL365203.2	2.10E-12
LDHAP5	1.12E-20	ZBTB8OS	4.16E-13	TMC6	2.34E-12
HNRNPKP4	1.16E-20	AC145285.2	4.21E-13	RHOBTB3	2.56E-12

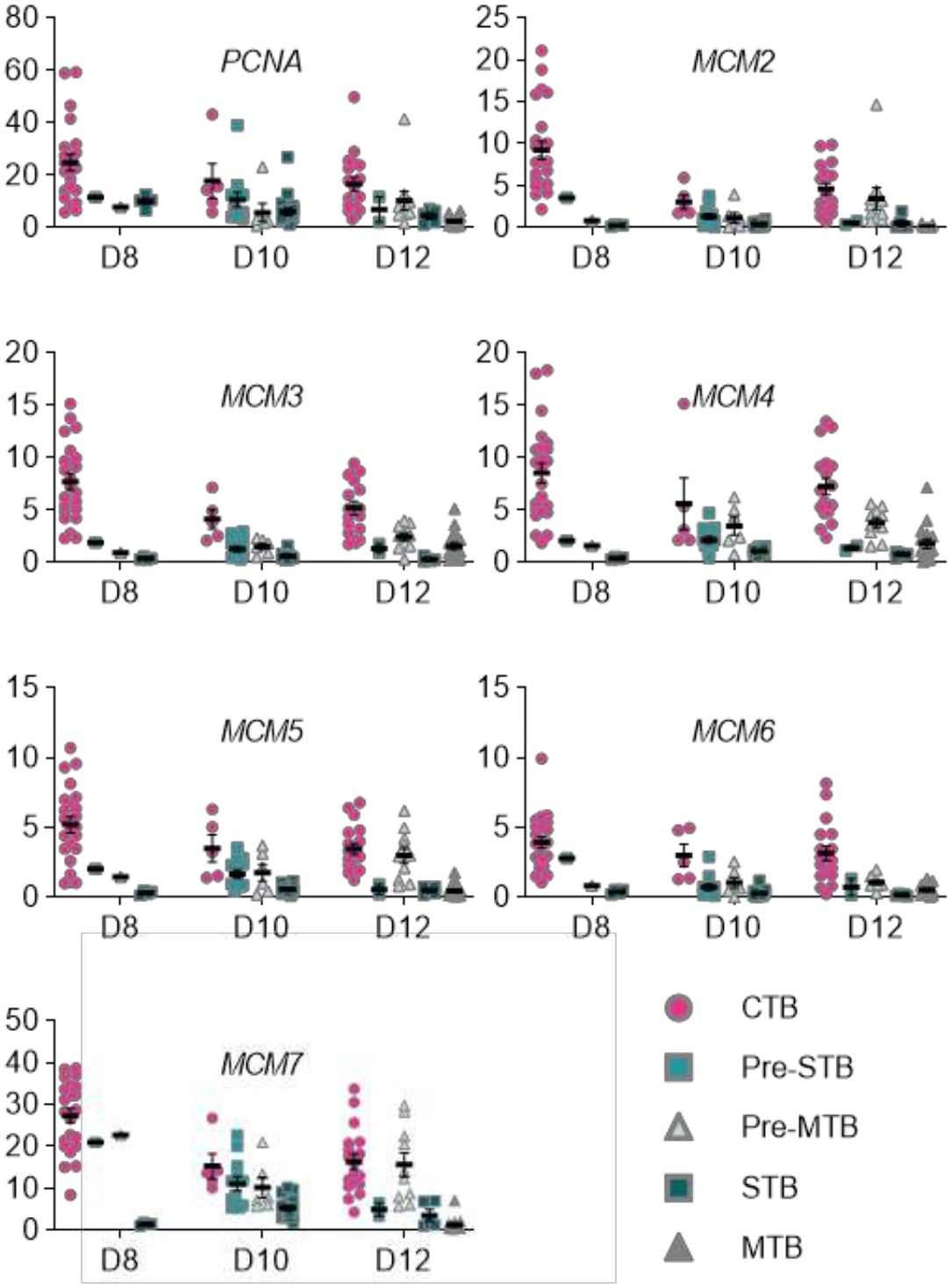

Figure 8.12. FPKM values of the cell proliferation marker *PCNA* and *MCM* genes in different sub-types of early TB cells.

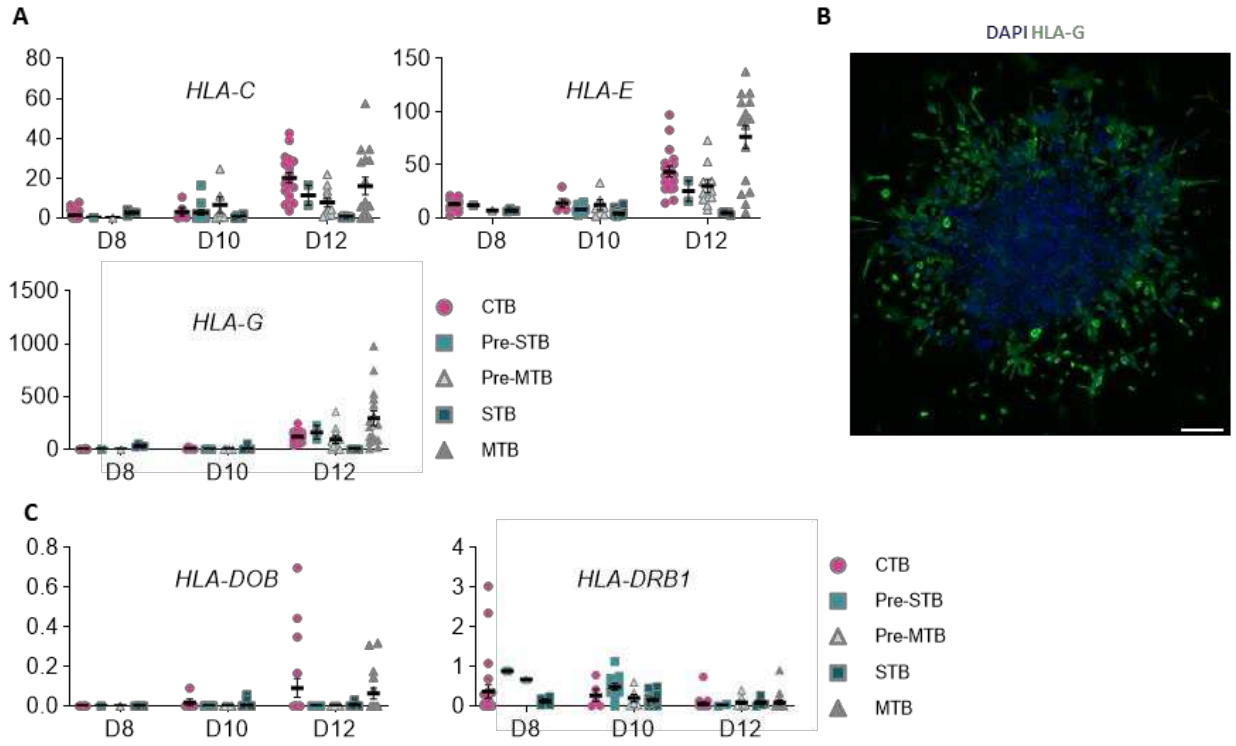

Figure 8.13. (A) FPKM values of MHC class I genes (*HLA-C, HLA-E* and *HLA-G*) in human embryos between D8 and D12. (B) Immunofluorescence of HLA-G in D12 human embryos (n=3). HLA-G is exclusively expressed in cells located on the periphery of the D12 embryo. (C) FPKM values of MHC class II genes (*HLA-DOB* and *HLA-DRB1*) in human embryos between D8 and D12.

REFERENCES

1. Jarvis G. E., Early embryo mortality in natural human reproduction: What the data say. *F1000 Res.* **5**, 2765 (2016).

2. Macklon N. S., Geraedts J. P., Fauser B. C., Conception to ongoing pregnancy: The 'black box' of early pregnancy loss. *Hum. Reprod. Update* **8**, 333–343 (2002).

3. Carter A. M., Animal models of human placentation–A review. *Placenta* **28** (suppl. A), S41–S47 (2007).

4. Enders A. C., Trophoblast-uterine interactions in the first days of implantation: Models for the study of implantation events in the human. *Semin. Reprod. Med.* **18**, 255–263 (2000).

5. Hertig A. T., Rock J., Adams E. C., A description of 34 human ova within the first 17 days of development. *Am. J. Anat.* **98**, 435–493 (1956).

6. Boyd J. D., Hamilton W. J., *The Human Placenta* (Heffer & Sons, Cambridge, 1970).

7. Amoroso E., "Placentation" in *Marshall's Physiology of Reproduction*, Parkes A., Ed. (Little Brown & Co., Boston, 1952), **vol. 2**, pp. 127–311.

8. Enders A. C., Trophoblast differentiation during the transition from trophoblastic plate to lacunar stage of implantation in the rhesus monkey and human. *Am. J. Anat.* **186**, 85–98 (1989).

9. Enders A. C., King B. F., Early stages of trophoblastic invasion of the maternal vascular system during implantation in the macaque and baboon. *Am. J. Anat.* **192**, 329–346 (1991).

10. Enders A. C., Lantz K. C., Peterson P. E., Hendrickx A. G., From blastocyst to placenta: The morphology of implantation in the baboon. *Hum. Reprod. Update* **3**, 561–573 (1997).

11. Hustin J., Schaaps J. P., Echographic [corrected] and anatomic studies of the maternotrophoblastic border during the first trimester of pregnancy. *Am. J. Obstet. Gynecol.* **157**, 162–168 (1987).

12. Foidart J. M., Hustin J., Dubois M., Schaaps J. P., The human placenta becomes haemochorial at the 13th week of pregnancy. *Int. J. Dev. Biol.* **36**, 451–453 (1992).

13. Burton G. J., Jauniaux E., Watson A. L., Maternal arterial connections to the placental intervillous space during the first trimester of human pregnancy: The Boyd collection revisited. *Am. J. Obstet. Gynecol.* **181**, 718–724 (1999).

14. James J. L., Carter A. M., Chamley L. W., Human placentation from nidation to 5 weeks of gestation. Part I: What do we know about formative placental development following implantation? *Placenta* **33**, 327–334 (2012).

15. Xu R. H., et al., BMP4 initiates human embryonic stem cell differentiation to trophoblast. *Nat. Biotechnol.* **20**, 1261–1264 (2002).

16. Yabe S., et al., Comparison of syncytiotrophoblast generated from human embryonic stem cells and from term placentas. *Proc. Natl. Acad. Sci. U.S.A.* **113**, E2598–E2607 (2016).

17. Okae H., et al., Derivation of human trophoblast stem cells. *Cell Stem Cell* **22**, 50–63.e6 (2018).

18. Haider S., et al., Self-renewing trophoblast organoids recapitulate the developmental program of the early human placenta. *Stem Cell Reports* **11**, 537–551 (2018).

19. Turco M. Y., et al., Trophoblast organoids as a model for maternal-fetal interactions during human placentation. *Nature* **564**, 263–267 (2018).

20. Deglincerti A., et al., Self-organization of the in vitro attached human embryo. *Nature* **533**, 251–254 (2016).

21. Shahbazi M. N., et al., Self-organization of the human embryo in the absence of maternal tissues. *Nat. Cell Biol.* **18**, 700–708 (2016).

22. Yan L., et al., Single-cell RNA-seq profiling of human preimplantation embryos and embryonic stem cells. *Nat. Struct. Mol. Biol.* **20**, 1131–1139 (2013).

23. Blakeley P., et al., Defining the three cell lineages of the human blastocyst by single-cell RNA-seq. *Development* **142**, 3613 (2015). Erratum in: *Development* 142, 3151–3165 (2015).

24. Petropoulos S., et al., Single-cell RNA-seq reveals lineage and X chromosome dynamics in human preimplantation embryos. *Cell* **165**, 1012–1026 (2016).

25. Knöfler M., Pollheimer J., Human placental trophoblast invasion and differentiation: A particular focus on Wnt signaling. *Front. Genet.* **4**, 190 (2013).

26. Tye B. K., MCM proteins in DNA replication. *Annu. Rev. Biochem.* **68**, 649–686 (1999).

27. Kelman Z., PCNA: Structure, functions and interactions. *Oncogene* **14**, 629–640 (1997).

28. Platanias L. C., Mechanisms of type-I- and type-II-interferon-mediated signalling. *Nat. Rev. Immunol.* **5**, 375–386 (2005).

29. de Parseval N., Lazar V., Casella J. F., Benit L., Heidmann T., Survey of human genes of retroviral origin: Identification and transcriptome of the genes with coding capacity for complete envelope proteins. *J. Virol.* **77**, 10414–10422 (2003). [

30. Johnson P. M., Lyden T. W., Mwenda J. M., Endogenous retroviral expression in the human placenta. *Am. J. Reprod. Immunol.* **23**, 115–120 (1990).

31. Rote N. S., Chakrabarti S., Stetzer B. P., The role of human endogenous retroviruses in trophoblast differentiation and placental development. *Placenta* **25**, 673–683 (2004).

32. Sugimoto J., Sugimoto M., Bernstein H., Jinno Y., Schust D., A novel human endogenous retroviral protein inhibits cell-cell fusion. *Sci. Rep.* **3**, 1462 (2013).

33. Jain A., Ezashi T., Roberts R. M., Tuteja G., Deciphering transcriptional regulation in human embryonic stem cells specified towards a trophoblast fate. *Sci. Rep.* **7**, 17257 (2017).

34. La Bonnardière C., et al., Production of two species of interferon by Large White and Meishan pig conceptuses during the peri-attachment period. *J. Reprod. Fertil.* **91**, 469–478 (1991).

35. Imakawa K., et al., Interferon-like sequence of ovine trophoblast protein secreted by embryonic trophectoderm. *Nature* **330**, 377–379 (1987).

36. Roberts R. M., Chen Y., Ezashi T., Walker A. M., Interferons and the maternal-conceptus dialog in mammals. *Semin. Cell Dev. Biol.* **19**, 170–177 (2008).

37. Inagaki N., et al., Analysis of intra-uterine cytokine concentration and matrix-metalloproteinase activity in women with recurrent failed embryo transfer. *Hum. Reprod.* **18**, 608–615 (2003).

38. Hardy G. A., et al., Desensitization to type I interferon in HIV-1 infection correlates with markers of immune activation and disease progression. *Blood* **113**, 5497–5505 (2009).
39. Apps R., et al., Human leucocyte antigen (HLA) expression of primary trophoblast cells and placental cell lines, determined using single antigen beads to characterize allotype specificities of anti-HLA antibodies. *Immunology* **127**, 26–39 (2009).
40. Murphy S. P., Choi J. C., Holtz R., Regulation of major histocompatibility complex class II gene expression in trophoblast cells. *Reprod. Biol. Endocrinol.* **2**, 52 (2004).
41. Holtan S. G., Creedon D. J., Haluska P., Markovic S. N., Cancer and pregnancy: Parallels in growth, invasion, and immune modulation and implications for cancer therapeutic agents. *Mayo Clin. Proc.* **84**, 985–1000 (2009).
42. Zhang B., et al., Effect of substrate topography and chemistry on human mesenchymal stem cell markers: a transcriptome study. *Int. J. Stem Cells* **12**, 84–94 (2019).
43. Darnell M., Gu L., Mooney D., RNA-seq reveals diverse effects of substrate stiffness on mesenchymal stem cells. *Biomaterials*. **181**, 182–188 (2018).
44. Fasano G., et al., A randomized controlled trial comparing two vitrification methods versus slow-freezing for cryopreservation of human cleavage stage embryos. *J. Assist. Reprod. Genet.* **31**, 241–247 (2014).
45. Jiang Z., et al., Transcriptional profiles of bovine in vivo pre-implantation development. *BMC Genomics* **15**, 756 (2014).

APPENDIX IV: SINGLE CELL COLLECTION OF TROPHOBLAST CELLS FROM PERI-IMPLANTATION HUMAN EMBRYOS

This work was published in the Journal of Visual Experiments in June 2020

Keywords Human, Embryo, Peri-implantation, Extended Culture, Single Cell Digestion

Summary

Here, we describe a method for warming vitrified human blastocysts, culturing them through the implantation period in vitro, digesting them into single cells and collecting early trophoblast cells for further investigation.

Human implantation, the apposition, adhesion, and invasion of the blastocyst into the maternal decidua, is a critical yet enigmatic biological event that has been historically difficult to study due to technical and ethical limitations. Implantation is initiated by the development of the trophectoderm to early trophoblast (TB) and subsequent differentiation into distinct TB sublineages. Aberrant early TB differentiation may lead to implantation failure, placental pathologies, fetal abnormalities, and miscarriage. Recently, methods have been developed to allow human embryos to grow until day (D) 14 post fertilization in vitro in the absence of maternal tissues, a time period that encompasses the implantation period in humans. This has given researchers the opportunity to investigate human implantation and recapitulate the dynamics of TB differentiation during this critical period without confounding maternal influences, and avoiding inherent obstacles to studying early embryo differentiation events in vivo. In order to characterize different TB sublineages during implantation, we have adopted the

existing two dimensional (2D) extended culture methods and developed a procedure to enzymatically digest and isolate different types of TB cells for downstream assays. Embryos cultured in 2D conditions have a relatively flattened morphology and may be suboptimal in modeling in vivo three dimensional (3D) embryonic architectures. However, TB differentiation seems to be less affected. Different TB sublineages, including cytoTB, syncytioTB and migratory TB can be separated by size, location, and temporal emergence, and used for further characterization or experimentation. Investigation of these early TB cells may be instrumental in understanding human implantation, treating common placental pathologies, and mitigating the incidence of pregnancy loss.

Introduction

Human implantation and the emergence of the early placenta are historically difficult to investigate and remain largely unknown because human tissues are inaccessible at this stage when pregnancy is clinically undetectable. Animal models are inadequate, as human placentation has its own unique features compared to other eutherian mammals[1-4]. Obtaining pre- implantation human embryos in vitro was not possible until clinical human in vitro fertilization (IVF) was routinely practiced as a treatment for infertility in the 1980's[5]. Now, human blastocysts can be grown in vitro to allow selection of more viable embryos for transfer, as well as enable safe genetic testing. Improvement in embryo culture techniques, as well as the increasing use of IVF has yielded a large number of surplus blastocysts remaining after patient's treatment cycles have been completed. With patient consent and with certain restrictions, these blastocysts may be utilized for research studies. They have become an invaluable resource to study human implantation since the development of extended culture of peri-implantation stage human embryos was reported in 2016 6, 7. By utilizing recently developed single cell omics approaches, the access to these implantation stage human embryo tissues has offered unique opportunities to describe the molecular mechanisms that regulate this highly dynamic cell differentiation process, which were previously impossible to explore8-11.

Here, we describe the methods used in our recent publication characterizing the dynamics of trophoblast differentiation during human implantation10. This protocol includes the warming of vitrified embryos, blastocyst extended culture up to D14 post IVF, enzymatic digestion of the embryo into single cells, and cell collection for downstream assays (Fig. 9.1). This extended culture system supports peri-implantation stage human embryo development without maternal input, and recapitulates TB differentiation that appears consistent with the observations made from histological specimens many years ago12-15. During implantation, the TB population is comprised of at least two cell types: the mononucleated progenitor-like cytoTB (CTB) and the terminally differentiated, multinucleated syncytioTB (STB). Upon trypsin digestion, the CTB are small, round cells that are morphologically indistinguishable from other cell lineages (Fig. 9.2A, left panel). Separation of CTB from other cell lineages, such as epiblast and primitive endoderm, can be achieved by their distinct transcriptomic profiles revealed by single cell RNA sequencing. SyncytioTB can be easily identified as irregular shaped structures that are significantly larger than the other cell types and mainly located at the periphery of the embryo (Fig. 9.2A, middle panel; 9.2B, left panel). Migratory TB cells (MTB) are another TB sublineage found during embryo extended culture, and can be recognized as seemingly moving away from the main body of the embryo (Fig. 9.2A, right panel, 2B, right panel). Migratory TB, although expressing many of the same markers as extra villous TB (EVT), should not be referred to as EVT, since the villous structures in the placenta have not emerged at this very early stage of development. Experimentally, we are able to collect the small CTB and large STB that are easily distinguishable after embryos are digested into single cells at D8, D10, and D12 (Fig. 2A and 9.2B). Migratory TB arise at the later stages of extended embryo culture and can be collected at D12 before enzymatic digestion of the whole embryo (Fig. 9.2A and 9.2B). By phenotypically separating these three TB sublineages before single cell analysis, we are able to identify specific transcriptomic markers and define the biological role of each cell type. CytoTB are highly proliferative and act as progenitor cells in supplying the STB and MTB differentiated lineages. SyncytioTB are involved in producing placental hormones to maintain pregnancy and

may be also responsible for the embryos burrowing into the endometrium. Migratory TB have even stronger features of an invasive, migratory phenotype and are likely responsible for deeper and more extensive colonization of the uterine endometrium10. After defining the transcriptomic signature of each cell type, clustering analyses have also revealed two additional subsets of cells that were morphologically indistinguishable from CTB and had transcriptomes with features of STB and MTB, respectively10. These intermediate stage cells are likely in the process of differentiating from CTB to either the MTB or STB sublineages, and would have been overlooked if embryos were blindly digested and cells were separated by transcriptome alone.

The protocol described here utilizes a 2D culture system and may not be optimal for supporting 3D structural development, as suggested by a recent publication describing a newly developed three-dimensional culture system11. Nevertheless, in this 2D system the differentiation of early TB seems to be consistent with observations made from in vivo specimens12-15. This protocol may also be easily adapted for use in the recently described 3D culture system11 with minimal changes.

Protocol

NOTE: all subsequent steps should be carried out with a handheld stripper pipette with commercially available disposable tips or a mouth pipette from a finely pulled glass pipette attached to rubber tubing, a filter, and a mouthpiece.

If culturing multiple embryos, be diligent to keep embryos separate to ensure proper identities are maintained.

Ethics Statement

All human embryos have been donated with consent for use in research. Protocols for extended human embryo culture have been approved by the Western Institutional Review Board (study no. 1179872) and follow international guidelines. Any use of human embryos should be

reviewed by the appropriate ethics and governing bodies associated with the research institution using this protocol.

1. Preparation

1.1 Prepare media and recovery plates one day prior to embryo warming in a sterile laminar flow hood

1.1.1 Embryos will recover in blastocyst culture media (BM) with 10% v/v serum protein substitute (SPS). Prepare approximately 2 mL of this media.

1.1.2 Fill two center-well organ culture wash dishes with 500 µL BM with 10% v/v SPS covered with 500 µL of embryo culture grade oil.

1.1.3 In a 60 mm tissue culture dish, layer 8 mL of embryo culture oil and prepare 20 µL drops of BM with 10% v/v SPS to the bottom of the culture plate. Make 1 drop for each embryo warmed. More media, drops, and wash dishes may be made as needed.

1.1.4 Equilibrate BM with 10% v/v SPS wash dishes and recovery plate in 37 °C, 6% CO2, 5% O2.

1.1.5 Thaw IVC1 in 4 °C or on the bench top.

1.1.6 Prepare one wash dish of 500 µL IVC1 with no oil overlay. Aliquot approximately 4 mL IVC1 into a 4 mL snap cap tube.

1.1.7 Equilibrate IVC1 wash dish and small snap cap tube of IVC1 in 37 °C, 6% CO2, and atmospheric O2.

1.2 Prepare extended culture plates one day prior to embryo warming in a sterile laminar flow hood.

1.2.1 Dilute fibronectin from human serum in PBS to 30 µg/mL. 250 µL per embryo will be needed to coat the chambers.

1.2.2 Open Ibidi ibi-treat 8-well chambered coverslip package under the hood while taking care not to touch the wells. Gently pipette 250 µL of 30 µg/mL fibronectin into each well.

1.2.3 Return the lid to the chambered coverslip and place in 4 °C for 20-24 h.

1.3 Prepare extended culture plate the morning of embryo warming.

1.3.1 Retrieve chambered coverslip with fibronectin and place in laminar flow hood. Remove fibronectin mixture with a 1 ml pipetteman and discard into waste.

1.3.2 Retrieve warmed, equilibrated IVC1 media from small 4 mL snap cap tube.

1.3.3 Pipette 300 µL of equilibrated IVC1 into each well. Be careful not to let any fluid touch the lid as this will increase the risk of contamination.

1.3.4 Return the Ibidi cambered coverslip with IVC1 to incubate in 37 °C, 6% CO2, and atmospheric O2 until embryos are dezonated in step 4.

2. Warming vitrified D5 human embryos

NOTE: The following procedure follows the vitrification protocol for the Cryotop® method. Other manufacturers may have slightly different protocols according to the vitrification technology. See manufacturer's instructions for use when applicable.

2.1 Warm 3.0mL thawing solution (TS) in 35 mm dish to 37 °C. Bring 300µL dilution solution (DS) and two wells of 300 µL washing solution (WS) in a six well plate to room temperature.

2.2 Vitrified embryos should be kept under liquid nitrogen at all times. Using forceps under liquid nitrogen, carefully remove the cryo device sleeve.

NOTE: Embryos should be warmed one at a time to retain embryo identity. Multiple cryo devices may be warmed simultaneously in separate dishes if the technician is comfortable.

2.3 Quickly move the cryo device from liquid nitrogen and plunge the tip of the cryo device in TS at 37 °C. Set a timer for 1 minute and keep the cryo device submerged until the embryo detaches into the TS.

2.4 During the one-minute incubation in TS, carefully remove the cryo device and gently pick up the embryo and move to the opposite side of the TS dish.

2.5 After 1 minute, gently pick up the embryo with a small amount of TS, approximately 2 µL. Move the embryo to the bottom of the 300 µL DS well while covering the embryo in a thin layer

of TS from the pipet. Set a timer for 3 minutes and place the 6-well plate on the bench top at room temperature (RT).

2.6 After 3 minutes, pick up the embryo with a small amount of DS, approximately 2 µL, and move the embryo to the bottom of the next well containing 300 µL WS. Again, gently layer a small amount of DS from the pipette over the embryo. Set a timer for 5 minutes and return to the bench top.

2.7 After 5 minutes, pick up the embryo with minimal volume of WS and move to the top of the last well of 300 µL WS. The embryo will slowly fall and wash through the WS to the bottom. Expel any retained DS from the pipette into an empty well.

2.8 Pick up the embryo with minimal volume and return to the top of the same 300 µL well of WS. The embryo will once again fall to the bottom of the well. Set a timer for 1 minute and return the 6-well plate to the bench top.

3. Recovery of warmed embryos

3.1 One at a time, move warmed embryos into a center-well organ tissue dish containing 500 µL equilibrated blastocyst culture media with 10% v/v SPS under 500 µL of equilibrated embryo culture grade oil.

3.2 Wash embryos by picking up each embryo and moving them around to several areas in the dish while blowing out old media between moves. Pick up the embryo and move it to an individual 20 µL culture drop of equilibrated blastocyst culture media with 10% v/v SPS under oil.

3.3 Let the warmed embryos recover for 2h in an incubator at 37 °C, 6% CO_2, 5% O_2. 231

4. Zona Removal

4.1 After a 2 h recovery, assess embryos for re-expansion and take pictures of each embryo.

4.2 Move embryos individually in 500 µL of a 3-(N-morpholino)-propanesulfonic acid (MOPS)-buffered handling medium with 5% (v/v) fetal calf serum (FCS) prior to treatment with acidic Tyrode’s solution. NOTE: An in-house handling media was used but may be substituted with a commercial handling media such as those listed in the table of materials.

4.3 Move one embryo quickly through 300 µL of warmed acidic Tyrode's solution while actively watching through the microscope. The zona pellucida will visually start to dissolve. This will take approximately 5 seconds.

4.4 Immediately move the embryo with dissolving zona into 300 µL of warmed MOPS buffered medium to quench the acid Tyrode's solution.

4.5 Move the embryo with minimal volume of MOPS buffered medium into a center-well organ tissue dish containing 500 µL equilibrated blastocyst culture media with 10% v/v SPS under 500 µL of equilibrated embryo culture grade oil to wash.

4.6 Return the dezonated embryo to the 20µL recovery drop from step 2.2.

4.7 Upon visual examination following zona removal, any embryos with retained zona pellucidae may be further treated with acidic Tyrode's solution if necessary by repeating steps 3.2-3.6. Minimizing exposure to the Tyrode's solution is desired.

5. Blastocyst Extended Culture

5.1 Move the dezonated embryos individually to the wash dish with equilibrated IVC1 media from step 1.1.6. Carefully move one embryo to each well of the Ibidi chambered coverslip with equilibrated IVC1 and maintain embryo identification. This step needs to be finished as quickly as possible to minimize medium evaporation.

5.2 Return Ibidi chambered coverslip to 37 °C, 6% CO_2, atmospheric O_2 for two days.

NOTE: Be sure to thaw and equilibrate media in 37 °C, 6% CO_2, atmospheric O_2 for the media exchange 4 hours in advance.

5.3 At outgrowth day 2 (D7 post fertilization), carefully examine the attachment of embryos under the microscope and perform media exchange.

5.3.1 Note which embryo is attached to the dish before exchanging media. This can be achieved by gently tapping the plate and examine whether an embryo has been securely attached to the plate under the microscope.

5.3.2 Remove the lid and carefully remove 150 µL of IVC1 and discard while not disturbing the attached embryo. If an embryo has not yet attached to the plate, do not exchange

the media, as the serum in IVC1 will aid in embryo attachment.

5.3.3 Pipette 150 µL of equilibrated IVC2 slowly into each well and return the lid to the chambered coverslip. NOTE: The time of removing the lid from the chambered coverslip should be minimized to avoid medium evaporation.

5.4 Carefully return the chambered coverslip to the incubator without splashing any media on the lid. Repeat media exchange and attachment check every day of extended culture until embryos are ready for fixation or single cell digestion.

6. Optional Collection of Spent Media

6.1 Collection of spent media is an optional step during the exchange of culture media after D7 or any day thereafter. During step 5.3.2, rather than discarding the medium snap- freeze the 150 µL of removed IVC1 into a low-bind 0.5 mL Eppendorf tube for future analysis.

7. Optional Fixation for Immunofluorescence

7.1 Use a 200 ul pipetteman to wash embryos with 1⁄2 media exchanges of PBS three times before fixation to remove any extracellular debris. Washing away excess debris and protein will help to optimize clarity and reduce background in images obtained with immunofluorescence.

7.2 Remove all media and slowly add 200 µL of 4% paraformaldehyde in PBS to the well. The embryo will want to stick to the surface of the fluid. Multiple 150 µL washes with 4% PFA before removing all fluid will help to minimize any damage to the embryo.

7.3 Incubate the embryos in 4% PFA for 20 min for fixation.

7.4 Wash embryos three times for 10 minutes per wash with 200 µL of 0.1% v/v Tween in fresh PBS.

7.5 Hold fixed embryos in 0.1% v/v Tween in PBS at 4 °C before proceeding with the

8. Single cell digestion with Trypsin

8.1 Fresh (not fixed) embryos should be used for single cell digestion.

8.2 Wash the embryo once with 200 µL of PBS and add 200 µL TrypLE to each well. Return the chambered coverslip to the incubator for 5 minutes.

8.3 Remove the chambered coverslip from the incubator and examine the embryos under a stereoscope. Cells on the periphery of the embryo will start to retract and MTB should still be attached to the plate where they are remotely located from the embryo. Use a small pipette of finely pulled mouth pipette to pick up individual MTB before breaking apart the whole embryo. Skip ahead to step 10.1 to save migratory trophoblast cells and return to step 8.4 after step 10.3.

8.4 Use a Stripper pipette or mouth pipette to gently dissociate the embryo by aspirating up and down.

8.5 Cells will begin to dissociate from the whole embryo. Continue to gently and repeatedly aspirate the embryo using a smaller diameter pipette tip or mouth pipette until the embryo has been incubated for a total of 10 minutes in TrypLE.

9. Single cell selection and sample collection.

9.1 With minimal TrypLE, move the dissociated cells through three wash drops of 20 µL PBS + 0.1% PVP under embryo culture oil with care not to lose and cells.

9.2 After washing the cells, use a finely pulled glass pipette to select one cell. Carefully pipette the single cell into a 0.2 mL-low bind Eppendorf tube with minimal volume of PBS + 0.1% PVP.

9.3 Snap freeze single cells in LN2, and store in -80 °C for future use.

Representative Results

Healthy embryos should exhibit continued proliferation over the course of extended culture (Fig. 9.2B). Abnormal embryos will begin to retract from their outer edges and disintegrate (Fig. 9.2C).

From our experience, approximately 75% of embryos should be attached to the bottom of the fibronectin coated dish at D7 and the attachment will increase to approximately 90% by D8 in culture. The success of embryo attachment may be largely impacted by the initial quality of the blastocysts. Embryos not attached by D8 likely will not survive.

At D8 post fertilization (day 3 of extended culture), most cells in the embryos are CTB that are positive for TB marker GATA3 (Fig. 9.3A). CytoTB have already began to differentiate into multinucleated STB on the periphery of the embryo (Fig. 9.2 B, left panel, dotted line). These STB have a sheet-like appearance and stain positive for the human chorionic gonadotropin subunit beta (CGB; Fig. 9.3A, middle panel). The embryos quickly grow in size between D8 and D10, suggesting a rapid cell proliferation of CTB during this period. At D10, the formation of CGB positive MTB is at a maximum, which can be confirmed by the upsurge of hCG production at this time (Fig. 9.3B). Migratory TB also begin to emerge and migrate away from the embryo body and are stained positive for HLA-G (Fig. 9.3A, right panel). By D12, STB differentiation is in decline and MTB production becomes more prominent, suggesting a shift of emphasis from hormone production on D10 to cell migration on D12. These changes can be observed by time-lapse video obtained during this peri-implantation period. Our single cell RNA sequencing data also reflected such dynamic changes in cell function. Together, these data suggest early trophoblast differentiation and the emergence of the early placenta is a dynamic process, during which the embryo is able to prioritize highly specialized cell functions at very specific time points to achieve successful implantation.

Discussion

The development of the protocol to culture human embryos through implantation has allowed scientists to explore a previously uncharted time in development[6, 7]. Here, we use an extended culture system to culture human embryos and study early trophoblast differentiation before the formation of villous placenta. The methods described here allow us to collect different TB sublineages for use in downstream single-cell analysis. This work allows the scientific community a chance to understand this critical and enigmatic period in human development, and may open new opportunities for therapeutic treatments for miscarriage or other placental

pathologies such as pre-eclampsia, as well as provide new insights about early human development.

This protocol requires skills in quickly manipulating embryos during embryo warming, zonal removal and plating to minimize embryo stress prior to extended culture. Minimizing media evaporation and thus an increase in medium osmolality by limiting the time of exposure during media exchange is essential. Taking care to use proper aseptic technique when exchanging medium and moving dishes will help minimize contamination. Stabilizing the dish when in use to minimize any mechanical disturbance once embryos have attached is also important. Embryos that become stressed will start to recede their syncytial projections and begin to apoptose. It is also critical to avoid allowing the meniscus of the culture media to touch the surface of the embryo, and to minimize any oil in the wells. Either of these scenarios may destroy the embryo.

Culturing human embryos beyond the blastocyst stage is a rapidly evolving field. A recent study[11 i8]demonstrated that a novel culture system which contains 10% Matrigel and a medium with additional supplementation of sodium pyruvate, lactate, and ROCK inhibitor is advantageous in modeling in vivo 3D embryonic architectures and yielded significantly more viable embryos at later stage of extended culture compared to the extended culture system described here. Validation of this new system to demonstrate its reproducibility will be required. We believe the procedures described here can be adapted to this new 3D system with minor changes, and may therefore benefit the advancement in methodology in this field.

This protocol may also be adapted to allow investigation into IVF culture media optimization. We have recently shown that in mouse, embryo development during extended culture may mimic embryo transfer success with regards to fetal development[16]. Abnormally fertilized and discarded human 3PN zygotes can be cultured to blastocysts on D5 in different conditions that may then influence their development during extended culture. Donated D5 human blastocysts

may be cultured for 48 h in novel conditions before being placed into the extended culture system for performance evaluation. Routine measurements of epiblast cell number, total cell number, outgrowth area, and hCG have allowed our laboratory to better understand how different culture media conditions may better support human pre-implantation embryo development and influence their post-implantation success.

Notes

We would like to acknowledge the many patients at the Colorado Center for Reproductive Medicine (CCRM) that have graciously donated their embryos for research. We would also like to thank Karen Maruniak and the clinical laboratory at CCRM for their help in processing hCG samples, as well as Sue McCormick and her clinical IVF embryology team at CCRM for their help with embryo collection, storage, tracking, and donation. Funding was provided internally by CCRM.

Disclosures

The authors have nothing to disclose.

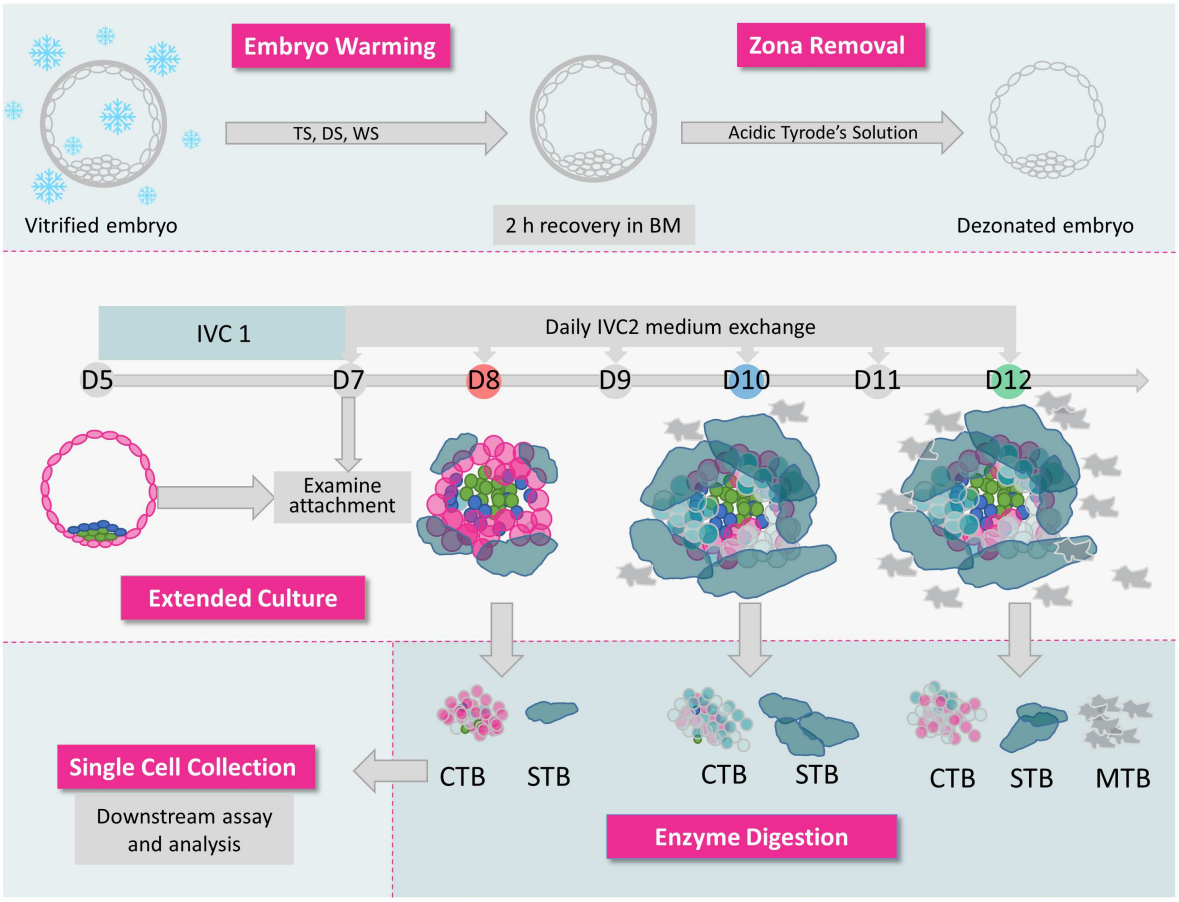

Figure 9.1. Procedural schematic of extended culture and enzymatic digestion. Workflow of warming vitrified embryos, zone pellucid removal, extended embryo culture, enzymatic digestion, and isolation of cytotrophoblast (CTB), syncytiotrophoblst (STB), and migratory trophoblast (MTB). This figure has been modified from West et al. 2019.

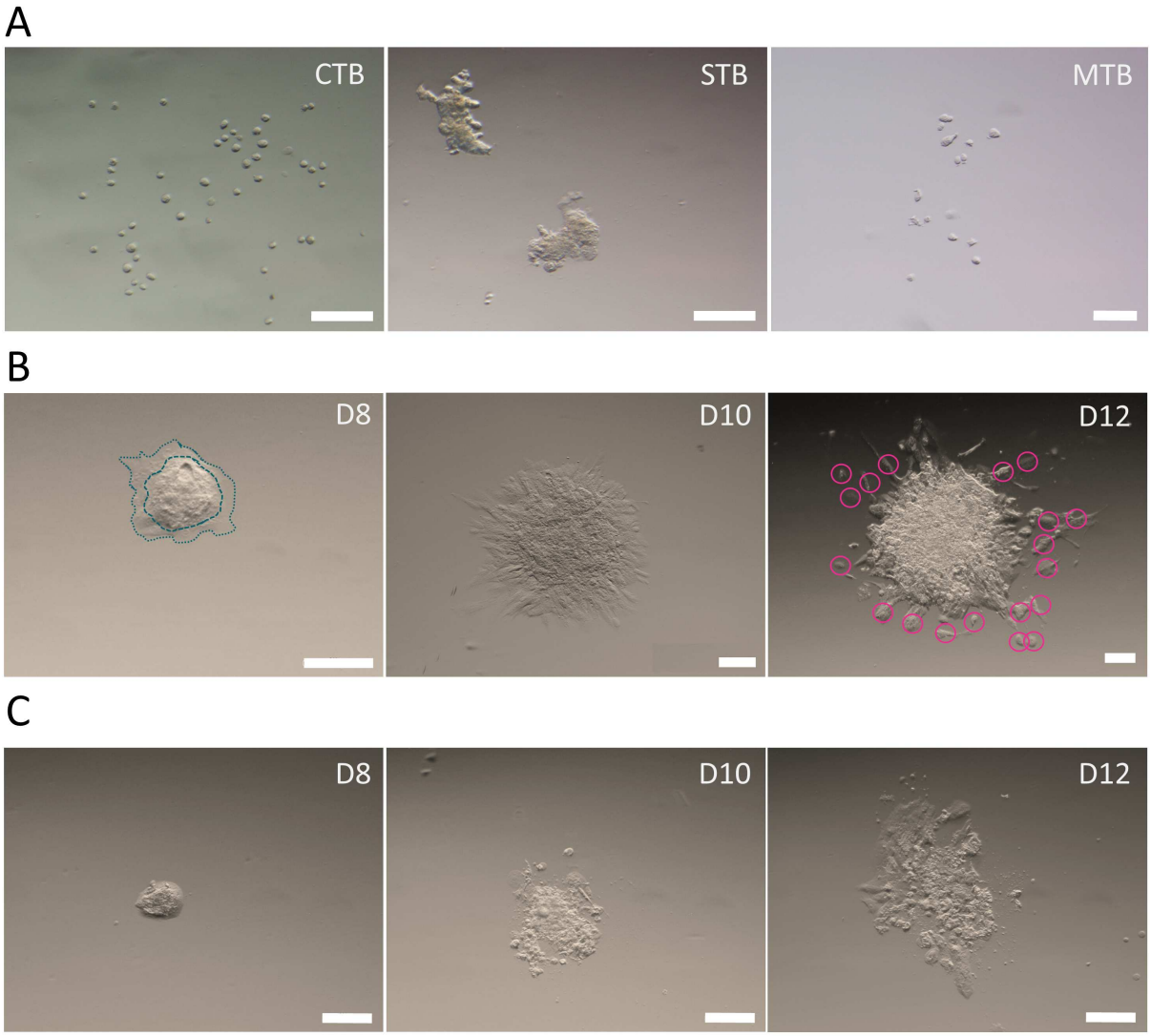

Figure 9.2. Healthy and unhealthy embryos in extended culture (A) Representative images of different cell types after enzymatic digestion with trypsin. Small CTB on the left, large syncytial in the center, and MTB on the right. Scale bars= 200 um. (B) Representative images of a healthy embryo at D8 (left), D10 (center), and D12 (right). Dashed lines in left panel outline presumably proliferative CTB population whereas dotted line outlines the flattened syncytium. Scale bars= 200 um. (C) Representative images of unhealthy embryos beginning to retract and disintegrate at D8 (left), D10 (center), and D12 (right). Scale bars= 200 um.

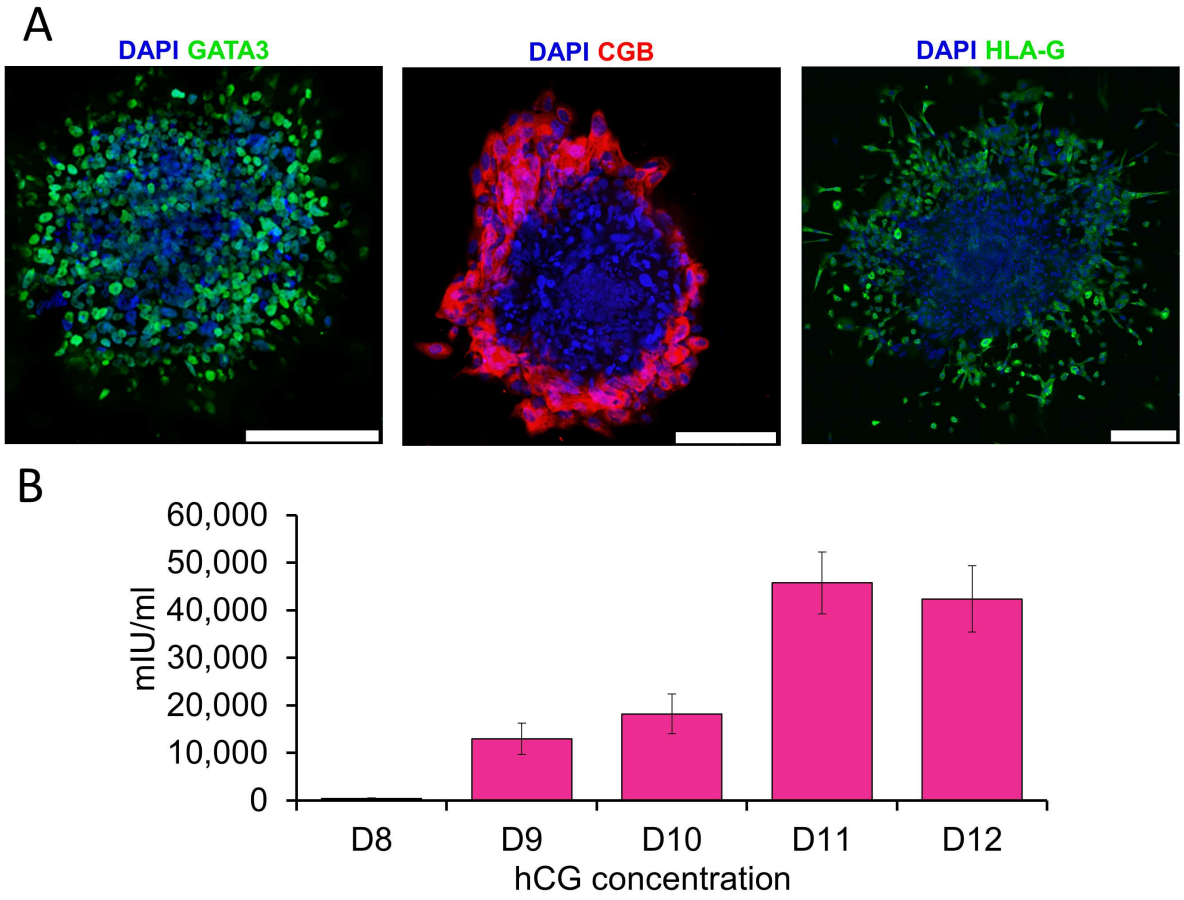

Figure 9.3. Representative images of expected development in extended culture embryos (A) Representative images of embryos showing expression of a trophoblast marker GATA3 at D10 (left), hCGB in STB at D10 (center), and a marker of MTB, HLA-G, at D12 (right). Scale bars= 200um. (B) Representative hCG concentration (mIU/mL) over the course of extended culture from D8 to D12 (mean +/- SEM). This figure has been adapted from West et al. 2019.

REFERENCES

1. Edwards, R.G., Bavister, B.D., Steptoe, P.C. Early stages of fertilization in vitro of human oocytes matured in vitro. Nature. 221 (5181) 632-635 (1969).
2. Carter, A.M. Animal models of human placentation--a review. Placenta. 28 Suppl A: S41-47 (2007).
3. Carter, A.M., Enders, A.C., Jones, C.J., Mess, A., Pfarrer, C., Pijnenborg, R. et al. Comparative placentation and animal models: patterns of trophoblast invasion -- a workshop report. Placenta 27 Suppl A: S30-33 (2006).
4. Pijnenborg, R., Robertson, W.B., Brosens, I. et al. Review article: trophoblast invasion and the establishment of haemochorial placentation in man and laboratory animals. Placenta 1981; 2: 71-91
5. Edwards, R.G., Bavister, B.D., Steptoe, P.C. Early stages of fertilization in vitro of human oocytes matured in vitro. Nature. 221 (5181) 632-635 (1969).
6. Shahbazi, M. N., Jedrusik, A., Vuoristo, S., Recher, G., Hupalowska, A., Bolton, V. et al. Self-organization of the human embryo in the absence of maternal tissues. Nature cell biology. 18 (6), 700-708 (2016).
7. Deglincerti, A., Croft, G. F., Pietila, L. N., Zernicka-Goetz, M., Siggia, E. D., Brivanlou, A. H. Self- organization of the in vitro attached human embryo. Nature. 533 (7602), 251-254 (2016).
8. Zhou, F., Wang, R., Yuan, P., Ren, Y., Mao, Y., Li, R., et al. Reconstituting the transcriptome and DNA methylome landscapes of human implantation. Nature. 572 (7771) 660-664 (2019).
9. Lv, B., An, Q., Zeng, Q., Zhang, X., Ping, L., Wang, Y., et al. Single cell RNA sequencing reveals regulatory mechanism or trophoblast ell-fate divergence in human peri-implantation conceptuses. PLoS Biology. 17 (10) art. no. e3000187 (2019).

10. West, R. C., Ming, H., Logsdon, D. M., Sun, J., Rajput, S. K., Kile, R. A., et al. Dynamics of trophoblast differentiation in peri-implantation-stage human embryos. PNAS. 116 (45) 22635-22644 (2019).
11. Xiang, L., Yin, Y., Zheng, Y., Ma, Y., Li, Y., Zhao, Z., et al. A developmental landscape of 3D-cultured human pre-gastrulation embryos. Nature. 577, 537-542 (2020).
12. Mall, F.P. Report upon the collection of human embryos at the johns hopkins university The Anatomical Record. 5 (7) 343-357 (2005).
13. Buettner, K.A., Franklin Paine Mall (1862-1917). In. Embryo Project Encyclopedia (2007). Carnegie Institution of Washington. Contributions to embryology. In. Washington, D.C.,:
14. Carnegie institution of Washington (1915).
Hertig, A.T., Rock, J., Adams, E.C. A description of 34 human ova within the first 17 days of development. Am J Anat. 98 (3) 435-493 (1956).
15. Logsdon, D. M., Ermisch, A. F., Kile, R., Schoolcraft, W. B., Krisher, R. L. Egg cylinder development during in vitro extended embryo culture predicts the post transfer developmental potential of mouse blastocysts. Journal of Assisted Reproduction and Genetics. [Epub ahead of print] (2020).

APPENDIX V: EVALUATION OF THE TMRW VAPOR PHASE CRYOSTORAGE PLATFORM USING REPRODUCTIVE SPECIMENS AND IN VITRO EXTENDED HUMAN EMBRYO CULTURE

Capsule: Cryogenic shipment, storage, and handling of reproductive specimens using novel labware and the TMRW vapor phase platform yields survival and viability results comparable to traditional storage in liquid nitrogen dewars.

Summary

Objective: To assess the impact of shipment and storage of sperm, oocytes, and blastocysts in vapor phase nitrogen compared with static storage in liquid phase nitrogen

Study Design: prospective cohort-matched study

Setting: Multiple IVF laboratories in an IVF Network

Patients/Animals: 58 human embryos, 32 human oocytes, 15 units of bovine semen

Intervention(s): Vapor vs. liquid nitrogen (LN_2)

Main Outcome Measure(s): Post-warming survival of oocytes, sperm, and blastocysts, and developmental potential of blastocysts during in vitro extended culture

Results**:** Custom designed labware, for use with the TMRW platform, enables continuous temperature monitoring during shipment and/or storage in the vapor phase robotic storage system. The highest temperature recorded for specimens shipped to a domestic lab was -180.2^{O}C with a mean of -190.4±0.5^{O}C during shipment and 181.1±0.6^{O}C during storage. Likewise, shipped internationally had a high of -180.2^{O}C with a mean of -193.5±0.6^{O}C during shipment and -181.2±0.7^{O}C during storage. Results from the extended culture assays have revealed no deleterious effect of shipment and storage in nitrogen vapor. The viability of mammalian gametes and embryos is equivalent between vapor and liquid phase storage.

Conclusion**:** The evaluated system does not have any deleterious effects on the post-warming survival of sperm, oocytes, and blastocysts. The post-warming developmental potential of

human blastocysts during in vitro extended culture was unaffected by storage and handling in the vapor phase nitrogen TMRW platform when compared with static liquid nitrogen phase storage. Our results suggest that the vapor phase cryostorage platform is a safe system to handle and store reproductive specimens for human ART.

Keywords: cryogovernance, cryostorage, assisted reproductive technology, blastocyst.

Introduction

The application of vitrification to the cryopreservation of human embryos and oocytes has corresponded with an increase in live birth rates (1, 2). Vitrification has enabled the convenient use of several technologies, such as preimplantation genetic screening for chromosome ploidy (PGT-A) or for a specific genetic disease (PGT-M), frozen donor oocyte cycles, and freeze-all cycles (1, 3-5). These technologies have improved patient care by decreasing adverse events associated with fertility treatment, specifically ovarian hyperstimulation syndrome (OHSS) and miscarriages, while simplifying donor oocyte cycles and expanding access to care (1, 2, 5, 6).

Although vitrification has improved and simplified the cryopreservation process, there is demand for increased stringency in cryogovernance; the set of protocols that ensure safe handling and storage of vitrified specimens (1). Cryogovernance guidelines give peace of mind to both in vitro fertilization (IVF) providers and patients that the risks associated with cryostorage have been minimized via appropriate storage, shipping, and inventory control (1).

Modern high efficiency vapor phase tanks, such as the Chart MVE 1500, allow for storage of specimens in the vapor phase at temperatures below -150°C (7). Similarly, shipment of reproductive specimens in a nitrogen vapor environment is common (8). Even though temperature is maintained below -150°C during shipment and storage in the vapor phase of nitrogen, current systems and processes in reproductive medicine provide for very little

proactive monitoring of environmental conditions (1). Minor temperature fluctuations occur during storage and shipment in the vapor phase of nitrogen, and the effect of these on survival and developmental potential of human oocytes and embryos is not well studied (8-10).

Vapor phase storage of gametes and embryos maximizes square footage while allowing for the application of automation to make handling safer and more efficient (Supplemental Material 1). Since the common goblet and cane configuration of reproductive specimen cryostorage is not easily adaptable to automation, TMRW has custom designed labware for the safe handling of specimens by humans and the automation of the platform. The TMRW platform consists of the Brooks BioStore™ III Cryo -190°C System including a Chart MVE 1500 series tank (7) with custom designed CryoGrids that hold RFID-enabled CryoBeacons to serve as vessels for commercially available cryodevices and cryostraws (Supplemental Material 1). These additional components were designed to make handling of specimens safer and provide for a digital chain of custody using RFID technology, while constantly providing environmental telemetry. The platform and the resulting digital chain of custody is enabled and controlled by TMRW software.

In addition to the temperature telemetry evaluation, post-warming evaluation of the viability and quality of the biological specimens is necessary to ensure the safety of any cryostorage system. Assessment of the cell viability immediately after warming is relatively easy. The damaged cells usually displayed shrinkage, membrane rupture, or loss of motility that can be assessed by morphology. However, only measuring the viability immediately post warming, though insightful, may give false-positive results (11), as damage during cryopreservation and/or cryostorage may have long-term effects on developmental potentials that cannot be evaluated at the time of warming.

Ongoing pregnancy and live birth are the gold standards to assess the success of human assisted reproductive technologies (ART). However, these measures do not allow experimental

manipulations that may pose any risks to the research participants. This can be a limitation for studies that aim to assess human embryo quality to optimize methods for in vitro manipulations, such as cryopreservation. A novel extended in vitro embryo culture system was developed to support peri-implantation stage human embryo development without maternal input (12, 13). Recently, this system was shown to predict the post-transfer developmental potential of mouse blastocysts (14). Preliminary work on human blastocysts also suggests that peri-implantation development during in vitro extended culture may reflect human blastocyst developmental potential following embryo transfer (15).

This study aims to assess the TMRW platform by evaluating temperature fluctuation, during shipping and storage with the TMRW platform, with static storage in liquid nitrogen dewars - using reproductive specimens, including oocytes, semen, and blastocysts as well as examining oocyte viability, sperm motility and blastocyst survival and developmental potential post-warming.

Materials and methods

Materials

All chemicals were purchased from Sigma-Aldrich (St. Louis, MO, USA) unless otherwise stated.

Study Setting and Design

This prospective, cohort case-controlled study was a single network, multi-site investigation of the impact of shipment and storage in the vapor phase of nitrogen using novel labware with automated handling and continuous telemetry of environmental conditions.

Oocyte and Embryo Storage and Assessment of Post-Warming Survival

All human embryos and donor oocytes used in this study were donated following completion of a consent for disposition to research and approved by WIRB (study numbers 20142468 and 1179872). A total of 58 human embryos and 32 donor oocytes were used in the study. To test the safety of the system, 30 embryos were transported and/or stored using TMRW labware, automated handling, and continuous telemetry. Five embryos and 5 units of bovine semen were shipped internationally and 5 were shipped to a second domestic location using a standard vapor phase shipping process where they were then handled and stored using traditional methods. Following storage for at least 5 days, specimens were handled and transferred to proprietary RFID labware (Fig. 10.1). Environmental telemetry was started at this time and measured each minute through return shipment and storage in the vapor phase platform under study using custom software, labware, and robotics. Additionally, 20 embryos were moved from conventional LN_2 dewars directly to the study system at the home laboratory and stored for 14 days. Matched controls (n=28) were shipped using a standard vapor phase shipping process, prior to study initiation, transferred to LN_2 dewars and were maintained in LN_2 dewars unitl assay. Post-warming survival of human blastocysts was confirmed by visualizing normal expansion after a 2-hour recovery period.

Twelve donor oocytes were transferred to custom designed labware at the home laboratory for storage in the vapor phase platform under study using custom software and robotics (Fig. 10.1). Cohort matched control oocytes (n=20) were shipped using a standard vapor phase shipping process, prior to study initiation, transferred to LN_2 dewars and were maintained in LN_2 dewars until assay. Following at least 7 days of storage, the oocytes were warmed, and post-warming survival was assessed by visually confirming the re-expansion of ooplasm and the integrity of cell membrane. Surviving oocytes were re-vitrified and returned to storage in the vapor phase TMRW platform or conventional LN_2 dewars, and a second assay of survival was performed following subsequent warming (Fig. 10.1).

Semen Storage and Sperm Motility Evaluation

Commercially available bovine semen was chosen because the specimens are well characterized, and the reproducibility of results ensured a robust assay. Following transport and storage in either the study system or in conventional vapor phase shippers and LN_2 dewars, semen samples were warmed in a 37°C water bath for 1 minute, then expelled into a 35 mm tissue culture dish without dilution. Evaluation of total sperm motility was performed by assessing the percentage of sperm that exhibit motility of any form under the microscope.

Assessment of Cell Apoptosis in Blastocysts by Cleaved Caspase-3 Staining

After warming, embryos stored and transported in the conventional dewar system (CON; n=8) or the study system (TMRW; n=10), were left to recover in 20 µL drops of Sage BM medium (Origio, Cooper Surgical, Denmark) + 20% Serum Protein Substitute (SPS, Origio, Cooper Surgical, Denmark) under oil (Spectrum, New Brunswick, NJ, USA) for 2 h in 5% O_2 and 7.5% CO_2 to maintain a medium pH between 7.2 and 7.3. Following recovery, embryos were immediately fixed using 4% paraformaldehyde (PFA, Electron Microscopy Sciences, Hatfield, PA, USA) in phosphate-buffered saline (PBS) for 20 minutes. Embryos were then washed three times in PBS + 0.1% (v/v) Tween 20 (Fisher scientific, Fair Lawn, NJ, USA) + 0.1% (w/v) polyvinyl pyrrolidone before permeabilization with 0.3% (v/v) Triton X-100 in PBS. Embryos were washed three times and moved to a blocking buffer with 0.1% Tween + 1.0% (w/v) bovine serum albumin (BSA, MP Biomedicals, Irvine, CA, USA) + 0.1 0 M glycine in PBS for 2 hours. Following the blocking step, embryos were immediately moved to primary antibodies against cleaved caspase-3 (1:200, 9661S, Cell Signaling, Danvers, MA, USA) in antibody buffer containing 0.1% (v/v) Tween 20 + 1.0% (w/v) BSA in PBS overnight at 4°C. Embryos were washed three times and moved to secondary antibody with NucBlue™ (Hoechst 33342, R37605, Life Technologies, Carlsbad, CA, USA) and Alexa Fluor 488 (1:200, A-21206, Invitrogen) in antibody buffer. After a 2-hour incubation, embryos were washed and mounted to

lysine-coated slides using 5-10 µL ProLong Diamond Antifade mountant with DAPI (P36962, Life Technologies).

Nuclei of approximately 5-10 µm with both positive staining for cleaved caspase-3 as well as granular degrading DNA were counted as one apoptotic cell. These granular nuclei were also included in the total cell nuclei count to achieve a proportion of apoptotic nuclei to the total number of nuclei.

Blastocyst Extended Culture

The method of human extended embryo culture has been previously described (14, 16). In brief, following transport and storage in either the study system or storage in LN_2 dewars, embryos were warmed using the Kitazato warming protocol (16) and left to recover for 2 hours in 20 µL drops of Sage BM medium with 10% SPS under oil in 21% O_2 and 7.5% CO_2 to maintain a medium pH between 7.2 and 7.3. Embryos were treated briefly with acidic Tyrode's solution to remove the zona pellucida and were plated for extended culture.

During extended embryo culture, embryo viability was quantified by the concentration of human chorionic gonadotropin (hCG) in the spent media from wells with attached embryos, the area of the trophectoderm outgrowth, and by the number of cells positive for pluripotency marker POU5F1 following immunoflourescent staining. Embryos were cultured in commercial IVC1/2 medium (Cell Guidance Systems, Cambridge, UK) in ibiTreat µ-Slide 8-chambered coverslips (80826 ibidi GmbH, Grafeling, Germany) coated in 30 µg/mL fibronectin from human serum in PBS. Embryos were examined for attachment to fibronectin-coated dishes, and 50% well volume was exchanged daily with IVC2 following initial inspection after 48 hours in culture. Spent media for hCG quantification was snap frozen in LN_2 and was analyzed by sandwich ELISA on a Roche cobas e601 analyzer. In addition to the collection of spent media, images were taken using an Olympus DP22 camera on a stereomicroscope for outgrowth area

measurements. All outgrowth area measurements were quantified using ImageJ software (17), which allows for the edges of the outgrowth to be traced for accurate measurement. On day 5 in extended embryo culture, embryos were fixed using 4% PFA in PBS for 20 minutes. Extended culture embryos were kept in PBS + 0.1% (v/v) Tween 20 (PBST) at 4°C until staining.

Embryo Immunofluorescence Staining and Confocal Analysis

Embryos were stained with antibodies against POU5F1 (sc-5279, Santa Cruz Biotechnology, Dallas, TX, USA), NucBlue™), and rhodamine phalloidin (Cytoskeleton, Denver, CO) to visualize the F-actin cytoskeleton. Embryos were washed in PBST and permeabilized with PBS + 0.5% (v/v) Triton X-100. Embryos were washed and held in blocking buffer containing 10% (v/v) fetal calf serum (Hyclone), 3% BSA (MP Biomedicals) and 0.1% Tween 20 in PBS overnight and subsequently moved to primary antibodies (1:200) in blocking buffer overnight. Embryos were washed and moved to secondary antibody Alexa Fluor 488 (1:200, A-11001, Invitrogen), Hoechst, and rhodamine phalloidin (1:200) in blocking buffer overnight. Embryos were washed and mounted using 5-10 µL ProLong Diamond Antifade mountant with DAPI.

Imaging experiments were performed using a 3i Marianas inverted spinning disk confocal microscope as previously described (14). Images were then analyzed for epiblast cell number using the surface tool and object identification within the surface of approximately 5-10 µM in diameter using Imaris x64 9.20 software.

Statistical Methods

Descriptive statistics of max, min, and mean ± SD were calculated for temperatures during shipment and/or storage in the TMRW platform to determine if an excursion of temperature occurred.

Assessment of binomial outcomes in extended culture embryos including attachment, normality, and presence of POU5F1 positive cells was completed using Fisher's exact test in GraphPad

Prism 8.4.2 software in place of Chi-squared analysis due to the small sample size. All continuous variables including cleaved caspase-3/DAPI ratio in blastocysts, hCG quantification from spent media, epiblast cell number, and trophectoderm outgrowth area were evaluated for normality using a Shapiro- Wilks test. Because data points were not normally distributed, a non-parametric rank- based Mann Whitney test was used to compare groups using GraphPad Prism 8.4.2 software. Significance was noted at $p<0.05$. Historical outgrowth areas from our laboratory were included in outgrowth area figures for comparison, but were not used in our statistical analysis due to the disproportionately large sample size.

Results

Platform Telemetry

No temperature reading approached the alert threshold (-160°C), the critical temperature (-150°C) set points for the study platform, or Glass Transition Temperature (T_g) during the study. A representative example of the temperature experienced by human embryos and bovine semen during shipment and storage in the TMRW platform is presented in Fig. 10.2. Summary statistics for all specimens during the shipment and storage portions of this study are listed in

Table 8. Temperature means (±SD) during shipment of embryos and semen from both a domestic laboratory and an international laboratory and storage at another domestic laboratory.

Shipment	Highest temperature recorded (°C)	Mean temperature during shipment (°C)	Mean temperature during storage (°C)
Domestic laboratory	–180.2	–190.4 ± 0.5	–181.1 ± 0.6
International laboratory	–180.2	–193.5 ± 0.6	–181.2 ± 0.7

Post-Warming Survival of Human Embryos, Human Oocytes, and Bovine Sperm

Following transport and storage in either the study system or in conventional dewars, bovine semen was alive and motile with approximately 70% motility and normal forward progression. No significant difference was noted between the two groups. All human donor oocytes survived

warming in both groups except for two oocytes frozen on the same cryodevice after the first warm in the conventional dewars (Fig. 10.3A). All oocytes survived an additional vitrification/ warming in the respective storage systems. All human blastocysts survived warming after storage and transport in both the study system and the conventional dewar system and showed normal blastocyst expansion after a 2-hour recovery period (Fig. 10.3B).

Expression of Cleaved Caspase-3 in Human Blastocysts

Embryos from both groups were evaluated for nuclei that stained positively for both markers of apoptosis, cleaved caspase 3, and granular DNA fragments (Fig. 10.3C). Both the total number of nuclei that stained positive for cleaved caspase-3 (CON: 5.00±1.31; TMRW: 7.75±0.82) and the total cell nuclei as determined by DAPI-positive staining (CON: 118.50±14.37; TMRW: 102.88±11.34) was similar between both groups, and no significant differences were noted. Additionally, the proportion of apoptotic cells as determined by the cleaved caspase-3 to total nuclei ratio was not different between the two groups (CON: 0.04±0.01; TMRW: 0.08±0.02, Fig 10.3D).

Assessment of Embryo Development in Extended Culture

Over the course of 5 days in extended embryo culture, the proportion of embryos attached to fibronectin-coated dishes was not different between embryos from the conventional dewar system compared to those in the study platform (Fig. 10.4A). The percentage of normal developing embryos was also not different between the two groups (Fig. 10.4B). Embryo health was assessed as normal or abnormal defined by continued proliferation and development of morphologically different cell populations including flattened syncytiotrophoblast and migratory trophoblast cells moving away from the embryo proper (Fig. 10.4C**)**. In addition to the morphological appearance, hCG was measured from the spent media over the duration of extended culture to evaluate the normal development of human embryos. There were no differences in secreted hCG levels between embryos from the conventional dewar system

compared to those in the study system (Fig. 10.4D). These measurements were also compared to historical extended embryo culture data from our lab, shown as “HIST” in Fig. 10.4D. Outgrowth areas over the course of extended culture were also not different between embryos in the conventional dewar system compared to those in the study system or to our historical dataset (Fig. 10.4E).

Confocal Analysis of Embryos in Extended Culture

Following five days in extended culture, the proportion of embryos with at least one cell positive for the pluripotency marker POU5F1 was not different between embryos in the conventional dewar system or the study system (Fig. 10.5A). The number of POU5F1-positive epiblast cells was also not different between the two groups (Fig. 10.5B). Organization of POU5F1 positive epiblast cells was relatively the same between the two groups, though this was not quantified (Fig. 10.5C).

Discussion

Cryogovernance of reproductive specimens encompasses many processes and systems. Among these are the systems used by IVF laboratories to manage inventory control, to provide for a specimen chain of custody, to monitor and ensure the maintenance of cryogenic temperatures, to control audits of the history of specimens under management, and to establish conditions for the safe handling of specimens for patients and laboratory personnel. Seldom are these systems integrated into a cohesive platform. Integration of all the facets of a successful ART cryosystem into a single, streamlined platform allows for a complete history of every specimen under management by an IVF laboratory. In the future, data gathered from fully integrated cryogovernance platforms can be used to continuously improve the safety and efficacy of cryogenic systems.

Of all the critical points controlled by cryogovernance to ensure specimen integrity, maintenance of temperatures to be well below the T_g, the point at which a material alters state, is of singular importance. While catastrophic loss of temperature undoubtedly results in specimen damage and loss, the magnitude and effect of minor fluctuations that occur during shipment and/or storage in nitrogen vapor is not well characterized (18).

T_g is known to vary, and there is debate around the exact temperature that should be used as the standard for vitrified specimens (18-20). The International Society of Biological and Environmental Repositories (ISBER) advises a conservative -136°C and -132°C T_g, while academic studies have reported a range -121°C to -126°C and a value of -130°C (18- 20). It is widely accepted that at temperatures lower than T_g, biological activity ceases; specifically, this temperature has been identified as below -150°C (21-23). To maintain the integrity of stored reproductive specimens indefinitely, cryogovernance operations either immerse specimens in the liquid phase of nitrogen with a temperature of approximately -196°C or suspend in the vapor phase of nitrogen with temperatures ranging from approximately -195°C and -150^{O}C (24-29). The temperature of nitrogen vapor also varies with the distance from the liquid vapor interface (30).

In our study, all specimens were initially shipped using vapor phase shippers without temperature monitoring. Temperature of the control groups is inferred from the presence of liquid nitrogen levels, but it is impossible to know if the specimens in our study were exposed to minor temperature excursions during static storage, like the treatment specimens in the vapor phase, as would happen when searching for a neighboring specimen. Continuous temperature monitoring of the treatment group of this study provides certainty that there were no temperature excursions that placed specimens in jeopardy. Similarly, extensive telemetry that includes specimen movement and particularly temperature during shipment and storage of reproductive

specimens allows for the investigation of any major temperature excursion that would otherwise go unnoticed.

Temperature telemetry from the TMRW platform allows for clarity that excursions did not occur during this study that would have put the specimens into jeopardy or confound the data collected. This allows for assurance that the results achieved are accurately reflecting the intended shipment and/or storage temperature of the specimens in the treatment and control groups.

Our results indicate that the TMRW platform is safe for the shipment and storage of gametes and embryos the advantages, including continuous telemetry, digital specimen inventory and management offer distinct improvements over current systems. Additionally, decreasing exposure to liquid nitrogen diminishes the chance for major liquid nitrogen burns *(data not shown).*

There was no difference in the post-warming survival of human oocytes, bovine sperm, and human blastocysts between the conventional dewar system and the study system. However, cryopreservation and storage may pose long-term damage on development that are difficult to evaluate at the time of warming by morphological assessment. Therefore, assessing whether there is a decline in the developmental potential of the stored samples becomes critical. Temperature fluctuations may activate caspase-3 and induce cell apoptosis (31), and the presence of cleaved caspase-3 is widely accepted as a biomarker to assess embryo quality (32-34). No significant differences in the expression of cleaved caspase-3 in human blastocysts between the study system and control suggests that the TMRW platform is as safe as the conventional dewar system and did not cause any additional damage that may trigger cell apoptosis (31). It is worth noting that caspase-3 experiments were underpowered due to travel restrictions and that caution should be used when interpreting these results. The study design

may introduce bias by assuming independence of each embryo and oocyte and not accounting for the embryo and oocyte donors.

Extended culture offers a valuable opportunity to measure the potential impact of the newly developed TMRW platform on human blastocyst developmental potential in lieu of pregnancy and live birth data from clinical studies. Extended culture of human blastocysts donated for research to test new techniques prior to clinical trials minimizes the risk for trial participants. Our research program has collected data from 653 human embryos in extended culture over the course of two years. Our data show that embryos with high morphological grade, which in our experience results in higher pregnancy rates after transfer, had significantly larger outgrowth areas than those with low morphological grade. Additionally, embryos from advanced maternal age patients tend to have fewer epiblast cells in extended culture and significantly smaller outgrowth areas than embryos from younger patients [15]. These results suggest that our extended culture system is a sensitive method to predict post transfer developmental potential of human blastocysts.

No significant differences were noted for any parameter measured during extended culture. Therefore, transportation and storage of human embryos in the TMRW platform are as safe as using a conventional dewar system. Our comparison of epiblast cell numbers may be underpowered due to the high variability of the dataset. However, measurements for outgrowth areas on extended culture day 3, 4, and 5 and hCG quantification 48 and 72 h post attachment are appropriately powered.

The multiple assays of gamete and embryo survival and quality coupled with the temperature telemetry in this study provides a thorough investigation of the effects of shipment and storage in nitrogen vapor compared with storage in the liquid phase of nitrogen. In addition to the increased clarity provided by the temperature telemetry that specimens are maintained at a safe

temperature, the results indicate that the TMRW designed labware in conjunction with automation is safe in handling frozen and vitrified reproductive specimens.

Conclusion

The TMRW platform does not have any deleterious effects on the post-warming viability of sperm, oocytes, or embryos.

Notes

The authors thank Mary Mahony, PhD and Frankie Michielli (supported by TMRW Life Sciences, Inc.) for editorial assistance in drafting the manuscript, and the TMRW team (Bill Garbarini, Cynthia Hudson, Robert Perkinson, Robert DeSanno, and Mischa Gresser) for site support assistance.

Disclosures

Deirdre Logsdon, Courtney Grimm, Sue McCormick, Terry Schlenker, Jason Swain, Rebecca Krisher and Ye Yuan have nothing to disclose. Michael Collins is an employee of TMRW Life Sciences, Inc.

William Schoolcraft is a shareholder of TMRW.

No employees of Colorado Center for Reproductive Medicine (CCRM) received compensation in any form from TMRW for the completion of this study. All experiments were designed by employees of CCRM with input from TMRW. Finally, all results for such experiments have been reported in full and no data was redacted in any way.

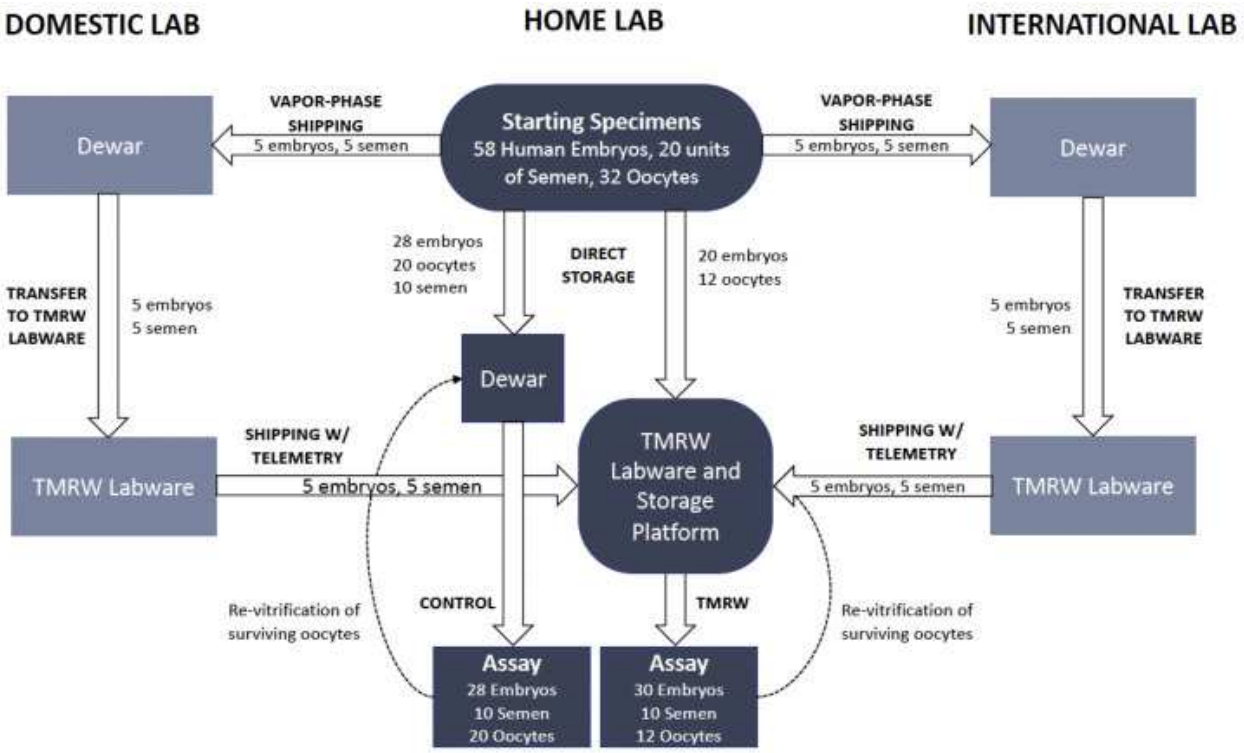

Figure 10.1. Shipment, treatment and assay of specimens. All control specimens, 28 embryos, 20 oocytes and 10 units of bovine semen did not leave the home lab, where they were stored in LN_2 dewars until assay. Five embryos and 5 units of bovine semen were shipped to both a domestic lab and an international lab. After at least 5 days of storage in LN_2 dewars they were transferred to TMRW labware with telemetry started and immediate shipment back to the home lab for storage in the TMRW automated storage unit. An additional 20 embryos and 10 oocytes were transferred at the home lab directly from LN_2 dewars to TMRW labware and storage in the TMRW automated storage unit. Surviving oocytes were revitrified and placed back into LN_2 dewars at the home lab or the TMRW labware and automated storage unit.

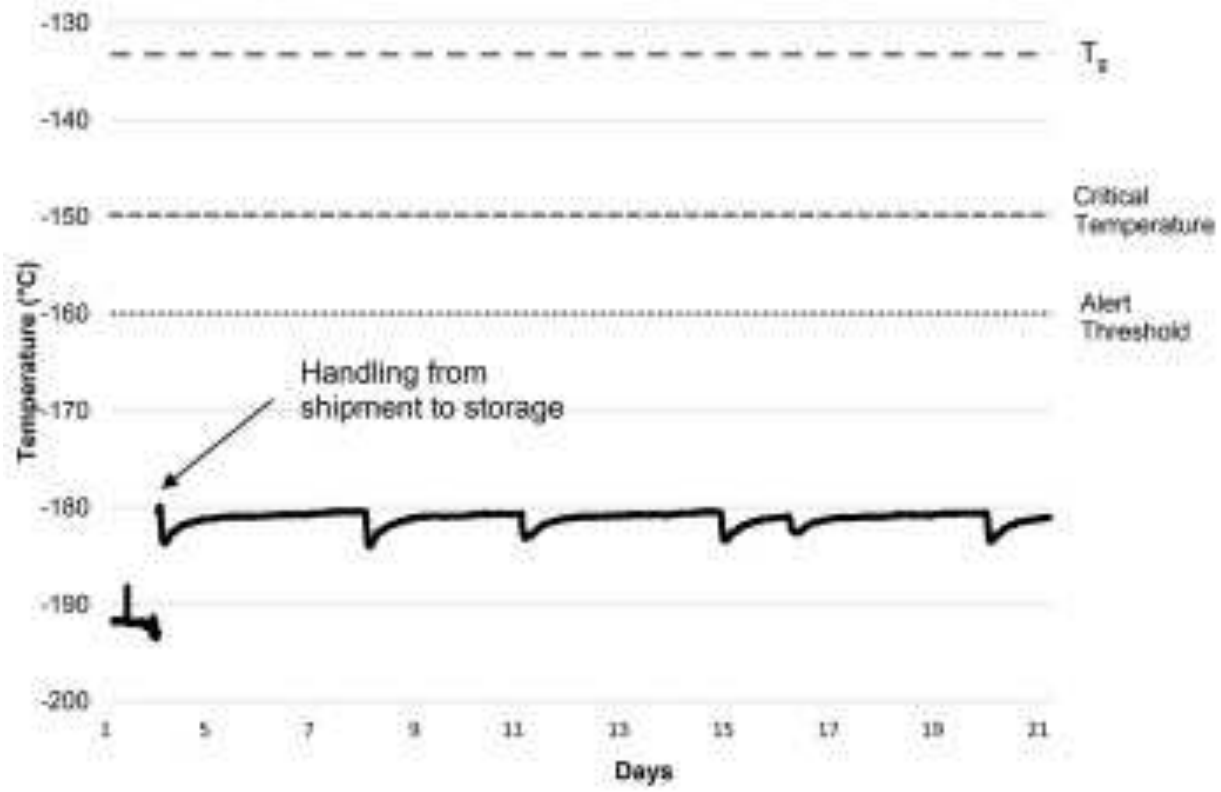

Figure 10.2. Nitrogen vapor phase temperature (°C) telemetry readings for embryos and semen during shipment from a domestic lab and storage at another domestic lab. The study platform was set to alert at -160^{O}C (Alert Threshold) and alarm at -150^{O}C (Critical Temperature). Telemetry (including temperature) was remotely monitored in New York City and logged through the course of the study. The T_g is assumed to be -132^{O}C based on literature reports.

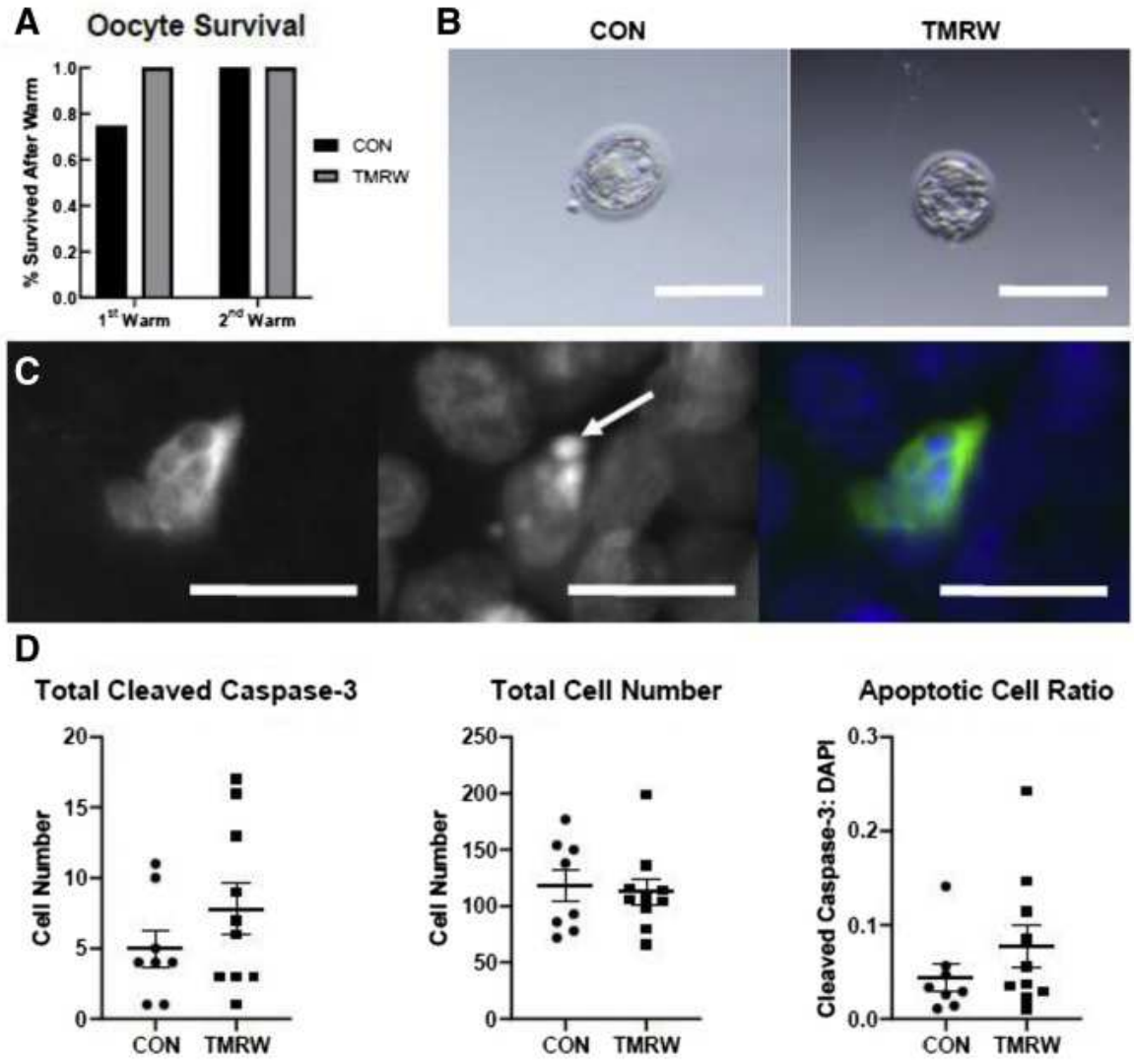

Figure 10.3. Post-warming viability of oocytes and embryos. A) Post-warming viability of oocytes that were transported and stored using the study system compared to those transported and stored in conventional liquid nitrogen (LN_2) dewars (CON) after a first and second warm. B) Representative stereomicroscope images of blastocysts after a 2-hour recovery following storage in conventional dewars (left) or TMRW (right). Scale bar = 200 µm. C) Representative images of cleaved caspase-3 staining in human embryos that were transported using the TMRW system. Cleaved caspase-3 (left), DAPI (center), and merged image (right). Green=cleaved caspase-3, Blue=DAPI. Scale bar = 5 µm. D) Total cleaved caspase-3 nuclei (left), total cell nuclei as measured by DAPI positive nuclei (center), and cleaved caspase-3:DAPI ratio (right). All data points are shown as well as mean ± SEM.

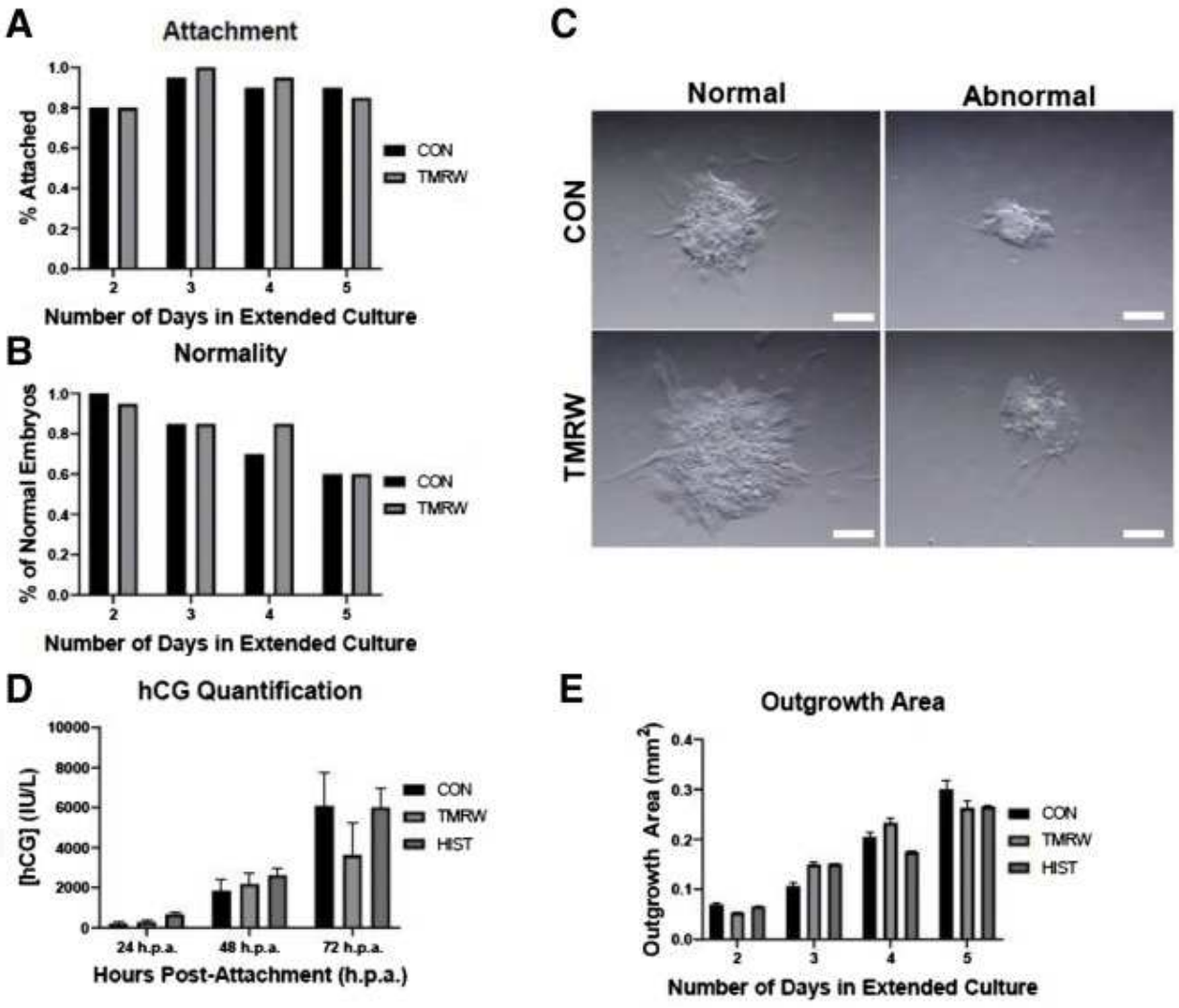

Figure 10.4. Assessment of embryo development during extended culture A) Proportion of embryos attached to fibronectin-coated dishes over the course of extended culture after storage in conventional dewars (CON) or the study platform (TMRW). B) Proportion of healthy embryos during extended embryo culture after storage in conventional dewars (CON) or the study system (TMRW). C) Representative images of normal and abnormal embryos after 5 days in extended culture after storage in conventional dewars (CON) or the study system (TMRW). Scale bar = 200 μm D) Human chorionic gonadotropin (hCG, IU/L) in 150 μL of spent media 24 hours post-attachment (h.p.a.), 48 h.p.a, and 72 h.p.a to fibronectin-coated dishes. CON= conventional dewar system, TMRW = study system, HIST = historical hCG concentrations over the course of two years. E) Outgrowth areas as measured by the outside edge of trophectoderm outgrowth in mm^2 between embryos stored in the conventional dewar system (CON), the study system (TMRW), or historically over the course of two years in our laboratory (HIST) during 5 days of extended embryo culture. Outgrowth areas shown are mean ± SEM.

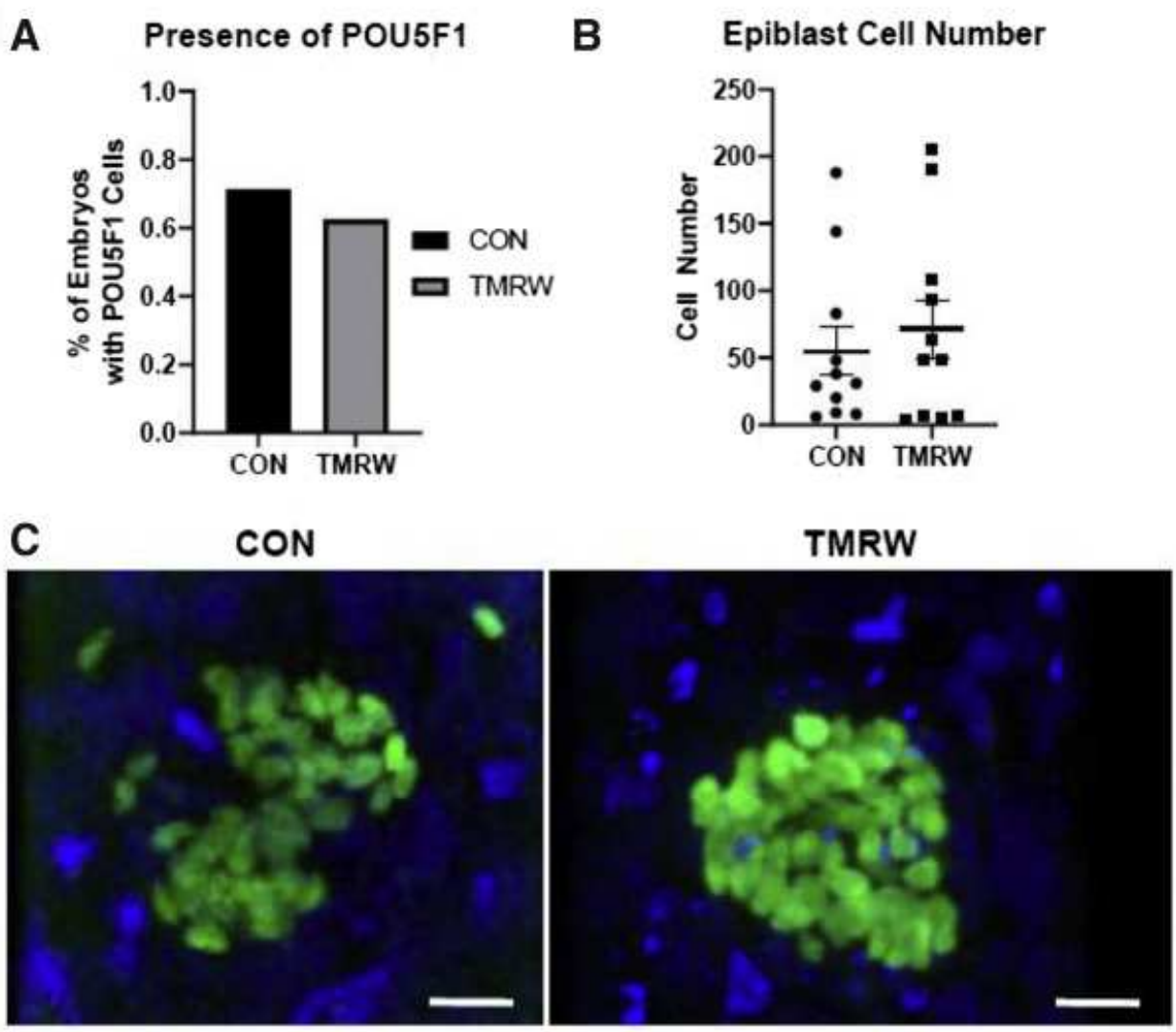

Figure 10.5. Confocal analysis of embryos in extended culture. A) Proportion of embryos stored in conventional dewars (CON) or the study system (TMRW) with at least one cell positive for the pluripotency marker POU5F1. B) Number of epiblast cells in embryos stored in conventional dewars (CON) or the study system (TMRW) with at least one epiblast cell as identified by positive POU5F1 staining. C) Representative images of POU5F1 staining in embryos that were stored in conventional dewars (CON) or the study system (TMRW). Scale bar= 10 μm. Blue= DAPI, Green= POU5F1. All epiblast cell numbers are shown as well as mean ± SEM.

REFERENCES

1. Alikani M. Cryostorage of human gametes and embryos: a reckoning. Reprod Biomed Online 2018; 37: 1–3.

2. Rienzi L, Gracia C, Maggiulli R, LaBarbera AR, Kaser DJ, Ubaldi FM, et al. Oocyte, embryo and blastocyst cryopreservation in ART: systematic review and meta-analysis comparing slow-freezing versus vitrification to produce evidence for the development of global guidance. Hum Reprod Update 2017; 23: 139–55.

3. Cobo A, Garcia-Velasco JA, Domingo J, Remohí J, Pellicer A. Is vitrification of oocytes useful for fertility preservation for age-related fertility decline and in cancer patients? Fertil Steril 2013; 99:1485–95.

4. Cobo A, Remohí J, Chang C-C, Nagy ZP. Oocyte cryopreservation for donor egg banking. Reprod Biomed Online 2011; 23: 341–6.

5. Simopoulou M, Asimakopoulos B, Bakas P, Boyadjiev N, Tzanakaki D, Creatsas G. Oocyte and embryo vitrification in the IVF laboratory: a comprehensive review. Folia Med (Plovdiv) 2014; 56: 161–9.

6. Homburg R, van der Veen F, Silber SJ. Oocyte vitrification-Women's emancipation set in stone. Fertil Steril 2009; 91(Suppl 4): 1319–20.

7. Chart Industries. MVE Cryopreservation for Life Science: Storage and Transport Systems for MVE Cryopreservation. Available at: http://files.chartindustries.com/Cryopreservation_Catalog_ML-CRYO0009.pdf. Accessed March 11, 2021.

8. Parmegiani L. Oocyte vitrification/storage/handling/transportation/warming, effect on survival and clinical results in donation programmes. Curr Trends Clin Embryol 2017; 4: 34.

9. Sansinena M, Santos MV, Zaritzky N, Chirife J. Numerical simulation of cooling rates in vitrification systems used for oocyte cryopreservation. Cryobiology 2011; 63: 32–7.

10. Sansinena M, Santos MV, Chirife J, Zaritzky N. In-vitro development of vitrified–warmed bovine oocytes after activation may be predicted based on mathematical modelling of cooling

and warming rates during vitrification, storage and sample removal. Reprod Boomed Online 2018; 36: 500–7.
11. Murray KA, Gibson MI. Post-thaw culture and measurement of total cell recovery is crucial in the evaluation of new macromolecular cryoprotectants. Biomacromolecules; 2020: 21: 2864-73.
12. Shahbazi MN, Jedrusik A, Vuoristo S, Recher G. Europe PMC Funders Group Self-organisation of the human embryo in the absence of maternal tissues. Nat Cell Biol 2016; 18: 700–8.
13. Deglincerti A, Croft GF, Pietila LN, Zernicka-Goetz M, Siggia ED, Brivanlou AH. Self-organization of the in vitro attached human embryo. Nature 2016; 533: 251–4.
14. Logsdon DM, Ermisch AF, Kile R, Schoolcraft WB, Krisher RL, Yuan Y. Egg cylinder development during in vitro extended embryo culture predicts the post transfer developmental potential of mouse blastocysts. J Assist Reprod Genet 2020; 37: 747–52.
15. Logsdon DM, West RC, Kile R, Grimm CK, Katz-Jaffe MG, McCormick S, et al. In Vitro Peri-Implantation Development of Good Quality Human Embryos Is Affected by Blastocyst Morphological Grade and Maternal Age. Fertil Steril 2020; 114: e315.
16. Logsdon, DM, Kile, RA, Schoolcraft, WB, Krisher, RL, Yuan, Y. Single Cell Collection of Trophoblast Cells in Peri-implantation Stage Human Embryos. J Vis Exp 2020; 160: e61476.
17. Schneider, CA, Rasband, WS, Eliceiri, KW. "NIH Image to ImageJ: 25 years of image analysis". Nat Methods 2012; 9: 671-675.
18. Campbell LD, Astrin JJ, DeSouza Y, Giri, J, Patel AA, Rawley-Payne M, et al. The 2018 Revision of the ISBER Best Practices: Summary of Changes and the Editorial Team's Development Process. Biopreservation and Biobanking. 2018 16: 3-6.
19. Mochida K, Hasegawa A, Li M-W, Fray MD, Kito S, Vallelunga JM, et al. High Osmolality Vitrification: A New Method for the Simple and Temperature-Permissive Cryopreservation of Mouse Embryos. PLoS One 2013; 8: e49316.

20. Sansinena M, Santos M V., Taminelli G, Zaritzky N. Implications of storage and handling conditions on glass transition and potential devitrification of oocytes and embryos. Theriogenology 2014; 82: 373–8.
21. Clarke A, Morris GJ, Fonseca F, Murray BJ, Acton E, Price HC. A Low Temperature Limit for Life on Earth. PLoS One 2013; 8: e66207.
22. Baust JG, Gao D, Baust JM. Cryopreservation: An emerging paradigm change. Organogenesis 2009; 5: 90–6.
23. Fuller B, Paynter S. Fundamentals of cryobiology in reproductive medicine. Reprod Biomed Online 2004; 9: 680–91.
24. Cobo A, Romero JL, Pérez S, De Los Santos MJ, Meseguer M, Remohí J. Storage of human oocytes in the vapor phase of nitrogen. Fertil Steril 2010; 94: 1903–7.
25. Eum JH, Park JK, Lee WS, Cha KR, Yoon TK, Lee DR. Long-term liquid nitrogen vapor storage of mouse embryos cryopreserved using vitrification or slow cooling. Fertil Steril 2009; 91: 1928–32.
26. Paoli D, Lombardo F, Lenzi A, Gandini L. Sperm cryopreservation: Effects on chromatin structure. Adv Exp Med Biol 2014; 791: 137–50.
27. Joaquim DC, Borges ED, Viana IGR, Navarro PA, Vireque AA. Risk of Contamination of Gametes and Embryos during Cryopreservation and Measures to Prevent Cross-Contamination. Biomed Res Int 2017; 2017: 1840417.
28. Hunt CJ. Cryopreservation: Vitrification and Controlled Rate Cooling. Methods Mol Biol 2017; 1590: 41-77.
29. Simione F, Sharp T. Best practices for storing and shipping cryopreserved cells. In Vitro Cell Dev Biol Anim 2017; 53: 888–95.
30. Hunt CJ, Pegg DE. Improved temperature stability in gas-phase nitrogen refrigerators: Use of a copper heat shunt. Cryobiology 1996; 33: 544–51.

31. Stroh C, Cassens U, Samraj AK, Sibrowski W, Schulze-Osthoff K, Los M. The role of caspases in cryoinjury: caspase inhibition strongly improves the recovery of cryopreserved hematopoietic and other cells. FASEB J 2002; 16: 1651–3.
32. Kaihola H, Yaldir FG, Bohlin T, Samir R, Hreinsson J, Åkerud H. Levels of caspase-3 and histidine-rich glycoprotein in the embryo secretome as biomarkers of good-quality day-2 embryos and high-quality blastocysts. PLoS One 2019; 14: 0226419.
33. Vandaele L, Mateusen B, Maes DGD, de Kruif A, Van Soom A. Temporal detection of caspase-3 and -7 in bovine in vitro procedure embryos of different developmental capacity. Reproduction 2007; 133: 709–18.
34. Hayashi M, Yoshida K, Kitada K, Kizu A, Tachibana D, Fukui M, et al. Low-dose irradiation of mouse embryos increases Smad-p21 pathway activity and preserves pluripotency. J Assist Reprod Genet 2018; 35: 1061–9.